

NEW REDOX-ACTIVE LIGANDS ON IRON AND COBALT FOR C–C BOND FORMING REACTIONS

A Thesis

Presented to

The Academic Faculty

by

Michael Bruce Bayless

In Partial Fulfillment

of the Requirements for the Degree

Doctorate in the

School of Chemistry and Biochemistry

Georgia Institute of Technology

August, 2014

Copyright © 2014 by Michael B. Bayless

NEW REDOX-ACTIVE LIGANDS ON IRON AND COBALT FOR C–C BOND FORMING REACTIONS

Approved by:

Dr. Jake D. Soper,
Advisor School of Chemistry and
Biochemistry
Georgia Institute of Technology

Dr. E. Kent Barefield
School of Chemistry and Biochemistry
Georgia Institute of Technology

Dr. W. John Zhang
School of Chemistry and Biochemistry
Georgia Institute of Technology

Dr. Angus P. Wilkinson
School of Chemistry and Biochemistry
Georgia Institute of Technology

Dr. Christopher W. Jones
School of Chemical and Biomolecular
Engineering
Georgia Institute of Technology

Date: June 11th, 2014

Acknowledgements

I would like to thank Dr. Jake Soper for helping me become the scientist I am today. Your guidance and scientific insight made working in the lab an enjoyable and educational experience. I would also like to thank the graduate students and post docs that I had the pleasure of working with over the years in Dr. Soper's lab. To Aubrey Smith, Cam Lippert and CJ Rolle, thanks for all the help and encouragement throughout my graduate career, I will always remember the good times had in lab between the four of us. To the current group members, Ashley McDaniel, Caleb Harris, and Lucas Evans thank you for your friendship and support. I would like to express my gratitude to all the friends I have made during my graduate career. I would like to thank Kyle Flack, Matt Hagy and Chelsea Wyss for providing me with parties, laughs and friendship. Thanks for always being there in my time of need to offer a shoulder to lean on. To my family, Olga and James Helmandollar, Brian, Diane, Jonathan, Matthew, Kayla, and Olivia Bayless, thank you for all your support and guidance during my graduate career. Your love and support gave me the strength to keep going when times were difficult. Finally, a special thanks to Laura Wally for supporting all my endeavors. Your encouragement means the world to me. Your support has carried me throughout my graduate career.

TABLE OF CONTENTS

	Page
Acknowledgements	iii
List of Tables	xi
List of Figures	xii
List of Symbols and Abbreviations	xv
Summary	xviii
<u>Chapter</u>	
1 Introduction	1
1.1 Significance of cross-coupling reactions in forming new C–C bonds	1
1.2 Palladium catalyzed C–C bond forming cross-coupling reactions	2
1.3 Late 3d metals and C–C bond forming reactions	4
1.4 Redox-active ligands	8
1.5 Redox-active ligands on metals: A well-defined platform for catalysis.	10

1.6	Redox-active amidophenolate ligands on 3d metals to carry out $2e^-$ transformations in C–C bond forming reactions.	12
1.7	Thesis hypothesis and goals.	16
1.8	Works cited	18
2	Development of Redox-Active Ligand $\text{FeCl}(\text{isq}^{\text{Ph}})_2$ Complex as Well-defined Catalyst for Aerobic Homocoupling of Grignard Reagents	26
2.1	Introduction	26
2.1.1	Iron salts for cross-coupling and homocoupling reactions and their mechanisms	26
2.1.2	Redox-active ligands as an electron reservoir for well-defined iron catalyst	27
2.1.3	The amidophenolate ligand as a redox active ligand on 3d metals	28
2.2	Results	29
2.2.1	Synthesis and characterization of $\text{Fe}^{\text{III}}\text{Cl}(\text{isq}^{\text{Ph}})_2$	29
2.2.2	Preparation of an ET series from reduction of $\text{FeCl}(\text{isq}^{\text{Ph}})_2$	31
2.2.3	Aerobic homocoupling of aryl Grignards using $\text{Fe}^{\text{III}}\text{Cl}(\text{isq}^{\text{Ph}})_2$	33
2.3	Discussion	36
2.3.1	Synthesis and characterization of $\text{Fe}^{\text{III}}\text{Cl}(\text{isq}^{\text{Ph}})_2$ and $\text{Na}[\text{Fe}(\text{ap}^{\text{Ph}})_2]$	36

2.3.2	C–C bond forming reactions using $\text{Fe}^{\text{III}}\text{Cl}(\text{isq}^{\text{Ph}})_2$	37
2.4	Conclusions	38
2.5	Methods	38
2.5.1	General considerations	38
2.5.2	Methods and materials	38
2.6	Works Cited	41
3	New Cobalt Electron-Transfer Series Featuring Redox-Active Pincer-Type N-Heterocyclic ligand for C–C Bond Forming Reactions	44
3.1	Introduction	44
3.2	Results	47
3.2.1	Synthesis and characterization of $\text{Co}^{\text{II}}((\text{tBuPhO})_2\text{NHC})\text{THF}$	47
3.2.2	Electrochemistry of the $\text{Co}^{\text{II}}((\text{tBuPhO})_2\text{NHC})(\text{THF})$	49
3.2.3	Synthesis and characterization of $[\text{Co}((\text{tBuPhO})_2\text{NHC})(\text{THF})_2]\text{BF}_4$	50
3.2.4	Synthesis and characterization of $[\text{Co}((\text{tBuPhO})_2\text{NHC})(\text{THF})_3](\text{PF}_6)_2$	51
3.2.5	Metrical parameters for the assignment of metal and ligand oxidation states of complexes 2 and 3	52
3.2.6	Cross-coupling reactions of aryl Grignard and alkylhalide	55

3.2.7	Reductive elimination and oxidative addition studies	57
3.3	Discussion	58
3.4	Conclusion	65
3.5	Methods	65
3.5.1	General considerations	65
3.5.2	Methods and materials	68
3.6	Works cited	72
4	Co^{II}((tBuPhO)₂NHC)THF Mediated Nitrile Transfer via C–O Activation	77
4.1	Introduction	77
4.1.1	Utility and prevalence of C–O activation	77
4.2	Results	80
4.2.1	C–O bond activation and cross-coupling	80
4.2.2	Scope of nucleophiles for cross-coupling	80
4.2.3	Scope of ether nitriles used for C–O activation	82
4.2.4	Oxidative addition of halide nitriles	84
4.3	Discussion	86
4.3.1	Scope of reactivity of 1 for C–O activation	86

4.3.2	Proposed catalytic cycle of C–O activation and cross-coupling using 1 as the catalyst	89
4.4	Conclusion	90
4.5	Materials and Methods	91
4.5.1	General	91
4.5.2	Synthesis	92
4.6	Work cited	94
5	Reactions studies of $\text{Co}^{\text{II}}((\text{tBuPhO})_2\text{NHC})\text{THF}$ and synthesis of $\text{Na}[\text{Fe}^{\text{III}}((\text{tBuPhO})_2\text{NHC})]$ and future directions	97
5.1	Introduction	97
5.1.1	Expanding the scope of $[\text{M}((\text{tBuPhO})_2\text{NHC})]$ ($\text{M} = \text{Co}, \text{Fe}$) toward C–H activation and oxygen atom transfer	98
5.2	Results	102
5.2.1	Attempts at C–H bond activation with $\text{Co}^{\text{II}}((\text{tBuPhO})_2\text{NHC})\text{THF}$	102
5.2.2	Stoichiometric reactions of $\text{Co}^{\text{II}}((\text{tBuPhO})_2\text{NHC})\text{THF}$ with O–atom transfer reagents	104
5.2.3	$[\text{Fe}((\text{tBuPhO})_2\text{NHC})\text{Cl}_2]^-$ and $[\text{Fe}((\text{tBuPhO})_2\text{NHC})]^+$ synthesis and characterization	108

5.2.4	[Fe((tBuPhO) ₂ NHC)(MeOH) ₂] ⁺ catalyzed cross-coupling of alkyl halides and Grignards	115
5.2.5	[Fe ^{III} ((tBuPhO) ₂ NHC)(MeOH) ₂]ClO ₄ reactivity with oxygen transfer reagents	117
5.3	Discussion	119
5.3.1	Co ^{II} ((tBuPhO) ₂ NHC)THF C–H bond activation and oxygen atom transfer reactions	119
5.3.2	Na[Fe((tBuPhO) ₂ NHC)Cl ₂] synthesis and reactivity	122
5.3.3	[Fe((tBuPhO) ₂ NHC)(MeOH) ₂]ClO ₄ synthesis and reactivity	123
5.4	Conclusion	125
5.4.1	Scope of reactivity of Co ^{II} ((tBuPhO) ₂ NHC)THF	125
5.4.2	[Fe ^{III} ((tBuPhO) ₂ NHC)] ⁺ synthesis and reactivity	126
5.5	Methods	127
5.5.1	General considerations	127
5.5.2	Na[Fe((tBuPhO) ₂ NHC)] synthesis	128
5.5.3	X-ray crystallography	129
5.5.4	General reaction for C–H bond activation	132
5.5.5	General reaction for oxygen atom transfer	132
5.6	Works Cited	133

6	Conclusions and Future Directions	138
6.1	Work cited	140
A	Work Towards a Pacman Type Redox-Active Ligand	142
A.1	Introduction	142
A.1.1	Pacman Type Ligands	142
A.1.2	Redox-Active Pacman Type Ligands	145
A.1.3	Retrosynthetic analysis of Redox-Active Pacman Type Ligands	147
A.2	Results	148
A.2.1	Attempts at Anthracene Backbone Pacman Type Ligand	148
A.2.2	Synthesis of Xanthene Backbone Pacman Type Ligand	148
A.3	Discussion	158
A.3.1	Cross-coupling attempts anthracene	159
A.3.2	Cross-coupling of a borate ester aryl diamine and dihalidexanthane	161
A.4	Conclusion	161
A.5	Materials and Methods	161
A.6	Work Cited	166

LIST OF TABLES

	Page
Table 3-1 Crystollographic data and parameters for complexes Co ^{II} ((tBuPhO) ₂ NHC)(THF) 1 , [Co ^{III} ((tBuPhO) ₂ NHC)(THF) ₂]BPh ₄ 2 , and [Co ^{II} ((tBuPhO) ₂ NHC)(THF) ₃](PF ₆) ₂ 3 .	66
Table 4-1. Reactions between various ether nitriles and PhMgBr catalyzed by 1 .	82
Table 5-1. Oxygen atom transfer to organic substrates using Co ^{II} ((tBuPhO) ₂ NHC)THF.	107
Table 5-2. Cross-coupling yields of PhMgBr and 1-bromohexane in the presence of [Fe ^{III} ((tBuPhO) ₂ NHC)Cl ₂] ⁻ under N ₂ or aerobic conditions.	115
Table 5-3. Cross-coupling yields of PhMgBr and 1-bromohexane in the presence of [Fe ^{III} ((tBuPhO) ₂ NHC)(MeOH) ₂]ClO ₄ under N ₂ or aerobic conditions.	116
Table 5-4. Oxygen atom transfer reactions to oragnic substrates in the presence of [Fe ^{III} ((tBuPhO) ₂ NHC)(MeOH) ₂]ClO ₄ .	118
Table 5-5. Crystallographic data and structure parameters for [(tBuPhO) ₂ NHC][FeCl ₄].	131
Table A-1. Reactions between anthracenedigrignard or diorganozinc and aryl halides catalyzed by Pd or Ni.	152
Table A-2 Reactions between aryl borate esters or boronic acid and aryl halides catalyzed by Pd.	153
Table A-3 Reaction conditions and results between dihalide xanthene and borate ester diamines catalyzed by Pd.	156

LIST OF FIGURES

	Page
Figure 1-1. Abundance of elements in earth's crust (U.S. Geological Survey Fact Sheet 087-02 courtesy of the U.S. Geological Survey).	3
Figure 2-1. Cyclic voltammogram of $\text{Fe}^{\text{III}}\text{Cl}(\text{isq}^{\text{Ph}})_2$ in CH_3CN containing 0.1 M $[\text{nBu}_4\text{N}][\text{PF}_6]$ at a 10 mm Pt electrode. Scan rate: 0.10 V s^{-1} . Temperature 25°C .	30
Figure 2-2. UV-vis absorption spectra in THF using a 0.50 mm pathlength cuvette for a) a reaction between isolated $\text{Na}[\text{Fe}^{\text{III}}(\text{ap}^{\text{Ph}})_2]$ (purple line) and air to produce $\text{Fe}^{\text{III}}(\text{isq}^{\text{Ph}})_3$ (green line) b) exposure of isolated $\text{Na}[\text{Fe}^{\text{III}}(\text{ap}^{\text{Ph}})_2]$ (purple line) to 1 equiv of 2,3,4,5,6,6-hexachlorocyclohexa-2,4-dien-1-one to produce $\text{Fe}^{\text{III}}\text{Cl}(\text{isq}^{\text{Ph}})_2$ (green line).	32
Figure 2-3. UV-vis spectra collected in a 0.54 mm path length in THF for a) comparison of the isolated $\text{Na}[\text{Fe}(\text{ap}^{\text{Ph}})_2]$ (dark purple) and the purple solution generated from the reaction between $\text{Fe}^{\text{III}}\text{Cl}(\text{isq}^{\text{Ph}})_2$ and 2 equiv of PhMgBr (light purple) b) exposure of $\text{Fe}^{\text{III}}\text{Cl}(\text{isq}^{\text{Ph}})_2$ (dark green line) to 2 equiv of PhMgBr (purple line) followed by exposure to air (light green line).	34
Figure 3-1. Proposed structure of $\text{Co}^{\text{II}}(\text{tBuPhO})_2\text{NHC}$.	46
Figure 3-2. UV-vis spectra of complexes 1 , 2 , and 3 in THF solutions at 22°C .	48
Figure 3-3. Cyclic voltammogram of $\text{Co}^{\text{II}}((\text{tBuPhO})_2\text{NHC})(\text{THF})$ CH_3CN containing 0.1 M $[\text{nBu}_4\text{N}][\text{PF}_6]$ at a 10 mm Pt electrode. Scan rate: 0.1 V s^{-1} . Temperature: 22°C .	50
Figure 3-4. Selected bond lengths (\AA) of the CoNHC electron-transfer series (red bond lengths represent contracted bond lengths and blue represents elongated bond lengths vs 1). Hydrogen, THF, and counter-ions have been omitted for clarity.	53
Figure 3-5. Schematic of selected bond lengths (\AA) in $\text{Co}^{\text{III}}(\text{ap}^{\text{Ph}})(\text{isq}^{\text{Ph}})$.	54
Figure 4-1. Cross-coupling and homocoupling yields generated from the	

catalytic reaction of a Grignard reagent and 3-phenylpropanenitrile using 1 as the catalyst. The yield is reported as the ratio of area of analyte vs area of decane (internal standard) in arbitrary units derived from the GC-MS trace of the crude reaction mixture after 24 hours.	81
Figure 4-2. ^1H NMR spectrum of 3-butoxybutanenitrile in CDCl_3 at 25 °C.	84
Figure 4-3. UV-vis absorption spectrum collected at 22 °C in THF (a) Bromoacetonitrile 10 min after addition to 1 (blue line); 3-bromopropanenitrile 12 hr after addition to 1 (red line) (b) 3 days after addition of: bromoacetonitrile (blue line), chloroacetonitrile (green line), and 3-bromopropanenitrile (red line) to 1.	85
Figure 5-1 UV-Vis spectra of a reaction between $\text{Co}^{\text{II}}((\text{tBuPhO})_2\text{NHC})\text{THF}$ and <i>m</i> -CPBA in CH_3CN . Red line represents $\text{Co}^{\text{II}}((\text{tBuPhO})_2\text{NHC})\text{THF}$ in CH_3CN prior to <i>m</i> -CPBA addition. Orange line represents 30 sec after <i>m</i> -CPBA addition. Green line represents 60 mins after <i>m</i> -CPBA addition. a) 0.5 equiv of <i>m</i> -CPBA. b) 1 equiv of <i>m</i> -CPBA c) 3 equiv of <i>m</i> -CPBA.	105
Figure 5-2. Proposed structure of $[\text{Fe}^{\text{III}}((\text{tBuPhO})_2\text{NHC})\text{Cl}_2]^-$.	108
Figure 5-3. UV-vis absorption spectrum for $[\text{Fe}^{\text{III}}((\text{tBuPhO})_2\text{NHC})\text{Cl}_2][\text{Na}]$ in THF at room temperature.	109
Figure 5-4. Cyclic voltammogram of $\text{Na}[\text{Fe}^{\text{III}}((\text{tBuPhO})_2\text{NHC})\text{Cl}_2]$ in THF containing 0.1 M $[\text{nBu}_4\text{N}][\text{PF}_6]$ at a 10 mm Pt electrode. Scan rate: 0.05 V s^{-1} . Temperature: 25 °C.	110
Figure 5-5. Solid-state structure of $[(\text{tBuPhO})_2\text{NHC})\text{H}_3][\text{FeCl}_4]$ shown with 50% probability ellipsoids. Hydrogen atoms omitted for clarity.	111
Figure 5-6. Cyclic voltammogram of $[\text{Fe}^{\text{III}}((\text{tBuPhO})_2\text{NHC})(\text{MeOH})_2]\text{ClO}_4$ in CH_3CN containing 0.1 M $[\text{nBu}_4\text{N}][\text{PF}_6]$ at a 10 mm Pt electrode. Temperature: 25 °C. a) Scan rate: 0.100 $\text{V}\cdot\text{s}^{-1}$. b) Scan rate: 0.500 $\text{V}\cdot\text{s}^{-1}$.	112
Figure 5-7. UV-vis absorption spectrum for $[\text{Fe}^{\text{III}}((\text{tBuPhO})_2\text{NHC})(\text{MeOH})_2]\text{ClO}_4$ in THF at room temperature.	113
Figure 6-1. Proposed ligands to increase electron density at the metal center.	140
Figure A-1. A pacman ligand with bis(Ni(II)oxocorrole) and an anthracene backbone.	143
Figure A-2. A redox-active pacman ligand consisting of an anthracene backbone	

and bis(Ru(terpyridine)(3,5-ditertbutylcatechol)). 145

Figure A-3. Proposed redox-active pacman complex. 146

Figure A-4. Chosen dihalidexanthenes and diamine nucleophiles for cross-coupling. 155

LIST OF SYMBOLS AND ABBREVIATIONS

API	Active pharmaceutical ingredient
ap ²⁻	Amidodphenolate
Å	Angstrom
CT	Charge transfer
δ	Chemical shift
CV	Cyclic voltammetry
°C	Degrees Celcius
DMSO	Dimethyl sulfoxide
z	Effective charge
ET	Electron transfer
ESI	Electrospray ionization
equiv	Equivalent
Et	Ethyl
Fc	Ferrocene
FTIR	Fourier transform infrared spectroscopy
GC	Gas chromatography
h	Hours
Hx	Hexyl
HOMO	Highest occupied molecular orbital

ibq	Imidobenzoquinone
isq ¹⁻	Iminosemiquinonate
iPr	Isopropyl
K	Kelvin
L	Ligand
LUMO	Lowest unoccupied molecular orbital
MS	Mass spectrometry
MHz	Megahertz
MeOH	Methanol
Me	Methyl
μL	Microliters
mL	Milliliters
M	Molar
ε	Molar absorbtivity
MO	Molecular orbital
nPr	n-Propyl
NHC	N-heterocyclic carbene
NMR	Nuclear magnetic resonance
ppm	Parts per million
PhO	Phenol
¹ H	Proton

s	Second
tBu	Tertbutyl
THF	Tetrahydrofuran
TMS	Tetramethylsilane
UV-vis	Ultraviolet-visible
V	Volts
λ	Wavelength

SUMMARY

Redox-active ligands can act as electron reservoirs to deliver redox equivalents and impart multi-electron functionality to 3d metals that typically undergo only one electron redox events. Previous work in the Soper lab generated several well-defined 3d metal complexes with redox-active ligands including $[\text{Co}(\text{ap}^{\text{Ph}})_2]^-$, and $\text{MnBr}(\text{isq}^{\text{Ph}})_2$. These complexes have been shown to facilitate $2e^-$ C–C bond forming reactions. Furthermore, key intermediates in the catalytic cycles were isolated and characterized demonstrating the redox-active ligands ability to store and deliver electrons is essential for catalytic function.

A new synthetic protocol has been developed to generate a previously reported iron complex containing redox-active ligands ($\text{Fe}^{\text{III}}\text{Cl}(\text{isq}^{\text{Ph}})_2$). The new synthetic route is higher yielding and more reproducible. $\text{Fe}^{\text{III}}\text{Cl}(\text{isq}^{\text{Ph}})_2$ was able to catalyze the homocoupling of PhMgBr using O_2 as the terminal oxidant to form new C–C bonds. Ligand redistribution precluded the isolation and identification of key intermediates in the catalytic cycle.

A previously known N-heterocyclic carbene with two phenol arms was metallated with cobalt forming a new complex ($\text{Co}^{\text{II}}((\text{tBuPhO})_2\text{NHC})\text{THF}$). The resulting $\text{Co}^{\text{II}}((\text{tBuPhO})_2\text{NHC})\text{THF}$ complex formed an electron transfer series in which the first oxidation was metal centered and the second oxidation was ligand centered. The ability of $\text{Co}^{\text{II}}((\text{tBuPhO})_2\text{NHC})\text{THF}$ to span multiple electrons was utilized for catalytic cross-coupling of alkyl halides with PhMgBr . However, the yield of the reaction was low. Mechanistic studies revealed that reductive elimination to the N-heterocyclic carbene hindered the cross-coupling yield.

$\text{Co}^{\text{II}}((\text{tBuPhO})_2\text{NHC})\text{THF}$ was found to activate C–O bonds in ether nitriles delivering an alkyl nitrile to aryl Grignards to form new C–C bonds. The reaction was not general to other C–O bonds that lacked a nitrile functional group, but was general to aryl Grignard reagents. Mechanistic studies suggest that η^2 -chelation of the nitrile might aid in C–O bond activation.

Attempts were made to utilize $\text{Co}^{\text{II}}((\text{tBuPhO})_2\text{NHC})\text{THF}$ for C–H bond activation and oxygen atom transfer. However, conditions were not found to facilitate either reaction. A new $[\text{Fe}^{\text{III}}((\text{tBuPhO})_2\text{NHC})\text{Cl}_2]^-$ complex was synthesized. $[\text{Fe}^{\text{III}}((\text{tBuPhO})_2\text{NHC})\text{Cl}_2]^-$ was shown to cross-couple alkyl halides to PhMgBr with an order of magnitude higher yields than $\text{Co}^{\text{II}}((\text{tBuPhO})_2\text{NHC})\text{THF}$. Oxygen atom transfer with $[\text{Fe}^{\text{III}}((\text{tBuPhO})_2\text{NHC})\text{Cl}_2]^-$ was also pursued with limited success. Although cross-coupling yields are much higher at $[\text{Fe}^{\text{III}}((\text{tBuPhO})_2\text{NHC})\text{Cl}_2]^-$, the lack of an X-ray structure has hindered mechanistic insight.

To carry out difficult multielectron reactions that require more than 2 redox equivalents such as O_2 reduction or nitrogen fixation, synthesis of a redox-active pacman-type ligand was pursued. The most challenging step of the synthetic procedure involved cross-coupling two 5-bromo-1,2-diaminebenzene to an activated xanthene. This step was accomplished and lays the foundation for a redox-active pacman ligand.

Chapter 1

Introduction

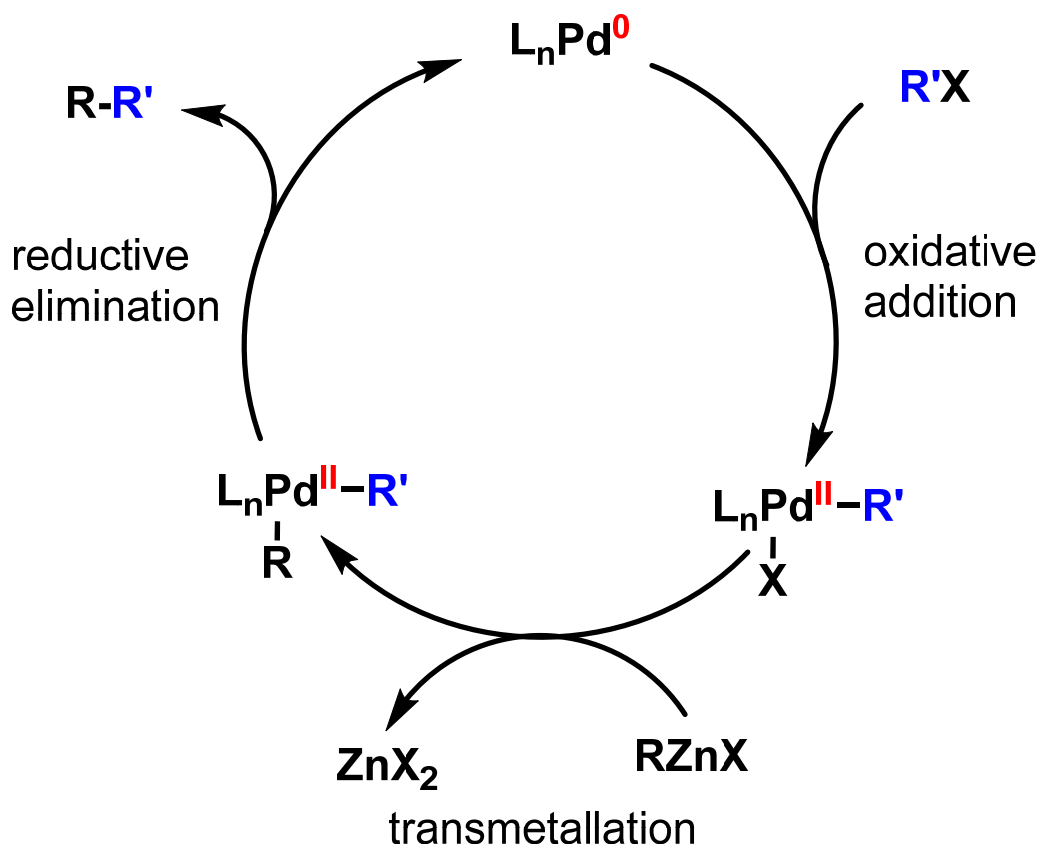
1.1 Significance of cross-coupling reactions in forming new C–C bonds

The ability to take two simple molecules and selectively make a new C–C bond to form a more complex system is a powerful tool for a synthetic chemist. In fact, five Nobel Prizes have been awarded for C–C bond forming reactions: The Grignard reaction (1912), the Diels-Alder reaction (1950), the Wittig reaction (1979), olefin metathesis (2005), and palladium-catalyzed cross couplings in organic synthesis (2010).¹ The Nobel prize in 2010, shared by Dr. Richard F. Heck, Dr. Ei-ichi Negishi, and Dr. Akira Suzuki, was awarded for demonstration of palladium as a catalyst to cross-couple two separate molecules to form a new C–C bond. From its humble beginnings in the late sixties,²⁻⁴ palladium catalysts have become an indispensable tool to couple C–C bonds in industrial settings. They are crucial for the production of pharmaceuticals (Taxol®⁵ and Morphine⁶), herbicides (Prosulfuron®⁷), monomer for electronic resins (Cyclotene®⁸), as well as in academic settings such as being a major step in (+)-dynemicin A⁹ synthesis and Pumiliotoxin A¹⁰ just to give a few examples.

1.2 Palladium catalyzed C–C bond forming cross-coupling reactions

What allows palladium to selectively couple C–C bonds? The answer is best illustrated by the mechanism of Negishi palladium-catalyzed cross-coupling of organozinc and aryl halides (**Scheme 1-1**). As shown in **Scheme 1-1** a Pd^0 complex first undergoes oxidative addition with an aryl halide leading to a Pd^{II} complex bound to a halide and an aryl fragment. Transmetalation of the organozinc with the palladium bound halide leads to a Pd^{II} complex with two organic fragments. From here reductive elimination forms the C–C bond and reduces the Pd^{II} back to Pd^0 , allowing the cycle to

Scheme 1-1. Mechanism of typical Negishi Palladium-catalyzed cross-coupling reaction



repeat. The ability of palladium to catalytically form new C–C bonds stems from its propensity to undergo two electron redox transformations.¹¹ Palladium shares this

functionality with many other late 4d and 5d metals (e.g. Ru, Ir, and Pt). A transition metal that undergoes two electron transformations provides the basis for selective catalyzed C–C bond forming reactions using a metal catalyst, by avoiding one e^- radical pathways. A tremendous amount of work has gone into understanding the mechanism and scope of palladium catalyst in C–C bond forming reactions.¹²⁻²² Knowledge of this well-defined catalytic system allows for catalyst design to optimize a wide array of cross-coupling reactions.²³

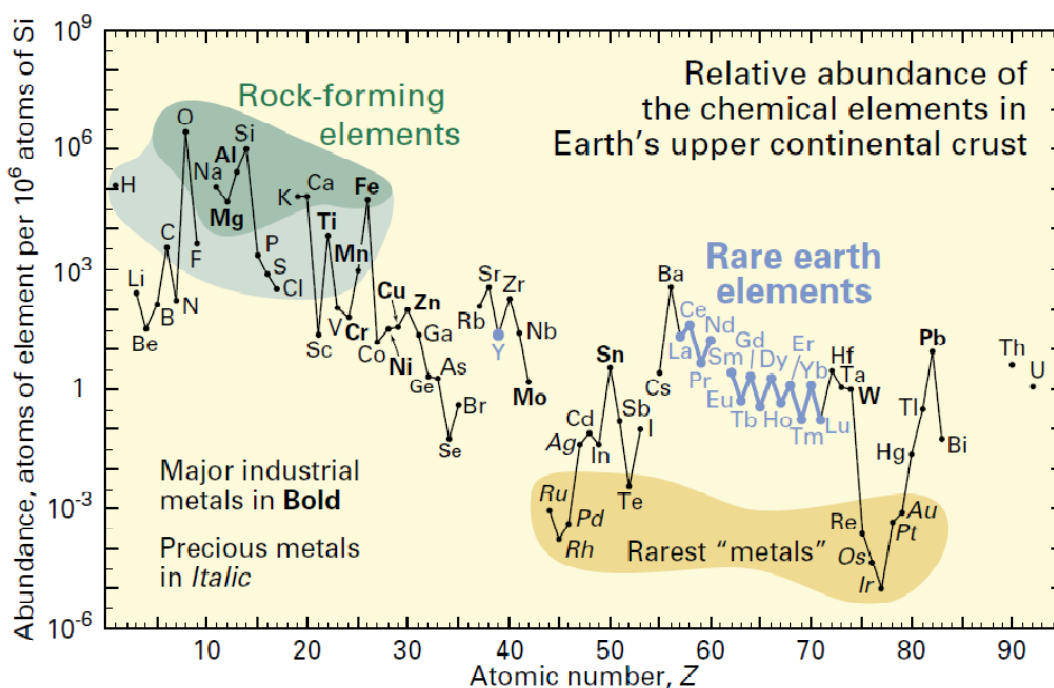


Figure 1-1. Abundance of elements in earth's crust (U.S. Geological Survey Fact Sheet 087-02 courtesy of the U.S. Geological Survey)

For all of the reactions that palladium (and other 4d and 5d metals) can catalyze it still has two significant drawbacks. First is the great expense of precious metals. Palladium is rare and therefore precious (**Figure 1-1**).²⁴ At the time of this thesis the market value of 1 troy oz (~31 g) of palladium was \$700.00 USD.²⁵ Although the catalyst loading of palladium complexes are generally low (0.5 mol % in the commercial

production of Prosulfuron®)²⁶ they still represent a significant initial cost especially on industrial scales where products are produced at hundreds of tons per year.²⁶ The second large drawback is the toxicity of palladium complexes. While the toxicity is not as much of a concern in fine chemicals or herbicides, it presents a risk and challenge in fragrance, dye, and medicinal chemistry. The pharmaceutical industry estimates that 22% of all reactions carried out in the development and production of active pharmaceutical ingredient (API) use a palladium catalyst.²⁷ In the pharmaceutical industry the acceptable limit of palladium remaining in the API is usually 10 ppm.²⁷ It is so important to remove the palladium catalyst that several techniques are employed to recover or remove the catalyst such as heterogenization (biphasic catalysis, supported liquid-phase catalysis, nonionic liquid solvents (NAILS), and perfluorinated solvents),²⁸ nanofiltration, and the application of temperature-dependent multi-component solvent systems (TMS systems) or switchable-polarity solvents (SPS).²⁹ This adds another layer of cost to using palladium catalysts.

1.3 Late 3d metals and C–C bond forming reactions

Given the drawbacks of using 4d and 5d metals to catalyze C–C bond forming reactions, opportunities abound for transition metals that are non-toxic, cheap and can carry out difficult C–C cross-coupling reactions. Late 3d transition metals are both cheap and environmentally benign. In fact, manganese (metalloenzymes including arginase, glutamine synthetase and glycosyltransferases in bone formation), iron (oxygen transport and storage in haemoglobin and myoglobin), cobalt (vitamin B₁₂), and copper (metalloenzyme acting as an oxidase in the reduction of molecular oxygen) are essential micronutrients for human function; nickel, although not an essential micronutrient, is consumed (~75 µg/day) in a normal diet due to its role in plant biochemistry to catalyze the hydrolysis of urea.^{11, 30} Not only are these metals cheap

and environmentally benign (except nickel, which is very toxic above the amount normally consumed in a daily diet)³¹⁻³² they have also demonstrated the ability to catalyze cross-coupling C–C bond forming reactions.³³⁻⁴⁰ However, late 3d metal catalysts suffer from a lack of mechanistic details that hinders their roles as industrially relevant catalysts.

A nickel phosphine complex made by Kumada *et al.* reported in 1972 catalyzes the coupling of alkenyl halides and Grignard reagents.⁴¹ From this discovery, nickel complexes have been used to carry out Negishi coupling and Suzuki–Miyaura reactions.^{33, 42} Beyond cost, nickel catalysts have some distinct advantages over palladium. Nickel catalysts excel at cross-coupling reactions involving secondary alkyl halides, which prove sluggish in palladium catalyzed systems.⁴³ However, the mechanism of nickel catalysts are much more complicated than that of palladium. While it is true that some reactions catalyzed by nickel proceed through oxidative addition to a Ni^I complex to generate a Ni^{III} complex followed by transmetalation and subsequent reductive elimination, this is an incomplete picture of the mechanistic details.³³ Kochi in 1980 demonstrated the complexities of nickel catalyzed cross-coupling. During the reaction Ni⁰, Ni^I, Ni^{II}, and Ni^{III} were detected and both closed-shell and radical mechanisms were operative.⁴⁴ This complexity lead to a mixture of homocoupling and cross-coupling products. Additionally, this lack of a well-defined mechanism hinders attempts to rationally design new nickel catalysts. Finally, nickel is also highly toxic in the zero oxidation state (Ni⁰). This means that even though most nickel catalysts are Ni^{II}, care must be taken to remove nickel from APIs or consumer products due to the possibility of Ni⁰ being present.

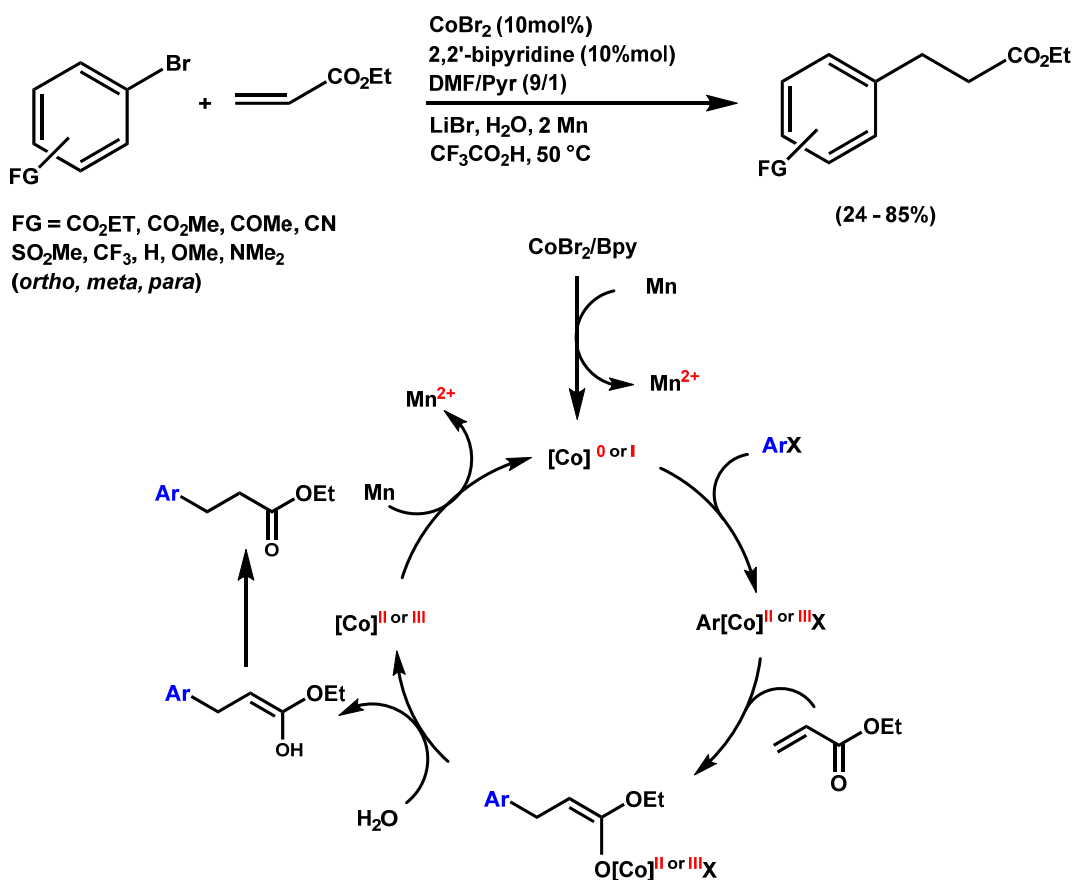
Copper catalyzed C–C bond forming reactions date back to 1901 where pioneering work by Ullmann *et. al.* discovered homocoupling of aryl reagents using

copper metal.⁴⁵ This Ullmann coupling consisted of homocoupling two aromatic halides (iodobenzene or bromobenzene) and copper metal to form a new C–C bond with CuX₂ as the byproduct. In the following century after the discovery of the Ullmann catalyst, copper complexes have been able to couple C–N, C–P, C–O, C–S, and C–Se bonds, demonstrating a large scope of reactivity.³⁷ However, as was the case with nickel, copper catalyzed reactions suffer from a lack of detailed mechanistic insight. In fact, Beletskaya and Cheprakov in a 2004 Coordination Chemistry Review article state "The most essential drawback of copper assisted cross-coupling chemistry as a whole is a complete lack of understanding of the effect of ligands. The catalytic systems are usually being developed by random trials."³⁷ This lack of predictability leaves copper catalysts unable to replace palladium catalysts. However, recent progress in elucidating key intermediates (Cu^{III}) in the copper catalyzed C–C cross-coupling mechanism should begin to aid catalyst design and optimization.⁴⁶

Significant recent progress has been made in the development of manganese, iron and cobalt protocols for selective cross coupling.^{35-36, 38, 40, 47-49} While it is beyond the scope of this thesis to explain all the ways that manganese, iron, and cobalt salts can form new C–C bonds, it is necessary to show that, like nickel and copper, the mechanisms of these reactions are still largely unknown. For instance, while Gosmini and co-workers were able to cross-couple aryl halides with activated olefins in moderate to good yields using a cobalt salt (**Scheme 1-2**), it is clear from their proposed catalytic cycle that the cobalt oxidation state and complex are still unknown.³⁶ The ambiguity in the identity of the active species slows the design of new catalysts. For instance, knowing if Co⁰ or Co^I is responsible for activation of the aryl halide, in the above mentioned reaction, would aid in designing ligands that stabilize that specific cobalt oxidation state. Two separate reasons have hindered insight into the mechanism of late

3d metals; first, identification of the intermediates in these reactions has been challenging due to their transient nature and to the paramagnetism of the generated

Scheme 1-2. Cobalt-catalyzed direct conjugate addition to activated and proposed mechanism adapted from ref [32].

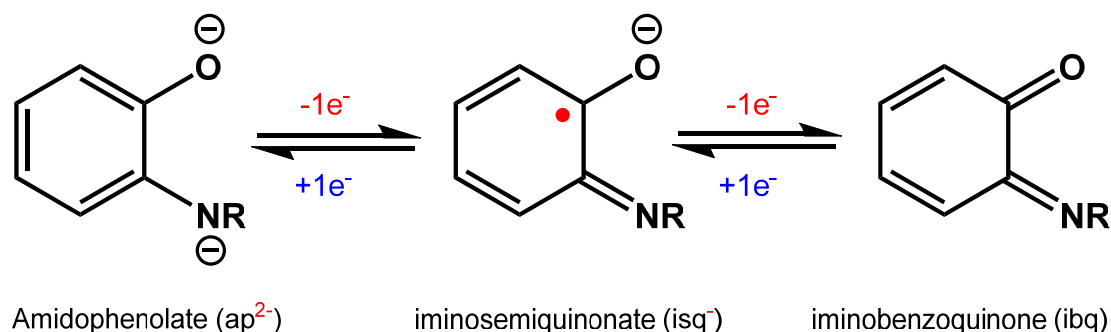


complexes, second, late 3d transition metals typically undergo 1e⁻ transformations, e.g. Fe^{II}/Fe^{III} or Co^{II}/Co^{III} leading to unselective and radical type reactivity. To make the catalytic cycles mirror palladium, mechanisms are often proposed that invoke atypical high and low oxidation states. This would undoubtedly introduce significant energetic barriers.⁵⁰ Both the high energetic barrier to achieve said oxidation states and the relative instability of the resulting complexes argues against their involvement. A further complication arising in the use of late 3d metals is potential contamination of the starting

metals salts with metal impurities that act as the true catalyst. This was demonstrated by Buchwald in 2009 where FeCl_3 purchased and used as received from several suppliers included trace copper (~ 10 ppm) contamination which was actually responsible for previously reported cross-coupling reactions.⁵¹ For instance, N-arylation of pyrazole with aryl iodide was originally reported as catalyzed by 10 mol % FeCl_3 ,⁵² however, analytically pure FeCl_3 (99.99%) at 10 mol % lead to only a 9 % yield whereas 5 ppm Cu_2O lead to a 77 % yield and was the true catalyst in the cross-coupling reaction.

1.4 Redox-active ligands

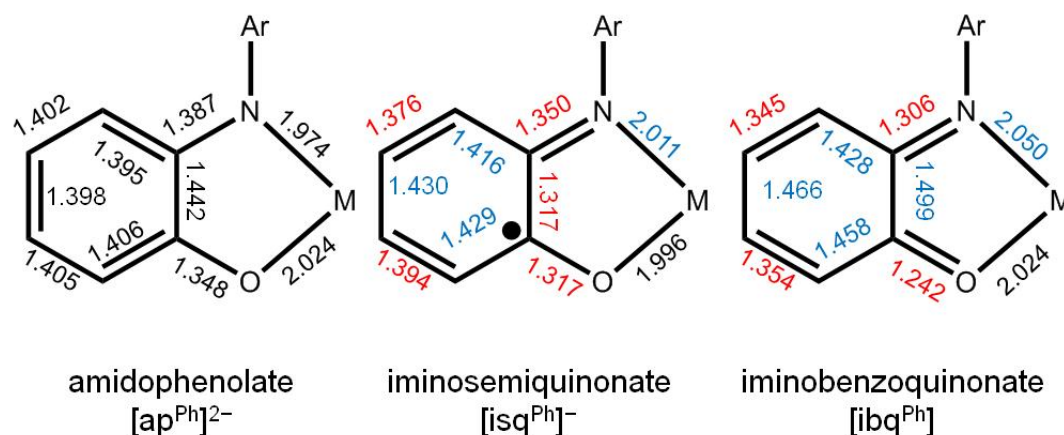
Scheme 1-3. Oxidation states of the amidophenolate ligand.



One approach to elaborating $2e^-$ chemistry at late 3d transition metals is to employ a ligand that is capable of acting as the electron reservoir, supplying electrons to avoid high or low oxidation states. This requires ligands that have the ability to be oxidized or reduced at modest potentials and electronic communication between metal and ligand. Ligands meeting this criteria have been known for over 40 years and are commonly referred to as redox-active or non-innocent. In 1964 Gray *et al.* proposed that certain dithiol ligands on nickel, platinum, and palladium were able to support a radical charge that was significantly mixed with the metal orbitals.⁵³ Following these pioneering studies, numerous other such ligands were identified as being able to support ligand centered radicals. This include the *ortho* chelating amidophenolates⁵⁴, catecholates⁵⁵,

and diimines.⁵⁶ As a prototypical example (Scheme 1-3), dianionic *o*-amidophenolates can be oxidized twice first generating a monoanionic semiquinonate radical and then

Scheme 1-4. Bond distances for the amidophenolate, the 1 e⁻ oxidized iminosemiquinonate, and the 2e⁻ oxidized iminobenzoquinonate bound to palladium. The red bond distances represent elongation of the bond compared to the amidophenolate. The blue bond distances represent contracted bonds.

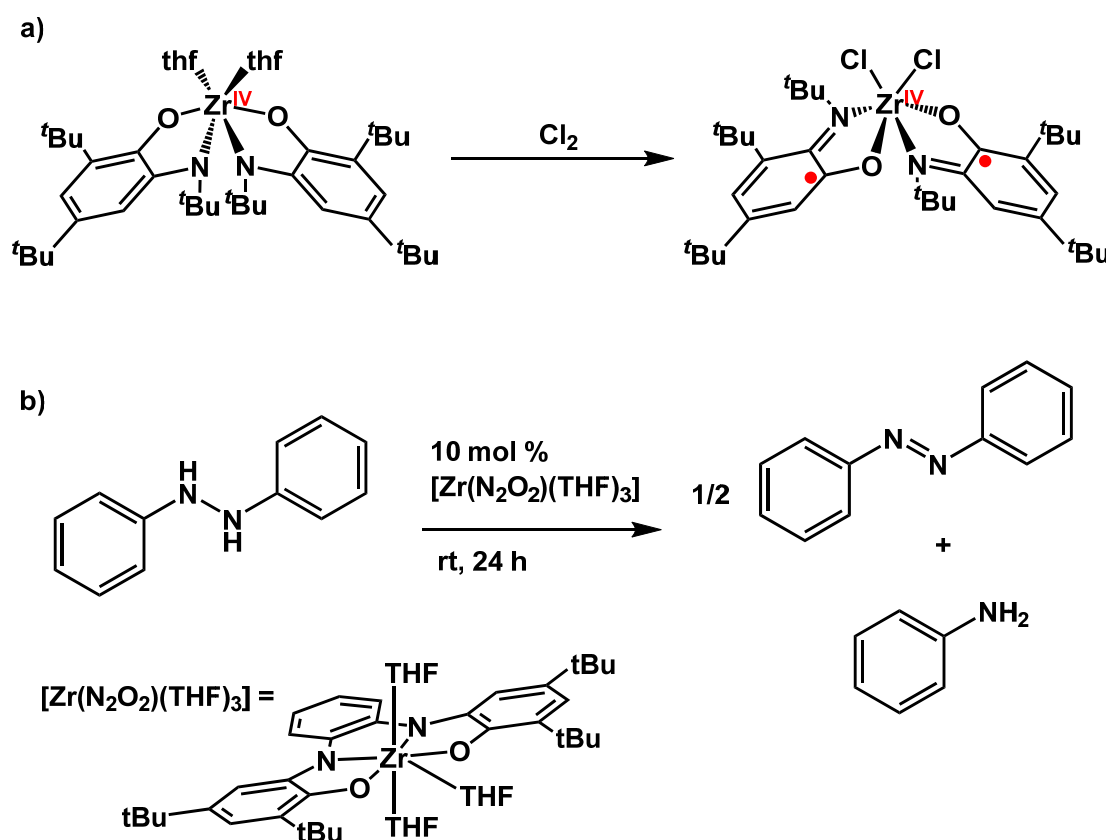


the neutral iminobenzoquinone. Typically crystallographic, spectroscopic, and magnetic data along with theoretical modeling are used to assign the oxidation states of the metal and the ligand.⁵⁷⁻⁶² For example, crystallographic data from several amidophenolate ligated metals show clear changes in bond lengths that correspond to the ligand oxidation state (**Scheme 1-4**).⁶³⁻⁶⁴ The fully reduced amidophenolate ligand shows the bonds lengths of the aryl ring to be aromatic (all bond lengths 1.39 ± 0.01 Å) however when the complex is oxidized there is a clear loss of aromaticity and a significant contraction of the C–N bond and C–O bond, which now more closely resembles a double bond.

1.5 Redox-active ligands on metals: A well-defined platform for catalysis.

The past decade has seen a rediscovery of redox-active ligands as electron reservoirs for 3d metal catalysts. Heyduk and co-workers in 2005 demonstrated oxidative addition of Cl_2 to a Zr^{IV} complex with two redox-active 2,4-di-*tert*-butyl-6-*tert*-butylamidophenolate(ap) ligands.⁶⁵ As shown in **Scheme 1-5**, Zr^{IV} has a d^0 electron configuration, so the ligands act as electron reservoirs supplying the two electrons needed to oxidatively add Cl_2 to Zr^{IV} . The oxidation state of the zirconium in the product $\text{Zr}^{\text{IV}}\text{Cl}_2(\text{isq})_2$ (isq = 2,4-di-*tert*-butyl-6-*tert*-butyliminosemiquinone) is unchanged because

Scheme 1-5. a) Oxidative addition of Cl_2 to a Zr^{IV} complex with redox-active ligands acting as an electron reservoir. b) Disproportionation of 1,2-diphenylhydrazine to azobenzene and aniline catalyzed by $[\text{Zr}^0(\text{N}_2\text{O}_2)(\text{THF})_3]$.

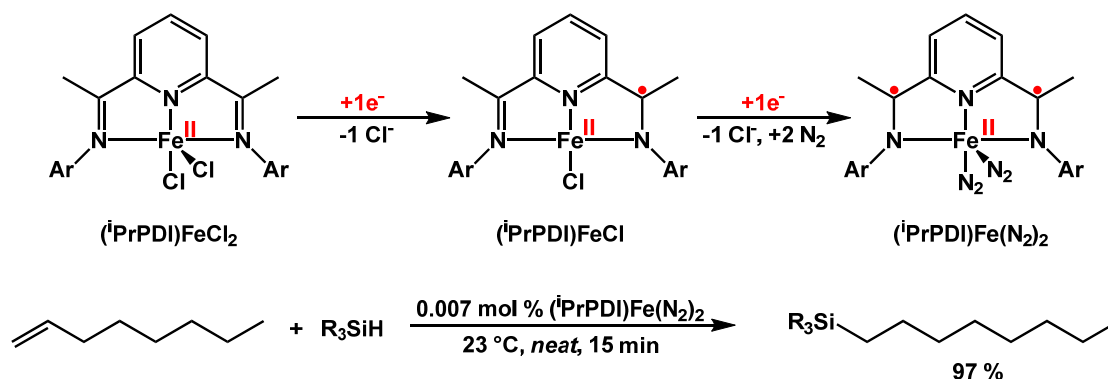


each ligand is oxidized by $1e^-$ (**Scheme 1-5 a**).⁶⁵ A related zirconium redox-active ligand

complex $[\text{Zr}^0(\text{N}_2\text{O}_2)(\text{THF})_3]$ ($\text{N}_2\text{O}_2 = N,N'$ -bis(3,5-di-*tert*-butyl-2-phenoxy)-1,2-phenylenediamide) produced by Heyduk and co-workers has been shown to catalyze the $2e^-$ disproportionation of diphenylhydrazine to azobenzene and aniline (**Scheme 1-5 b**).⁶⁶ This further demonstrates the utility of using redox-active ligands as an electron reservoir to impart new reactivity to 3d metals in a well-defined system.

Berben and Myers were able to catalytically convert CO_2 into a carbonate salt⁶⁷ using aluminum(III) and a redox-active ligand (2,6-diisopropyl-N-(pyridin-2-ylmethyl)aniline (IP), which can adopt three states: neutral(IP), singly reduced (IP^-), and doubly reduced (IP^{2-})).⁶⁸ In this system 2 equiv of $\text{Al}^{\text{III}}(\text{OH})(\text{IP}^-)_2$ reversibly bind CO_2 with a loss of water to make a dimetallic complexes with a bridging carbonate. Subsequent

Scheme 1-6. Electron transfer series of (iPrPDI)Fe and its role in the catalyzed hydrosilylation of alkenes with tertiary silanes.



reduction of the two Al complexes ($2 [\text{Al}^{\text{III}}(\text{IP}^{2-})_2]^-$) release carbonate and in the presence of an oxygen atom donor regenerates then starting complex $\text{Al}^{\text{III}}(\text{OH})(\text{IP}^-)_2$.

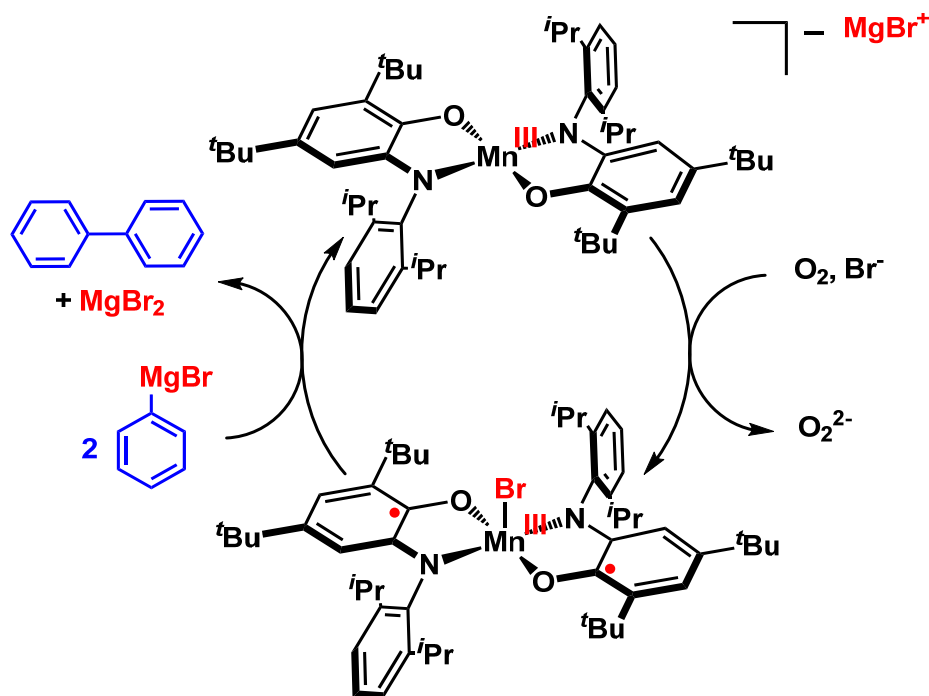
Chirik and co-workers demonstrated the commercial viability of redox active ligand containing catalysts with an iron complex featuring a redox-active pincer-type ligand. The selective anti-Markovnikov hydrosilylation of alkenes using tertiary silanes

was performed on a kilogram scale using only 0.007 mol% catalyst loading of with the redox-active catalyst (*i*PrPDI)Fe(N₂)₂ (**Scheme 1-6**).^{61, 69}

1.6 Redox-active amidophenolate ligands on 3d metals to carry out 2e⁻ transformations in C–C bond forming reactions.

Previous work in the Soper lab has led to the development of 3d metal redox-active ligand supported catalysts for C–C coupling and aerobic alcohol oxidations.

Scheme 1-7. Catalytic aerobic homocoupling of PhMgBr by Mn^{III}Br(isq^{Ph(*i*Pr)₂})₂.

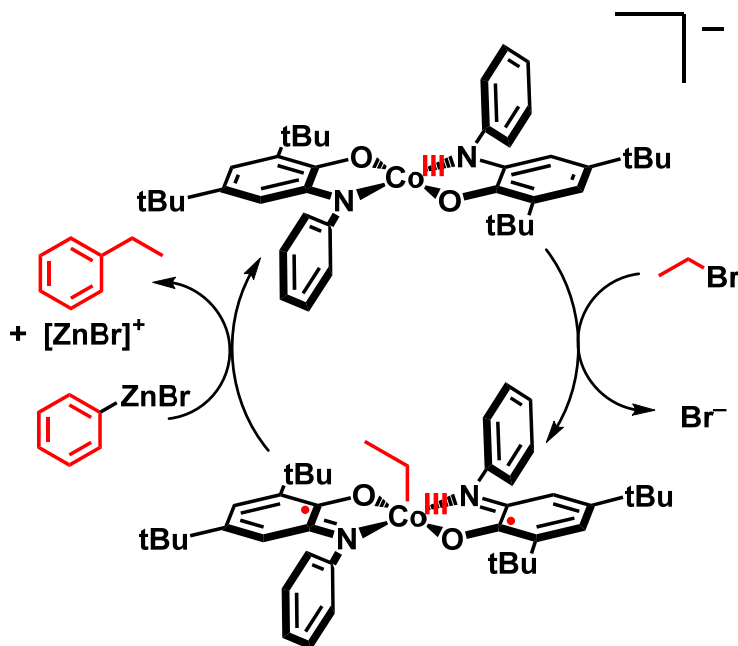


Using a [Mn^{III}(Br₄cat)₂]⁻ (Br₄cat²⁻ = tetrabromo-1,2-catecholate) complex, Rolle *et al.* was able to catalytically (0.2 mol % catalyst loading) and selectively carry out the 2e⁻ dehydrogenation of tetrabromo-1,2-catechol to form tetrabromo-1,2-benzoquinone using dioxygen as the oxidant.⁷⁰ Although aerobic catechol oxidations with metal-quinone

complexes are known,⁷¹⁻⁷² Rolle was able to elucidate key aspects of the mechanism. The selective oxidation of catechol is an overall $2e^-$ process under the reaction conditions used, but it proceeds through $1e^-$ steps involving both ligand and metal based redox events. Furthermore, binding of the catechol to the metal happens prior to the O_2 reaction and facilitates an intramolecular redox process. A related complex, $[Mn^{III}(ap^{Ph(iPr)_2})_2]^-$ ($[ap^{Ph(iPr)_2}]^{2-} = 2,4\text{-di-tert-butyl-6-(2,6-diisopropylphenylimino)phenolate}$), catalyzes homocoupling of aryl Grignards (72 % yield) under 1 atm of O_2 using 5 mol % catalyst loading.⁷³ Although 3d metals have been known to catalyze these reactions, Rolle's work clearly shows the $2e^-$ mechanism involved.^{34, 74-76} A reaction between $Mn^{III}Br(isq^{Ph(iPr)_2})_2$ ($isq^{Ph(iPr)_2} = 2,4\text{-di-tert-butyl-6-(2,6-diisopropylphenylimino)semiquinonate}$) and 1 equiv of $PhMgBr$ quantitatively lead to 0.5 equiv of biphenyl and $[Mn^{III}(ap^{Ph(iPr)_2})_2]^-$ which clearly shows the reductive elimination half of the catalytic cycle where the ligands are reduced instead of the metal center. A reaction between $[MgBr][Mn^{III}(ap^{Ph(iPr)_2})_2]$ (generated *in situ* from $Mn^{III}Br(isq^{Ph(iPr)_2})_2$ and 2 equiv of $PhMgBr$) and O_2 lead to doubly oxidized $Mn^{III}Br(isq^{Ph(iPr)_2})_2$. The use of 2-(3-butenyl)phenyl magnesium iodide as a substrate did not lead to the radical induced cyclized product, suggesting the coupling reaction occurs without the intermediacy of free radicals. Combining the two individual steps makes a well-defined catalytic cycle that demonstrates selective and concerted $2e^-$ process can be accomplished at manganese and applied to the homocoupling of Grignard reagents (**Scheme 1-7**).

Further evidence for the capacity of redox-active ligand to effect organometallic $2e^-$ steps at later first row metals was obtained by Smith *et al.* in cross-coupling of ethyl bromide with aryl and alkylzinc halides.⁷⁷ Starting with $[\text{Co}^{\text{III}}(\text{ap}^{\text{Ph}})_2]^-$ ($\text{ap}^{\text{Ph}2-}$ = 2,4-di-tert-butyl-6-(phenylamido)phenolate), exposure of this cobalt complex to ethyl bromide lead to a stable alkyl cobalt complex. A solid state structure of the alkyl cobalt complex shows an axial ethyl group bound to a Co^{III} center and two singly oxidized ligands, $\text{Co}^{\text{III}}(\text{Et})(\text{isq}^{\text{Ph}})_2$ (isq^{Ph} = 2,4-di-tert-butyl-6-(phenylimino)semiquinone). This alkyl complex generates a new C–C bond in the presence of an aryl organozinc reagent and

Scheme 1-8. Cobalt catalyzed cross-coupling of an aryl organozinc reagent with ethyl bromide.

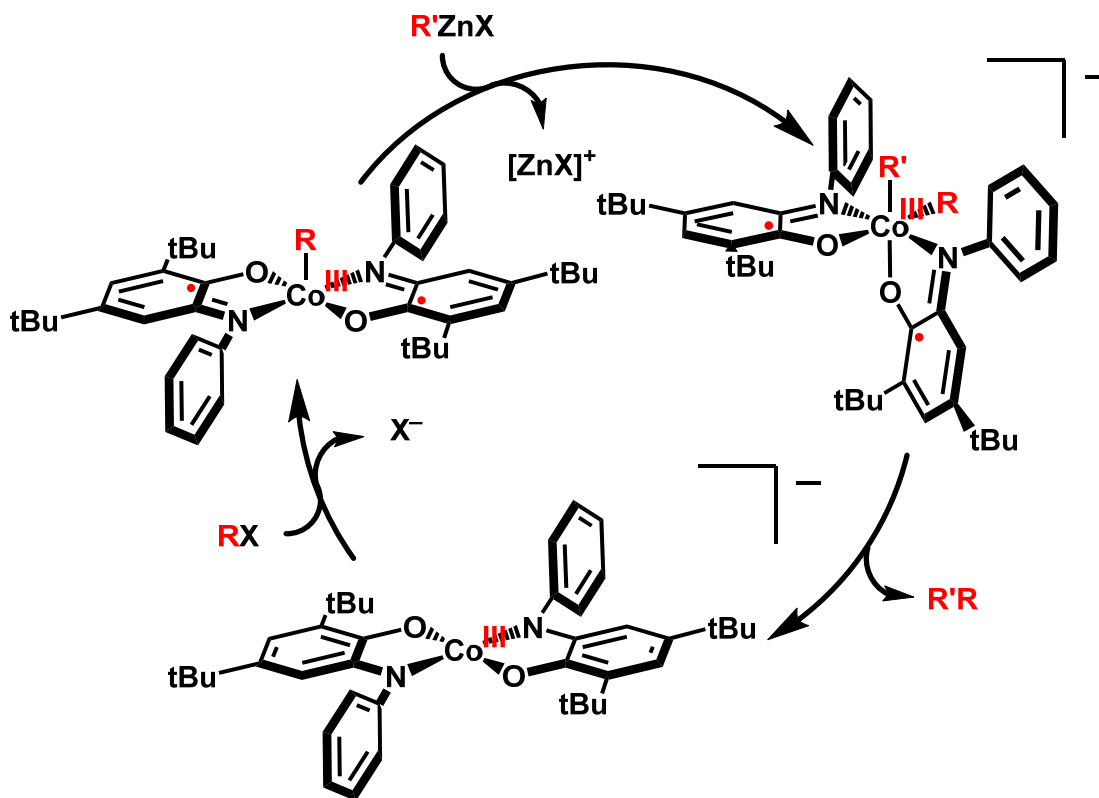


produces the cross-coupled product. Together the two reaction steps comprise a well-defined catalytic system for Co Negishi-type cross coupling. In sum, the catalytic pathway to generate new C–C bonds closely resembles the palladium catalyzed Negishi reaction (**Scheme 1-8**) in which pseudo-oxidative addition of C–X bond leads to a doubly

oxidized metal complex followed by addition of a carbanion results in reductive elimination to make a new C–C bond and regenerate the starting catalyst. However the C–C coupled products were only obtained in low yields ca. (15%) that reflect the low yields of C–C reductive elimination reactions. Strategies to address the low C–C coupling yields are presented in Chapters 2 and 3 of this thesis.

Recent advances have made the strategy of combining redox-active ligands with 3d metals to impart $2e^-$ functionality for C–C bond forming reactions an interesting area of research. However, only a handful of redox-active ligand based complexes have

Scheme 1-9. Proposed mechanism of the Berry-pseudo rotation needed to cross-couple ethyl bromide with PhZnBr using $[\text{Co}^{\text{III}}(\text{ap}^{\text{Ph}})_2]^-$.



been utilized as catalysts and the chemical space of these kinds of reactions remains largely unknown. Furthermore, questions and opportunities arise from the research already done. For instance, oxidative addition to the $[\text{Mn}^{\text{III}}(\text{ap}^{\text{Ph}(\text{iPr})_2})_2]^-$ is challenging

even though the redox potentials for $[\text{Mn}^{\text{III}}(\text{ap}^{\text{Ph}(\text{iPr})_2})_2]^-$ (-0.85 V and -0.29 V vs Fc^+/Fc) are very similar to that of the analogous $[\text{Co}^{\text{III}}(\text{ap}^{\text{Ph}(\text{iPr})_2})_2]^-$ (-0.80 V and -0.33 V vs Fc^+/Fc).^{73, 78} The reported $[\text{Co}^{\text{III}}(\text{ap}^{\text{Ph}})_2]^-$ is able to carry out oxidative addition and reductive elimination reactions in concerted $2e^-$ steps, however it suffers from low cross-coupling yield ($\sim 15\%$). However, because it is a well-defined catalyst, problem areas can be indentified and tested in a systematic way. Dr. Smith in her doctoral thesis, concluded that the product from oxidative addition of ethyl bromide to $[\text{Co}^{\text{III}}(\text{ap}^{\text{Ph}})_2]^-$ leads to a square pyramidal complex $[\text{Co}^{\text{III}}(\text{Et})(\text{ap}^{\text{Ph}(\text{iPr})_2})_2]$ that must undergo a Berry-pseudo rotation after the addition of the carbanion to allow the organic fragments to arrange *cis* to one another and allow reductive elimination to occur (**Scheme 1-9**).⁷⁹ It is this isomerization that seems to be limiting the yield.

1.7 Thesis hypothesis and goals.

The $[\text{Mn}^{\text{III}}(\text{ap}^{\text{Ph}(\text{iPr})_2})_2]^-$ complex demonstrated an high affinity $2e^-$ reduction chemistry. For instance, $[\text{Mn}^{\text{III}}(\text{ap}^{\text{Ph}(\text{iPr})_2})_2]^-$ can catalytically homocouple PhMgBr and, in a separate reaction, catalytically dihydrogenate catechol. In both reactions the terminal oxidant was O_2 . However, the $[\text{Mn}^{\text{III}}(\text{ap}^{\text{Ph}(\text{iPr})_2})_2]^-$ complex was unable to oxidatively add alkyl halides, a step need for cross-coupling. The $[\text{Co}^{\text{III}}(\text{ap}^{\text{Ph}})_2]^-$ complex was able to oxidatively add alkyl halides quantitatively. However, reductive elimination of the alkyl fragment was challenging. This thesis explores the question, can an $[\text{Fe}^{\text{III}}(\text{ap}^{\text{Ph}})_2]^-$ complex both oxidatively add alkyl halides and reductively eliminate organic fragments to produce a well-defined cross-coupling catalyst for C–C bond formation (Chapter 2). Subsequently, the lessons learned from the manganese, iron, and cobalt amidophenolate systems are used to design new redox-active ligands. A new redox-active ligand featuring two phenol arms attached to an N-heterocyclic carbene bound to cobalt ($\text{Co}^{\text{II}}((\text{tBuPhO})_2\text{NHC})(\text{THF})$) was synthesized and demonstrated the ability to

cross-couple alkyl halides and aryl Grignards to form new C–C bonds (Chapter 3). Furthermore, this new $\text{Co}^{\text{II}}((\text{tBuPhO})_2\text{NHC})(\text{THF})$ complex can activate C–O bonds in ether nitriles (Chapter 4). Chapter 5 will explore expanding the scope and utility of $\text{Co}^{\text{II}}((\text{tBuPhO})_2\text{NHC})(\text{THF})$ toward difficult C–H bond activation and oxygen atom transfer. Additionally, synthetic work towards a new redox-active complex $\text{Na}[\text{Fe}^{\text{III}}((\text{tBuPhO})_2\text{NHC})\text{Cl}_2]$ will be discussed and its ability to catalyze C–C bond forming reactions will be explored. Finally, synthetic work towards a redox-active pacman-type ligand that can deliver 6 redox equivalence will be discussed in Appendix A.

1.8 Works cited

1. The Nobel Prize in Chemistry 2010 - Advanced Information *Nobelprize.org* [Online], p. Nobel Media AB 2013. <http://www.nobelprize.org/nobel_prizes/chemistry/laureates/2010/advanced.html> (accessed Web. 2 Sep 2013).
2. Heck, R. F., The arylation of allylic alcohols with organopalladium compounds. A new synthesis of 3-aryl aldehydes and ketones. *J. Am. Chem. Soc.* **1968**, *90*, 5526-5531.
3. Heck, R. F., The palladium-catalyzed arylation of enol esters, ethers, and halides. A new synthesis of 2-aryl aldehydes and ketones. *J. Am. Chem. Soc.* **1968**, *90*, 5535-5538.
4. Heck, R. F., Acylation, methylation, and carboxyalkylation of olefins by Group VIII metal derivatives. *J. Am. Chem. Soc.* **1968**, *90*, 5518-5526.
5. Danishefsky, S. J.; Masters, J. J.; Young, W. B.; Link, J. T.; Snyder, L. B.; Magee, T. V.; Jung, D. K.; Isaacs, R. C. A.; Bornmann, W. G.; Alaimo, C. A.; Coburn, C. A.; Di Grandi, M. J., Total Synthesis of Baccatin III and Taxol. *J. Am. Chem. Soc.* **1996**, *118*, 2843-2859.
6. Hong, C. Y.; Kado, N.; Overman, L. E., Asymmetric synthesis of either enantiomer of opium alkaloids and morphinans. Total synthesis of (-)- and (+)-dihydrocodeinone and (-)- and (+)-morphine. *J. Am. Chem. Soc.* **1993**, *115*, 11028-11029.
7. Hirashima, S.; Aoyagi, S.; Kibayashi, C., Total Synthesis of Pumiliotoxins A and 225F. *J. Am. Chem. Soc.* **1999**, *121*, 9873-9874.
8. Schrock, A. K. Polyorganosiloxane-bridged bisbenzocyclobutene monomers. U.S Patent US4812588 A, **1989**.
9. Myers, A. G.; Tom, N. J.; Fraley, M. E.; Cohen, S. B.; Madar, D. J., A Convergent Synthetic Route to (+)-Dynemicin A and Analogs of Wide Structural Variability. *J. Am. Chem. Soc.* **1997**, *119*, 6072-6094.
10. P. Baumeister, G. S., H. Steiner European Patent EP584043, **1994**.
11. Greenwood, N. N.; Earnshaw, A., Chemistry of the Elements (2nd Edition). Butterworth Heinemann: **1997**.

12. Beletskaya, I. P.; Cheprakov, A. V., The heck reaction as a sharpening stone of palladium catalysis. *Chem. Rev. (Washington, DC, U. S.)* **2000**, *100*, 3009-3066.
13. Hassan, J.; Sevignon, M.; Gozzi, C.; Schulz, E.; Lemaire, M., Aryl-aryl bond formation one century after the discovery of the Ullmann reaction. *Chem. Rev. (Washington, DC, U. S.)* **2002**, *102*, 1359-1469.
14. Littke, A. F.; Fu, G. C., Palladium-catalyzed coupling reactions of aryl chlorides. *Angew. Chem., Int. Ed.* **2002**, *41*, 4176-4211.
15. Miyaura, N.; Suzuki, A., Palladium-catalyzed cross-coupling reactions of organoboron compounds. *Chem. Rev. (Washington, DC, U. S.)* **1995**, *95*, 2457-2483.
16. Miyaura, N.; Yanagi, T.; Suzuki, A., The palladium-catalyzed cross-coupling reactions of phenylboronic acid with haloarenes in the presence of bases. *Synth. Commun.* **1981**, *11*, 513-519.
17. Stille, J. K., The palladium-catalyzed cross-coupling reactions of organotin reagents with organic electrophiles. *Angew. Chem., Int. Ed. Engl.* **1986**, *25*, 508-523.
18. Barder, T. E.; Walker, S. D.; Martinelli, J. R.; Buchwald, S. L., Catalysts for Suzuki-Miyaura coupling processes: Scope and studies of the effect of ligand structure. *J. Am. Chem. Soc.* **2005**, *127*, 4685-4696.
19. Chen, X.; Engle, K. M.; Wang, D. H.; Yu, J. Q., Palladium(II)-Catalyzed C-H Activation/C-C Cross-Coupling Reactions: Versatility and Practicality. *Angew. Chem., Int. Ed.* **2009**, *48*, 5094-5115.
20. Nicolaou, K. C.; Bulger, P. G.; Sarlah, D., Palladium-catalyzed cross-coupling reactions in total synthesis. *Angew. Chem., Int. Ed.* **2005**, *44*, 4442-4489.
21. Amatore, C.; Jutand, A., Mechanistic and kinetic studies of palladium catalytic systems. *J. Organomet. Chem.* **1999**, *576*, 254-278.
22. Amatore, C.; Jutand, A., Anionic Pd(0) and Pd(II) intermediates in palladium-catalyzed Heck and cross-coupling reactions. *Acc. Chem. Res.* **2000**, *33*, 314-321.

23. Nicolaou, K. C.; Bulger, P. G.; Sarlah, D., Palladium-Catalyzed Cross-Coupling Reactions in Total Synthesis. *Angew. Chem., Int. Ed.* **2005**, *44*, 4442-4489.
24. Haxel, G. B. H., James B.; Orris, Greta J.; edited by Stauffer, Peter H.; Hendley, James W., II *Rare earth elements: critical resources for high technology*; **2002**; p 4.
25. Kitco. <http://www.kitco.com/charts/livepalladium.html> (accessed 12/10/2013).
26. de Vries, J. G., The Heck reaction in the production of fine chemicals. *Can. J. Chem.* **2001**, *79*, 1086-1092.
27. Cooper, T. W. J.; Campbell, I. B.; Macdonald, S. J. F., Factors Determining the Selection of Organic Reactions by Medicinal Chemists and the Use of These Reactions in Arrays (Small Focused Libraries). *Angew. Chem., Int. Ed.* **2010**, *49*, 8082-8091.
28. Bhanage, B. M.; Arai, M., Catalyst Production Separation Techniques in Heck Reaction. *Catalysis Reviews* **2001**, *43*, 315-344.
29. Torborg, C.; Beller, M., Recent Applications of Palladium-Catalyzed Coupling Reactions in the Pharmaceutical, Agrochemical, and Fine Chemical Industries. *Adv. Synth. Catal.* **2009**, *351*, 3027-3043.
30. *Dietary Reference Intakes for Vitamin A, Vitamin K, Arsenic, Boron, Chromium, Copper, Iodine, Iron, Manganese, Molybdenum, Nickel, Silicon, Vanadium, and Zinc*. The National Academies Press: **2001**.
31. Donskoy, E.; Donskoy, M.; Forouhar, F.; Gillies, C.; Marzouk, A.; Reid, M.; Zaharia, O.; FW, S., Hepatic toxicity of nickel chloride in rats. *Annals of Clinical & Laboratory Science* **1986**, *16*, 108-117.
32. Sunderman Jr, F. W.; Shen, S. K.; Mitchell, J. M.; Allpass, P. R.; Damjanov, I., Embryotoxicity and fetal toxicity of nickel in rats. *Toxicol. Appl. Pharmacol.* **1978**, *43*, 381-390.
33. Phapale, V. B.; Cardenas, D. J., Nickel-catalysed Negishi cross-coupling reactions: scope and mechanisms. *Chem. Soc. Rev.* **2009**, *38*, 1598-1607.
34. Moncomble, A.; Le Floch, P.; Gosmini, C., Cobalt-Catalyzed Formation of Symmetrical Biaryls and Its Mechanism. *Chem. Eur. J.* **2009**, *15*, 4770-4774.

35. Hess, W.; Treutwein, J.; Hilt, G., Cobalt-Catalysed Carbon-Carbon Bond-Formation Reactions. *Synthesis* **2008**, 2008, 3537-3562.
36. Gosmini, C.; Begouin, J.-M.; Moncomble, A., Cobalt-catalyzed cross-coupling reactions. *Chem. Commun. (Cambridge, U. K.)* **2008**, 3221-3233.
37. Beletskaya, I. P.; Cheprakov, A. V., Copper in cross-coupling reactions: The post-Ullmann chemistry. *Coord. Chem. Rev.* **2004**, 248, 2337-2364.
38. Jana, R.; Pathak, T. P.; Sigman, M. S., Advances in Transition Metal (Pd,Ni,Fe)-Catalyzed Cross-Coupling Reactions Using Alkyl-organometallics as Reaction Partners. *Chem. Rev. (Washington, DC, U. S.)* **2011**, 111, 1417-1492.
39. Yoshikai, N.; Nakamura, E., Mechanisms of Nucleophilic Organocopper(I) Reactions. *Chem. Rev. (Washington, DC, U. S.)* **2011**, 112, 2339-2372.
40. Fürstener, A.; Martin, R., Advances in Iron Catalyzed Cross Coupling Reactions. *Chem. Lett.* **2005**, 34, 624-629.
41. Tamao, K.; Sumitani, K.; Kumada, M., Selective carbon-carbon bond formation by cross-coupling of Grignard reagents with organic halides. Catalysis by nickel-phosphine complexes. *J. Am. Chem. Soc.* **1972**, 94, 4374-4376.
42. Kotha, S.; Lahiri, K.; Kashinath, D., Recent applications of the Suzuki-Miyaura cross-coupling reaction in organic synthesis. *Tetrahedron* **2002**, 58, 9633-9695.
43. Frisch, A. C.; Beller, M., Catalysts for Cross-Coupling Reactions with Non-activated Alkyl Halides. *Angew. Chem., Int. Ed.* **2005**, 44, 674-688.
44. Kochi, J. K., The Role of Electron Transfer and Charge Transfer in Organometallic Chemistry. *Pure Appl. Chem.* **1980**, 52, 34.
45. Lindley, J., Tetrahedron report number 163 : Copper assisted nucleophilic substitution of aryl halogen. *Tetrahedron* **1984**, 40, 1433-1456.
46. Casitas, A.; Ribas, X., The role of organometallic copper(III) complexes in homogeneous catalysis. *Chem. Sci.* **2013**, 4, 2301-2318.
47. Khusnutdinov, R. I.; Bayguzina, A. R.; Dzhemilev, U. M., Manganese compounds in the catalysis of organic reactions. *Russ. J. Org. Chem.* **2012**, 48, 309-348.

48. Sherry, B. D.; Fürstner, A., The Promise and Challenge of Iron-Catalyzed Cross Coupling. *Acc. Chem. Res.* **2008**, *41*, 1500-1511.
49. Cahiez, G.; Moyeux, A., Cobalt-Catalyzed Cross-Coupling Reactions. *Chem. Rev. (Washington, DC, U. S.)* **2010**, *110*, 1435-1462.
50. Alan Earnshaw, N. G., *Chemistry of the Elements*. Second ed.; Pergamon Press: 30 Corporate Drive, Burlington, Ma 01803, **1997**.
51. Buchwald, S. L.; Bolm, C., On the Role of Metal Contaminants in Catalyses with FeCl₃. *Angew. Chem., Int. Ed.* **2009**, *48*, 5586-5587.
52. Correa, A.; Bolm, C., Iron-Catalyzed N-Arylation of Nitrogen Nucleophiles. *Angew. Chem., Int. Ed.* **2007**, *46*, 8862-8865.
53. Shupack, S. I.; Williams, R.; Gray, H. B.; Billig, E.; Clark, R. J. H., Electronic Structures of Square-Planar Metal Complexes .V. Spectral Properties of Maleonitriledithiolate Complexes of Nickel Palladium + Platinum. *J. Am. Chem. Soc.* **1964**, *86*, 4594-&.
54. Chaudhuri, P.; Verani, C. N.; Bill, E.; Bothe, E.; Weyhermüller, T.; Wieghardt, K., Electronic Structure of Bis(o-iminobenzosemiquinonato)metal Complexes (Cu, Ni, Pd). The Art of Establishing Physical Oxidation States in Transition-Metal Complexes Containing Radical Ligands. *J. Am. Chem. Soc.* **2001**, *123*, 2213-2223.
55. Pierpont, C. G.; Buchanan, R. M., Transition-Metal Complexes of Ortho-Bezoquinone, Ortho-Semiquinone, and Catecholate Ligands. *Coord. Chem. Rev.* **1981**, *38*, 45-87.
56. Nawn, G.; Waldie, K. M.; Oakley, S. R.; Peters, B. D.; Mandel, D.; Patrick, B. O.; McDonad, R.; Hicks, R. G., Redox-Active Bridging Ligands Based on Indigo Diimine ("Nindigo") Derivatives. *Inorg. Chem.* **2011**, *50*, 9826-9837.
57. Sokolowski, A.; Bothe, E.; Bill, E.; Weyhermuller, T.; Wieghardt, K., Phenoxyl radical complexes of chromium(III). *Chem. Commun. (Cambridge, U. K.)* **1996**, 1671-1672.
58. Adam, B.; Bill, E.; Bothe, E.; Goerdts, B.; Haselhorst, G.; Hildenbrand, K.; Sokolowski, A.; Steenken, S.; Weyhermuller, T.; Wieghardt, K., Phenoxyl radical complexes of gallium, scandium, iron and manganese. *Chem. Eur. J.* **1997**, *3*, 308-319.

59. Penkert, F. N.; Weyhermuller, T.; Bill, E.; Hildebrandt, P.; Lecomte, S.; Wieghardt, K., Anilino radical complexes of cobalt(III) and manganese(IV) and comparison with their phenoxyl analogues. *J. Am. Chem. Soc.* **2000**, *122*, 9663-9673.
60. Lu, C. C.; Weyhermuller, T.; Bill, E.; Wieghardt, K., Accessing the Different Redox States of alpha-Iminopyridines within Cobalt Complexes. *Inorg. Chem.* **2009**, *48*, 6055-6064.
61. Stieber, S. C. E.; Milschmann, C.; Hoyt, J. M.; Turner, Z. R.; Finkelstein, K. D.; Wieghardt, K.; DeBeer, S.; Chirik, P. J., Bis(imino)pyridine Iron Dinitrogen Compounds Revisited: Differences in Electronic Structure Between Four- and Five-Coordinate Derivatives. *Inorg. Chem.* **2012**, *51*, 3770-3785.
62. Fox, G. A.; Pierpont, C. G., Periodic trends in charge distribution for transition metal complexes containing catecholate and semiquinone ligands. Metal-mediated spin coupling in the bis(3,5-di-tert-butyl-1,2-semiquinone) complexes of palladium(II) and platinum(II) M(DBSQ)₂ (M = Pd, Pt). *Inorg. Chem.* **1992**, *31*, 3718-3723.
63. Kokatam, S. L.; Chaudhuri, P.; Weyhermuller, T.; Wieghardt, K., Molecular and electronic structure of square planar complexes Pd-II((t)bpy)(L-N,(IP)(O)) (0), Pd-II((t)bpy)(L-N,O(ISQ)) (PF₆), and Pd-II((t)bpy)(L-N,O(IBQ)) (PF₆)(BF₄)center dot 2CH₂Cl₂: an o-iminophenolato based ligand centered, three-membered redox series. *Dalton Trans.* **2007**, 373-378.
64. Sun, X. R.; Chun, H.; Hildenbrand, K.; Bothe, E.; Weyhermuller, T.; Neese, F.; Wieghardt, K., omicron-Iminobenzosemiquinonato(1-) and omicron-amidophenolato(2-) complexes of palladium(II) and platinum(II): A combined experimental and density functional theoretical study. *Inorg. Chem.* **2002**, *41*, 4295-4303.
65. Blackmore, K. J.; Ziller, J. W.; Heyduk, A. F., "Oxidative Addition" to a Zirconium(IV) Redox-Active Ligand Complex. *Inorg. Chem.* **2005**, *44*, 5559-5561.
66. Blackmore, K. J.; Lal, N.; Ziller, J. W.; Heyduk, A. F., Catalytic Reactivity of a Zirconium(IV) Redox-Active Ligand Complex with 1,2-Diphenylhydrazine. *J. Am. Chem. Soc.* **2008**, *130*, 2728-2729.
67. Myers, T. W.; Berben, L. A., Redox active aluminium(iii) complexes convert CO₂ into MgCO₃ or CaCO₃ in a synthetic cycle using Mg or Ca metal. *Chem. Commun. (Cambridge, U. K.)* **2013**, *49*, 4175-4177.

68. Myers, T. W.; Berben, L. A., A Sterically Demanding Iminopyridine Ligand Affords Redox-Active Complexes of Aluminum(III) and Gallium(III). *Inorg. Chem.* **2012**, *51*, 1480-1488.
69. Tondreau, A. M.; Atienza, C. C. H.; Weller, K. J.; Nye, S. A.; Lewis, K. M.; Delis, J. G. P.; Chirik, P. J., Iron Catalysts for Selective Anti-Markovnikov Alkene Hydrosilylation Using Tertiary Silanes. *Science* **2012**, *335*, 567-570.
70. Rolle, C. J.; Hardcastle, K. I.; Soper, J. D., Reactions of tetrabromocatecholatomanganese(III) complexes with dioxygen. *Inorg. Chem.* **2008**, *47*, 1892-1894.
71. Hitomi, Y.; Ando, A.; Matsui, H.; Ito, T.; Tanaka, T.; Ogo, S.; Funabiki, T., Aerobic Catechol Oxidation Catalyzed by a Bis(μ -oxo)dimanganese(III,III) Complex via a Manganese(II)-Semiquinonate Complex. *Inorg. Chem.* **2005**, *44*, 3473-3478.
72. Triller, M. U.; Pursche, D.; Hsieh, W. Y.; Pecoraro, V. L.; Rompel, A.; Krebs, B., Catalytic oxidation of 3,5-Di-tert-butylcatechol by a series of mononuclear manganese complexes: synthesis, structure, and kinetic investigation. *Inorg. Chem.* **2003**, *42*, 6274-83.
73. Rolle, C. J., III. Selective Aerobic Oxidations Catalyzed by Manganese(III) Complexes Using Redox-Active Ligands. Ph.D. Dissertation, Georgia Institute of Technology, Georgia, USA, **2011**.
74. Hatakeyama, T.; Hashimoto, S.; Ishizuka, K.; Nakamura, M., Highly Selective Biaryl Cross-Coupling Reactions between Aryl Halides and Aryl Grignard Reagents: A New Catalyst Combination of N-Heterocyclic Carbenes and Iron, Cobalt, and Nickel Fluorides. *J. Am. Chem. Soc.* **2009**, *131*, 11949-11963.
75. Hua, S. K.; Hu, Q. P.; Ren, J. M.; Zeng, B. B., Dilithium Tetrachlorocuprate(II) Catalyzed Oxidative Homocoupling of Functionalized Grignard Reagents. *Synthesis-Stuttgart* **2013**, *45*, 518-526.
76. Zhou, Z. M.; Xue, W. Z., Manganese-catalyzed oxidative homo-coupling of aryl Grignard chlorides. *J. Organomet. Chem.* **2009**, *694*, 599-603.
77. Smith, A. L.; Hardcastle, K. I.; Soper, J. D., Redox-Active Ligand-Mediated Oxidative Addition and Reductive Elimination at Square Planar Cobalt(III): Multielectron Reactions for Cross-Coupling. *J. Am. Chem. Soc.* **2010**, *132*, 14358-14360.

78. Smith, A. L.; Clapp, L. A.; Hardcastle, K. I.; Soper, J. D., Redox-active ligand-mediated Co-Cl bond-forming reactions at reducing square planar cobalt(III) centers. *Polyhedron* **2010**, 29, 164-169.
79. Smith, A. L. Facilitating Multi-Electron Reactivity at Low-Coordinate Cobalt Complexes Using Redox-Active Ligands. Ph.D. Dissertation, Georgia Institute of Technology, Atlanta, Georgia, **2011**.

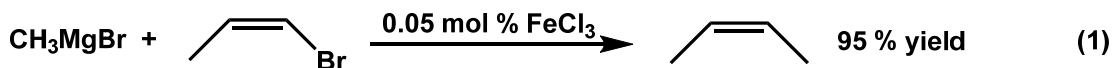
Chapter 2

Development of Redox-Active Ligand FeCl(isq^{Ph})₂ Complex as Well-defined Catalyst for Aerobic Homocoupling of Grignard Reagents

2.1 Introduction

2.1.1 Iron salts for cross-coupling and homocoupling reactions and their mechanisms

Iron catalyzed cross-coupling and homocoupling reactions have recently been reviewed.¹⁻³ Iron salts such as FeCl₃ and FeBr₂, can catalyze the homocoupling of Grignards⁴⁻⁵ and the cross-coupling of Grignards to alkenyl electrophiles (ethylene bromide),⁶ aryl electrophiles (chloro and iodobenzene),⁷ and alkyl halides.⁸⁻⁹ However, the mechanism of these transformations remains unclear. For instance, Kochi speculated that a soluble reduced iron species, either Fe^I or Fe⁰, was the active catalyst in the cross-coupling reaction of ethyl bromide and ethyl magnesium bromide.⁶ Although the oxidation state and coordination environment could not be identified, evidence for a concerted 2e⁻ process, included the high conversion (>95 %) and the stereoselectivity

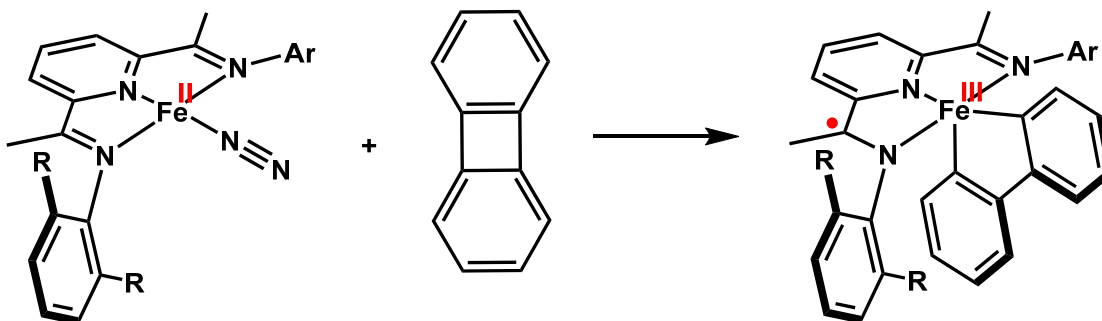


seen between *cis*-propenyl bromide and methyl magnesium bromide to generate *cis*-butene-2 exclusively **Equation 1**. However, Bogdanovic and co-workers have suggested a completely different mechanism, in which a Fe^{II}(MgCl)₂ complex is the active catalyst in homocoupling and cross-coupling reactions.¹⁰⁻¹¹ Unfortunately,

because no isolated or well-characterized iron containing complex was observed in either study the mechanism for cross-coupling or homocoupling using FeCl_3 or FeBr_2 is unknown. The problem with the lack of mechanistic detail limits rational ligand design. For instance, if an Fe^{I} species is the active catalyst then ligands that support low-valent metals should increase reactivity. However, electron rich low-valent iron complexes are difficult to isolate and study due to the high reactivity of low-valent iron complexes, and the intermediacy of paramagnetic species during catalysis limits the utility of NMR and X-ray diffractometry measurements.³

2.1.2 Redox-active ligands as an electron reservoir for well-defined iron catalyst

Scheme 2-1. Oxidative addition of biphenylene to $(^{\text{iPr}}\text{PDI})\text{Fe}^{\text{II}}(\text{N}_2)$



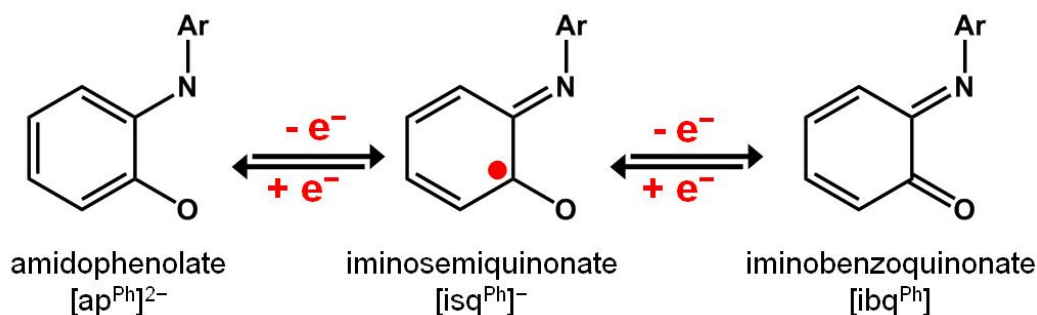
One attractive strategy to generate well-defined 3d metal complexes that are catalytically active, is the use of redox-active ligands to act as an electron reservoir. As shown in Chapter 1, several redox-active ligands have been used to generate well-defined 3d metal catalysts.¹²⁻¹⁴ Chirik and co-workers were able to isolate the oxidative addition of biphenylene to $(^{\text{iPr}}\text{PDI})\text{Fe}(\text{N}_2)$.¹⁵ Based on spectral evidence and solid state structure of the well-defined $(^{\text{iPr}}\text{PDI})\text{Fe}(\text{N}_2)$ catalyst, both the metal and ligand were oxidized by one e^- in the final product **Scheme 2-1**. This catalyst demonstrates how a redox-active ligand on a 3d metal can make a well-defined catalyst for mechanistic

investigation. However, C–C bond forming reactions are unexplored with iron complexes containing redox-active ligands.

2.1.3 The amidophenolate ligand as a redox active ligand on 3d metals

Another interesting redox-active ligand is the amidophenolate ligand. The amidophenolate ligand $[\text{ap}^{\text{Ph}}]^{2-}$ can be oxidized twice in two, 1 e^- steps to produce the iminosemiquinonate $[\text{isq}^{\text{Ph}}]^-$ and the iminobenzenequinonate $[\text{ibq}^{\text{Ph}}]$ (**Scheme 2-2**).¹⁶

Scheme 2-2. The amidophenolate ET series.



Furthermore, the amidophenolate ligand has frontier orbitals that favorably mix with the frontier metal orbitals in manganese, iron, and cobalt to allow for electron movement throughout the metal containing complex.¹⁷⁻¹⁹ Stable complexes of $\text{MnBr}(\text{isq}^{\text{Ph}})_2$ and $[\text{Co}(\text{ap}^{\text{Ph}})_2]^-$ have been prepared and shown to effect C–C bond forming reactions.²⁰⁻²¹ As described in Chapter 1, $\text{MnBr}(\text{isq}^{\text{Ph}})_2$ is capable of catalytically homocoupling PhMgBr using O_2 as the terminal oxidant.²⁰ However, cross-coupling remains challenging. $[\text{Co}(\text{ap}^{\text{Ph}})_2]^-$ has recently been explored for C–C bond forming reactions involving ethyl bromide and PhZnBr .^{20, 22-23} $[\text{Co}(\text{ap}^{\text{Ph}})_2]^-$ oxidatively adds alkyl halides such as ethyl bromide but is sluggish at reductive elimination of the ethyl fragment to a carbon nucleophile. In this context, it seems reasonable that L_2Fe ($\text{L} = [\text{ap}^{\text{Ph}}]^{2-}$ or $[\text{isq}^{\text{Ph}}]^-$) complexes might be candidates for C–C coupling. Furthermore, we hypothesize that $\text{Fe}^{\text{III}}\text{Cl}(\text{isq}^{\text{Ph}})_2$ will serve as a stable platform for detailed mechanistic study. Earlier

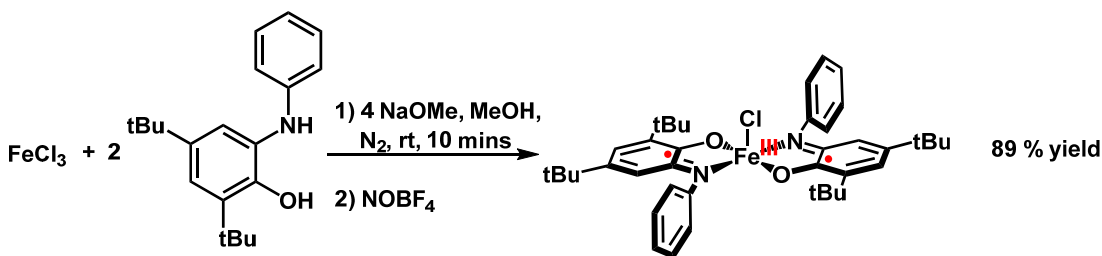
efforts at producing the L_2Fe analogs of $MnBr(isq^{Ph})_2$ and $[Co(ap^{Ph})_2]^-$ yielded only intractable mixtures of reactants and products. Presented herein are the syntheses of new L_2Fe complexes that exhibit significantly enhanced stability, and mechanistic studies of their use for Kumada-type C–C cross coupling. Limitations of the catalysts, including lack of cross-coupling and ligand redistribution are discussed.

2.2 Results

2.2.1 Synthesis and characterization of $Fe^{III}Cl(isq^{Ph})_2$

The synthesis of $Fe^{III}Cl(isq^{Ph})_2$ in modest yield was previously reported from the reaction of 2 equiv of 3,5-di-*tert*-butylamidophenol, 4 equiv of triethylamine, and $FeCl_3$ in methanol refluxed in air for 1 h.²⁴ In my hands, this procedure sometimes afforded the desired complex $Fe^{III}Cl(isq^{Ph})_2$, but the reaction was not consistently reproducible. In air, a significant amount of the tris ligated iron complex, $Fe^{III}(isq^{Ph})_3$ was formed. The $Fe^{III}(isq^{Ph})_3$ complex has been previously reported.¹⁸ The reported synthetic protocol to generate $Fe^{III}(isq^{Ph})_3$ involves the deprotonated ligand $[ap^{Ph}]^{2-}$ (5 equiv) and $FeCl_2 \cdot 4 H_2O$ in MeOH under reflux in air for 1 h. Improved yields and reproducibility were

Scheme 2-3. New synthetic procedure of $Fe^{III}Cl(isq)_2$.



achieved by the reaction of 2 equiv of 3,5-di-*tert*-butylamidophenolate, generated *in situ* from 4 equiv NaOMe, with $FeCl_3$ under a N_2 atmosphere which immediately afforded a purple solution. After 15 min of stirring, 2 equiv of $NOBF_4$ were added and the solution turned dark green. Subsequent filtration through a porous frit lead to isolation of

$\text{Fe}^{\text{III}}\text{Cl}(\text{isq}^{\text{Ph}})_2$ in high yield 89% (**Scheme 2-3**), a significant increase on the reported yield of 51% using the above procedure. The UV–vis spectrum and X-ray crystallographic data match those previously reported. However, the CV has not been reported. The

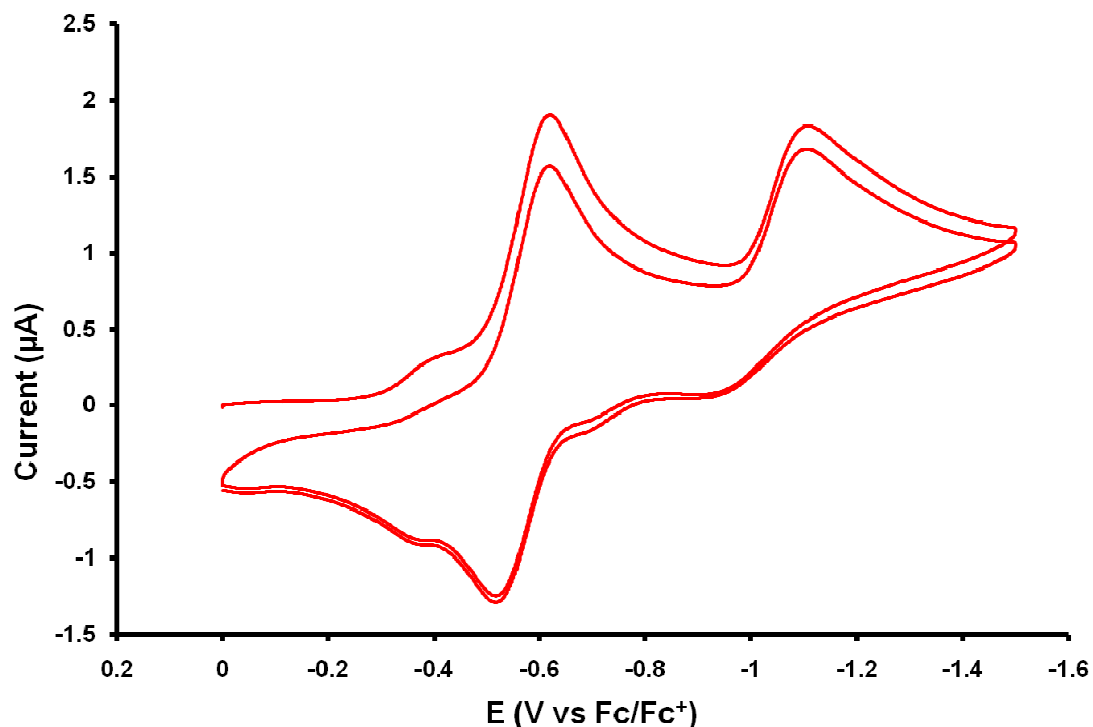
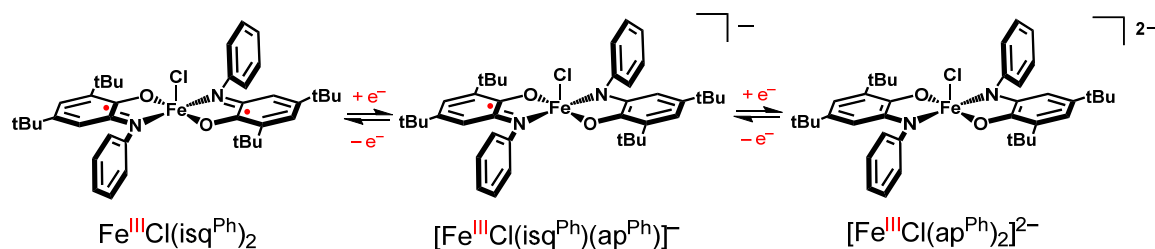


Figure 2-1. Cyclic voltammogram of $\text{Fe}^{\text{III}}\text{Cl}(\text{isq}^{\text{Ph}})_2$ in CH_3CN containing 0.1 M $[\text{nBu}_4\text{N}][\text{PF}_6]$ at a 10 mm Pt electrode. Scan rate: 0.10 V s^{-1} . Temperature 25°C .

$\text{Fe}^{\text{III}}\text{Cl}(\text{isq}^{\text{Ph}})_2$ open circuit potential in MeCN is -0.08 V vs Fc/Fc^+ and one quasi reversible reduction wave is observed at -0.57 V followed by an irreversible reduction peak at -1.11 V (**Figure 2-1**).

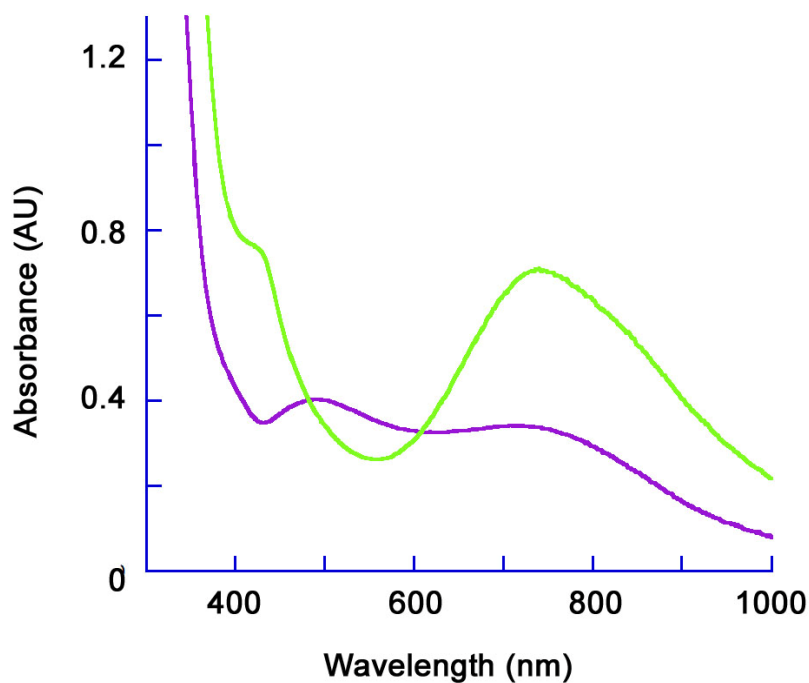
2.2.2 Preparation of an ET series from reduction of $\text{FeCl}(\text{isq}^{\text{Ph}})_2$

Scheme 2-4. Proposed ET series of $\text{Fe}^{\text{III}}\text{Cl}(\text{isq}^{\text{Ph}})$.



The accessibility of two reductions in the CV led us to speculate that reduced variants of $\text{Fe}^{\text{III}}\text{Cl}(\text{isq}^{\text{Ph}})_2$ might be accessible. By parallel to the $[\text{Co}(\text{ap}^{\text{Ph}})_2]^-$ and $\text{MnBr}(\text{isq}^{\text{Ph}})_2$ ET series, we hypothesized that species such as $[\text{Fe}^{\text{III}}\text{Cl}(\text{ap}^{\text{Ph}})(\text{isq}^{\text{Ph}})]^-$ and $[\text{Fe}^{\text{III}}\text{Cl}(\text{ap}^{\text{Ph}})_2]^{2-}$ might be accessed (**Scheme 2-4**). The synthetic method to produce $\text{Fe}^{\text{III}}\text{Cl}(\text{isq}^{\text{Ph}})_2$ involves the deprotonated closed shell ligand $[\text{ap}^{\text{Ph}}]^{2-}$ reacting with $\text{Fe}^{\text{III}}\text{Cl}_3$. This implies that $[\text{Fe}^{\text{III}}\text{Cl}(\text{ap}^{\text{Ph}})_2]^{2-}$ is the initial complex formed prior to NOBF_4 addition in the above mentioned reaction. The purple solution, from the reaction of deprotonated 3,5-di-*tert*-butylamidophenol and FeCl_3 turns green over the course of hours even in an inert atmosphere dry box. The resulting green solution contained a mixture of $\text{Fe}^{\text{III}}(\text{isq}^{\text{Ph}})_3$, and $\text{Fe}^{\text{III}}\text{Cl}(\text{isq}^{\text{Ph}})_2$, as evidenced by ESI-MS. Filtration to remove NaCl and removal of the solvent *in vacuo* produces a purple powder that turns green over the course of 24 h under N_2 to afford the $\text{Fe}^{\text{III}}(\text{isq}^{\text{Ph}})_3$ complex **Figure 2-2 a**. Preparation of 60 μM solution of the purple material in THF for UV-vis experiments gave $\text{Fe}^{\text{III}}(\text{isq}^{\text{Ph}})_3$ presumably by ligand redistribution. This could be avoided through the use of a 0.5 mm path length cuvette, because higher concentrations (6 mM, $[\text{Fe}]$) gave more stable solutions of the reduced iron complex. Metathesis reactions to generate $\text{M}[\text{Fe}(\text{ap}^{\text{Ph}})_2]$, M = bis(triphenylphosphine)iminium (PPN^+) or tertbutylammonium (TBA^+) were performed, but an increase in the stability in either the solution or solid state was not observed. However, addition of 2 equiv of pyridine to a THF solution of the purple material

a)



b)

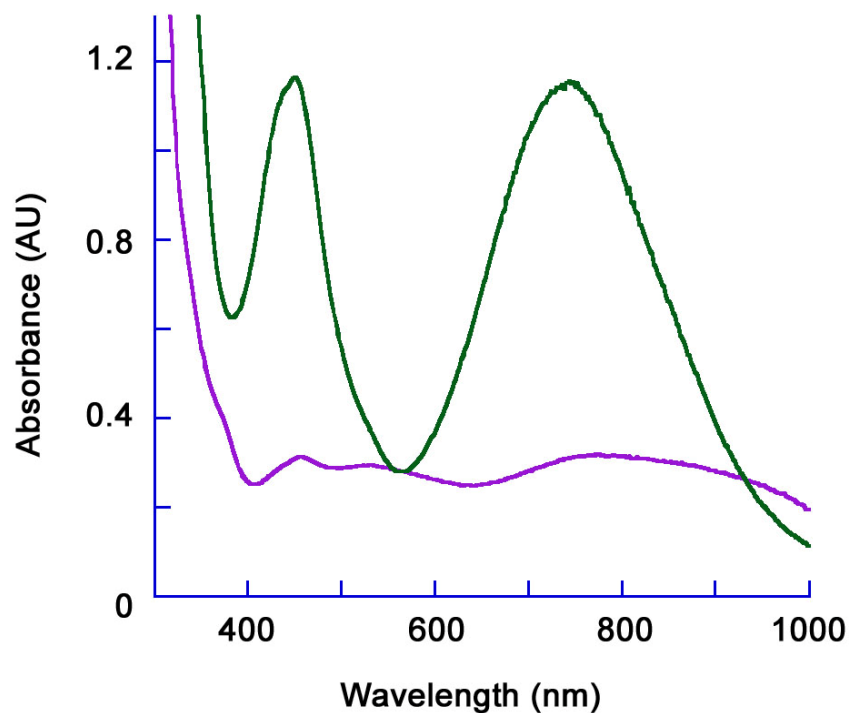
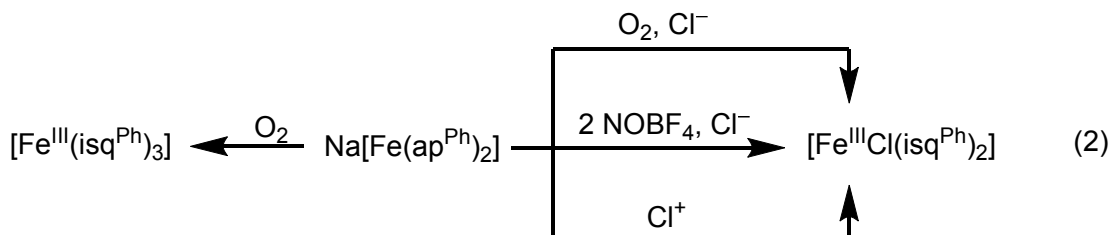


Figure 2-2. UV-vis absorption spectra in THF using a 0.50 mm pathlength cuvette for a) a reaction between isolated Na[Fe^{III}(ap^{Ph})₂] (purple line) and air to produce Fe^{III}(isq^{Ph})₃ (green line) b) exposure of isolated Na[Fe^{III}(ap^{Ph})₂] (purple line) to 1 equiv of 2,3,4,5,6,6-hexachlorocyclohexa-2,4-dien-1-one to produce Fe^{III}Cl(isq^{Ph})₂ (green line).

increased the stability of the solution (1 day) and the solid state complex (3 weeks).

Single crystals of the putative pyridine adduct were obtained from diffusion of pentane into a concentrated THF solution, but attempts to mount the air-sensitive crystals on the X-ray diffractometer led to dissolution of the of purple crystals in both Paratone–N and silicone grease.

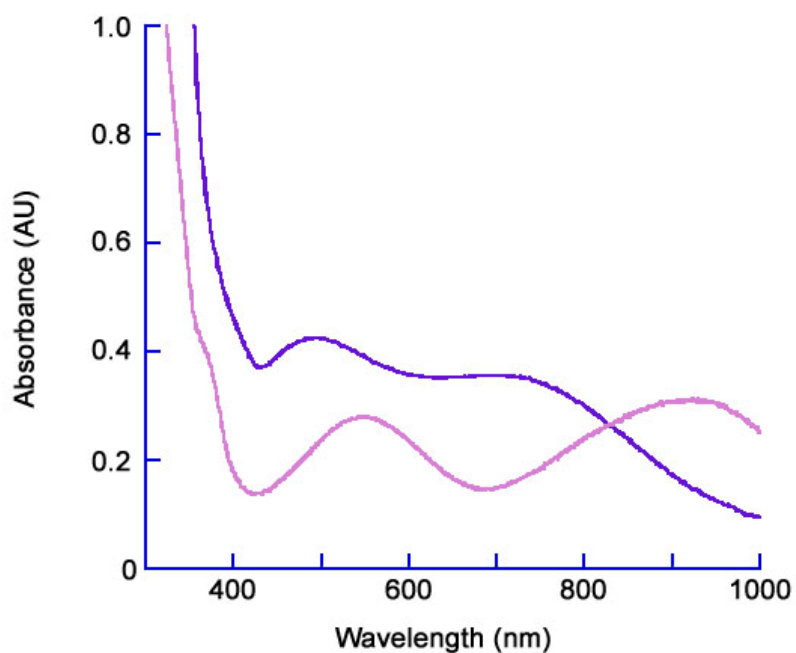
All direct methods for determining the structure or identity of the reduced iron compound have been unsuccessful, but some insights regarding the formulation of the purple material comes from its chemical reactivity. Addition of 1 equiv of a Cl^+ reagent (2,3,4,5,6,6-hexachlorocyclohexa-2,4-dien-1-one) to the purple solution resulted in an immediate color change to green producing $\text{Fe}^{\text{III}}\text{Cl}(\text{isq}^{\text{Ph}})_2$ quantitatively (**Figure 2-2 b**). The purple powder in a solution of THF and MgCl_2 , when exposed to dry air for limited amounts of time (5 s), would also immediately turn green, quantitatively generating $\text{Fe}^{\text{III}}\text{Cl}(\text{isq}^{\text{Ph}})_2$. A summary of the conversion of the reduced iron species by various oxidants is shown in **Equation 2**.



2.2.3 Aerobic homocoupling of aryl Grignards using $\text{Fe}^{\text{III}}\text{Cl}(\text{isq}^{\text{Ph}})_2$

Reactivity of **1** with 2 equiv of PhMgBr produced a purple solution and a 40 % yield of the homocoupled product biphenyl. Again the purple solution was only observed (stable) when concentrated (6mM, $\text{Fe}^{\text{III}}\text{Cl}(\text{isq}^{\text{Ph}})_2$ in THF), necessitating the use of a 0.5 mm path length cuvette. In dilute solution, addition of 2 equiv of PhMgBr to **1** lead to a yellow solution and featureless absorption spectrum. The purple solution produced is different than that of isolated $\text{Na}[\text{Fe}^{\text{III}}(\text{ap}^{\text{Ph}})_2]$ (**Figure 2-3 a**). Furthermore, the resulting

a)



b)

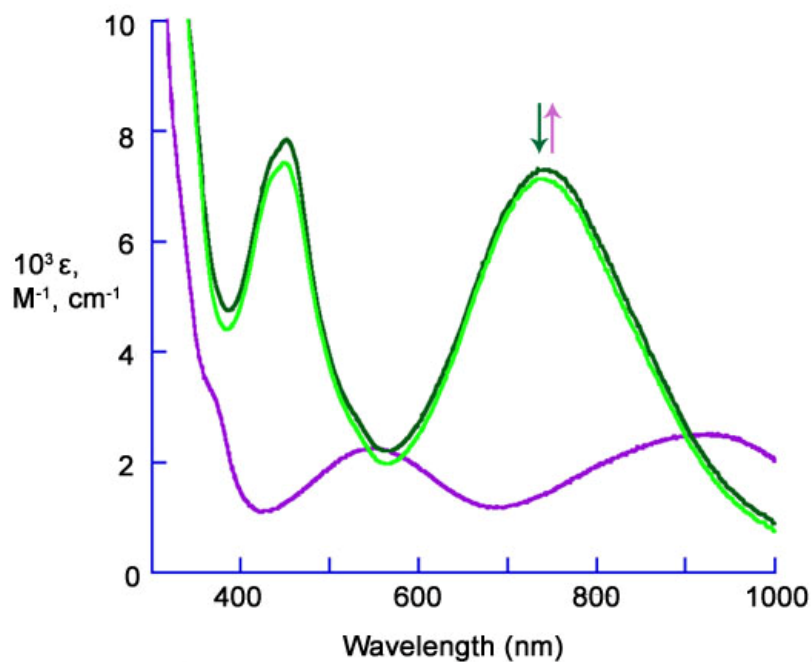
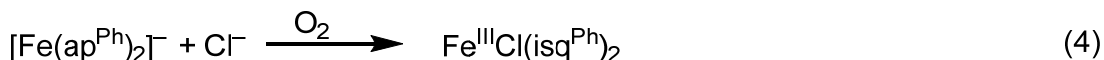
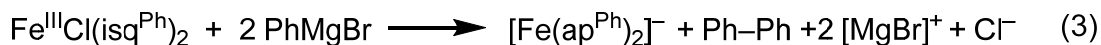


Figure 2-3. UV-vis spectra collected in a 0.54 mm path length in THF for a) comparison of the isolated $\text{Na}[\text{Fe}(\text{ap}^{\text{Ph}})_2]$ (dark purple) and the purple solution generated from the reaction between $\text{Fe}^{\text{III}}\text{Cl}(\text{isq}^{\text{Ph}})_2$ and 2 equiv of PhMgBr (light purple) b) exposure of $\text{Fe}^{\text{III}}\text{Cl}(\text{isq}^{\text{Ph}})_2$ (dark green line) to 2 equiv of PhMgBr (purple line) followed by exposure to air (light green line).

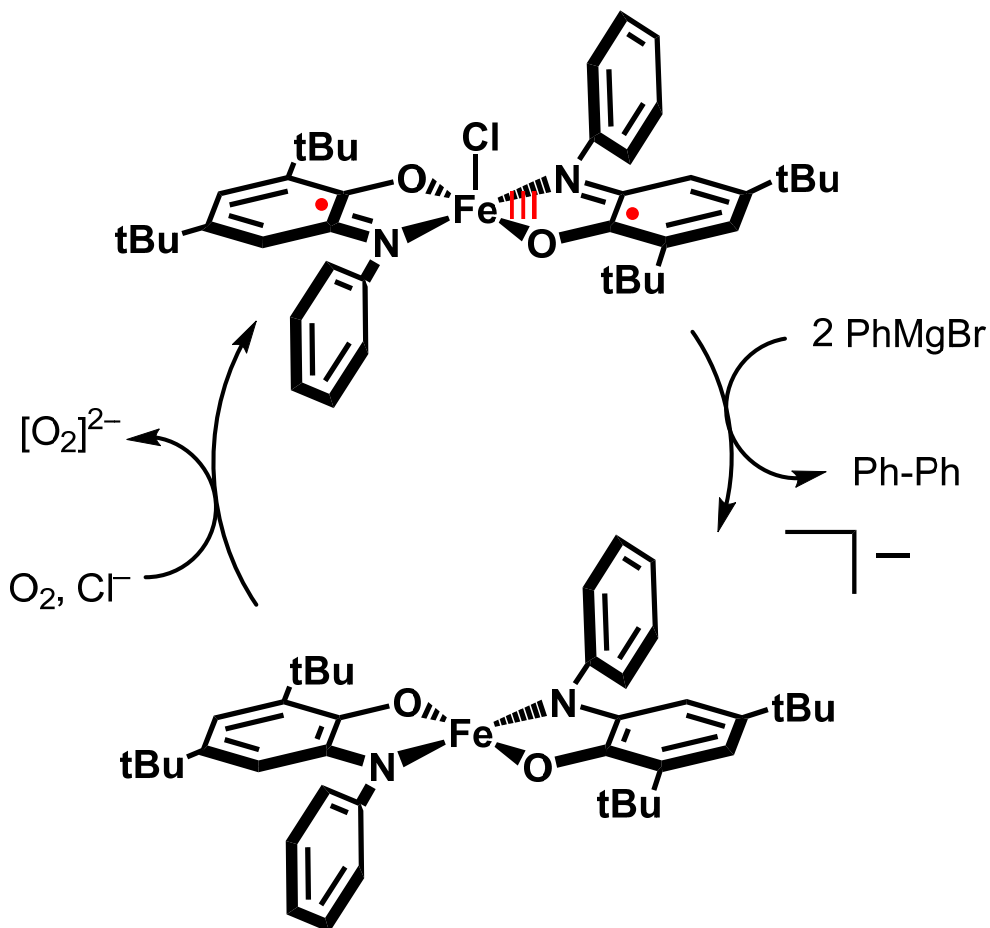
purple solution when exposed to air regenerated $\text{Fe}^{\text{III}}\text{Cl}(\text{isq}^{\text{Ph}})_2$ (98 % yield, **Figure 2-3**

b). The combination of the PhMgBr coupling reaction (**Equation 3**) and the O₂ oxidation (**Equation 4**) comprise a complete cycle for aerobic homocoupling of PhMgBr,



as shown in **Scheme 2-5**. When the reaction is run catalytically (5 mol % of **1**) in air the biphenyl yield, after 6 h, is 45 % demonstrating a turnover number (TON) of 4.5. When

Scheme 2-5. Proposed mechanism of aryl Grignard homocoupling via Fe^{III}Cl(isq^{Ph})₂ using O₂ as the terminal oxidant.



the reaction is carried out in an inert atmosphere at 5 mol % loading of **1** the yield of biphenyl is decreased to 20% or 2 TON vs. **1**.

Cross-coupling of alkyl halides and either alkyl or aryl Grignards was attempted. For example, octylmagnesium bromide and 1-chlorohexane were reacted using 5 mol % of **1** for 24 h at room temperature. This reaction produced only homocoupled product hexadecane, suggesting the alkyl halide functions as a sacrificial oxidant. To probe this reaction, ethyl bromide was added to the purple solutions of the putative $\text{Na}[\text{Fe}(\text{ap}^{\text{Ph}})_2]$ complex, affording immediate conversion to the $\text{Fe}^{\text{III}}(\text{isq}^{\text{Ph}})_3$ complex.

2.3 Discussion

2.3.1 Synthesis and characterization of $\text{Fe}^{\text{III}}\text{Cl}(\text{isq}^{\text{Ph}})_2$ and $\text{Na}[\text{Fe}(\text{ap}^{\text{Ph}})_2]$

Problems with reproducibility in the published procedure for the preparation of $\text{Fe}^{\text{III}}\text{Cl}(\text{isq}^{\text{Ph}})_2$ necessitated the development of a new synthetic protocol that used a chemical oxidant (NOBF_4) for the controlled oxidation and synthesis of $\text{Fe}^{\text{III}}\text{Cl}(\text{isq}^{\text{Ph}})_2$. Beyond increasing the yield and purity of $\text{Fe}^{\text{III}}\text{Cl}(\text{isq}^{\text{Ph}})_2$, this protocol also provided a way to study the reduced iron complex, which based on parallels to $\text{MnBr}(\text{isq}^{\text{Ph}})_2$ and $[\text{Co}(\text{ap}^{\text{Ph}})_2]^-$ is here formulated as $\text{Na}[\text{Fe}(\text{ap}^{\text{Ph}})_2]$. Chemical characterization of the reduced species was difficult because of its extreme air-sensitivity and its proclivity for ligand redistribution in dilute solutions. The reduced iron complex, in the solid state, is stable for only 24 h under N_2 at $-30\text{ }^\circ\text{C}$. The decomposition product in all cases was the $\text{Fe}^{\text{III}}(\text{isq}^{\text{Ph}})_3$ complex. This oxidation and ligand redistribution was also seen when FeCl_3 and deprotonated $[\text{ap}^{\text{Ph}}]^{2-}$ were reacted in air.

This ease of oxidation and ligand redistribution also precluded structural analysis but evidence for the presence of an $[\text{Fe}^{\text{III}}(\text{ap}^{\text{Ph}})_2]$ core comes from reactivity studies. A summary of the reactivity of the reduced iron species is shown in **Equation 2**. The reduced iron complex can be quantitatively converted to $\text{Fe}^{\text{III}}\text{Cl}(\text{isq}^{\text{Ph}})_2$ using either air or 2 equiv of chemical oxidant in the presence of halide. When a halide is not present the tris complex is formed exclusively. In sum, these reactions suggest that $\text{Na}[\text{Fe}^{\text{III}}(\text{ap}^{\text{Ph}})_2]$,

$\text{Na}[\text{Fe}^{\text{II}}(\text{isq}^{\text{Ph}})(\text{ap}^{\text{Ph}})]$ or $\text{Na}[\text{Fe}^{\text{I}}(\text{isq}^{\text{Ph}})_2]$ could be the chemical identity of the purple solution. However, the oxidation state of the ligand and metal remain unknown.

2.3.2 C–C bond forming reactions using $\text{Fe}^{\text{III}}\text{Cl}(\text{isq}^{\text{Ph}})_2$

The putative $[\text{Fe}(\text{ap}^{\text{Ph}})_2]^-$ did not react with alkyl halides including methyl iodide to give oxidative addition products. This prevented cross-coupling from occurring in this system. Interestingly, $\text{Fe}^{\text{III}}\text{Cl}(\text{isq}^{\text{Ph}})_2$ catalytically homocouples PhMgBr to generate biphenyl using alkyl halide as a terminal oxidant. When $\text{Fe}^{\text{III}}\text{Cl}(\text{isq}^{\text{Ph}})_2$ is exposed to 2 equiv of PhMgBr a purple solution is generated with concomitant production of biphenyl, suggesting that transmetallation and reductive elimination from $\text{FeCl}(\text{isq})_2$ is viable. However, the resulting purple solution is different than that of the independently generated $[\text{Fe}(\text{ap}^{\text{Ph}})_2]^-$ as seen in **Figure 2-3 a**. Together these results imply that $\text{Fe}^{\text{III}}\text{Cl}(\text{isq}^{\text{Ph}})_2$ is reduced twice, but the reduced iron complex from this reaction has not been identified perhaps rationalizing the disparate reactivity with alkyl halides noted above. The re-oxidation step can also be accomplished with O_2 . When the purple solution generated from the reaction between $\text{Fe}^{\text{III}}\text{Cl}(\text{isq}^{\text{Ph}})_2$ and 2 equiv of PhMgBr are exposed to air for 5 s, $\text{Fe}^{\text{III}}\text{Cl}(\text{isq}^{\text{Ph}})_2$ is regenerated at 98 % yield, but longer times afford $\text{Fe}^{\text{III}}(\text{isq}^{\text{Ph}})_3$ as the dominant product. Together, these reactions comprise catalytic cycles for biphenyl using chemical oxidants, including O_2 . For instance, at 5 mol % catalyst loading of $\text{Fe}^{\text{III}}\text{Cl}(\text{isq}^{\text{Ph}})_2$ a 45 % yield of biphenyl is achieved over the course of 6 h.

While both the $\text{MnBr}(\text{isq}^{\text{Ph}})_2$ and $[\text{Co}(\text{ap}^{\text{Ph}})_2]^-$ ET series complexes have been isolated and characterized, the high spin d^5 electron configuration of Fe^{III} bound to weak field ligands ($[\text{ap}^{\text{Ph}}]^{2-}$) does not produce any ligand field stabilization energy. This leads to ligand redistribution and the prevention of fully characterizing the reduced iron complex.

2.4 Conclusions

A new synthetic procedure has been developed for the preparation of $\text{Fe}^{\text{III}}\text{Cl}(\text{isq}^{\text{Ph}})_2$. While the new complex can catalytically homocouple PhMgBr using O_2 as the terminal oxidant, the yields are less than that of previously reported iron salts, such as FeCl_3 and FeBr_2 . It was believed that this system could shed light of the mechanism of Grignard homocoupling reactions, however, the instability of the reduced iron complex $\text{Na}[\text{Fe}(\text{ap}^{\text{Ph}})_2]$ prevents detailed mechanistic study. However, it is clear that ligand redistribution must be avoided to produce a well-defined catalyst. Work towards this goal is shown in Chapter 3.

2.5 Methods

2.5.1 General considerations

Unless otherwise noted, all manipulations were performed under anaerobic conditions using standard vacuum line techniques, or in an inert atmosphere glove box under purified nitrogen. UV–visible absorption spectra were acquired using a Varian Cary 50 spectrophotometer. Unless otherwise specified, all electronic absorption spectra were recorded at ambient temperatures in 1cm quartz cells. All mass spectra were recorded in the Georgia Institute of Technology Bioanalytical Mass Spectrometry Facility.

2.5.2 Methods and materials

Anhydrous dichloromethane and pentane solvents for air- and moisture-sensitive manipulations were purchased from Sigma-Aldrich, further dried by passage through columns of activated alumina, degassed by at least three freeze-pump-thaw cycles, and stored under N_2 . Anhydrous tetrahydrofuran (THF) purchased from Sigma-Aldrich was further dried by stirring over Na (s) in the presence of benzophenone until a dark purple

color was achieved (~1 day), followed by THF removal *in vacuo* and stored under N₂. The ligand (2,4-di-tert-butyl-6-(lphenylamino)phenol (H₂ap^{Ph}) was prepared by literature methods and all characterization data matched those referenced.²⁵ Anhydrous FeCl₃ was purchased from Strem Chemical, Inc. All other chemicals were purchased from Sigma-Aldrich and used as received.

Synthesis of [FeCl(isq^{Ph})₂] (1)

In a procedure modified from literature,²⁶ a 20 mL scintillation vial was charged with anhydrous FeCl₃ (0.081 g, 0.5 mmol), a Teflon stir bar, H₂ap^{Ph} (0.297 g, 1 mmol), and 0.5 M NaOMe in MeOH (4 mL, 2 mmol) to afford a dark purple solution. After 1 min of stirring NOBF₄ (0.161 g, 1 mmol) was added and the solution turned dark green with the evolution of a colorless gas. **Caution:** NO gas is generated during the reaction and proper ventilation is required. After an additional minute of stirring, the solvent was removed *in vacuo* to generate a dark green powder. The collected dark green solid was dissolved in THF (5 mL) and filtered through a fine Buchner funnel and the filtrate was dried *in vacuo* to generate [FeCl(isq^{Ph})₂] (0.299 g, 89% yield) UV-vis (CH₂Cl₂) λ_{max}, nm (ε, M⁻¹, cm⁻¹): 290 (1.8 x 10⁴), 455 (0.82 x 10⁴), 760 (0.78 x 10⁴); (THF) λ_{max}, nm (ε, M⁻¹, cm⁻¹): 290 (1.6 x 10⁴), 455 (0.77 x 10⁴), 740 (0.73 x 10⁴).

Synthesis of Na[Fe(ap^{Ph})₂] (2) and Na[Fe(ap^{Ph})₂(py)₂] (3)

A 20 mL scintillation vial was charged with anhydrous FeCl₃ (0.162 g, 1 mmol), a Teflon stir bar, H₂ap^{Ph} (0.594 g, 2 mmol), and 0.5 M NaOMe in MeOH (8 mL, 4 mmol) to afford a dark purple solution. After 1 min of stirring, the solvent was removed *in vacuo* to generate a dark purple powder. The collected dark purple solid was dissolved in THF (5 mL) and filtered through a fine Buchner funnel and the filtrate was dried *in vacuo* to

generate $\text{Na}[\text{Fe}(\text{ap}^{\text{Ph}})_2]$ (0.629 g, 94% yield). Pyridine (54 μL , 0.6 mmol) was added to **2** (0.2243 g, 0.3 mmol) in 2 mL of THF and layered with 15 mL of pentane and stored at -30°C for 2 days to generate dark green crystals **3**.

Catalytic Homocoupling of PhMgBr

In a representative procedure, a 20 mL scintillation vial was charged with **1** (2mM), 2M PhMgCl in THF (4mM), and 5 mL of THF under N_2 and fitted with a teflon lined cap. The reaction was monitored in a quartz, 0.5 mm path length cuvette and a greased # 9 glass stopper with UV-vis spectroscopy (300–1000 nm). Yield of the iron species was determined by the absorption peak at 740 nm with $\epsilon = 7300 \text{ M}^{-1}, \text{ cm}^{-1}$. To determine the biphenyl yield the solution (400 μL) was quenched with HCl in ether (100 μL) and analyzed with GC-MS using decane as an internal standard and compared to a calibration plot. Oxidation of the resulting reduced iron species was accomplished by opening the cuvette to ambient air for 30 s followed by resealing.

2.6 Works Cited

1. Fürstner, A.; Martin, R., Advances in Iron Catalyzed Cross Coupling Reactions. *Chem. Lett.* **2005**, *34*, 624-629.
2. Jana, R.; Pathak, T. P.; Sigman, M. S., Advances in Transition Metal (Pd,Ni,Fe)-Catalyzed Cross-Coupling Reactions Using Alkyl-organometallics as Reaction Partners. *Chem. Rev. (Washington, DC, U. S.)* **2011**, *111*, 1417-1492.
3. Sherry, B. D.; Fürstner, A., The Promise and Challenge of Iron-Catalyzed Cross Coupling. *Acc. Chem. Res.* **2008**, *41*, 1500-1511.
4. Kharasch, M. S.; Fields, E. K., Factors Determining the Course and Mechanisms of Grignard Reactions. IV. The Effect of Metallic Halides on the Reaction of Aryl Grignard Reagents and Organic Halides¹. *J. Am. Chem. Soc.* **1941**, *63*, 2316-2320.
5. Cahiez, G.; Moyer, A.; Buendia, J.; Duplais, C., Manganese- or Iron-Catalyzed Homocoupling of Grignard Reagents Using Atmospheric Oxygen as an Oxidant. *J. Am. Chem. Soc.* **2007**, *129*, 13788-13789.
6. Tamura, M.; Kochi, J. K., Vinylation of Grignard reagents. Catalysis by iron. *J. Am. Chem. Soc.* **1971**, *93*, 1487-1489.
7. Fürstner, A.; Leitner, A.; Méndez, M.; Krause, H., Iron-Catalyzed Cross-Coupling Reactions. *J. Am. Chem. Soc.* **2002**, *124*, 13856-13863.
8. Nakamura, M.; Matsuo, K.; Ito, S.; Nakamura, E., Iron-Catalyzed Cross-Coupling of Primary and Secondary Alkyl Halides with Aryl Grignard Reagents. *J. Am. Chem. Soc.* **2004**, *126*, 3686-3687.
9. Nakamura, M.; Ito, S.; Matsuo, K.; Nakamura, E., Iron-Catalyzed Chemoselective Cross-Coupling of Primary and Secondary Alkyl Halides with Arylzinc Reagents. *Synlett* **2005**, *2005*, 1794-1798.
10. Aleandri, L. E.; Bogdanovic, B.; Bons, P.; Duerr, C.; Gaidies, A.; Hartwig, T.; Hockett, S. C.; Lagarden, M.; Wilczok, U.; Brand, R. A., Inorganic Grignard Reagents. Preparation and Their Application for the Synthesis of Highly Active Metals, Intermetallics, and Alloys. *Chem. Mater.* **1995**, *7*, 1153-1170.
11. Bogdanović, B.; Schwickardi, M., Transition Metal Catalyzed Preparation of Grignard Compounds. *Angew. Chem., Int. Ed.* **2000**, *39*, 4610-4612.
12. Blackmore, K. J.; Lal, N.; Ziller, J. W.; Heyduk, A. F., Catalytic Reactivity of a Zirconium(IV) Redox-Active Ligand Complex with 1,2-Diphenylhydrazine. *J. Am. Chem. Soc.* **2008**, *130*, 2728-2729.

13. Myers, T. W.; Berben, L. A., A Sterically Demanding Iminopyridine Ligand Affords Redox-Active Complexes of Aluminum(III) and Gallium(III). *Inorg. Chem.* **2012**, *51*, 1480-1488.
14. Tondreau, A. M.; Atienza, C. C. H.; Weller, K. J.; Nye, S. A.; Lewis, K. M.; Delis, J. G. P.; Chirik, P. J., Iron Catalysts for Selective Anti-Markovnikov Alkene Hydrosilylation Using Tertiary Silanes. *Science* **2012**, *335*, 567-570.
15. Darmon, J. M.; Stieber, S. C. E.; Sylvester, K. T.; Fernández, I.; Lobkovsky, E.; Semproni, S. P.; Bill, E.; Wieghardt, K.; DeBeer, S.; Chirik, P. J., Oxidative Addition of Carbon–Carbon Bonds with a Redox-Active Bis(imino)pyridine Iron Complex. *J. Am. Chem. Soc.* **2012**, *134*, 17125-17137.
16. Poddel'sky, A. I.; Cherkasov, V. K.; Abakumov, G. A., Transition metal complexes with bulky 4,6-di-tert-butyl-N-aryl(alkyl)-o-iminobenzoquinonato ligands: Structure, EPR and magnetism. *Coord. Chem. Rev.* **2009**, *253*, 291-324.
17. Bill, E.; Bothe, E.; Chaudhuri, P.; Chlopek, K.; Herebian, D.; Kokatam, S.; Ray, K.; Weyhermüller, T.; Neese, F.; Wieghardt, K., Molecular and electronic structure of four- and five-coordinate cobalt complexes containing two o-phenylenediamine- or two o-aminophenol-type ligands at various oxidation levels: An experimental, density functional, and correlated ab initio study. *Chem. Eur. J.* **2005**, *11*, 204-224.
18. Chun, H.; Verani, C. N.; Chaudhuri, P.; Bothe, E.; Bill, E.; Weyhermüller, T.; Wieghardt, K., Molecular and Electronic Structure of Octahedral o-Aminophenolato and o-Iminobenzosemiquinonato Complexes of V(V), Cr(III), Fe(III), and Co(III). Experimental Determination of Oxidation Levels of Ligands and Metal Ions. *Inorg. Chem.* **2001**, *40*, 4157-4166.
19. Chun, H. P.; Bill, E.; Weyhermüller, T.; Wieghardt, K., S=3/2 reversible arrow S=1/2 spin crossover behavior in five-coordinate halido- and pseudohalido-bis(o-iminobenzosemiquinonato)iron(III) complexes. *Inorg. Chem.* **2003**, *42*, 5612-5620.
20. Rolle, C. J., III. Selective Aerobic Oxidations Catalyzed by Manganese(III) Complexes Using Redox-Active Ligands. Ph.D. Dissertation, Georgia Institute of Technology, Georgia, USA, **2011**.
21. Smith, A. L.; Clapp, L. A.; Hardcastle, K. I.; Soper, J. D., Redox-active ligand-mediated Co-Cl bond-forming reactions at reducing square planar cobalt(III) centers. *Polyhedron* **2010**, *29*, 164-169.
22. Smith, A. L.; Hardcastle, K. I.; Soper, J. D., Redox-Active Ligand-Mediated Oxidative Addition and Reductive Elimination at Square Planar Cobalt(III): Multielectron Reactions for Cross-Coupling. *J. Am. Chem. Soc.* **2010**, *132*, 14358-14360.
23. Smith, A. L. Facilitating Multi-Electron Reactivity at Low-Coordinate Cobalt Complexes Using Redox-Active Ligands. Ph.D. Dissertation, Georgia Institute of Technology, Atlanta, Georgia, **2011**.

24. Chun, H.; Weyhermuller, T.; Bill, E.; Wieghardt, K., Tuning the electronic structure of halidobis(o-imino-benzosemiquinonato)iron(III) complexes. *Angew. Chem., Int. Ed.* **2001**, *40*, 2489-+.
25. Chaudhuri, P.; Verani, C. N.; Bill, E.; Bothe, E.; Weyhermüller, T.; Wieghardt, K., Electronic Structure of Bis(o-iminobenzosemiquinonato)metal Complexes (Cu, Ni, Pd). The Art of Establishing Physical Oxidation States in Transition-Metal Complexes Containing Radical Ligands. *J. Am. Chem. Soc.* **2001**, *123*, 2213-2223.
26. Chun, H.; Weyhermüller, T.; Bill, E.; Wieghardt, K., Tuning the Electronic Structure of Halidobis(o-imino-benzosemiquinonato)iron(III) Complexes. *Angewandte Chemie International Edition* **2001**, *40*, 2489-2492.

Chapter 3

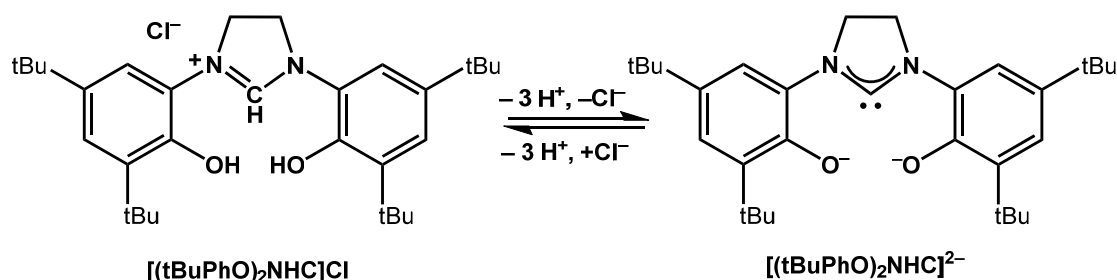
New Cobalt Electron-Transfer Series Featuring Redox-Active Pincer-Type N-Heterocyclic ligand for C–C Bond Forming Reactions

3.1 Introduction

The use of redox-active ligands as electron reservoirs for multielectron transformations at 3d metals has become an increasingly versatile tool to mimic 4d and 5d metals.¹⁻⁶ The ability of the ligand to store electrons allows for species to be stable over an atypically wide range of oxidation states, permitting detailed studies of catalytic mechanisms and new reactivity at 3d metals. For example, Chirik and co-workers recently used an Fe catalyst supported by a pincer-type redox-active ligand to achieve the industrially relevant selective anti-Markovnikov addition of sterically hindered tertiary silanes to alkenes.⁷ Our lab has demonstrated the ability of a square-planar redox-active ligand $[\text{Co}^{\text{III}}(\text{ap}^{\text{Ph}})]^-$ complex to mediate C–C cross-coupling between alkyl halides and aryl Grignards, in the process demonstrating the ability of a redox-active ligand to mediate oxidative addition and reductive elimination at a 3d metal center.³⁻⁴ However, only low yields of the cross-coupled product 10-15% were obtained with $[\text{Co}^{\text{III}}(\text{ap}^{\text{Ph}})]^-$ due to low yielding C–C reductive elimination that apparently stems from slow formation of *cis*- $[\text{Co}(\text{ap}^{\text{Ph}})_2(\text{R})_2]$.

To address this issue, and to expand the library of redox-active ligated 3d metal complexes, we pursued the development of new chelating redox-active ligands. Diphenolated imidazolyl-carbene ligands have recently been used to support a variety of metals (Mn, Ir, Zn, V, Ti).⁸⁻¹⁹ The tridentate, pincer-type N-heterocyclic carbene 1,3-bis(3,5-di-tert-butylphenol)dihydroimidazolium chloride $[(tBuPhO)_2NHC]Cl$ ligand (**Scheme 3-1**) was chosen to address the challenges in C-C coupling with the $[Co^{III}(ap^{Ph})]^-$ complex. The $[(tBuPhO)_2NHC]Cl$ is cationic in its protonated state, however, upon deprotonation of both hydroxyl groups and the carbene the ligand becomes dianionic $[(tBuPhO)_2NHC]^{2-}$. The tridentate pincer-type $[(tBuPhO)_2NHC]^{2-}$ binds in a meridional orientation and the strong σ -donating character disfavors bis-ligated complexes, which allows for vacant axial and equatorial sites that can potentially accommodate *cis* binding of substrates. Although the ligand has not been definitively

Scheme 3-1. Protonated and deprotonated version of 1,3-bis(3,5-di-tert-butylphenol)dihydroimidazolium chloride.



shown to support a radical, its similarity to the known amidophenolate ligand warrants further investigation.²⁰ Work by Bercaw and co-workers, using a similar ligand 1,3-bis(2-hydroxy-5-tert-butylphenyl)imidazolium chloride, bound to Ir^{III} could be oxidized twice. Oxidizing the $Ir^{III}(NHC)$ complex led to either an Ir^V complex or an Ir^{IV} ligand radical complex; however, the identity of the doubly oxidized complex could not be ascertained.

To understand the behavior of $[(t\text{BuPhO})_2\text{NHC}]^{2-}$ as a ligand, a Co complex bearing the $[(t\text{BuPhO})_2\text{NHC}]^{2-}$ was chosen **Figure 3-1**. Reported here, is the first

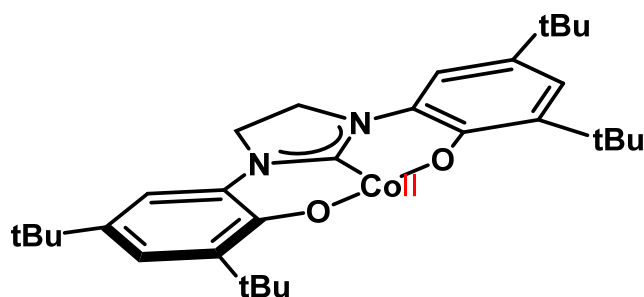


Figure 3-1. Proposed structure of $\text{Co}^{\text{II}}(t\text{BuPhO})_2\text{NHC}$.

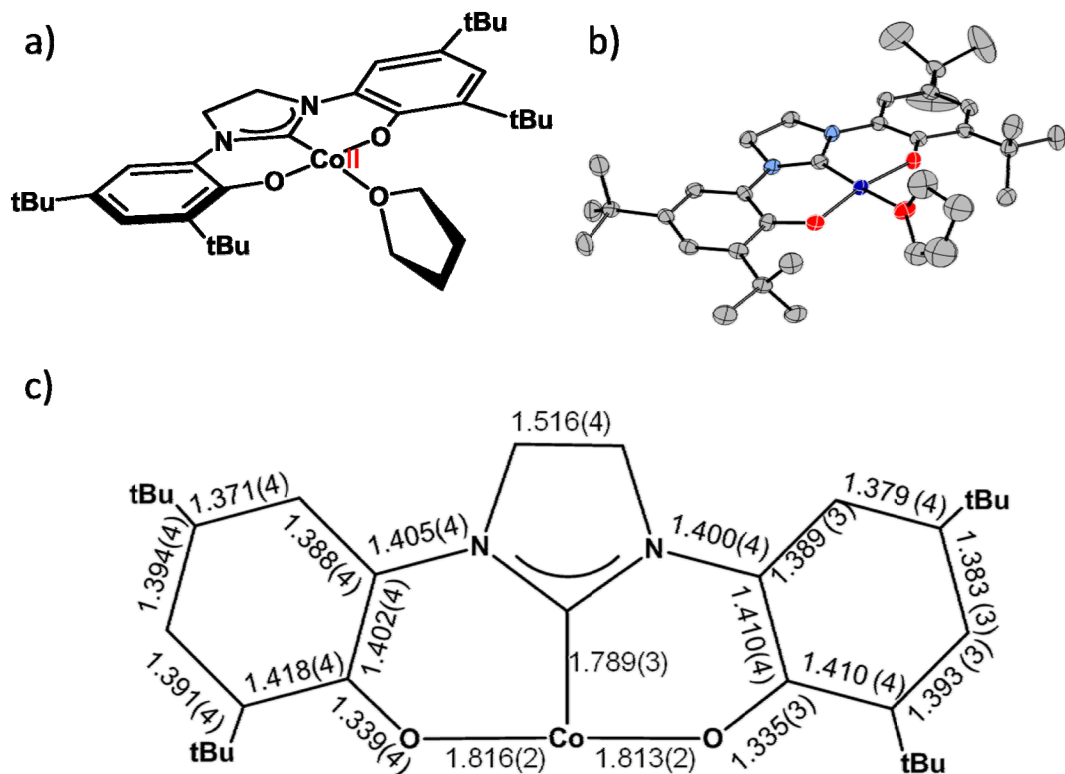
isolated and characterized redox-active ET series bearing a $[(t\text{BuPhO})_2\text{NHC}]^{2-}$ ligand bound to cobalt. The ability of this new complex to span multiple redox states is used for C–C coupling including Kumada cross-coupling and homocoupling of aryl Grignard reagents. Limitations of the $\text{Co}^{\text{II}}((t\text{BuPhO})_2\text{NHC})\text{THF}$ as a cross coupling catalyst are discussed in the context of an unexpected degradation pathway.

3.2 Results

3.2.1 Synthesis and characterization of $\text{Co}^{\text{II}}((\text{tBuPhO})_2\text{NHC})\text{THF}$

The reaction of triply deprotonated 1,3-bis(3,5-di-tert-

Scheme 3-2. a) $\text{Co}^{\text{II}}((\text{tBuPhO})_2\text{NHC})\text{THF}$ (**1**) b) Solid-state structures of **1** drawn with 50 % probability ellipsoids. Hydrogen and counter ions omitted for clarity. c) Selected bond lengths (Å) of **1**.



butylphenolate)dihydroimidazol-2-ylidene $[(\text{tBuPhO})_2\text{NHC}]^{2-}$ (generated *in situ* from the reaction of $[(\text{tBuPhO})_2\text{NHC}]\text{Cl}$ with 3.0 equiv NaOMe) and CoCl_2 in MeOH under N_2 generates an orange solution. Subsequent drying and addition of THF followed by filtration and removal of solvent *in vacuo* affords $\text{Co}^{\text{II}}((\text{tBuPhO})_2\text{NHC})(\text{THF})$ (**1**) as an orange powder in good yield (**Scheme 3-2 a**). The UV–Vis spectrum shows a large charge transfer band at 420 nm ($\epsilon = 5300 \text{ M}^{-1}, \text{cm}^{-1}$) in THF (**Figure 3-2**). Evan's

method analysis in oxygen-free THF- d_6 gives a $\mu_{\text{eff}} = 2.37$ for **1** which is in-between the calculated spin only values of 1.73 for $S = 1/2$ and 2.82 for the $S = 1$. Cobalt can have significant contribution from the angular momentum term L leading to a higher μ_{eff} than expected

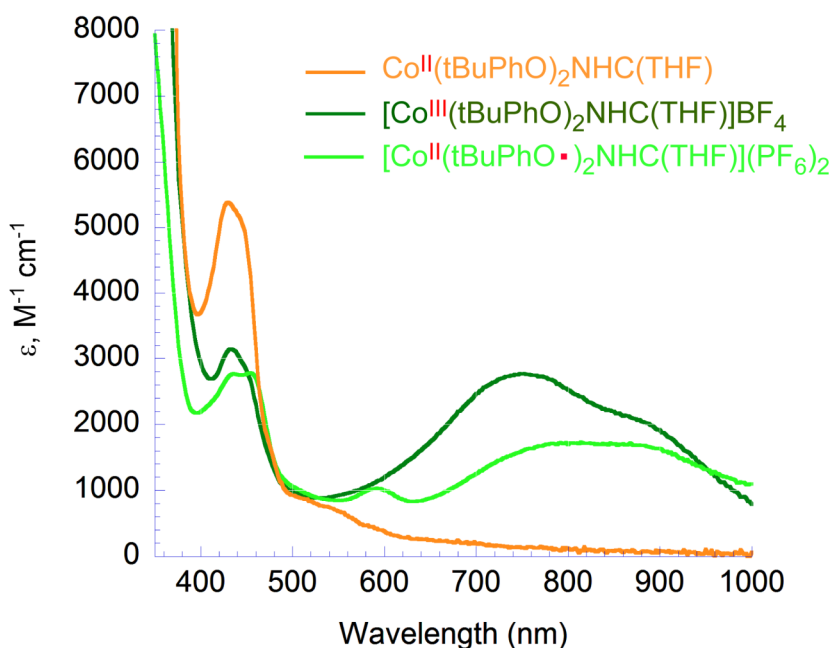


Figure 3-2. UV–vis spectra of complexes **1**, **2**, and **3** in THF solutions at 22 °C.

for the spin-only value, so we have assigned **1** as having one unpaired electron ($S = 1/2$).²¹ Single crystals suitable for X-ray diffraction were obtained from slow diffusion of pentane into a THF solution containing **1** at $-30\text{ }^{\circ}\text{C}$ over 24 hours (**Scheme 3-2 b**). The crystal structure of **1** shows a square planar arrangement of the tridentate $[(\text{tBuPhO})_2\text{NHC}]^{2-}$ ligand and THF *trans* to the carbene, giving the complex approximate C_{2v} symmetry. Selected bond lengths for **1** are shown in **Scheme 3-2 c**. Complex **1** shows an average C–C bond length of 1.394 Å for both phenol rings. This is

consistent with aromaticity as seen in comparable $[\text{ap}^{\text{Ph}}]^{2-}$ ligands bound to 3d metals where the average C–C bond distance in the phenol ring is 1.39–1.41 Å.²² Complex **1** has a very short C–Co bond length of 1.789(3) Å. This much shorter than the next shortest C–Co bond length of 1.941 Å.²³ The O–C bond lengths of 1.339(4) Å and 1.335(3) Å in the phenols are typical for complexed phenolates.²² For instance, the C–O bond length in the closed-shell fully reduced amidophenolate ligand bound to Co ($[\text{Co}^{\text{III}}(\text{ap}^{\text{Ph}})_2]^-$) is 1.353(3) Å.²⁴ The Co–O bond length of 1.816(2) Å is shorter than those in comparable Co^{II} phenolate complexes (typical Co–O bond length of 2.10–1.91 Å).^{25–28} The contraction of the C–O is due to the geometric constraints of the pincer-type architecture and the C–O bond distance is best described as a C–O single bond.³ The C–C bond in the imidazole linker is saturated as shown by the bond length between the two carbons in the ring of 1.516 Å, which is indicative of a single bond. The combined data are consistent with a low-spin d^7 Co^{II} center bound to a fully reduced tridentate $[(\text{tBuPhO})_2\text{NHC}]^{2-}$ ligand with two aromatic phenolates as depicted in **Scheme 3-2 a**.

3.2.2 Electrochemistry of the $\text{Co}^{\text{II}}((\text{tBuPhO})_2\text{NHC})(\text{THF})$

Cyclic voltammetry on **1** shows three quasi-reversible peaks at -0.350 V, 0.356

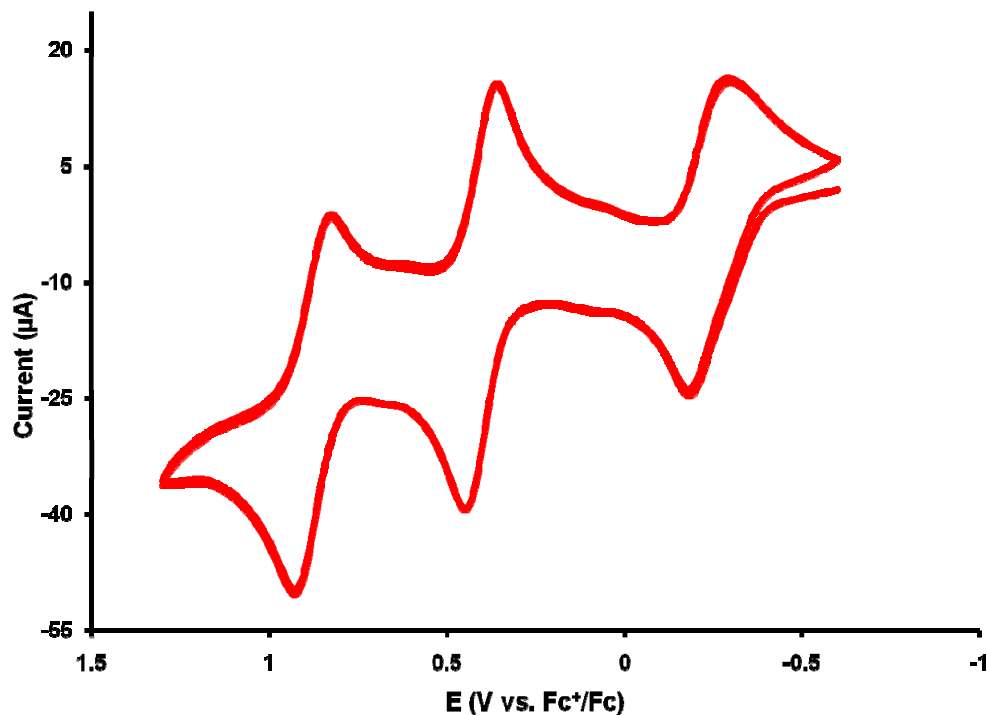


Figure 3-3. Cyclic voltammogram of $\text{Co}^{\text{II}}((\text{tBuPhO})_2\text{NHC})(\text{THF})$ in CH_3CN containing 0.1 M $[\text{nBu}_4\text{N}][\text{PF}_6]$ at a 10 mm Pt electrode. Scan rate: 0.1 V s^{-1} . Temperature: 22°C .

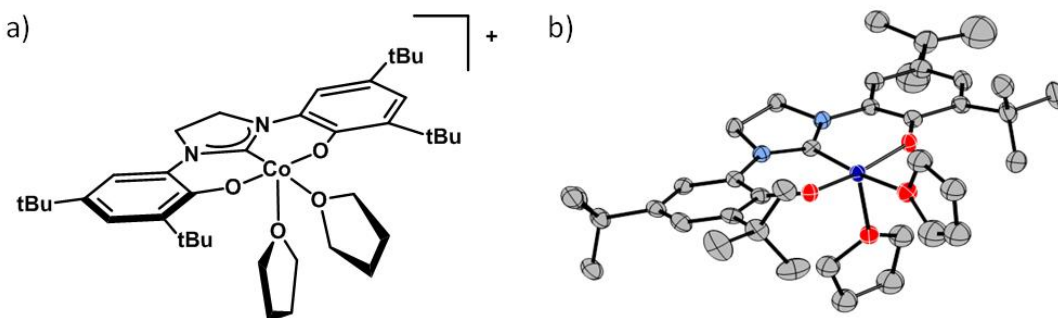
V, and 0.830 V from the open circuit potential of -1.16 V vs Fc^+/Fc in a 0.1 M solution of $[\text{nBu}_4\text{N}][\text{PF}_6]$ in CH_3CN (**Figure 3-3**). The three oxidation waves correspond to formal oxidation of the Co^{II} center to Co^{III} , Co^{IV} , and Co^{V} . These formally correspond to generation of Co^{IV} and Co^{V} but the paucity of stable $\text{Co}^{\text{IV}}/\text{Co}^{\text{V}}$ complexes makes such an assignment unlikely. Therefore chemical oxidation/isolation of the oxidized material was pursued.

3.2.3 Synthesis and characterization of $[\text{Co}((\text{tBuPhO})_2\text{NHC})(\text{THF})_2]\text{BF}_4$

Addition of 1 equiv of AgBF_4 to a THF solution containing **1** immediately generated a green solution. Filtration and drying *in vacuo* gave a green powder. Crystals suitable for X-ray diffraction were grown from a metathesis reaction between the green powder and $\text{Na}[\text{B}(\text{Ph})_4]$ in THF. The resulting green solution was layered with pentane at $-30\text{ }^\circ\text{C}$ for 24 h to precipitate green crystals of $[\text{Co}((\text{tBuPhO})_2\text{NHC})(\text{THF})_2](\text{BPh}_4)$ (**2**). The solid-state structure of **2** shows a cationic, quasi-square pyramidal arrangement of the $[(\text{tBuPhO})_2\text{NHC}]^{2+}$ ligand and two THF molecules in axial and equatorial positions about cobalt with a $[\text{BPh}_4]^-$ counter ion with approximate C_s symmetry. The UV–Vis spectrum of **2** shows a charge transfer bands at 434 nm ($\epsilon = 3100\text{ M}^{-1}\text{ cm}^{-1}$), 747 ($\epsilon = 2700\text{ M}^{-1}\text{ cm}^{-1}$), and 878 ($\epsilon = 2000\text{ M}^{-1}\text{ cm}^{-1}$) in THF (**Figure 3-2**). Evan's method analysis in oxygen-free THF-d_6 gives a $\mu_{\text{eff}} = 2.96$ of **2** suggesting a $S = 1$ spin state.

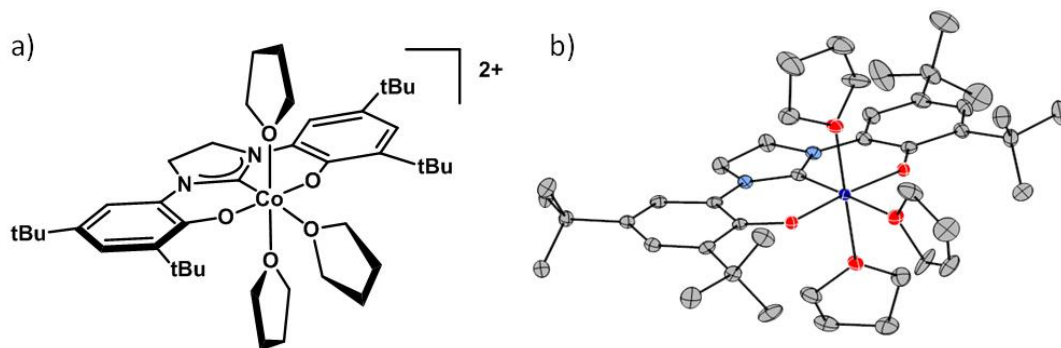
3.2.4 Synthesis and characterization of $[\text{Co}((\text{tBuPhO})_2\text{NHC})(\text{THF})_3](\text{PF}_6)_2$

Scheme 3-3. a) $[\text{Co}((\text{tBuPhO})_2\text{NHC})(\text{THF})_2]^+$ (**2**) b) Solid-state structure of $[\text{Co}^{\text{III}}((\text{tBuPhO})_2\text{NHC})(\text{THF})_2]\text{BPh}_4$ (**2**) drawn with 50 % probability ellipsoids. Hydrogen and counter ions omitted for clarity.



The addition of 2 equiv of $[\text{N}(\text{PhBr-}i>p\text{)}_3]\text{PF}_6$ to a CH_2Cl_2 solution containing **1** lead to an immediate color change to green. The green solution was filtered and dried in

Scheme 3-4. a) $[\text{Co}((\text{tBuPhO})_2\text{NHC})(\text{THF})_3]^{2+}$ (**2**) b) Solid-state structures of $[\text{Co}^{\text{III}}((\text{tBuPhO})_2\text{NHC})(\text{THF})_3](\text{PF}_6)_2$ (**3**) drawn with 50 % probability ellipsoids. Hydrogen and counter ions omitted for clarity.



vacuo to produce a green powder. Dissolution in THF followed by layering with pentane afford green single crystals suitable for X-ray diffractometry, which shows a dicationic, octahedral arrangement of the $[(\text{tBuPhO})_2\text{NHC}]^{2-}$ ligand and three THF molecules in meridian arrangement about cobalt with approximate C_{2v} symmetry (**Scheme 3-4 a**). Evan's method analysis in oxygen-free THF-d_6 gives a $\mu_{\text{eff}} = 2.51$. Complex **3** has an $\mu_{\text{eff}} = 2.51$ larger than the spin only case of 1.73, and like **1** is assigned a spin state of $S = 1/2$ with one unpaired electron. The UV–Vis spectrum of **2** shows charge transfer bands at 436 nm ($\epsilon = 2700 \text{ M}^{-1}, \text{ cm}^{-1}$), 456 ($\epsilon = 2700 \text{ M}^{-1}, \text{ cm}^{-1}$), 585 ($\epsilon = 1000 \text{ M}^{-1}, \text{ cm}^{-1}$), 805 ($\epsilon = 1700 \text{ M}^{-1}, \text{ cm}^{-1}$), and 874 ($\epsilon = 1600 \text{ M}^{-1}, \text{ cm}^{-1}$) in THF (**Figure 3-2**). Complex **3** shows a similar broad absorption spectra around 800 nm as seen in complex **2**.

3.2.5 Metrical parameters for the assignment of metal and ligand oxidation states of complexes **2** and **3**

A comparison of the metrical parameters for **1**, **2**, and **3**, shown in **Figure 3-4**, is informative. Using **1**, Co^{II} bound to a closed-shell fully reduced [(tBuPhO)₂NHC]²⁻ ligand, as a reference point, the respective bond lengths in complexes **2** and **3** can be compared. Complex **2** has an average C–C bond length of 1.398 Å which is similar to the average C–C bond length seen in **1** (1.394 Å), demonstrating that both phenolate rings are aromatic. Therefore the oxidation is metal centered to generate a Co^{III}. The consequence of metal centered oxidation is observed in the Co–O and Co–C bonds.

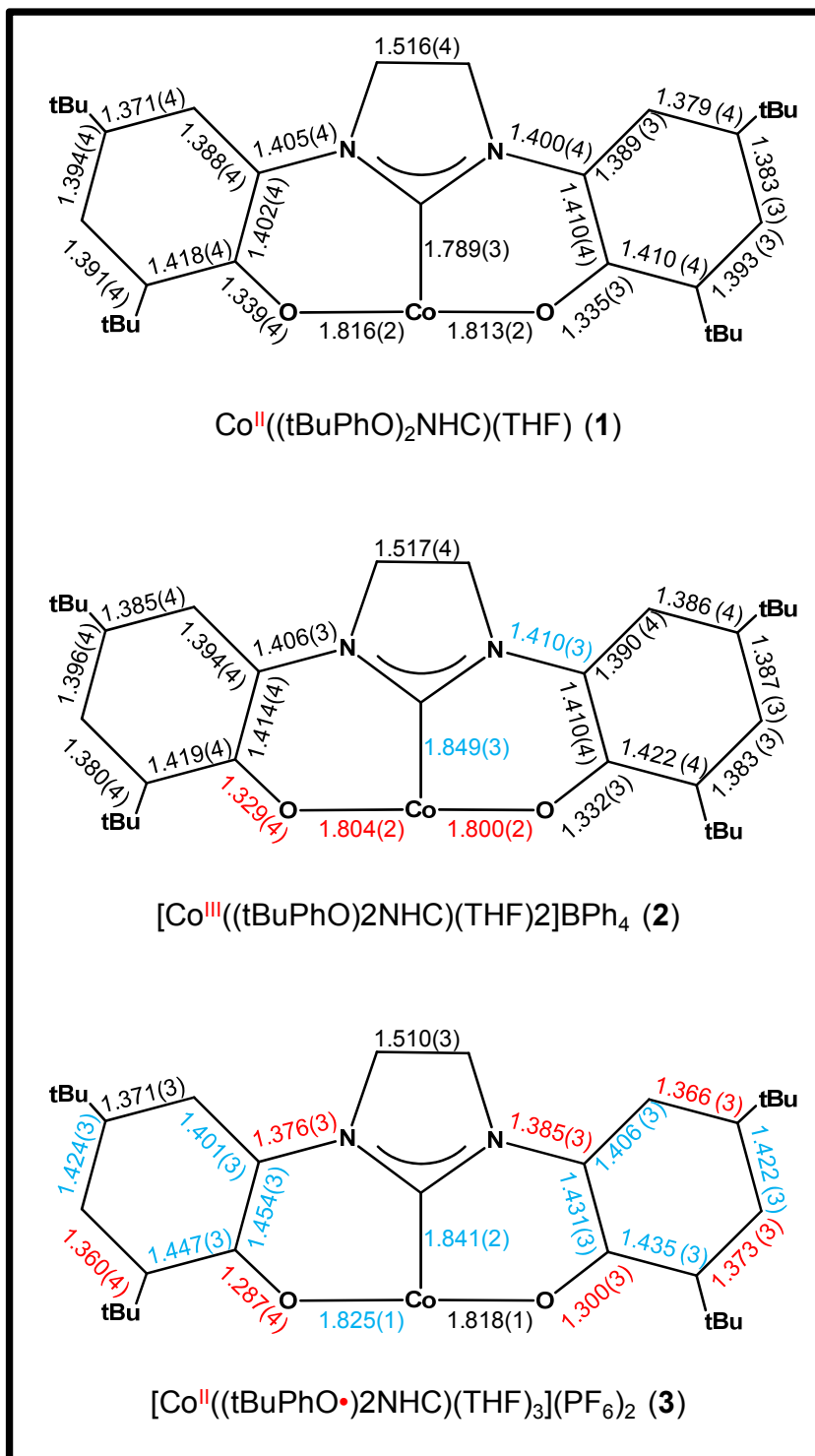
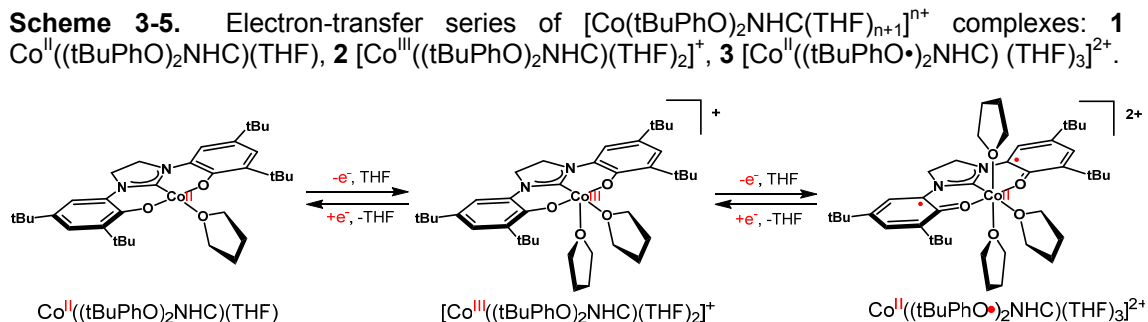


Figure 3-4. Selected bond lengths (Å) of the CoNHC electron-transfer series (**red** bond lengths represent contracted bond lengths and **blue** represents elongated bond lengths vs 1). Hydrogen, THF, and counter-ions have been omitted for clarity.

the C–O bond is most consistent with a C=O. Further evidence for the assignment of C=O comes from the IR spectra where a CO stretching frequency at 1681 cm^{-1} and its overtone at 3326 cm^{-1} are indicative of a C=O stretch. Both IR bands are lacking in complexes **1** and **2**. The Co–O bond distances of **3** ($1.825(3)\text{ \AA}$ and $1.818(3)\text{ \AA}$) are comparable to **1** and implies a lack of oxidation at the metal center consistent with Co^{II} . Complex **3** is thus more similar to a bis-quinone complex $[\text{Co}^{\text{II}}(\text{tBuPhO}\cdot)_2\text{NHC}]^{2+}$.³² Taken together, complex **1**, **2**, and **3** form an new ET series capable of spanning $2e^-$ as shown in

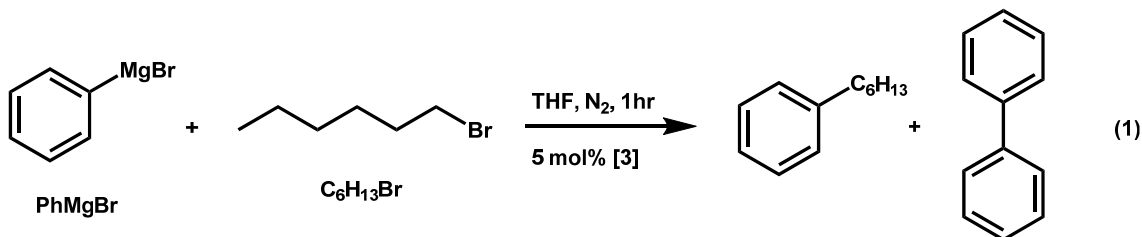
Scheme **3-5.**



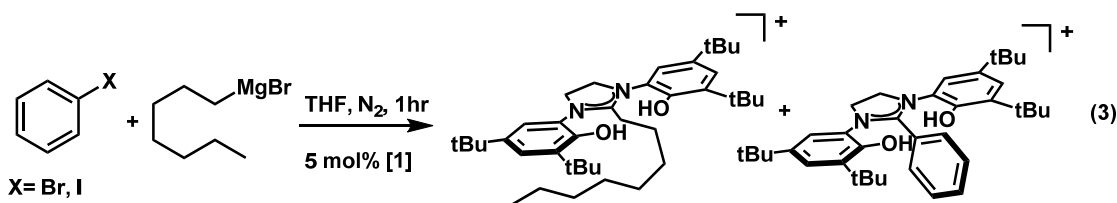
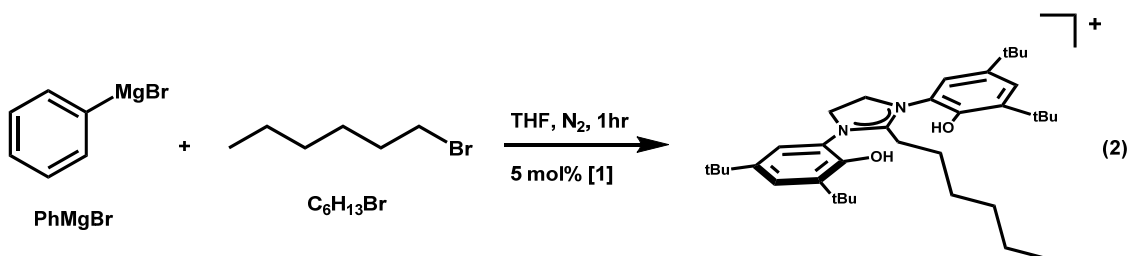
3.2.6 Cross-coupling reactions of aryl Grignard and alkylhalide

Cross-coupling of 1-bromohexane and PhMgBr was accomplished using 5 mol% of **3** under N_2 in THF for 1 hour and led to yield of 38% cross-coupled product Ph-Hx vs **3** or 1.2 % vs PhMgBr (**Equation 1**). Biphenyl was obtained as a byproduct in 26% yields vs. the PhMgBr reactant. The cross-coupled product represents 3x increase in yield vs metal compared to the previously reported $[\text{Co}^{\text{III}}(\text{ap}^{\text{Ph}})]^{1-}$ complex.³³ The high yield of the homocoupled product biphenyl suggested 1-bromohexane could be functioning as a sacrificial oxidant, evidenced by observation of hexane at the end of the reaction. Increasing the catalyst loading of **1** to 10 mol % for the reaction in **Equation 1** yielded 60% of 1-phenylhexane cross-coupling product vs. metal and a 6% overall yield

of 1-phenylhexane along with 43% of the biphenyl homocoupling product vs Grignard. If



3 equiv of triphenylphosphine were added to the reaction of **1** the yield of cross-coupling increases to 10 % vs. the organic reactants (100 % vs. **1**). The biphenyl production is also increased to 62% vs. the PhMgBr reactant. After 24 hrs **1** has degraded and no metal containing species are observed via ESI-MS spectroscopy. However, ligand degradation was observed in ESI-MS, where a peak of 563.6 m/z was assigned to the alkylated ligand (563.4 m/z) as shown in **Equation 2**. This ligand degradation was also observed with other alkyl halides (ethyl bromide, 1-bromooctane). In all three cases no metal containing species was observed by ESI-MS, the crossed coupled product



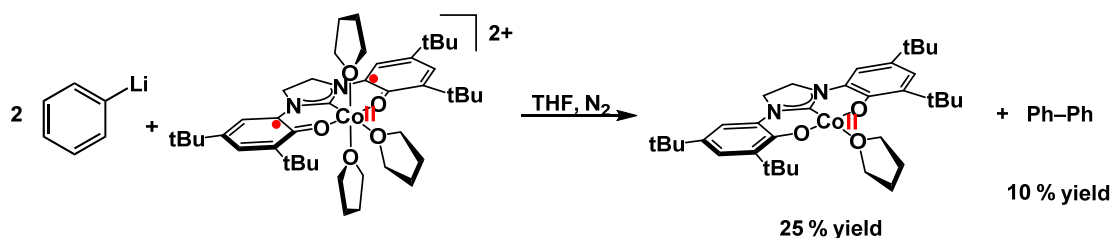
between the ligand and the alkyl halide were the only identifiable peaks. Phenyl from the Grignard reagent was never incorporated into the ligand. However when an aryl halide (bromobenzene or iodobenzene) and octyl magnesium bromide were reacted in the

presence of 10 mol % of **1**, both an alkylated and arylated ligand were formed (**Equation 3**).

3.2.7 Reductive elimination and oxidative addition studies

A reaction between **3** and 2 equiv of PhMgBr gives a 50% yield of biphenyl and a metal species with a UV–vis spectrum that is distinct from **1**, **2**, or **3**. A reaction of **3** with 2 equiv of PhLi leads to a smaller yield (10%) of biphenyl but generated **1** in a 25% yield. The observation of biphenyl and **1** suggest $2 e^-$ reductive elimination is viable (**Scheme 3-6**), however the low yields of homocoupled product and the new unknown metal-containing species highlights the potential for off cycle reactions. To probe off cycle

Scheme 3-6. PhLi homocoupling via reductive elimination using **3** to generate 25 % **1** and 10 % Ph–Ph.



pathways in reductive elimination, **1** was titrated with PhMgBr. On addition of 2.0 equiv of PhMgBr, the Co^{II}((tBuPhO)₂NHC)THF concentration was reduced to 19% of its initial concentration, as determined by UV–vis spectroscopy. Addition of 3.0 equiv of PhMgBr resulted in a complete loss of absorbance at 420 nm and a 35% yield of biphenyl. When methanol was added to quench the Grignard, 65% of **1** was regenerated as judged by UV–vis.

Oxidative addition to complex **1** was attempted using ethyl bromide (EtBr) or methyl iodide (MeI) in a 1:1 ratio. However, neither alkyl halide induced a color change of the aforementioned **1** within 24 hrs, however in the case of MeI, a reaction is

observed in the course of 7 days that lead to a green solution. The UV–vis spectra shows a loss of absorption at 420 nm and broad feature at 650 nm ($\epsilon = 500 \text{ M}^{-1}, \text{ cm}^{-1}$). No metal containing peaks could be identified by ESI–MS. Furthermore, the solid powder produced did not yield single crystals.

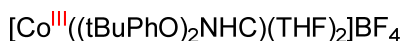
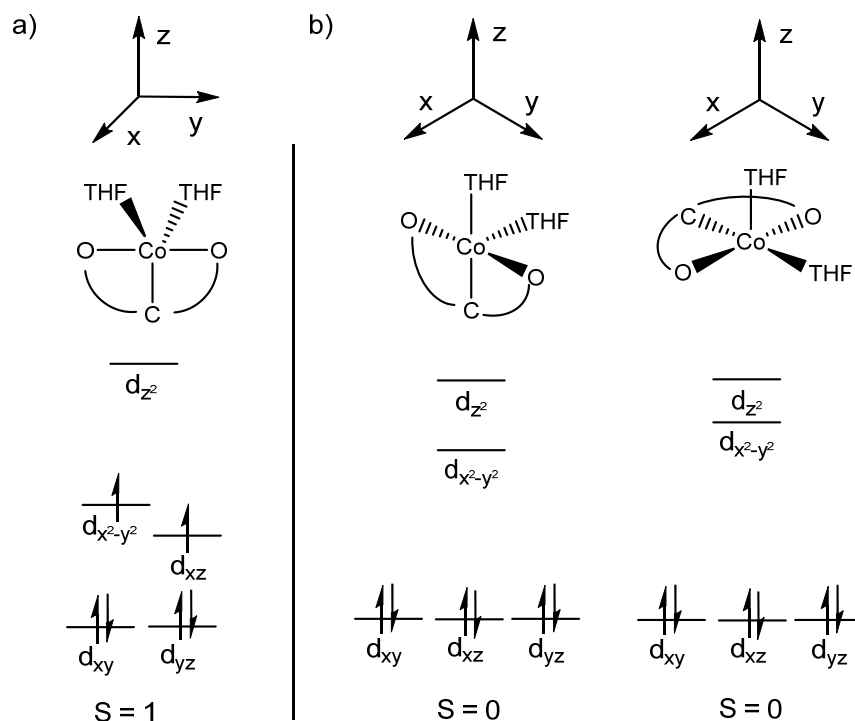
3.3 Discussion

To improve the cross-coupling ability of $[\text{Co}^{\text{III}}(\text{ap}^{\text{Ph}})_2]^-$, a cobalt complex with available *cis* sites and redox-active ligands was desired. A tridentate N-heterocyclic carbene with two phenol arms was chosen to accomplish these goals. Addition of the deprotonated $[(\text{tBuPhO})_2\text{NHC}]^{2-}$ ligand to CoCl_2 lead to a square planer complex with the $[(\text{tBuPhO})_2\text{NHC}]^{2-}$ coordinated in a meridional fashion with a THF *trans* to the carbene $\text{Co}^{\text{II}}((\text{tBuPhO})_2\text{NHC})(\text{THF})$ **1**. This allowed for two vacant axial positions and a labile equatorial THF. This satisfies the first objective of obtaining available *cis* sites on a cobalt complex. The CV of **1** shows three oxidation waves assigned to the formal oxidation of the metal center to Co^{III} , Co^{IV} , and Co^{V} . However, experimentally, these are unlikely do to how exceedingly rare and unstable Co^{IV} and Co^{V} complexes are.³⁴ This suggests that the ligand is acting as an electron reservoir which avoids high oxidation states of cobalt, and gives evidence that the second objective could be accomplished.

Complex **1** is best described as a Co^{II} bound to a triply deprotonated tridentate meridional bound $[(\text{tBuPhO})_2\text{NHC}]^{2-}$ with one THF bound *trans* to the carbene. The X-ray crystal structure reveals the ligand to be in the fully reduced closed-shell dianionic form. The 1 and 2 e^- oxidized forms of **1**, a new ET series as shown above **Scheme 3-5**, are best described as metal oxidation (complex **2**) followed by a re-reduction of the metal concomitant with a $2e^-$ oxidation of the ligand (complex **3**). In contrast, the $(\text{Co}^{\text{III}}(\text{ap}^{\text{Ph}})_2)^-$ ET series when oxidized is only oxidized at the ligands and remains Co^{III} in the ET series. The $(^{\text{IPr}}\text{PDI})\text{Fe}^0(\text{CO})_2$ ET series, produced by Chirik and co-workers, also

shows the same interesting redox chemistry. For instance, a 1 e⁻ oxidation of (ⁱPrPDI)Fe⁰(CO)₂ affords an Fe^I complex ((ⁱPrPDI)Fe^I(CO)₂)⁺ and 1 e⁻ reduction lead to an Fe^I complex with a doubly reduced ligand ((ⁱPrPDI²⁻)Fe^I(CO)₂)⁻.³⁵

Scheme 3-7 A simplified MO diagram for complex **2**.

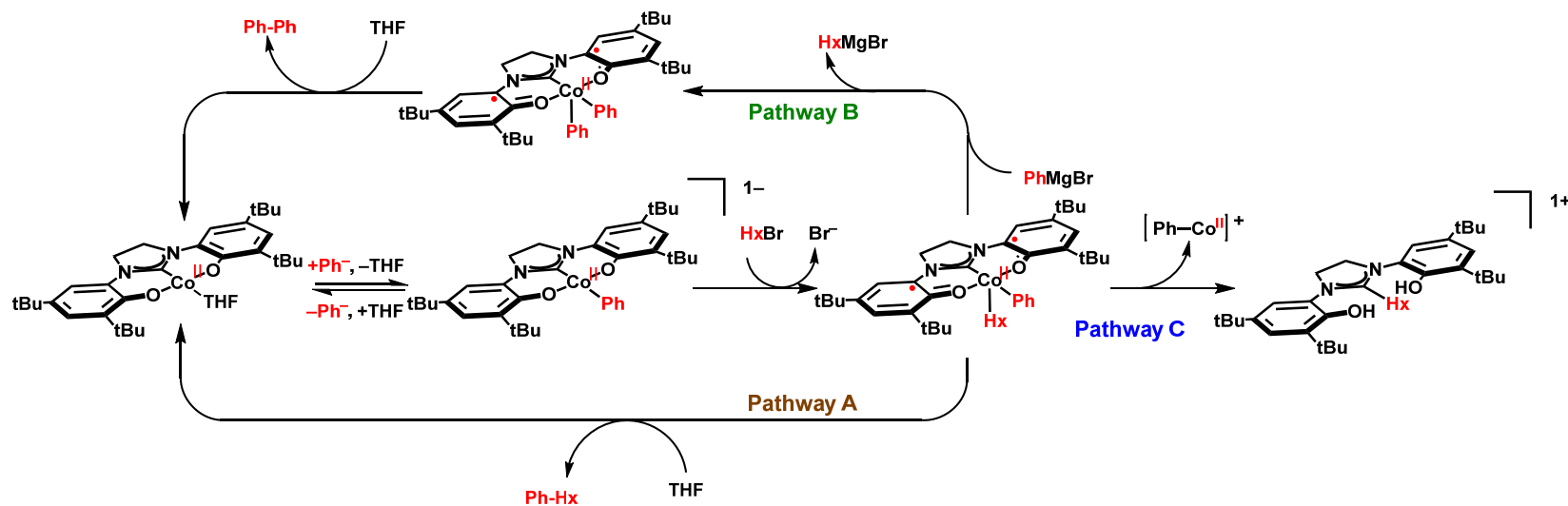


Assignment of the spin states for complexes **1** and **3** is straightforward. In the case of **1** a low spin d⁷ Co^{II} bound to a closed shell ligand in an square planar field has one unpaired e⁻, and in agreement with this prediction the measured magnetic moment observed $\mu_{\text{eff}} = 2.37$ leads to an assigned spin state of $S = 1/2$. Complex **3** has a magnetic moment $\mu_{\text{eff}} = 2.51$ and a spin state of $S = 1/2$. Assuming the Co^{II} center in **3** is also in a strong ligand field, there are a total of three spins to account for, one on the metal and two on the radical ligands, giving possible $S = 1/2$ and $S = 3/2$ spin states. The experimentally observed moment of $\mu_{\text{eff}} = 2.51$ implies that a ligand spin couples

antiferromagnetically with the metal. Complex **2** has a magnetic moment $\mu_{\text{eff}} = 2.96$ and a spin state of $S = 1$. A spin state of $S = 1$ precludes a high spin assignment which would be $S = 2$ for a d^6 Co in a square pyramidal field. This is in agreement with how rare high spin octahedral Co^{III} complexes are.³⁶ A simple molecular orbital (MO) diagram (**Scheme 3-7**) offers a possible explanation. If complex **2** has a square pyramidal geometry, as seen in the solid state, then both high spin and intermediate spin complex seem unlikely due to the large energy difference between the HOMO and LUMO which arises from molecular overlap of the ligand and THF molecules with the d_{z^2} and $d_{x^2-y^2}$ exclusively (**Scheme 3-7 b**). However, if a trigonal bipyramidal geometry is adopted in solution (**Scheme 3-7 a**) then the energy difference between the $d_{x^2-y^2}$ and d_{xz} orbitals decreases and the two orbitals ($d_{x^2-y^2}$, d_{xz}) become nearly degenerate. Furthermore, the gap between the d_{z^2} and $d_{x^2-y^2}$ and d_{xz} orbitals becomes large due to the strong σ -donation from the carbene to the d_{z^2} orbital, precluding it from being occupied. This arrangement gives rise to the intermediate spin $S = 1$ observed in complex **2**. A similar square planar intermediate spin Co^{III} complex $\text{Co}^{\text{III}}(\text{ap}^{\text{Ph}})(\text{isq}^{\text{Ph}})$ has also been reported.³ In this system, an intermediate spin $S = 1$ Co^{III} ion is antiferromagnetically coupled with the ligand radical $[\text{isq}^{\text{Ph}}]^-$ yielded an $S = 1/2$ spin state.

Given the ability of this new electron-transfer series to span multiple oxidation states, Kumada-type cross coupling was attempted (PhMgBr and 1-bromohexane (HxBr)) with 5 % mol or 10% of **3** or **1** respectively. In all cases, cross-coupled product were low (1.4 - 10%) and homocoupled products were high (26 %). There are several possibilities to explain the high homocoupled product compared to the cross-coupled product (**Scheme 3-8**).

Scheme 3-8. Proposed cross-coupling catalytic cycle mechanism between PhMgBr and 1-bromohexane in the presences of **1**



Pathway A consists of a carboanion (Ph^-) first binding to the cobalt, followed by oxidative addition then reductive elimination to regenerate complex **1**. The first oxidation potential of complex **1** is much more positive of (-0.35 mV vs Fc^+/Fc) than that of the cobalt bisamidophenolate species (-1.4 mV) which can oxidatively add alkyl halides.³ Accordingly, oxidative addition of alkyl halide does not happen with complex **1** except in the case of methyl iodine which takes 7 days to produce a color change. But binding an aryl nucleophile should make the complex much more reducing and might initiate an oxidative addition reaction with HxBr . To probe this assumption 1 equiv of triphenylphosphine or pyridine were added, and an increase in both the homocoupled and cross-coupled product yields were observed. Although the imposed steric congestion upon addition of $\text{P}(\text{Ph})_3$ or pyridine can not be ruled out as the driving force for increased coupling. Oxidative addition of the alkyl halide to complex **1** with a bound aryl (Co-Ph) then leads to complex **3** with two *cis* organic products positioned to carry out C–C bond forming cross-coupling. Pathway A is slow compared to the other pathways as evidenced by the low amount of cross-coupling that is achieved.

Pathway B is proposed to explain the increase in homocoupled product biphenyl compared to cross-coupled Ph-Hx . Here transmetalation between PhMgBr and Hx^- lead to HxMgBr and $\text{Co}(\text{Ph})_2((\text{tBuPhO}\bullet)_2\text{NHC})$, as evidenced by hexane present in the solution after a MeOH quench. Then reductive elimination could occur to regenerate **1** and produce biphenyl. Reactions with isolated **3** and 2 equiv of PhMgBr lead to a homocoupled yield of 50 % demonstrating the viability of this proposed step. However, the stoichiometric reactions produce an unidentified metal species. In contrast, addition of 2 equiv of PhLi to **3** gives 25 % yield of biaryl and 25 % of complex **1** as judged by UV–Vis. This pathway must be very fast given the high yields and competing pathways.

Pathway C represents a decomposition pathway that might occur under these conditions. The observation of the alkylated and arylated $[\text{tBuPhO})_2\text{NHC}(\text{R})]^+$ (**Equation 2** and

Equation 3) ligand suggests that $\text{Co}^{\text{II}}(\text{Ph})(\text{Hx})(\text{tBuPhO})_2\text{NHC}$, generated by oxidative addition, might be prone to C–C reductive elimination to the carbene carbon in the ligand or alkyl migration. Consistent with this hypothesis, no metal containing species were observed by ESI after the reaction. Presumably because the metal byproduct would be a dissolved form of Co^{II} . The migration of an alkyl to the carbene carbon of the NHC ligand has been shown in an analogous structure $\text{ZnCl}(\text{CH}_2\text{Ph})((\text{tBuPhO})_2\text{NHC})\text{THF}$ reported by Dagorne and co-workers.¹⁰ The $\text{ZnCl}(\text{CH}_2\text{Ph})((\text{tBuPhO})_2\text{NHC})\text{THF}$ complex decomposed upon heating to transfer the benzyl group to the carbene. Furthermore, $\text{Co}^{\text{II}}\text{Cl}_2$ is known to homocouple Grignards, which could also explain the large increase in biphenyl yield compared to Ph-Hx.³⁷ Pathway C must be faster than Pathway A but significantly slower than pathway B to allow both a high yield of homocoupled product and keep the complex intact long enough for cross-coupling of the PhMgBr and the 1-bromohexane.

While this mechanism explains most of the observed results it can not encompass all the reactivity present. For instance, alkyl halides, aryl halides and alkyl Grignards couple to the carbene ligand, however, aryl Grignards do not. Furthermore, if HxMgBr is generated in solution then cross-coupling of this alkyl Grignard (Hx-Hx) should be observed, however, Hx-Hx is not observed at the end of the reaction. Lastly, it cannot be ruled out at this time that a purely radical mechanism is driving the cross-coupling and homocoupling reactions, although this seems unlikely given that lack of diversity in the corresponding organic products e.g. no branched alkanes.

The new $\text{Co}^{\text{II}}((\text{tBuPhO})_2\text{NHC})\text{THF}$ ET series is able to span multiple electrons and has available *cis* sites for coupling reactions. However, oxidative addition could not be accomplished in the stoichiometric reactions between **1** and alkyl halides. Although $\text{Co}^{\text{II}}((\text{tBuPhO})_2\text{NHC})\text{THF}$ ET series can cross-couple 1-bromohexane to PhMgBr under catalytic

conditions, the yields 10 % is low. Interaction with the ligand hinders cross-coupling and ultimately the utility of this ET series towards Kumada-type coupling.

3.4 Conclusion

Utilizing cobalt and the redox-active 1,3-bis(3,5,-di-tert-butylphenolate)dihydroimidazol-2-ylidene $[(tBuPhO)_2NHC]^{2-}$ produces a new electron-transfer series spanning 3 accessible oxidation states. Solid-state structures of the three isolated complexes reveals oxidation events occurring at both the metal and ligand. The $[Co((tBuPhO)_2NHC)(THF)_{n+1}]^{n+}$ series can be used for homocoupling (carbanions) or cross-coupling of (alkyl halides (sp^2) and aryl Grignards (sp^3)), forming C–C bonds using the ligand as an electron reservoir, but the C–C bond forming yields are low. Further work is focused on exploring the mechanistic aspects of the cross-coupling reaction in hopes of overcoming the challenges presented here.

3.5 Methods

3.5.1 General considerations

Unless otherwise noted, all manipulations were performed under anaerobic conditions using standard vacuum line techniques, or in an inert atmosphere glove box under purified nitrogen. UV–visible absorption spectra were acquired using a Varian Cary 50 spectrophotometer. IR spectra were obtained using attenuated total reflection (ATR) with a diamond plate on a Thermo-Scientific Nicolet 4700 Fourier-transform infrared spectrophotometer. All NMR spectra were acquired on a Varian Mercury 300 spectrometer (300.323 MHz for 1H) at ambient temperature. Chemical shifts are reported in parts per million (ppm) relative to TMS, with the residual solvent peak serving as an internal reference. Solution state magnetic moments were determined by Evans' NMR method.³⁸⁻³⁹ Unless otherwise

Table 3-1 Crystallographic data and parameters for complexes $\text{Co}^{\text{II}}((\text{tBuPhO})_2\text{NHC})(\text{THF})$ **1**, $[\text{Co}^{\text{III}}((\text{tBuPhO})_2\text{NHC})(\text{THF})_2]\text{BPh}_4$ **2**, and $[\text{Co}^{\text{II}}((\text{tBuPhO})_2\text{NHC})(\text{THF})_3](\text{PF}_6)_2$ **3**.

Complex	1	2	3
Empirical formula	$\text{C}_{35}\text{H}_{52}\text{CoN}_2\text{O}_3$	$\text{C}_{63}\text{H}_{80}\text{BCoN}_2\text{O}_4$	$\text{C}_{43}\text{H}_{68}\text{CoF}_{12}\text{N}_2\text{O}_5\text{P}_2$
Formula weight	607.72	999.03	1041.86
T (K)	173(2)	173(2)	110.15
Crystal system	Triclinic	Monoclinic	Orthorhombic
Space group	$\text{p}\bar{1}$	$\text{P2}_1/\text{n}$	Pbca
Unit cell dimensions			
<i>a</i> (Å)	10.371(3)	10.3466(15)	11.2128(3)
<i>b</i> (Å)	13.964(4)	21.707(3)	18.8423(4)
<i>c</i> (Å)	24.225(6)	25.532(4)	46.5193(11)
α (°)	84.881(4)	90	90
β (°)	81.155(4)	97.871(2)	90
γ (°)	72.358(4)	90	90
<i>V</i> (Å ³)	3300.2(14)	5680.3(14)	9828.4(4)
<i>Z</i>	4	4	8
<i>D</i> _{calc} (g cm ⁻³)	1.223	1.168	1.408
Absorption coefficient (mm ⁻¹)	0.555	0.349	0.504
Crystal size (mm)	0.22 x 0.10 x 0.05	0.34 x 0.27 x 0.13	0.53 x 0.16 x 0.08
θ range for data collection (°)	1.53 to 27.48	1.24 to 28.50	1.75 to 26.37
Index ranges	-13 ≤ <i>h</i> ≤ 13 -18 ≤ <i>k</i> ≤ 18 -31 ≤ <i>l</i> ≤ 31	-13 ≤ <i>h</i> ≤ 13 -28 ≤ <i>k</i> ≤ 29 -34 ≤ <i>l</i> ≤ 34	-14 ≤ <i>h</i> ≤ 11 -23 ≤ <i>k</i> ≤ 23 -40 ≤ <i>l</i> ≤ 57
Reflections collected/unique	55151/15117	98957/14288	58160/10017
Goodness of fit on <i>F</i> ²	1.038	1.020	1.039
<i>R</i> [<i>I</i> > 2σ(<i>I</i>)]	<i>R</i> 1 = 0.0607, <i>wR</i> 2 = 0.1274	<i>R</i> 1 = 0.0689, <i>wR</i> 2 = 0.1690	<i>R</i> 1 = 0.0464, <i>wR</i> 2 = 0.1092
<i>wR</i> ₂ (all data)	<i>R</i> 1 = 0.1198, <i>wR</i> 2 = 0.1513	<i>R</i> 1 = 0.1170, <i>wR</i> 2 = 0.1908	<i>R</i> 1 = 0.0667, <i>wR</i> 2 = 0.1196

specified, all electronic absorption spectra were recorded at ambient temperatures in 1cm

quartz cells. All mass spectra were recorded in the Georgia Institute of Technology Bioanalytical Mass Spectrometry facility. Cyclic voltammetric measurements were made using a CH Instruments CHI620C potentiostat in a three component cell consisting of a platinum disk working electrode, a platinum wire auxiliary electrode, and a non-aqueous AgNO_3/Ag reference electrode. All electrochemical experiments were performed in CH_3CN with 0.1 M $[\text{nBu}_4\text{N}][\text{PF}_6]$ as the supporting electrolyte. Electrochemical data are referenced and reported to Fc^+/Fc as an internal standard. Elemental analyses were performed by Atlantic Microlab, Inc., Norcross, GA. All analyses were performed in duplicate, and the reported compositions are the average of the two runs.

Single crystals of $[\text{Co}((\text{tBuPhO})_2\text{NHC})]$, $[\text{Co}((\text{tBuPhO})_2\text{NHC})](\text{BPh}_4)$, and $[\text{Co}((\text{tBuPhO})_2\text{NHC})](\text{PF}_6)_2$ suitable for X-ray diffraction analysis were coated with Paratone N, suspended in a small fiber loop and placed in a cooled nitrogen gas stream at 173 K on a Bruker D8 APEX II CCD sealed tube diffractometer. Diffraction data for $[\text{Co}((\text{tBuPhO})_2\text{NHC})]$, $[\text{Co}((\text{tBuPhO})_2\text{NHC})](\text{BPh}_4)$, and $[\text{Co}((\text{tBuPhO})_2\text{NHC})](\text{PF}_6)_2$ was collected using graphite monochromated $\text{Cu K}\alpha$ ($\lambda = 1.54178 \text{ \AA}$) radiation. Data were measured using a series of combinations of phi and omega scans with 10 second frame exposures and 0.5° frame widths. Data collection, indexing and initial cell refinements were all carried out using APEX II software.⁴⁰ Frame integration and final cell refinements were done using SAINT software.⁴¹ The final cell parameters were determined from least-squares refinement on 55151 reflection for $\text{Co}((\text{tBuPhO})_2\text{NHC})$, 98957 reflection for $[\text{Co}((\text{tBuPhO})_2\text{NHC})](\text{BPh}_4)$, and 59074 for $[\text{Co}((\text{tBuPhO})_2\text{NHC})](\text{PF}_6)_2$. The structure was solved using direct methods and difference Fourier techniques using the SHELXTL program package.⁴² Hydrogen atoms were placed in their expected chemical positions using the HFIX command and were included in the final cycles of least-squares with isotropic U_{ij} 's related to the atoms ridden upon. All non-hydrogen

atoms were refined anisotropically. Details of data collection and structure refinement are provided in **Table 1**.

3.5.2 Methods and materials

Anhydrous dichloromethane and pentane solvents for air- and moisture-sensitive manipulations were purchased from Sigma–Aldrich, further dried by passage through columns of activated alumina, degassed by at least three freeze-pump-thaw cycles, and stored under N₂. Anhydrous tetrahydrofuran (THF) purchased from Sigma–Aldrich was further dried by stirring over Na(s) in the presence of benzophenone until a dark purple color was achieved (~1 day), followed by THF removal *in vacuo* and storage under N₂. The ligand (N,N'-Bis(2-hydroxy-3,5-di-tert-butylphenyl)ethylenediamine = H₄en^{ap/ap}) was prepared by literature methods and all characterization data matched those referenced.⁴³ All chemicals were purchased from Sigma–Aldrich and used as received.

Synthesis of 1,3-bis(2-hydroxy-3,5-di-tert-butylphenyl)imidazolium chloride ([(tBuPhO)₂NHC]Cl)

In a modified procedure from literature,⁴⁴ a 500 mL round bottom flask was charged with H₄en^{ap/ap} (2.00 g, 4.27 mmol), NH₄Cl (0.224 g, 4.57 mmol), triethyl orthoformate (0.710 mL, 4.27 mmol), stir bar and 75 mL of isopropanol. The resulting green solution was refluxed at 120 °C for 4 hours producing a golden solution. Removal of solvent *in vacuo* produced a white powder. Recrystallization from anhydrous ether gave a white crystalline product of [(tBuPhO)₂NHC]Cl (1.75 g, 76% yield). All characterization data matched those referenced.¹²

Synthesis of Co((tBuPhO)₂NHC)THF (1)

A 20 mL scintillation vial was charged with anhydrous CoCl₂ (0.0649 g, 0.5 mmol), a Teflon stir bar, [(tBuPhO)₂NHC]Cl (0.257 g, 0.5 mmol), and 0.5 M NaOMe in MeOH (3 mL, 1.5

mmol) to afford an orange solution. After an additional minute of stirring, the solution was removed *in vacuo* to generate an orange powder. The collected orange powder was dissolved in THF (5 mL) and filtered through a fine Buchner funnel and the filtrate was dried *in vacuo* to generate Co((tBuPhO)₂NHC)THF (0.275 g, 90% yield) UV-vis (THF) λ_{max} , nm (ϵ , M⁻¹, cm⁻¹): 430 (5.3 x 10³) Anal. Calc. for C₃₅H₅₃CoN₂O₃Na_{0.5}Cl_{0.5}: C, 66.00; H, 8.23; N, 4.40. Found: C, 65.89; H, 8.44; N, 4.43%. FTIR (ATR): 2947(m), 2899(m), 2866(m), 1506(s), 1478(m), 1447(m), 1389(m), 1358(m), 1325(s), 1283(m), 1270(m), 1240(m), 1200(m), 1159(m), 1076(m), 1051(m), 914(m), 894(m), 869(m), 836(m), 756(m), 699(m), 643(m), 605(m), 578(m), 545(m), 512(m), 466(m), 434(m), 419(m) cm⁻¹.

Synthesis of [Co((tBuPhO)₂NHC)(THF)₂]BF₄ (2)

A 20 mL scintillation vial was charged with **1** (0.103 g, 0.164 mmol), a Teflon stir bar, THF, and AgBF₄ (0.032 g, 0.164 mmol) to afford a dark green solution. After 5 min of stirring, the green solution was layered with pentane and stored at -30 °C for 24 hours to collect green crystals of [Co((tBuPhO)₂NHC)(THF)₂]BF₄ (0.105 g, 83% yield). Single crystals suitable for X-ray analysis were generated from the metathesis reaction between a THF solution containing **2** and NaB(Ph)₄. The resulting green solution was filtered and layered with pentane to generate crystals of [Co((tBuPhO)₂NHC)(THF)₂]B(Ph)₄ UV-vis (THF) λ_{max} , nm (ϵ , M⁻¹, cm⁻¹): 434 (3.1 x 10³), 747 (2.7 x 10³), 878 (2.0 x 10³). The report analysis is for [Co((tBuPhO)₂NHC)(THF)_{2.65}]]BF₄ • 0.2 AgBF₄. Anal. Calc. for C₃₉H₅₈BCoF₄N₂O₄ • (THF)_{0.65} • (AgBF₄)_{0.2}: Calc., 58.75; H, 7.49; N, 3.29. Found: C, 58.40; H, 7.84; N, 3.63%. FTIR (ATR): 3054(m), 2953(m), 2902(m), 2865(m), 1588(m), 1556(m), 1478(m), 1440(m), 1388(m), 1359(m), 1311(m), 1241(m), 1200(m), 1124(m), 1071(m), 1026(m), 913(m), 843(m), 733(s), 700(s), 647(w), 625(m), 610(w), 580(w), 543(w), 518(w), 498(w), 471(w), 446(w), 400(w) cm⁻¹.

Synthesis of $[\text{Co}((\text{tBuPhO})_2\text{NHC})(\text{THF})_3](\text{PF}_6)_2$ (**3**)

A 20 mL scintillation vial was charged with $\text{N}(\text{C}_6\text{H}_4\text{Br-p})_3$ (0.0799 g, 0.166 mmol), a Teflon stir bar, NOPF_6 (0.032 g, 0.178 mmol), and CH_2Cl_2 (5 mL) to afford a dark blue solution. **Safety Caution:** NO gas is generated and proper ventilation is required! After 15 min of stirring, **1** (0.046 g, 0.075 mmol) was added to generate a brown/green solution. The collected brown/green solid was washed with MeCN (2 x 5 mL) through a fine Buchner funnel and the filtrate was dried *in vacuo*, taken up in THF (2 mL), filtered again through Celite, layered with pentane, and stored at -30°C to generate green crystals of $[\text{Co}((\text{tBuPhO})_2\text{NHC})(\text{THF})_3](\text{PF}_6)_2$ (0.064 g, 81% yield) UV-vis (THF) λ_{max} , nm (ϵ , M^{-1} , cm^{-1}): 436 (2.7×10^3), 456 (2.7×10^3), 585 (1.0×10^3), 805 (1.7×10^3), 874 (1.6×10^3). The report analysis is for $[\text{Co}((\text{tBuPhO})_2\text{NHC})(\text{THF})_3](\text{PF}_6)_2$. Anal. Calc. for $\text{C}_{35}\text{H}_{52}\text{CoF}_{12}\text{N}_2\text{O}_3\text{P}_2$: C, 46.83; H, 5.84; N, 3.12. Found: C, 46.48; H, 6.14; N, 3.34% FTIR (ATR): 3326 (w), 2956(m), 2905(m), 2872(m), 1681(w), 1627(w), 1592(m), 1531(w), 1484(s), 1352(m), 1309(m), 1284(m), 1266(m), 1239(m), 1195(m), 1159(m), 1117(m), 1059(m), 1024(w), 1007(w), 948(w), 902(w), 818(s), 739(m), 711(w), 694(w), 650(w), 556(s), 493(s), 436(w), 416(w).

Production of homocoupled product Ph-Ph.

In a representative procedure, a 20 mL scintillation vial was charged with **1** (0.500 mL, of a 1.60 mM stock solution in THF), PhMgBr (0.082 mL, of a 0.2 M stock solution in THF), and 5 mL of THF under N_2 and fitted with a teflon lined cap. The reaction was monitored by UV-vis spectroscopy (300-1000 nm). Yield of the cobalt species was determined by the absorption peak at 430 nm with $\epsilon = 5300 \text{ M}^{-1}$, cm^{-1} . To determine the biphenyl yield the solution was analyzed with GC-MS using decane as an internal standard and compared to a calibration plot.

Production of cross-coupled product Ph–Ph.

In a representative procedure, a 5 mL volumetric flask was charged with **1** (0.500 mL, of a 1.60 mM stock solution in THF), 1-bromohexane (0.289 mL, of a 0.28 M stock solution in THF), PhMgBr (0.412 mL, of a 0.2 M stock solution in THF), and filled to the line with THF under N₂. The solution was immediately transferred to a 20 mL scintillation vial charged with a stir bar and fitted with a teflon lined cap. The reaction was allowed to stir for 24 hours at room temperature. Yield of the cobalt species was determined by the absorption peak at 430 nm with $\epsilon = 5300 \text{ M}^{-1}, \text{ cm}^{-1}$. To determine the yield of both homo and cross-coupled products, the solution was analyzed with GC-MS using decane as an internal standard and compared to a calibration plot.

3.6 Works cited

1. Chirik, P. J.; Wieghardt, K., Radical Ligands Confer Nobility on Base-Metal Catalysts. *Science* **2010**, 327, 794-795.
2. Lyaskovskyy, V.; de Bruin, B., Redox Non-Innocent Ligands: Versatile New Tools to Control Catalytic Reactions. *ACS Catalysis* **2012**, 2, 270-279.
3. Smith, A. L.; Clapp, L. A.; Hardcastle, K. I.; Soper, J. D., Redox-active ligand-mediated Co–Cl bond-forming reactions at reducing square planar cobalt(III) centers. *Polyhedron* **2010**, 29, 164-169.
4. Smith, A. L.; Hardcastle, K. I.; Soper, J. D., Redox-Active Ligand-Mediated Oxidative Addition and Reductive Elimination at Square Planar Cobalt(III): Multielectron Reactions for Cross-Coupling. *J. Am. Chem. Soc.* **2010**, 132, 14358-14360.
5. Szigethy, G.; Heyduk, A. F., Steric and Electronic Consequences of Flexibility in a Tetradentate Redox-Active Ligand: Ti(IV) and Zr(IV) Complexes. *Inorg. Chem.* **2011**, 50, 125-135.
6. Zarkesh, R. A.; Heyduk, A. F., Reactivity of Organometallic Tantalum Complexes Containing a Bis(phenoxy)amide (ONO)(3-) Ligand with Aryl Azides and 1,2-Diphenylhydrazine. *Organometallics* **2011**, 30, 4890-4898.
7. Tondreau, A. M.; Atienza, C. C. H.; Weller, K. J.; Nye, S. A.; Lewis, K. M.; Delis, J. G. P.; Chirik, P. J., Iron Catalysts for Selective Anti-Markovnikov Alkene Hydrosilylation Using Tertiary Silanes. *Science* **2012**, 335, 567-570.
8. Romain, C.; Brelot, L.; Bellemin-Laponnaz, S. p.; Dagorne, S., Synthesis and Structural Characterization of a Novel Family of Titanium Complexes Bearing a Tridentate Bis-phenolate-N-heterocyclic Carbene Dianionic Ligand and Their Use in the Controlled ROP of rac-Lactide. *Organometallics* **2010**, 29, 1191-1198.
9. Romain, C.; Heinrich, B.; Laponnaz, S. B.; Dagorne, S., A robust zirconium N-heterocyclic carbene complex for the living and highly stereoselective ring-opening polymerization of rac-lactide. *Chem. Commun. (Cambridge, U. K.)* **2012**, 48, 2213-2215.
10. Romain, C.; Miqueu, K.; Sotiropoulos, J.-M.; Bellemin-Laponnaz, S.; Dagorne, S., Non-Innocent Behavior of a Tridentate NHC Chelating Ligand Coordinated onto a Zirconium(IV) Center. *Angew. Chem., Int. Ed.* **2010**, 49, 2198-2201.

11. Aihara, H.; Matsuo, T.; Kawaguchi, H., Titanium N-heterocyclic carbene complexes incorporating an imidazolium-linked bis(phenol). *Chem. Commun. (Cambridge, U. K.)* **2003**, 2204-2205.
12. Bellemin-Laponnaz, S.; Welter, R.; Brelot, L.; Dagorne, S., Synthesis and structure of V(V) and Mn(III) NHC complexes supported by a tridentate bis-aryloxide-N-heterocyclic carbene ligand. *J. Organomet. Chem.* **2009**, 694, 604-606.
13. Manna, C. M.; Shavit, M.; Tshuva, E. Y., Structural characterization of dinuclear Ti(IV) complexes of rigid tetradentate dianionic diamine bis(phenolato) ligands; effect of steric bulk on coordination features. *J. Organomet. Chem.* **2008**, 693, 3947-3950.
14. Weinberg, D. R.; Hazari, N.; Labinger, J. A.; Bercaw, J. E., Iridium(I) and Iridium(III) Complexes Supported by a Diphenolate Imidazolyl-Carbene Ligand. *Organometallics* **2009**, 29, 89-100.
15. Xu, X.; Yao, Y.; Zhang, Y.; Shen, Q., Synthesis, Reactivity, and Structural Characterization of Sodium and Ytterbium Complexes Containing New Imidazolidine-Bridged Bis(phenolato) Ligands. *Inorg. Chem.* **2007**, 46, 3743-3751.
16. Yagyu, T.; Oya, S.; Maeda, M.; Jitsukawa, K., Syntheses and Characterization of Palladium(II) Complexes with Tridentate N-Heterocyclic Carbene Ligands Containing Aryloxy Groups and Their Application to Heck Reaction. *Chem. Lett.* **2006**, 35, 154-155.
17. Zhang, D., Dinuclear Titanium(IV) Complexes Bearing Phenoxide-Tethered N-Heterocyclic Carbene Ligands with cisoid Conformation through Control of Hydrolysis. *Eur. J. Inorg. Chem.* **2007**, 2007, 4839-4845.
18. Zhang, D.; Aihara, H.; Watanabe, T.; Matsuo, T.; Kawaguchi, H., Zirconium complexes of the tridentate bis(aryloxide)-N-heterocyclic-carbene ligand: Chloride and alkyl functionalized derivatives. *J. Organomet. Chem.* **2007**, 692, 234-242.
19. Zhang, D.; Liu, N., Titanium Complexes Bearing Bisaryloxy-N-heterocyclic Carbenes: Synthesis, Reactivity, and Ethylene Polymerization Study. *Organometallics* **2008**, 28, 499-505.
20. Chun, H.; Verani, C. N.; Chaudhuri, P.; Bothe, E.; Bill, E.; Weyhermüller, T.; Wieghardt, K., Molecular and Electronic Structure of Octahedral o-Aminophenolato and o-Iminobenzosemiquinonato Complexes of V(V), Cr(III), Fe(III), and Co(III). Experimental Determination of Oxidation Levels of Ligands and Metal Ions. *Inorg. Chem.* **2001**, 40, 4157-4166.

21. Miessler, G. L.; Tarr, D. A., *Inorganic Chemistry*. Prentice Hall: Upper Saddle River, NJ, **1998**; p 642.
22. Poddelsky, A. I.; Cherkasov, V. K.; Abakumov, G. A., Transition metal complexes with bulky 4,6-di-tert-butyl-N-aryl(alkyl)-o-iminobenzoquinonato ligands: Structure, EPR and magnetism. *Coord. Chem. Rev.* **2009**, 253, 291-324.
23. Gibson, S. E.; Johnstone, C.; Loch, J. A.; Steed, J. W.; Stevenazzi, A., Novel Structures and Pauson–Khand Activities of N-Heterocyclic Carbene Dicobalt Complexes. *Organometallics* **2003**, 22, 5374-5377.
24. Smith, A. L.; Clapp, L. A.; Hardcastle, K. I.; Soper, J. D., Redox-active ligand-mediated Co-Cl bond-forming reactions at reducing square planar cobalt(III) centers. *Polyhedron* **2010**, 29, 164-169.
25. Du, M.; An, D.-L.; Guo, Y.-M.; Bu, X.-H., Synthesis, spectral and structural characterization of a novel phenoxo-bridged dinuclear CoII complex with a tridentate phenol-functionalized diazamacrocyclic ligand. *J. Mol. Struct.* **2002**, 641, 193-198.
26. Benisvy, L.; Bill, E.; Blake, A. J.; Collison, D.; Davies, E. S.; Garner, C. D.; Guindy, C. I.; McInnes, E. J. L.; McArdle, G.; McMaster, J.; Wilson, C.; Wolowska, J., Phenolate and phenoxyl radical complexes of Co(II) and Co(III). *Dalton Trans.* **2004**, 3647-3653.
27. Shakya, R.; Hindo, S. S.; Wu, L.; Allard, M. M.; Heeg, M. J.; Hratchian, H. P.; McGarvey, B. R.; da Rocha, S. R. P.; Verani, C. N., Archetypical Modeling and Amphiphilic Behavior of Cobalt(II)-Containing Soft-Materials with Asymmetric Tridentate Ligands. *Inorg. Chem.* **2007**, 46, 9808-9818.
28. Arora, H.; Philouze, C.; Jarjayes, O.; Thomas, F., CoII, NiII, CuII and ZnII complexes of a bipyridine bis-phenol conjugate: Generation and properties of coordinated radical species. *Dalton Trans.* **2010**, 39, 10088-10098.
29. Abakumov, G.; Cherkasov, V.; Bubnov, M.; Abakumova, L.; Ikorskii, V.; Romanenko, G.; Poddelsky, A., Synthesis and structures of five-coordinate bis- π -o-iminobenzosemiquinone complexes $M(\text{ISQ-R})_2X$ ($X = \text{Cl, Br, I, or SCN}$; $M = \text{Co}^{III}, \text{Fe}^{III}, \text{or Mn}^{III}$). *Russ. Chem. Bull.* **2006**, 55, 44-52.
30. Herebian, D.; Ghosh, P.; Chun, H.; Bothe, E.; Weyhermüller, T.; Wieghardt, K., Cobalt(II)/(III) Complexes Containing o-Iminothiobenzosemiquinonato(1-) and o-Iminobenzosemiquinonato(1-) π -Radical Ligands. *Eur. J. Inorg. Chem.* **2002**, 2002, 1957-1967.

31. Poddel'sky, A. I.; Cherkasov, V. K.; Fukin, G. K.; Bubnov, M. P.; Abakumova, L. G.; Abakumov, G. A., New four- and five-coordinated complexes of cobalt with sterically hindered o-iminobenzoquinone ligands: synthesis and structure. *Inorg. Chim. Acta* **2004**, 357, 3632-3640.
32. Van Anh, N.; Williams, R. M., Bis-semiquinone (bi-radical) formation by photoinduced proton coupled electron transfer in covalently linked catechol-quinone systems: Aviram's hemiquinones revisited. *Photochem. Photobiol. Sci.* **2012**, 11, 957-961.
33. Smith, A. L. Facilitating Multi-Electron Reactivity at Low-Coordinate Cobalt Complexes Using Redox-Active Ligands. Ph.D. Dissertation, Georgia Institute of Technology, Atlanta, Georgia, **2011**.
34. Greenwood, N. N.; Earnshaw, A., Chemistry of the Elements (2nd Edition). Butterworth Heinemann: **1997**.
35. Bart, S. C.; Chłopek, K.; Bill, E.; Bouwkamp, M. W.; Lobkovsky, E.; Neese, F.; Wieghardt, K.; Chirik, P. J., Electronic Structure of Bis(imino)pyridine Iron Dichloride, Monochloride, and Neutral Ligand Complexes: A Combined Structural, Spectroscopic, and Computational Study. *J. Am. Chem. Soc.* **2006**, 128, 13901-13912.
36. Garcia, Y.; Gütllich, P., Thermal Spin Crossover in Mn(II), Mn(III), Cr(II) and Co(III) Coordination Compounds. In *Spin Crossover in Transition Metal Compounds II*, Springer Berlin Heidelberg: **2004**; Vol. 234, pp 49-62.
37. Mayer, M.; Czaplik, W. M.; Jacobi von Wangelin, A., Thieme Journal Awardees - Where Are They Now? On Cobalt-Catalyzed Biaryl Coupling Reactions. *Synlett* **2009**, 2009, 2919-2923.
38. Evans, D. F., 400. The determination of the paramagnetic susceptibility of substances in solution by nuclear magnetic resonance. *Journal of the Chemical Society (Resumed)* **1959**, 2003-2005.
39. Live, D. H.; Chan, S. I., Bulk susceptibility corrections in nuclear magnetic resonance experiments using superconducting solenoids. *Anal. Chem.* **1970**, 42, 791-792.
40. Systems, A. X.-r. *APEX II*, Bruker AXS, Inc.: Madison, WI, **2005**.
41. Systems, A. X.-r. *saint Version 6.45A*, Bruker AXS, Inc.: Madison, WI, **2003**.
42. Systems, A. X.-r. *shelxtl Version 6.12*, Bruker AXS, Inc.: Madison, WI, **2002**.

43. Min, K. S.; Weyhermüller, T.; Bothe, E.; Wieghardt, K., Tetradentate Bis(o-
iminobenzosemiquinonate(1-)) π Radical Ligands and Their o-Aminophenolate(1-)
Derivatives in Complexes of Nickel(II), Palladium(II), and Copper(II). *Inorg. Chem.* **2004**,
43, 2922-2931.
44. Saba, S.; Brescia, A.; Kaloustian, M. K., One-pot synthesis of cyclic amidinium
tetrafluoroborates and hexafluorophosphates; the simplest models of
N⁵,N¹⁰-methenyltetrahydrofolate coenzyme. *Tetrahedron Lett.* **1991**, 32, 5031-5034.

Chapter 4

Co^{II}((tBuPhO)₂NHC)THF Mediated C–O Activation

4.1 Introduction

4.1.1 Utility and prevalence of C–O activation

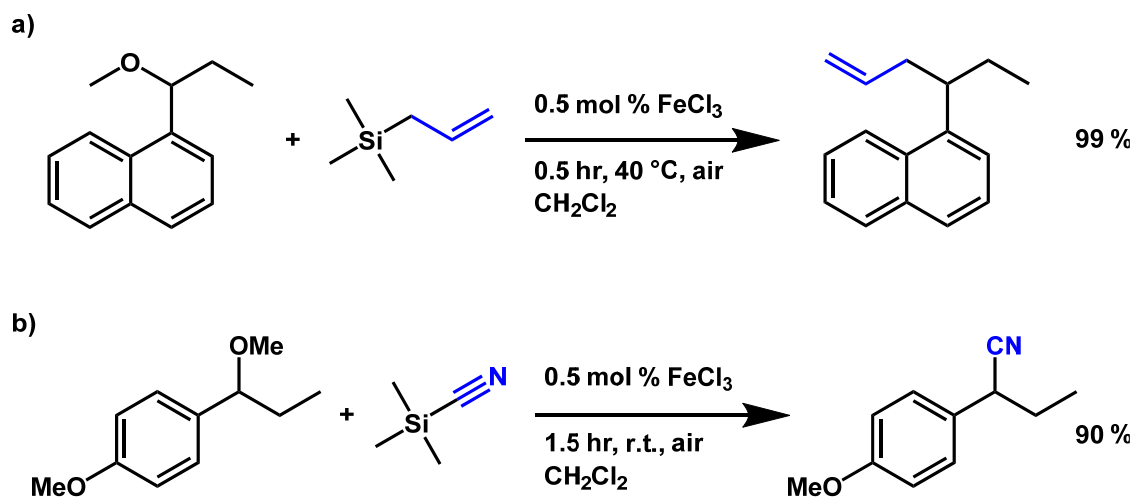
Almost all natural products contain carbon-oxygen bonds, in the form of alcohols, ester, and ethers.¹ For instance, lignin, a natural polymer found in plants ((C₃₁H₃₄O₁₁)_n), is a paper industry byproduct yielding 50 million tons per year as waste.² Lignin has C–O bonds in the form of alcohols, phenols, and ethers. Ethers represent the largest functional group in lignin.³⁻⁴ Developing a catalyst to selectively activate the C–O bonds in lignin could turn this industrial waste product into a valuable chemical feed stock. For instance, depolymerization of lignin via C–O activation would lead to the production of simple aromatics such as benzene, toluene, and xylene. Global production of benzene, largest source from catalytic reforming of naphthas distilled from crude oil, is estimated at 40.2 million metric tonnes annually.⁵⁻⁶ Therefore, strategies that can activate these C–O bonds remain a worthy goal. However, selective C–O bond activation in lignin has not yet been realized. Direct cross-coupling of C–O by transition metals is difficult due to the relatively inert C–O bond. This is not due to thermodynamics because the bond dissociation energy (BDE) of C–O bonds in aryl or alkyl ethers is roughly the same as for C–Cl bonds. For instance, butyl ether has a BDE of 85 kcal/mol for the C–O bond vs. 83 kcal/mol for the C–Cl bond in 1-chloropentane.⁷ While many protocols have been devised for cross-coupling reactions involving C–Cl substrates,⁸⁻¹² comparatively less is known about ether C–O bond activation and coupling. In fact, because C–O bonds are

inert, alkyl and aryl ethers are used as protecting groups for alcohols. The ether linkage functions to prevent reactivity at oxygen centers.¹³ Alcohols can be converted to methyl, aryl, and prenyl ethers to name a few. For instance, conversion of an alcohol group to methoxymethyl ether (MOM) renders the new ether linkage unreactive towards: nucleophiles (NaOMe, NaCN); Grignards; oxidants (OsO₄, O₃ at -50 °C, KMnO₄ at pH7); reductants (Na (s), Al(Hg)); and temperature (<350 °C).¹³ Many strategies exist to remove the different ether protecting group, i.e. to cleave the C–O bonds, such as acidic and basic conditions, hydrogenolysis, reductive or oxidative cleavage, and photochemical cleavage.¹³⁻¹⁴ However, these strategies can only convert the ether to an alcohol. Thus far, there does not exist a general atom economical method for direct C–O activation that avoids the simple conversion of the ether to an alcohol.

To date, examples of metal mediated C–O bond activation have mostly focused on aryl C–O bond cleavage. Work done by Chatterjee and co-workers involving a heterogeneous Rh/C catalyst in super critical CO₂ lead to the cleavage of aryl ether bonds in diphenyl ether.¹⁵ Several homogenous and heterogeneous Ni complexes have recently been shown to cleave aryl C–O bonds.¹⁶⁻²⁴ Sergeev and co-workers developed a heterogeneous Ni catalyst that could cleave the C–O bond in diphenyl ether under 1 bar H₂ and only 0.25 mol % catalyst loading.²⁵ Shi and co-workers have developed several homogeneous Ni catalysts for the cleavage of C–O bond followed by cross-coupling to a nucleophilic carbon.² Recently two papers by, Fan and co-workers have shown FeCl₃ can catalytically cleave secondary C_{sp3}–O bonds and form new C_{sp3}–C_{sp3} and C_{sp3}–C_{sp} bonds.²⁶⁻²⁷ For example, Fan, *et. al.* demonstrated that 0.5 mol % FeCl₃ were able to carry out allylic alkylation of an ether, 1-(1-methoxypropyl)naphthalene, using allyltrimethylsilane to form 1-(hex-5-en-3-yl)naphthalene (**Scheme 4-1 a**). This reaction is general to most secondary carbons at the C–O linkage, but could not cross-couple primary carbons. Interestingly, when a cyclopropyl group was attached to the

carbon bound to oxygen, no ring opening event was observed. This suggests a concerted C–O bond activation. Fan was also able to catalytically form α -aryl nitriles compounds by C–O activation of an ether followed by addition of cyanide (**Scheme 4-1 b**). However, this reaction could not activate primary C–O ethers. To the best of my knowledge, no examples exist of primary C_{sp^3} –O ether bond activation in a well-defined cross-coupling reaction. Furthermore, in the few systems that can cross couple ethers

Scheme 4-1. C–O bond activation and cross-coupling using $FeCl_3$, a) Allylic alkylation of ether with allylTMS, b) α -arylation of nitrile using TMSCN and an $FeCl_3$ catalyst.



there is a general lack of mechanistic understanding of how these reactions occur. While the authors suggest that $FeCl_3$ acts only as a Lewis acid in the in the above mentioned reactions, the reaction does not work with other Lewis acids such as $FeCl_2$, $Fe(acac)_2$, BF_3 , or $ZnCl_2$. The reaction is also extremely solvent dependent. Using CH_2Cl_2 as the solvent results in a 99 % yield, but no cross-coupling is observed in THF, EtOAc or DMF. When toluene, benzene, $CHCl_3$, and 1,2-dichloroethane were used the yield decreased to 60 %. When $FeCl_3 \cdot 6H_2O$ was used as a catalyst only a 46 % yield was realized, however all reaction were run in ambient atmosphere. Even if the reaction is purely Lewis acid catalyzed, the metal coordination environment is unknown.

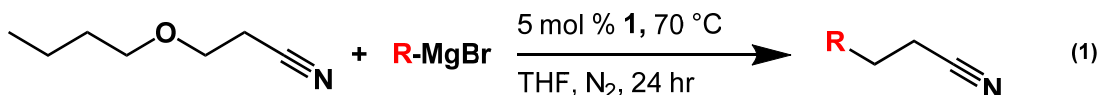
Determining the metal coordination environment and mechanistic steps involved in C–O bond activation will aid in rational ligand design.

This chapter explores the catalytic cross-coupling of a nitrile containing ether (3-butoxypropanenitrile) and Grignard substrates via C–O bond activation using $\text{Co}^{\text{II}}((\text{tBuPhO})_2\text{NHC})\text{THF}$ as the catalyst. This represents the first primary $\text{C}_{\text{sp}^3}\text{--O}$ activation followed by C–C bond formation. Mechanistic studies suggest that nitrile binding is important for C–O activation by cobalt.

4.2 Results

4.2.1 C–O bond activation and cross-coupling

A reaction between 3-butoxypropanenitrile and PhMgBr with 5 mol % of $\text{Co}^{\text{II}}((\text{tBuPhO})_2\text{NHC})(\text{THF})$ **1** in THF under N_2 at 70 °C for 1 hour lead to 70 % of the cross-coupled product 3-phenylpropanenitrile **Equation 1**. When the reaction is run at



room temperature the yield was decreased to 38 %. At colder temperatures (–30 °C) the yield was 27 %. When no metal is present, no cross-coupling was detected. When CoBr_2 , at 5 mol % loading, was used as the catalyst a 10 % yield of 3-phenylpropanenitrile was observed. Increasing or decreasing the amount of Grignard used in the catalytic reaction dramatically reduced the yield. For instance, increasing or decreasing the equiv of PhMgBr used by 25 % lead to a 75 % reduction in product.

4.2.2 Scope of nucleophiles for cross-coupling

Several aryl Grignard reagents were screened for C–C coupling with ether nitrile (**Figure 4-1**). The ratio of analyte (cross-coupled product or homocoupled product) vs.

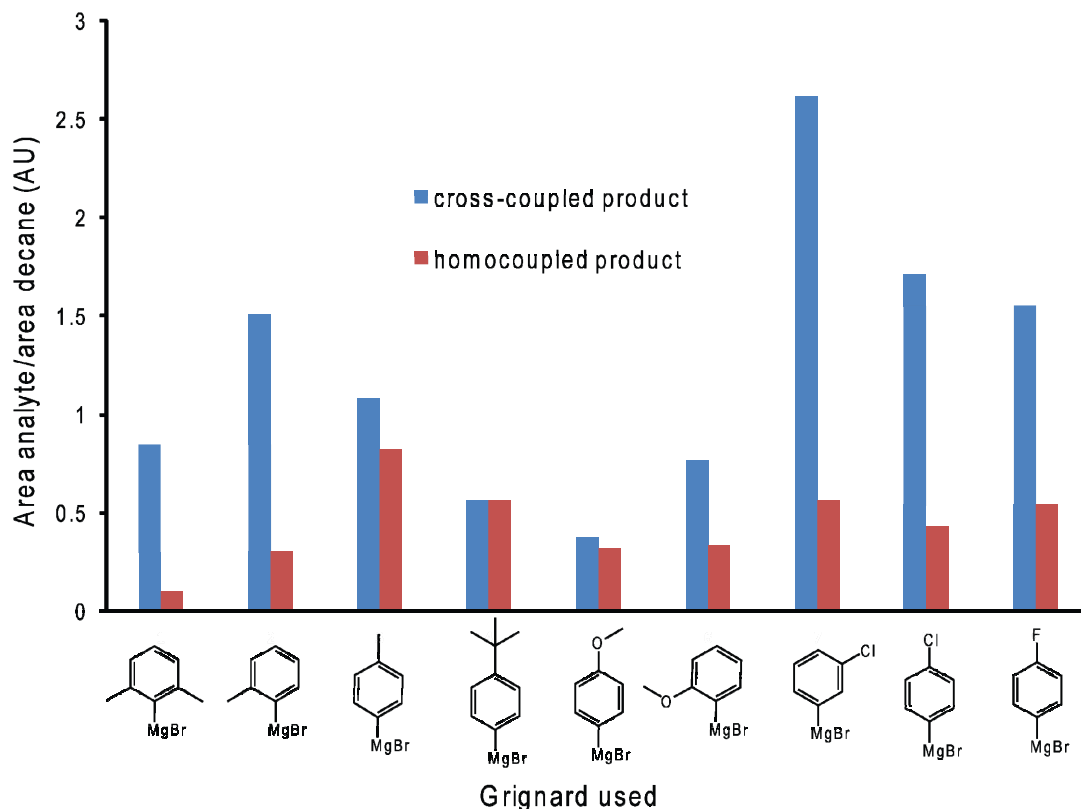


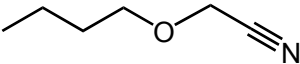
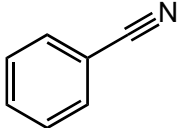
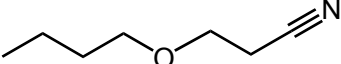
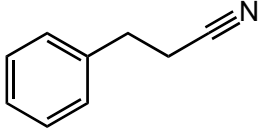
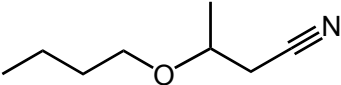
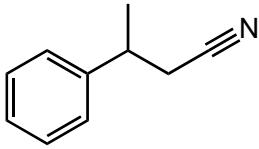
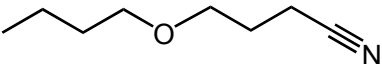
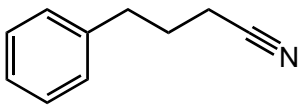
Figure 4-1. Cross-coupling and homocoupling yields generated from the catalytic reaction of a Grignard reagent and 3-phenylpropanenitrile using **1** as the catalyst. The yield is reported as the ratio of area of analyte vs area of decane (internal standard) in arbitrary units derived from the GC-MS trace of the crude reaction mixture after 24 hours.

internal standard (decane) allows for some qualitative comparison between the different Grignard reagents used and their respective products since isolated yields have not yet been determined. Isolation of the resulting aryl nitrile has been difficult due to high boiling points $>300\text{ }^{\circ}\text{C}$, which preclude distillation, and difficulty in finding a suitable solvent system for column chromatography. Both electron donating and withdrawing groups were tolerated on the aryl Grignard. Steric crowding at C-Mg (2,6 dimethylphenyl magnesium bromide, o-tolylmagnesium bromide) disfavors homocoupling, but still allowed cross-coupling to occur. Electron donating groups (OMe) in either the *ortho* or *para* position did not increase the yield of cross-coupled product. However, electron withdrawing groups (halide) in the *meta* position increased cross-coupling yield.

The reaction was not general to other nucleophilic aryl complexes. Reactions of 3-butoxypropanenitrile with PhLi, PhZnCl, or PhB(OH)₂ did yield any observable cross-coupling products under the reaction conditions outlined in **Equation 1**. Alkyl Grignard reagents (octylmagnesium bromide, pentylmagnesium bromide) were also unsuccessful at cross-coupling.

4.2.3 Scope of ether nitriles used for C–O activation

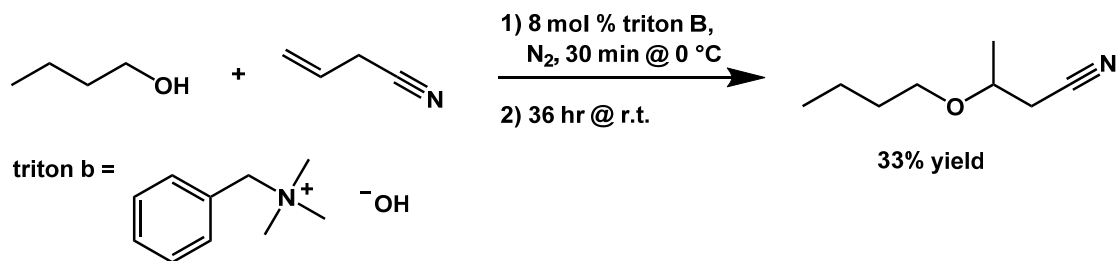
Table 4-1. Reactions between various ether nitriles and PhMgBr catalyzed by **1**.

Ether + PhMgBr		5 mol % Co ^{II} ((tBuPhO) ₂ NHC)THF N ₂ , THF, 70 °C, 4 hrs.	Ph-(CH ₂) _n -C≡N
Entry	Ether	Desired product	Yield
1	 2-butoxyacetonitrile		n.r.
2	 3-butoxypropanenitrile		70 %
3	 3-butoxybutanenitrile		5 %
4	 4-butoxybutanenitrile		n.r.

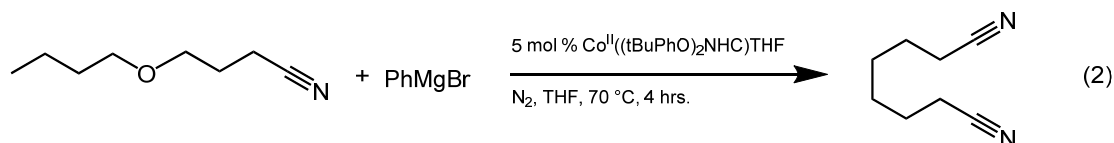
Changes to the ether nitrile produced interesting results as summarized in **Table 4-1**. Decreasing the carbon count between the nitrile (2-butoxyacetonitrile) and ether lead to no cross-coupling. Adding an additional carbon between the nitrile and ether (4-butoxybutanenitrile **Table 4-1**, entry 4) did not cross-couple with PhMgBr. However, octanedinitrile, was observed by GC-MS (**Equation 2**). In addition to primary C–O

bonds, secondary carbon centers cross-coupled but only produced a 5 % yield of the

Scheme 4-2. Synthesis of 3-butoxybutanenitrile



aryl nitrile. The compound 3-butoxybutanenitrile was formed from the reaction between 3-butenitrile and butanol using a solid organic base (benzyltrimethylammonium hydroxide, triton B) (**Table 4-1**). This reaction was originally reported to yield the anti-Markovnikov addition product 4-butoxybutanenitrile.²⁸ However, the only characterization that the authors used for identification was boiling point and refractive



index. Using 1H , ^{13}C NMR and GC-MS, lead to an assignment of 3-butoxybutanenitrile as the major product as seen in **Figure 4-2**. A reaction between 3-butoxybutanenitrile and $PhMgBr$ using **1** as the catalyst at 10 mol % loading lead to cross-coupling to produce 3-phenylbutanenitrile in poor yield. The majority of 3-butoxybutanenitrile remained, unreacted, at the end of reaction.

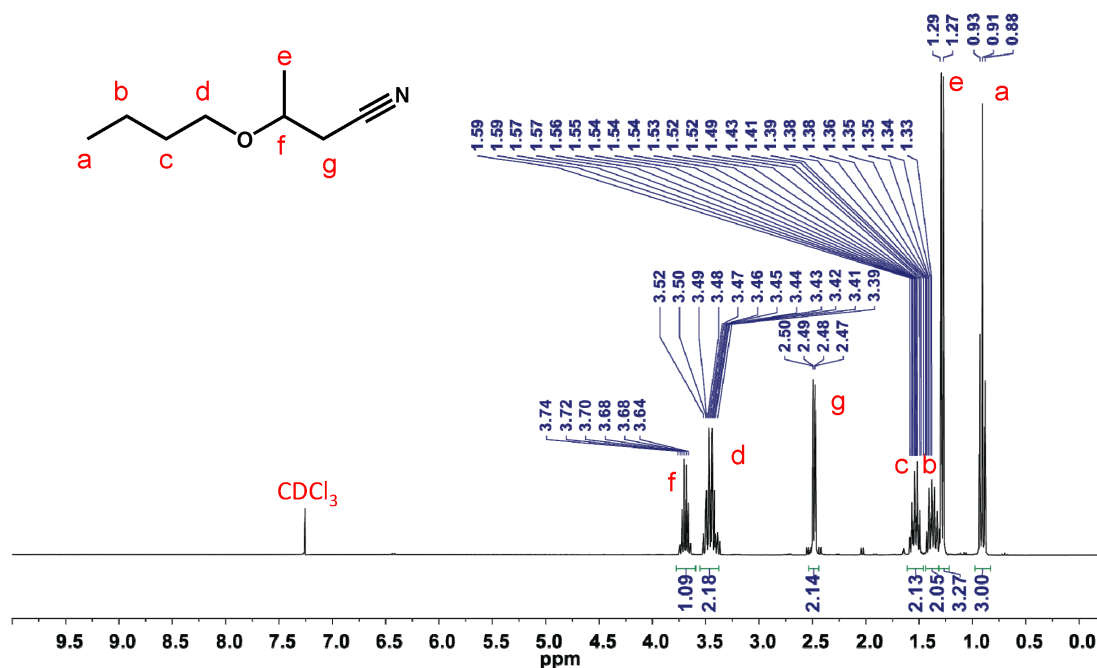


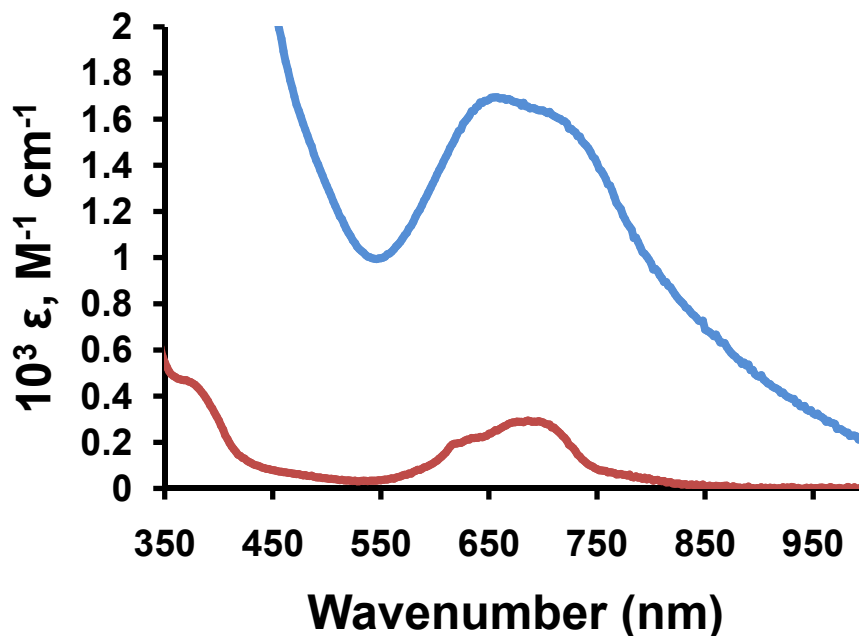
Figure 4-2. ¹H NMR spectrum of 3-butoxybutanenitrile in CDCl₃ at 25 °C.

Interestingly, when 1 equiv of **1**, 3-butoxypropanenitrile, and PhMgBr are reacted in THF under N₂, both Ph⁻ and 3-butoxypropanenitrile can be seen bound to **1** in the ESI-MS spectrum; both the mass and isotopic pattern match the spectrum generated. When the reaction is run catalytically, 10 mol % of **1**, after 24 hr 3-butoxypropanenitrile is still bound to the metal center, again judged by ESI-MS.

4.2.4 Oxidative addition of halide nitriles

When any of the above mentioned ether nitriles (**Table 4-1**) are added either

a)



b)

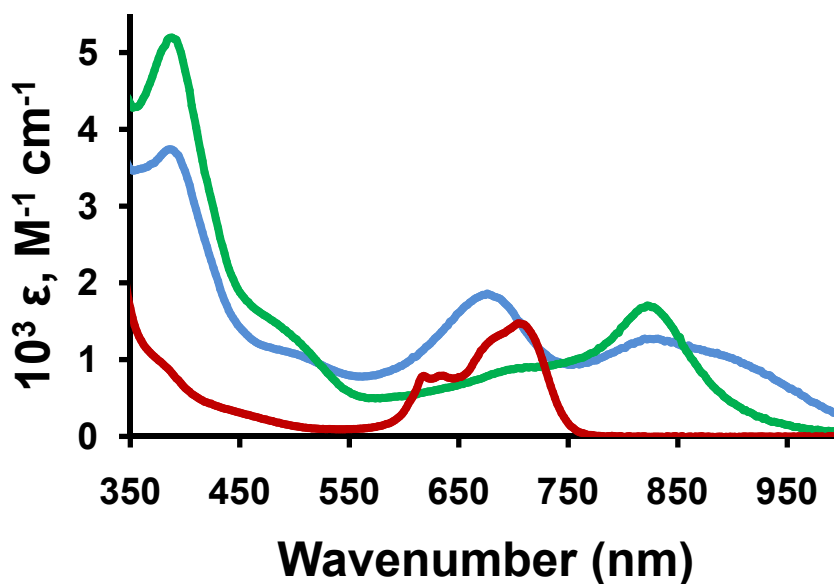


Figure 4-3. UV-vis absorption spectrum collected at 22 °C in THF (a) Bromoacetonitrile 10 min after addition to **1** (blue line); 3-bromopropanenitrile 12 hr after addition to **1** (red line) (b) 3 days after addition of: bromoacetonitrile (blue line), chloroacetonitrile (green line), and 3-bromopropanenitrile (red line) to **1**.

stoichiometrically or in excess no oxidative addition occurs between the ether nitrile and $\text{Co}^{\text{II}}((\text{tBuPhO})_2\text{NHC})\text{THF}$. Butoxide is a poor leaving group, this prompted the investigation of better leaving groups such as halides. When bromoacetonitrile is added to $\text{Co}^{\text{II}}((\text{tBuPhO})_2\text{NHC})\text{THF}$ the solution immediately changed color from orange to dark green with a broad peak at 650 nm (**Figure 4-3 (a)** blue line). After three days the peak at 650 nm shifts to 675 nm and an additional broad peak appears at 820 nm (**Figure 4-3 (b)** blue line). When an orange solution of **1** in THF was exposed to 1 equiv of 3-bromopropanenitrile the solution turned green over the course of 12 hr (**Figure 4-3 (a)** red line). The green solution has a broad peak at 690 nm with a shoulder at 617 nm. After 3 days, the epsilon value tripled and the spectrum was red shifted by 10 nm (**Figure 4-3 (b)** red line). In the both reactions, the initially formed green solutions are similar and both show a large broad peaks around 680 nm. Addition of chloroacetonitrile effects a similar conversion to a green solution over 20 mins, but the UV-vis spectrum is different (**Figure 4-3 (b)** green line). Over the course of several days the reaction between bromoacetonitrile or 3-bromopropanenitrile with **1** led to different UV-vis spectrum (**Figure 4-3 (b)**). None of the above mentioned spectra share any UV-vis absorption features with the isolated doubly oxidized Co complex, $[\text{Co}^{\text{II}}((\text{tBuPhO}\cdot)_2\text{NHC})(\text{THF})]^{2+}$, Chapter 3 of this thesis.

Addition of 1.4 equiv of PhMgBr to the green solution containing **1** and bromoacetonitrile lead to 2-phenylacetonitrile and 50 % regeneration of $\text{Co}^{\text{II}}((\text{tBuPhO})_2\text{NHC})\text{THF}$ as evidenced by appearance of a characteristic UV-vis absorption at 420 nm.

4.3 Discussion

4.3.1 Scope of reactivity of **1** for C–O activation

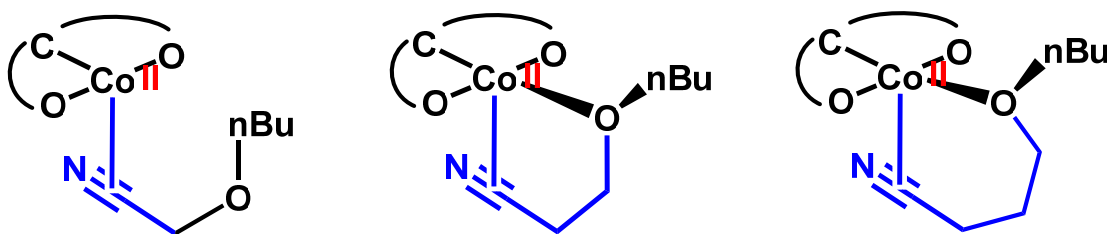
FeCl_3 can activate secondary C–O bonds to form new C–C bonds. Presented here is the first primary C_{sp^3} –O bond activation followed by the generation of a new C–C bond. Furthermore, **1** can deliver alkyl nitriles to aryl compounds (**Figure 4-1**) via C–O bond activation. Delivery of nitriles is advantageous due to their presence in natural products. Nitriles are present in cyanogenic glycosides and bisindole alkaloids, which have been shown to have antitumor behavior and act as part of organisms defense mechanism.²⁹ It is therefore no surprise that several pharmaceutical products PPAR- γ -active triterpenoid (2-cyano-3,12-dioxooleana-1,9-dien-28-oic acid) which is used to combat acute promyelocytic leukemia, contain nitriles.³⁰ Furthermore, nitriles function as precursors to a vast array of functional groups including, amines,³¹ amides,³² esters,³³ and ketones.³⁴ All of these factors make delivery of a nitrile an attractive goal for cross-coupling reactions.

$\text{Co}^{\text{II}}((\text{tBuPhO})_2\text{NHC})\text{THF}$ was able to catalytically activate a primary C_{sp^3} –O in 3-butoxypropanenitrile followed by cross-coupling to an aryl Grignard to produce an aryl nitrile compound. The reaction was tolerant of a wide variety of aryl Grignard reagents. Steric bulk at the nucleophilic carbon did not prevent cross-coupling, however it did decrease Grignard homocoupling. Although the *ortho*- and *para*- methoxy Grignards increase the nucleophilicity at the Mg bound carbon, the relative yields of the cross-coupled product were much lower. Halides *ortho* or *meta* to the Mg bound carbon lead to the largest increase in cross-coupling yield. Since halides are *ortho* and *para* directing it is unusual that both *ortho* and *meta* halides on the ring increase the cross-coupling yield. It is difficult to propose a mechanism that is consistent with all of these observations. Although cross-coupling is general to aryl Grignards, cross-coupling does

not occur with alkyl Grignards or other nucleophiles such as PhLi or PhZnBr. It is surprising that PhLi cannot cross-couple with the ether nitrile, due to its increased nucleophilicity. Although that is in line with *ortho*- and *para*- methoxyphenyl magnesium bromide, which should also increase the nucleophilicity at the C bound to Mg, having a lower cross-coupling yield. The aryl organozinc, on the other hand, is less nucleophilic than PhMgBr and was not competent for cross-coupling. Again it is difficult to propose a mechanism that encompass these results.

Stoichiometric oxidative addition of **1** with ether nitriles was unsuccessful due to butoxide being a poor leaving group. In the case of bromo or chloro acetonitrile, the electrophilicity of the α -carbon increased due to both the electronegativity of the halide and the adjacent nitrogen which is only one carbon away. This seems to allow for facile oxidative addition, making even chloro a good leaving group. In the case of 3-bromopropanenitrile, the α -carbon's electrophilicity is only slightly effected by the nitrile due the increased chain length. Also, as seen in chapter 3 of this thesis, thus far no alkyl halides has oxidatively added to the $\text{Co}^{\text{II}}((\text{tBuPhO})_2\text{NHC})\text{THF}$ complex independent of Grignard addition. Also, diphenyl ether or dibutyl ether did not undergo C–O

Scheme 4-3. The proposed structures of η^2 -bound ether nitriles to **1**.



activation (Chapter 5). Therefore, it is reasonable to believe that nitrile coordination to the metal facilitates C–O bond activation.

Interestingly, the number of carbons between the oxygen and the nitrogen plays a large role in C–O activation pathway. If the nitrile binds in a η^1 fashion through the

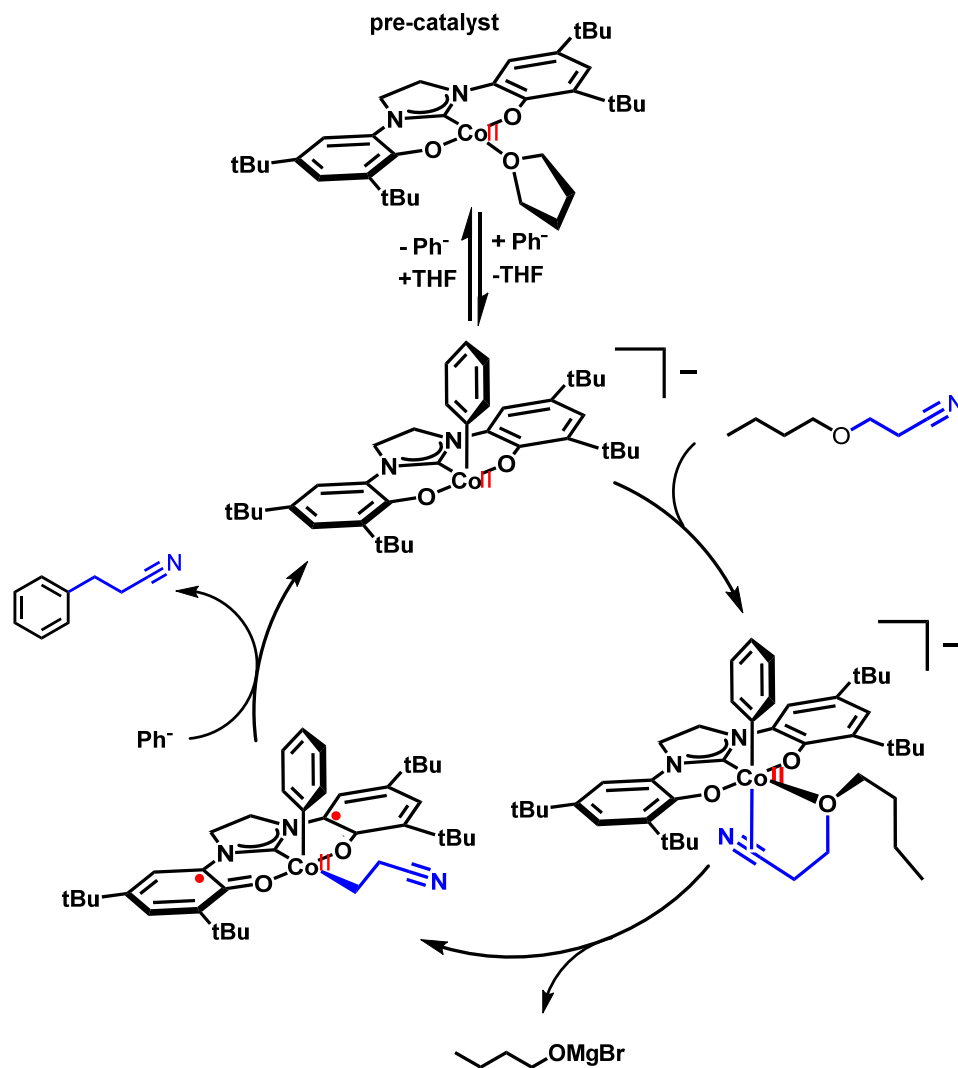
nitrogen then the differences between the ether nitriles studied (**Table 4-1**) become less obvious. If η^2 -binding of the nitrile is necessary for C–O activation then decreasing the number of carbons, 2-butoxyacetonitrile, would decrease C–O activation due to inability of both the nitrile and oxygen to bind to Co simultaneously **Scheme 4-3**. Increasing the chain length between the oxygen and nitrogen, 4-butoxybutanenitrile, should reduce the steric strain of the binding of 4-butoxybutanenitrile. However, 4-butoxybutanenitrile did not cross-couple, and instead generated the homocoupled product **Equation 2**.

4.3.2 Proposed catalytic cycle of C–O activation and cross-coupling using **1** as the catalyst

A proposed catalytic cycle as shown in **Scheme 4-4** begins with $\text{Co}^{\text{II}}((\text{tBuPhO})_2\text{NHC})\text{THF}$ as a pre-catalyst. The first step involves Grignard binding to the metal center $[\text{Co}^{\text{II}}((\text{tBuPhO})_2\text{NHC})\text{Ph}]^-$. It could also be the case that the ether nitrile binds first; however, there is no color change observed when any ether nitrile is added. Only the addition of Grignard changes the color of the solution. Grignard addition increases the nucleophilicity of Co and allows C–O activation of the ether nitrile, which leads to oxidative addition and loss of *n*-butoxide, which is seen as butanol when the reaction is quenched with MeOH. After oxidative addition has occurred the organic fragments are positioned for reductive elimination leading to the desired product and regeneration of the starting catalyst. This proposed mechanism explains why 2-butoxyacetonitrile does not cross-couple due to η^2 -binding of the nitrile not having enough flexibility to allow for the oxygen to bind to the metal. The ether nitrile 4-butoxybutanenitrile not being able to cross-couple is more troubling. If the mechanism above is correct then an additional carbon between nitrogen and oxygen should be poised to make a better bidentate ligand by relieving the steric strain with 3-butoxypropanenitrile. Although cross-coupling did not occur, homocoupling of the two

nitrile fragments did. This implies that C–O bond activation and oxidative addition are still occurring, however this mechanism becomes more complicated.

Scheme 4-4. Proposed catalytic cycle for the generation of 4-phenylbutanenitrile from 3-butoxypropanenitrile and PhMgBr using **1** as the catalyst.



4.4 Conclusion

This novel C–O bond activation represents a gateway into a variety of new possibilities. The use of an inexpensive and environmentally benign redox-active ligand bound to a 3d metal to cleave an unactivated ether could be used to turn industrial waste, such as lignin, to a useful chemical feed stock. The reaction between ether

nitriles and Grignards using catalytic amounts of **1** is still limited in scope. Finding conditions that expand this reactivity to other nucleophilic carbon centers remains a significant goal. One way to address this issue is to increase the nucleophilicity at cobalt using auxiliary electron donating ligands, such as triphenylphosphine. Furthermore, identifying the reason nitrile groups aid in oxidative addition could lead to other functional groups that mimic this binding motif. Finally, more mechanistic studies could elucidate more opportunities to expand the scope of substrates and include other ethers.

4.5 Materials and Methods

4.5.1 General

Unless otherwise noted, all manipulations were performed under anaerobic conditions using standard vacuum line techniques, or in an inert atmosphere glove box under purified nitrogen. All NMR spectra were acquired on a Varian Mercury 300 spectrometer (300.323 MHz for ¹H) at ambient temperature. Chemical shifts are reported in parts per million (ppm) relative to TMS, with the residual solvent peak serving as an internal reference. All mass spectra were recorded in the Georgia Institute of Technology Bioanalytical Mass Spectrometry Facility. Anhydrous tetrahydrofuran (THF), and pentane solvents for air- and moisture-sensitive manipulations were purchased from Sigma–Aldrich, and further dried by passage through columns of activated alumina, degassed by at least three freeze–pump–thaw cycles, and stored under N₂ prior to use. In a septum capped round bottom flask, *n*-butanol was dried over 3 Å molecular sieves under N₂ for 24 hr and sparged with N₂ for 1 hour prior to use. The compound 4-butoxybutanenitrile was prepared according to literature methods.³⁵ All characterization data matched those referenced. All other chemicals were purchased from Sigma–Aldrich and used as received.

4.5.2 Synthesis

Synthesis of 2-butoxyacetonitrile

A three-neck round bottom flask was charged a stir bar, and freshly cut Na (s) (2.0 g, 0.086 mol) in an inert atmosphere glove box. A reflux condenser was attached to the three-neck round bottom flask and all opening were sealed with rubber septa. The reaction flask was removed from the glove box and kept under N₂ using a Schlenk line. A round bottom flask was charged with n-butanol (40 mL) and molecular sieves and capped with a rubber septum. After 24 hrs in the presence of molecular sieves, n-butanol was sparged with N₂ for 1 hour and then transferred by cannula to the round bottom flask containing the Na (s). The Na/n-butanol mixture was stirred and heated to reflux until all the Na was consumed. Chloroacetonitrile (5.2 mL, 82.1 mmol) was added slowly over the course of 10 mins to produce a dark solution. The reaction was allowed to reflux with stirring for 24 hrs and then cooled to room temperature. The reflux condenser was replaced with a distillation head and the dark solution was fractionally distilled *in vacuo* to produce 2-butoxyacetonitrile as a colorless oil (0.501 g, 4.42 mmol, 5% yield). ¹H NMR (300 MHz, CDCl₃, δ): 4.23 (s, 2H), 3.57 (t, *J* = 7 Hz, 2H), 1.59 (quin, *J* = 7 Hz, 2H), 1.38 (sex, *J* = 7 Hz, 2H), 0.92 (t, *J* = 7 Hz, 3H). ¹³C NMR (300 MHz, CDCl₃): 116.31, 71.71, 56.31, 31.24, 19.11, 13.80. HRMS (ESI) Calcd for C₆H₁₀NO: [M] = 112.0762 m/z. Found 112.0759 m/z.

Synthesis of 3-butoxybutanenitrile

The synthesis of 3-butoxybutanenitrile is from a modified version in literature.²⁸ A three-neck round bottom flask with a reflux condenser was charged with *n*-butanol (18.00 mL, 196 mmol), benzyltrimethylammonium hydroxide (triton b) (2.50 mL, 14.2 mmol) and a magnetic stir bar. The solution was cooled to 0 °C with an ice bath and but-3-enenitrile (16 mL, 198 mmol) was added slowly over the course of 30 mins. After addition of the nitrile the solution was allowed to warm to room temperature and stirring continued for 36 hrs. At the end of 36 hrs, the solution was washed with water and the organic layer was removed and distilled *in vacuo* to produce 3-butoxybutanenitrile as a clear liquid (9.021 g, 63.8 mmol, yield 33 %) ¹H NMR (300 MHz, CDCl₃, δ): 3.69 (p, *J* = 6.0 Hz, 1H), 3.46 (qt, *J* = 9.0, 6.4 Hz, 2H), 2.49 (dd, *J* = 5.8, 1.5 Hz, 2H), 1.54 (ddt, *J* = 11.4, 8.4, 6.4 Hz, 2H), 1.44 – 1.32 (m, 2H), 1.28 (d, *J* = 6.2 Hz, 3H), 0.91 (t, *J* = 7.3 Hz, 3H). ¹³C NMR (75 MHz, CDCl₃) δ 117.61, 71.02, 68.93, 31.85, 24.89, 19.74, 19.22, 13.81. HRMS (ESI) Calcd C₈H₁₅NO: [M] = 142.1232 m/z. Found 142.1234 m/z.

Cross-coupling reaction between phenyl magnesium bromide and 3-phenylpropanenitrile

In a representative procedure, a scintillation vial was charged with a magnetic stir bar, 5 mL of THF, decane (0.005 mL, 25 μmol, (internal standard)), 2-butoxyacetonitrile (2.28 mL (165 μmol) of a 0.07244 M stock solution) and **1** (0.500 mL (8.26 μmol) of a 0.01653 M stock solution). PhMgBr (0.826 mL (165 μmol) of a 0.200 M stock solution) was added turning the orange solution dark green. The vial was capped and stirred for 24 hr. After 24 hr the solution was quenched with 1 mL of dried MeOH.

4.6 Work cited

1. Hartwig, J. F., Carbon-Heteroatom Bond Formation Catalysed by Organometallic Complexes. *Nature* **2008**, 455, 8.
2. Yu, D.-G.; Li, B.-J.; Shi, Z.-J., Exploration of New C–O Electrophiles in Cross-Coupling Reactions. *Acc. Chem. Res.* **2010**, 43, 1486-1495.
3. Wong, D. S., Structure and Action Mechanism of Ligninolytic Enzymes. *Appl. Biochem. Biotechnol.* **2009**, 157, 174-209.
4. He, J.; Zhao, C.; Lercher, J. A., Ni-Catalyzed Cleavage of Aryl Ethers in the Aqueous Phase. *J. Am. Chem. Soc.* **2012**, 134, 20768-20775.
5. Rachel Massey, R. W. C., Louise, A. Gallagher, Andrew Dlugolecki, Laura Cochran, Ken Geiser, Sally Edwards, , Global Chemicals Outlook - Towards Sound Management of Chemicals. Programme, U. N. E., Ed. GPS Publishing: Nairobi, Kenya, **2013**; p 245.
6. Netzer, D.; Ghalayini, O. J., Improve benzene production from refinery sources. *Hydrocarb. Process.* **2002**, 81, 71.
7. Luo, Y.-R., *Handbook of Bond Dissociation Energies in Organic Compounds*. CRC Press LLC: 2000 N.W. Corporate Blvd., Boca Raton, Florida 33431, **2003**.
8. Ackermann, L.; Althammer, A., Air-stable PinP(O)H as preligand for palladium-catalyzed Kumada couplings of unactivated tosylates. *Org. Lett.* **2006**, 8, 3457-3460.
9. Chen, Y.; Sun, H. J.; Floeke, U.; Li, X. Y., Cyclometalation reactions involving C–Cl bond activation of ortho-chlorinated substrates with imine as anchoring groups by cobalt complexes. *Organometallics* **2008**, 27, 270-275.
10. Shi, Y. J.; Li, M.; Hu, Q. P.; Li, X. Y.; Sun, H. J., C–Cl Bond Activation of ortho-Chlorinated Imine with Iron Complexes in Low Oxidation States. *Organometallics* **2009**, 28, 2206-2210.
11. Li, J.; Li, X.; Sun, H., Synthesis and characterization of novel organonickel and organocobalt complexes via carbon–chlorine bond activation. *J. Organomet. Chem.* **2013**, 743, 114-122.
12. Littke, A. F.; Fu, G. C., Palladium-catalyzed coupling reactions of aryl chlorides. *Angew. Chem., Int. Ed.* **2002**, 41, 4176-4211.
13. Wuts, P. G. M.; Greene, T. W., Protection for Phenols and Catechols. In *Greene's Protective Groups in Organic Synthesis*, John Wiley & Sons, Inc.: **2006**; pp 367-430.
14. Bhatt, M. V.; Kulkarni, S. U., Cleavage of Ethers. *Synthesis* **1983**, 1983, 249-282.

15. Chatterjee, M.; Ishizaka, T.; Suzuki, A.; Kawanami, H., An efficient cleavage of the aryl ether C-O bond in supercritical carbon dioxide-water. *Chem. Commun. (Cambridge, U. K.)* **2013**, *49*, 4567-4569.
16. Kelley, P.; Lin, S.; Edouard, G.; Day, M. W.; Agapie, T., Nickel-Mediated Hydrogenolysis of C-O Bonds of Aryl Ethers: What Is the Source of the Hydrogen? *J. Am. Chem. Soc.* **2012**, *134*, 5480-5483.
17. Dankwardt, J. W., Nickel-Catalyzed Cross-Coupling of Aryl Grignard Reagents with Aromatic Alkyl Ethers: An Efficient Synthesis of Unsymmetrical Biaryls. *Angew. Chem., Int. Ed.* **2004**, *43*, 2428-2432.
18. Johnstone, R. A. W.; Neil McLean, W., Catalysed ipso replacement of phenolic ethers by Grignard reagents. *Tetrahedron Lett.* **1988**, *29*, 5553-5556.
19. Guan, B.-T.; Xiang, S.-K.; Wu, T.; Sun, Z.-P.; Wang, B.-Q.; Zhao, K.-Q.; Shi, Z.-J., Methylation of arenes via Ni-catalyzed aryl C-O/F activation. *Chem. Commun. (Cambridge, U. K.)* **2008**, 1437-1439.
20. Tobisu, M.; Shimasaki, T.; Chatani, N., Nickel-Catalyzed Cross-Coupling of Aryl Methyl Ethers with Aryl Boronic Esters. *Angew. Chem., Int. Ed.* **2008**, *47*, 4866-4869.
21. Quasdorf, K. W.; Tian, X.; Garg, N. K., Cross-coupling reactions of aryl pivalates with boronic acids. *J. Am. Chem. Soc.* **2008**, *130*, 14422-3.
22. Alvarez-Bercedo, P.; Martin, R., Ni-catalyzed reduction of inert C-O bonds: a new strategy for using aryl ethers as easily removable directing groups. *J. Am. Chem. Soc.* **2010**, *132*, 17352-3.
23. Tobisu, M.; Yamakawa, K.; Shimasaki, T.; Chatani, N., Nickel-catalyzed reductive cleavage of aryl-oxygen bonds in alkoxy- and pivaloxyarenes using hydrosilanes as a mild reducing agent. *Chem. Commun. (Cambridge, U. K.)* **2011**, *47*, 2946-2948.
24. Wenkert, E.; Michelotti, E. L.; Swindell, C. S., Nickel-induced conversion of carbon-oxygen into carbon-carbon bonds. One-step transformations of enol ethers into olefins and aryl ethers into biaryls. *J. Am. Chem. Soc.* **1979**, *101*, 2246-2247.
25. Sergeev, A. G.; Webb, J. D.; Hartwig, J. F., A Heterogeneous Nickel Catalyst for the Hydrogenolysis of Aryl Ethers without Arene Hydrogenation. *J. Am. Chem. Soc.* **2012**, *134*, 20226-20229.
26. Fan, X. H.; Guo, K.; Guan, Y. H.; Fu, L. A.; Cui, X. M.; Lv, H.; Zhu, H. B., Efficient assembly of alpha-aryl and alpha-vinyl nitriles via iron-catalyzed ether bond activation. *Tetrahedron Lett.* **2014**, *55*, 1068-1071.

27. Ren, Y. L.; Yan, M. J.; Wang, J. J.; Zhang, Z. C.; Yao, K. S., Selective Reductive Cleavage of Inert Aryl C-O Bonds by an Iron Catalyst. *Angew. Chem., Int. Ed.* **2013**, 52, 12674-12678.
28. Jambon, D.; Gaiffe, A., Systematique de l'etude comparative de la reactivite de differents nitriles ethyleniques sur des alcools aliphatiques. Utilisation du triton B comme catalyseur. *Comptes Rendus Hebdomadaires Des Seances De L'Academie Des Sciences, Serie C: Sciences Chimiques* **1971**, 273, 2.
29. F. Fleming, F., Nitrile-containing natural products. *Nat. Prod. Rep.* **1999**, 16, 597-606.
30. Tabe, Y.; Konopleva, M.; Kondo, Y.; Contractor, R.; Tsao, T.; Konoplev, S.; Shi, Y.; Ling, X.; Watt, J. C.; Tsutsumi-Ishii, Y.; Ohsaka, A.; Nagaoka, I.; Issa, J. P.; Kogan, S. C.; Andreeff, M., PPARgamma-active triterpenoid CDDO enhances ATRA-induced differentiation in APL. *Cancer Biol Ther* **2007**, 6, 1967-77.
31. Cogley, C. J.; van den Heuvel, M.; Abbadi, A.; de Vries *, J. G., Platinum catalysed hydrolytic amidation of unactivated nitriles. *Tetrahedron Lett.* **2000**, 41, 2467-2470.
32. Allen, C. L.; Williams, J. M. J., Metal-catalysed approaches to amide bond formation. *Chem. Soc. Rev.* **2011**, 40, 3405-3415.
33. Kornblum, N.; Singaram, S., The conversion of nitriles to amides and esters to acids by the action of sodium superoxide. *The Journal of Organic Chemistry* **1979**, 44, 4727-4729.
34. Wang, R.; Falck, J. R., Transformations of X (C, O, N)-CN bonds: cases of selective X (C, O, N)-C activation. *Rsc Advances* **2014**, 4, 1062-1066.
35. Benati, L.; Leardini, R.; Minozzi, M.; Nanni, D.; Scialpi, R.; Spagnolo, P.; Strazzari, S.; Zanardi, G., A novel tin-free procedure for alkyl radical reactions. *Angewandte Chemie - International Edition* **2004**, 43, 3598 - 3601.

Chapter 5

Reactions studies of $\text{Co}^{\text{II}}((\text{tBuPhO})_2\text{NHC})\text{THF}$ and synthesis of $\text{Na}[\text{Fe}^{\text{III}}((\text{tBuPhO})_2\text{NHC})]$ and future directions

5.1 Introduction

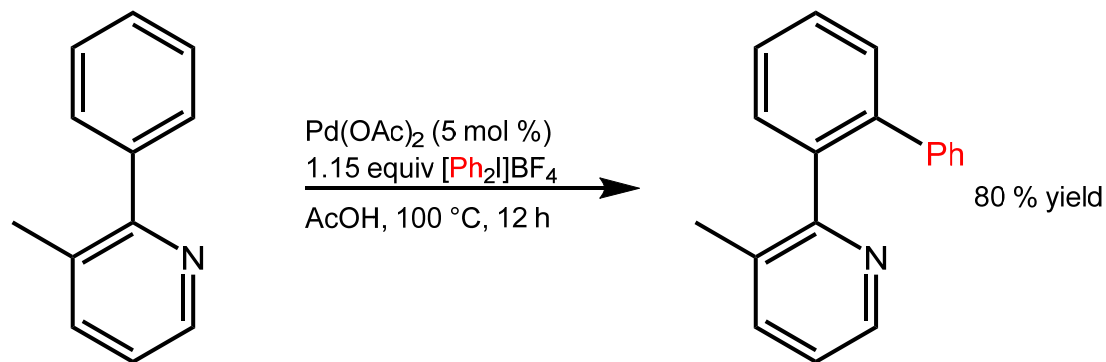
As shown in Chapter 3 of this thesis, $\text{Co}^{\text{II}}((\text{tBuPhO})_2\text{NHC})\text{THF}$ was able to generate new C–C bonds via cross-coupling that proceeds through palladium-like 2e^- organometallic steps. For example, $\text{Co}^{\text{II}}((\text{tBuPhO})_2\text{NHC})\text{THF}$ was able to cross-couple 1-bromohexane with PhMgBr to form hexylbenzene in a novel demonstration of Kumada-type C–C coupling at a well-defined base metal catalyst. The $\text{Co}^{\text{II}}((\text{tBuPhO})_2\text{NHC})\text{THF}$ complex is believed to undergo oxidative addition, transmetallation, and reductive elimination in a fashion similar to palladium catalyzed cross-coupling reactions. The oxidative addition and subsequent reductive elimination are 2e^- redox steps, but the $[\text{Co}^{\text{II}}((\text{tBuPhO})_2\text{NHC})]$ catalyst can be oxidized by 2e^- without a change in oxidation state at the cobalt center, because the redox-active ligand acts as an electron reservoir. In Chapter 4 of this thesis, the reactivity was expanded to include a novel C–O bond activation for cross-coupling of aryl Grignard reagents with ether nitriles. This reaction demonstrates the potential of this complex to perform fundamentally new 2e^- redox catalysis. Presented in this chapter are efforts to utilize this ligand-derived 2e^- redox capacity for other reactions, including C–H bond activation, and oxygen atom transfer.

5.1.1 Expanding the scope of $[M((tBuPhO)_2NHC)]$ ($M = Co, Fe$) toward C–H activation and oxygen atom transfer

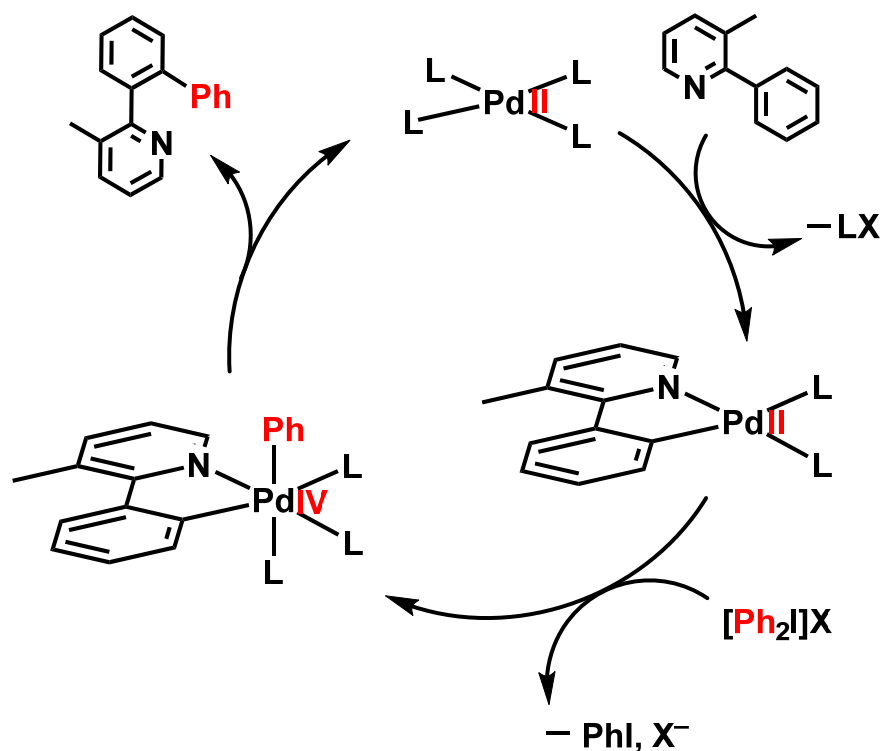
The past 10 years have seen an exponential rise in palladium methods for the selective activation and functionalization of C–H bonds.¹⁻⁴ Atom-economic routes to C–C bond forming reactions starting from unactivated C–H bonds is especially desirable in the context of sustainable (green) transformations.⁵ Because most C–C bond forming reactions involve C–X bonds, C–H bonds must first be functionalized by substitution of hydrogen for X (where X = N, O, S, Cl, Br).⁶ This activation step increases the reactivity and selectivity at a desired carbon. However, this procedure introduces extra synthetic steps and waste and selective functionalization can be challenging for many substrates. Although C–H bond activation with palladium has been known for over four decades, selective C–H bond activation has been difficult to achieve.⁷⁻⁸ A major problem with C–H bond activation, under mild conditions, has been poor regioselectivity.⁹⁻¹³ For example, $Pd(OAc)_2$ activates the C–H bond in benzene in the presence of $NaNO_2$ and HOAc at 100 °C to generate both nitrobenzene and phenylacetate (in a 1:1 ratio).¹⁴

Scheme 5-1. a) A reaction between 3-methyl-2-phenylpyridine and diphenyliodide catalyzed by $\text{Pd}(\text{OAc})_2$ to produce 2-([1,1'-biphenyl]-2-yl)-3-methylpyridine.¹⁶ b) proposed mechanism for C–H bond activation at Pd^{II} (L = ancillary ligands).

a)



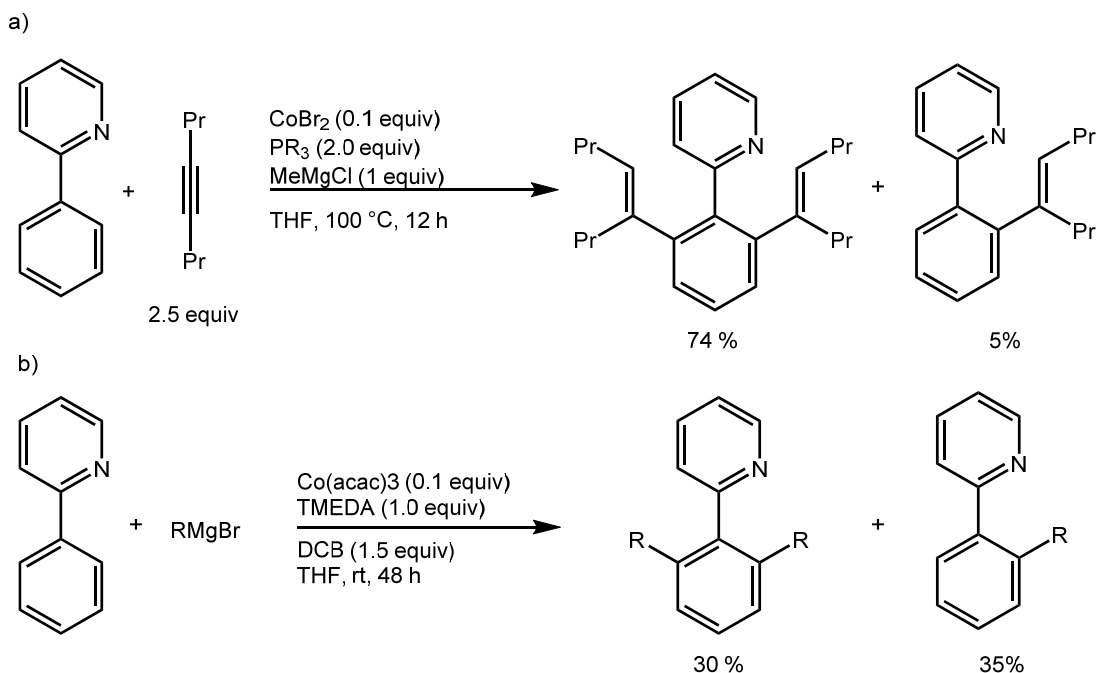
b)



Pioneering work from Sanford and co-workers elaborated a new method for selectively activating aryl C–H bonds using a palladium catalyst (**Scheme 5-1 a**).¹⁵⁻¹⁶ This strategy involves combining the substrate and ligand into one. For example, combining pyridine and benzene in the form of 2-phenylpyridine allows the nitrogen to bind to the metal center and exposes only two C–H bonds to the palladium. The proposed mechanism

involves 2-phenylpyridine binding to Pd^{II} and electrophilic C–H bond activation (Scheme 5-1 b).¹⁵ Then $2e^-$ oxidation of Pd^{II} to Pd^{IV} permits for reductive elimination to produce a substituted 2-phenylpyridine and regenerate the starting Pd^{II} catalyst.¹⁷

Scheme 5-2. C-H activation of 2-phenylpyridine using Co salts in the presence of a) alkyne
b) Grignard reagent to generate the mono and disubstituted aryl.

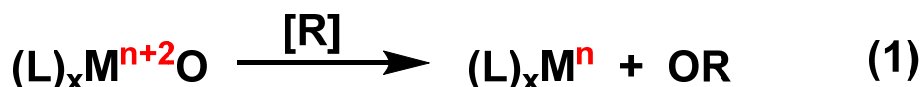


Recently, Fujita and co-workers have demonstrated analogous C–H bond activation reactivity using CoBr_2 .¹⁸ As shown in **Scheme 5-2**, the C–H bond on 2-phenylpyridine with 2-octyne to produce the *ortho*-dialkenylated product (74 % yield) and the mono-alkenylated product.¹⁸ The reaction only proceeds in the presence of a phosphine ligand and under a very reducing environment (stoichiometric amounts of methyl magnesium chloride) at 100 °C for 12 hours. The yields are good, but the overall mechanism is still not known. Also, the oxidation state of the metal catalyst is unknown. Shi and co-workers expanded this reactivity to include using Grignard reagents to cross-couple to the 2-phenylpyridine (**Scheme 5-2 b**).¹⁹ Their mechanistic studies seem to

preclude a radical mechanism, leading the authors to favor a $2e^-$, $\text{Co}^{\text{I}}/\text{Co}^{\text{III}}$ catalytic cycle.

Since $\text{Co}^{\text{II}}((\text{tBuPhO})_2\text{NHC})\text{THF}$ can be oxidized by $2e^-$, it was hypothesized that this complex might be able to activate C–H bonds. While 2-phenylpyridine is an attractive substrate for C–H bond activation, the $\text{Co}^{\text{II}}((\text{tBuPhO})_2\text{NHC})\text{THF}$ electron transfer (ET) series has an affinity for oxygen atoms, as evidenced by the fact that all three oxidation states of $\text{Co}^{\text{II}}((\text{tBuPhO})_2\text{NHC})\text{THF}$ contain THF as a ligand. Therefore, oxygen containing ether moieties could be better directing groups for the $\text{Co}^{\text{II}}((\text{tBuPhO})_2\text{NHC})\text{THF}$ ET series.

Metal mediated oxygen atom transfer reactions are essential redox steps in chemical processes ranging from energy conversion and storage,²⁰⁻²¹ to *in vivo* processing of cytotoxic materials,²²⁻²³ and the production of industrial chemicals.²⁴⁻²⁵ As illustrated in **Equation 1**, delivery of an oxygen equivalent from an oxo metal species is a $2e^-$ redox process at the metal center. Inspired by biological oxo-transfer, the past



two decades have seen significant progress in the development of later 3d metals for oxo transfer catalysis.²⁶ However, complexes containing multiply bonded metal oxygen fragments with base metals later than group 8 are rare due to lack of vacant d orbitals with π symmetry to stabilize the M–O linkage.²⁷ This is the so called "oxo wall" which states that d electron counts higher than five in an octahedral complex will be unable to stabilize the oxygen atom p-orbitals.²⁷ Since metals in groups 9, 10, 11, and 12 have high energetic barriers to generate d^4 oxidation states, they are no longer stable towards

H₂O₂ or O₂.²⁷ Although there are several group 9 metals that have metal oxo bonds (Ir^V(O)(mesityl)₃²⁸ and Pt^{IV}(O)²⁹) which do not break the “oxo wall” rule due to coordination geometries and ligand choice that allow for vacant d orbitals with π symmetry. Furthermore, work done by Nocera *et. al.* using a thin film Co–Pi (Pi = methylphosphonate) catalyst demonstrated H₂O oxidation, where a Co^{IV}=O complex is believed to be an intermediate, in O₂ production.^{21, 30-32}

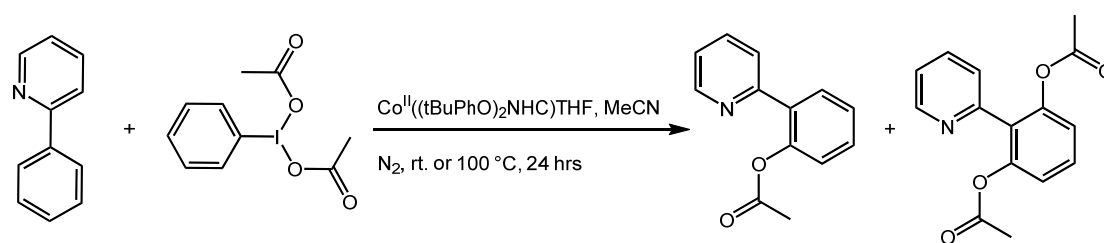
The multielectron redox capacity of Co^{II}((tBuPhO)₂NHC)THF complex makes it an interesting candidate for oxygen atom transfer. I therefore set out to evaluate oxygen atom transfer to/from Co^{II}((tBuPhO)₂NHC)THF, with the aim of preparing and characterizing unusual oxo intermediates and/or developing new cobalt-catalyzed oxo transfer cycles to an organic substrate.

5.2 Results

5.2.1 Attempts at C–H bond activation with Co^{II}((tBuPhO)₂NHC)THF

Attempting to mimic C–H bond activation seen in Pd^{II} systems, 2-phenylpyridine and iodosobenzene diacetate (PhI(OAc)₂) were reacted in the presence of a catalytic amount of Co^{II}((tBuPhO)₂NHC)THF (10 mol %) for 24 hr (**Scheme 5-3**). The desired

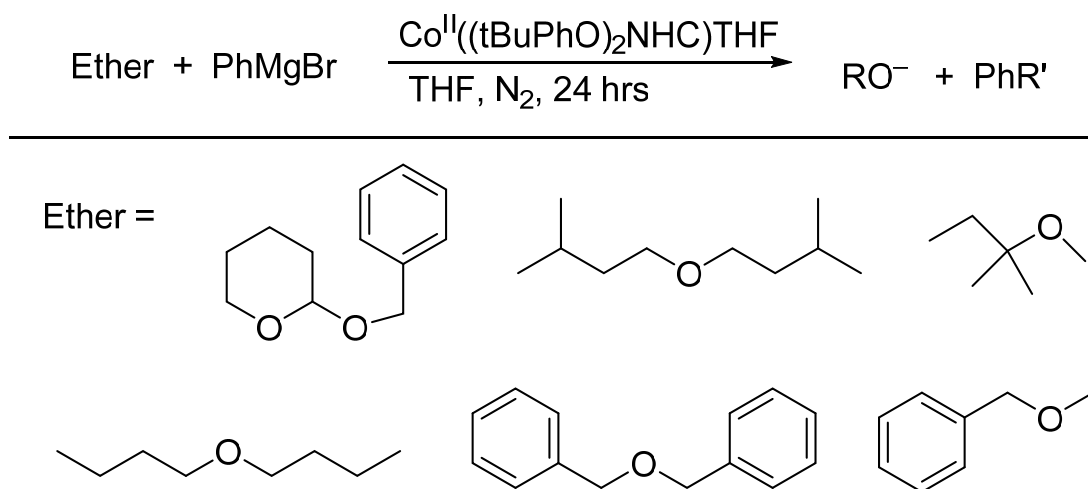
Scheme 5-3. Proposed C–H activation reaction between 2-phenyl pyridine and iodosobenzene diacetate catalyzed by Co^{II}((tBuPhO)₂NHC)THF



product was not observed in either reaction. However, ESI–MS analysis showed a peak

at 690 m/z which corresponds to the molecular weight of the starting $\text{Co}^{\text{II}}((\text{tBuPhO})_2\text{NHC})\text{THF}$ complex and 2-phenylpyridine. No other metal containing species was observed by ESI. Although product was not detected, several other peaks were present in the GC-MS trace, however, they could not be assigned to any oxidized 2-phenyl pyridine complex. Using 2,3,4,5,6,6-hexachlorocyclohexa-2,4-dien-1-one (HCP) as a 2e^- oxidant, a Cl^+ reagent, a reaction between 2-phenylpyridine and HCP in the presence of either $\text{Co}^{\text{II}}((\text{tBuPhO})_2\text{NHC})\text{THF}$ or $[\text{Co}^{\text{III}}((\text{tBuPhO})_2\text{NHC})\text{THF}_2]^+$ lead to an immediate color change to green and a very small amount ($< 1\%$) of 2-(2-chlorophenyl)pyridine as judged by GC-MS. In a separate reaction *m*-CPBA was used as the oxidant, replacing $\text{PhI}(\text{OAc})_2$ in **Scheme 5-3**. Unfortunately, no C–H bond activation followed by cross-coupling was observed.

Scheme 5-4 .Reactions between ethers and PhMgBr using $\text{Co}^{\text{II}}((\text{tBuPhO})_2\text{NHC})\text{THF}$.



Since the $[\text{Co}((\text{tBuPhO})_2\text{NHC})(\text{THF})_{n+1}]^{n+}$ ET series, Chapter 3 of this thesis, has an affinity for ethers (in the form of THF), we proposed that an ether might be a better chelation ligand to direct a C–H bond towards the metal center. To test this theory several ethers were chosen and tested for C–H bond activation (**Scheme 5-4**).

Exposure of $\text{Co}^{\text{II}}((\text{tBuPhO})_2\text{NHC})\text{THF}$ to the ethers in **Scheme 5-4** did not lead to a color change. Adding PhMgBr lead to an immediate color change and the production of biphenyl. However, no cross-coupling between the ether and aryl Grignard was observed by GC-MS.

5.2.2 Stoichiometric reactions of $\text{Co}^{\text{II}}((\text{tBuPhO})_2\text{NHC})\text{THF}$ with O-atom transfer reagents

Attempts were made to oxidize $\text{Co}^{\text{II}}((\text{tBuPhO})_2\text{NHC})\text{THF}$ using meta-chloroperoxybenzoic acid (*m*-CPBA) and iodosylbenzene (PhIO). Dissolving $\text{Co}^{\text{II}}((\text{tBuPhO})_2\text{NHC})\text{THF}$ in CH_3CN affords an orange solution with several new low intensity peaks at 542 nm, 589 nm, and 778 nm, which are not present when $\text{Co}^{\text{II}}((\text{tBuPhO})_2\text{NHC})\text{THF}$ is dissolved in THF. Exposure of this orange solution to 1 equiv *m*-CPBA results in a decrease in the intensity of the peak at 423 nm by 50 % (**Figure 5-1 b**) with a commensurate increase in the 542 nm, 589 nm, and 778 nm peaks during the first 30 seconds of the reaction. Over the course of an hour, the peaks at 423, 589 and 778 nm decrease to produce a broad low intensity peak at 750 nm in a UV-vis spectrum corresponding to a green solution. In contrast, when 0.5 equiv *m*-CPBA was added no increase in any peaks were noticed after an hour. The solution still remained a light orange (**Figure 5-1 a**) and after an hour, the solution turned green, and the spectra matched that obtained with 1 equiv of *m*-CPBA after one hour. Addition of 3 equiv of *m*-CPBA to the $\text{Co}^{\text{II}}((\text{tBuPhO})_2\text{NHC})\text{THF}$ containing solution immediately turned green and no increase in absorbance was seen (**Figure 5-1 c**).

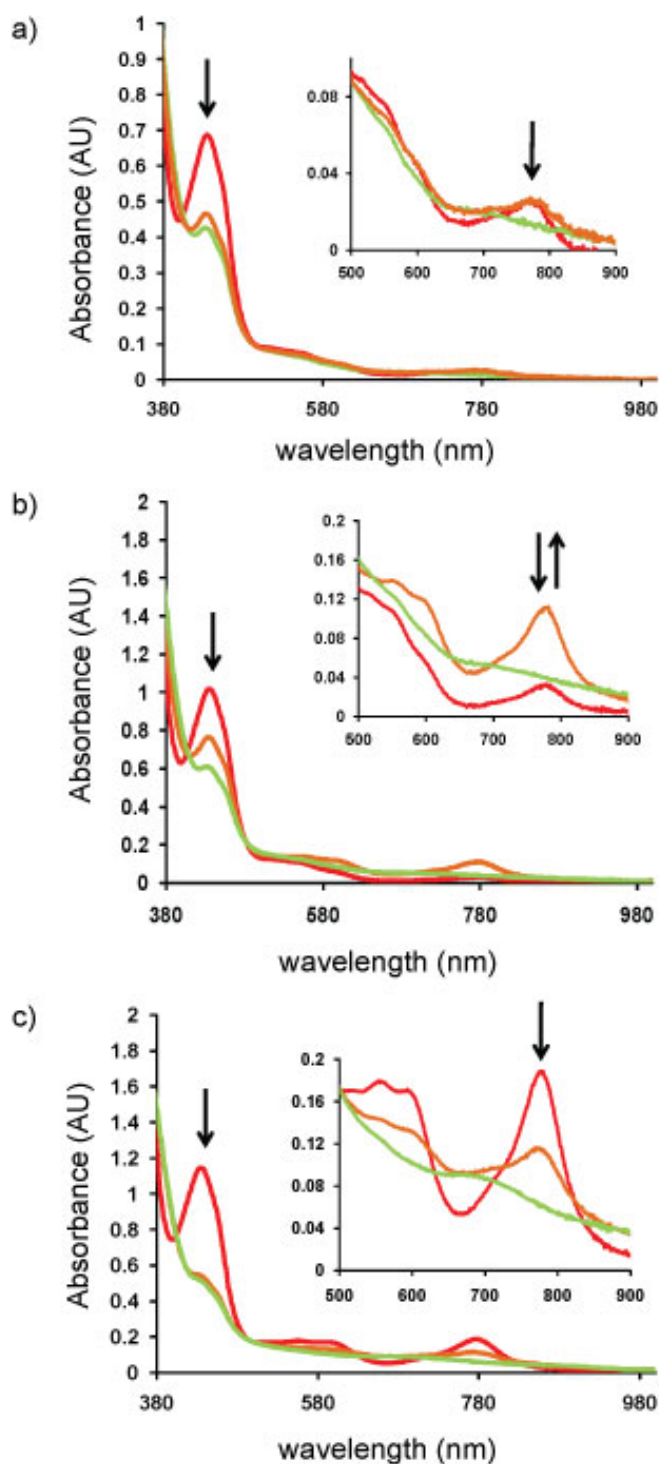

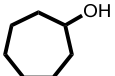
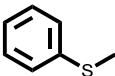
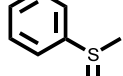
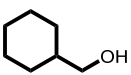
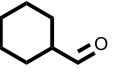

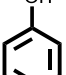
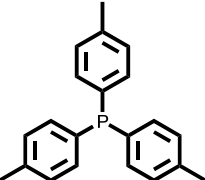
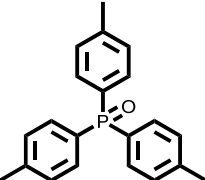
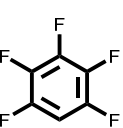
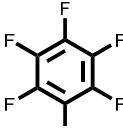
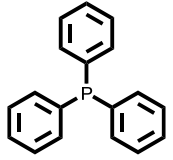
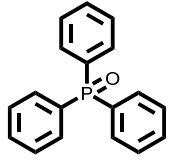
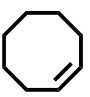
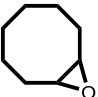
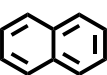
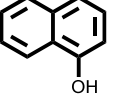
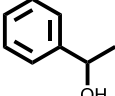
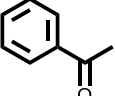
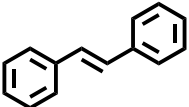
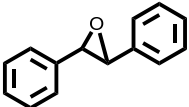
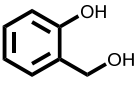
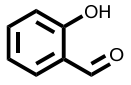
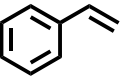
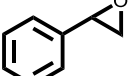


Figure 5-1 UV-Vis spectra of a reaction between $\text{Co}^{\text{II}}((\text{tBuPhO})_2\text{NHC})\text{THF}$ and m-CPBA in CH_3CN . Red line represents $\text{Co}^{\text{II}}((\text{tBuPhO})_2\text{NHC})\text{THF}$ in CH_3CN prior to m-CPBA addition. Orange line represents 30 sec after m-CPBA addition. Green line represents 60 mins after m-CPBA addition. a) 0.5 equiv of m-CPBA. b) 1 equiv of m-CPBA c) 3 equiv of m-CPBA.

The peak at 428 nm is converted to a shoulder which is not seen when stoichiometric or substoichiometric amounts of *m*-CPBA is used. When $\text{Co}^{\text{II}}((\text{tBuPhO})_2\text{NHC})\text{THF}$ was reacted with 1 equiv of PhIO in THF, a similar color change from orange to green occurred over the course of 60 mins at ambient temperature. However, the two oxidants, PhIO and *m*-CPBA, produced two different absorption spectra. The UV-Vis spectrum of the PhIO reaction with $\text{Co}^{\text{II}}((\text{tBuPhO})_2\text{NHC})\text{THF}$ showed a loss of the peak at 423 nm and a new low absorbance peak at 671 nm. However when 10 equiv of PhIO is added to $\text{Co}^{\text{II}}((\text{tBuPhO})_2\text{NHC})\text{THF}$ the absorption spectra generated matches that of 3 equiv of *m*-CPBA. ESI-MS analysis of all three reactions in **Figure 5-1** contained $\text{Co}^{\text{II}}((\text{tBuPhO})_2\text{NHC})\text{THF}$, however, there were no *m/z* peaks indicative of a metal oxo species. Attempts to grow crystals of the green solution produced only an amorphous powder.

To test oxygen atom transfer to an organic substrate, $\text{Co}^{\text{II}}((\text{tBuPhO})_2\text{NHC})\text{THF}$, 2 equiv of an organic substrate, and 2 equiv of an oxygen atoms transfer reagent (*m*-CPBA) were allowed to react for 24 hours in THF under N_2 (**Table 5-1**). The result in all cases studied, as judged by GC-MS, did not lead to oxygen atom transfer (**Table 5-1**), except in the case of triphenylphosphine ($\text{P}(\text{Ph})_3$) and tri(*p*-tolyl)phosphine ($\text{P}(\text{tol})_3$) where the amount of $\text{O}=\text{P}(\text{Ph})_3$ or $\text{O}=\text{P}(\text{tol})_3$ did not exceed the control, in which no metal was present.

Table 5-1. Oxygen atom transfer to organic substrates using $\text{Co}^{\text{II}}((\text{tBuPhO})_2\text{NHC})\text{THF}$

$[\text{S}] + \text{m-CPBA} \xrightarrow[\text{N}_2, \text{MeCN}, 24 \text{ hr, rt}]{\text{Co}^{\text{II}}((\text{tBuPhO})_2\text{NHC})\text{THF}} [\text{S}=\text{O}] \text{ or } [\text{S}-\text{OH}]$					
Organic Substrate [S]	Desired Product [S=O] or [S-OH]	yield % ¹	Organic Substrate [S]	Desired Product [S=O] or [S-OH]	yield % ¹
		N.R.			N.R.
		N.R.			N.R.
		N.R.*			N.R.
		N.R.*			N.R.
		N.R.			N.R.
		N.R.			N.R.
					N.R.

¹ Yield judged by GC-MS. * Oxygenated products were observed however the yield was significantly less than control (in which no metal was present).

No by-product of the oxygen atom transfer reagents was observed by GC-MS. The $\text{Co}^{\text{II}}((\text{tBuPhO})_2\text{NHC})\text{THF}$ complex remains in the final solution as judged by ESI and MALDI, however, the amount could not be quantified.

5.2.3 $[\text{Fe}((\text{tBuPhO})_2\text{NHC})\text{Cl}_2]^-$ and $[\text{Fe}((\text{tBuPhO})_2\text{NHC})]^+$ synthesis and characterization

Iron with redox-active ligands has already been shown to be of interest in both the $\text{Fe}^{\text{III}}(\text{ap}^{\text{Ph}})_2$, Chapter 2, and the $(^{\text{Pr}}\text{PDI})\text{Fe}(\text{N}_2)_2$ complex from the Chirik group.³³ Generating the $[\text{Fe}^{\text{III}}((\text{tBuPhO})_2\text{NHC})]^+$ complex could not only expand the reactions that the NHC ligand could afford, its designed to remedy many of the challenges seen with the $[\text{Fe}^{\text{III}}(\text{ap}^{\text{Ph}})_2]^-$ including ligand rearrangement, and ease of oxidation. The $[\text{Fe}((\text{tBuPhO})_2\text{NHC})]^+$ ET series is also a better candidate for metal-oxo chemistry. For example, previously reported $\text{Fe}^{\text{IV}}=\text{O}$ complexes could oxygenate olefins³⁴, $\text{P}(\text{Ph})_3$ ³⁵, sulides³⁶, and alkanes³⁷. To this end, $[\text{Fe}((\text{tBuPhO})_2\text{NHC})]^+$ will be synthesized and tested for chemistry requiring 2e^- transformations, such as selective C-C bond forming reactions and oxygen atom transfer.

A solution of FeCl_3 in CH_3CN was added to a yellow, MeOH solution of deprotonated $[(\text{tBuPhO})_2\text{NHC}]^{2-}$ to immediately afford a purple solution.

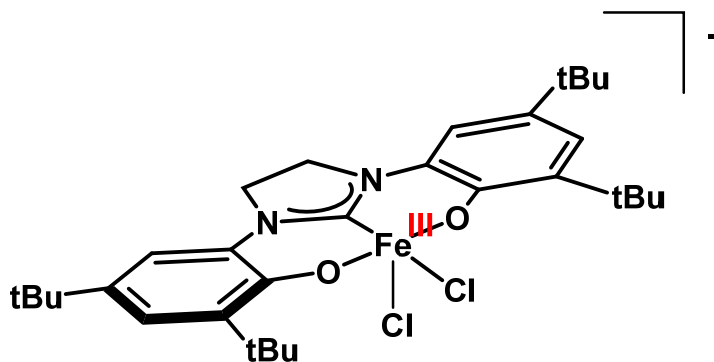


Figure 5-2. Proposed structure of $[\text{Fe}^{\text{III}}((\text{tBuPhO})_2\text{NHC})\text{Cl}_2]^-$.

The resulting purple solution was filtered, dried, taken up in THF, filtered and dried again to afford a purple powder in moderate (47 %) yield. ESI-MS showed a parent ion peak at 602.2 m/z with an isotopic splitting pattern matched that for the $[(\text{tBuPhO})_2\text{NHC}]^{2-}$

bound to one iron metal with two chlorides associated (calculated 602.21 m/z).

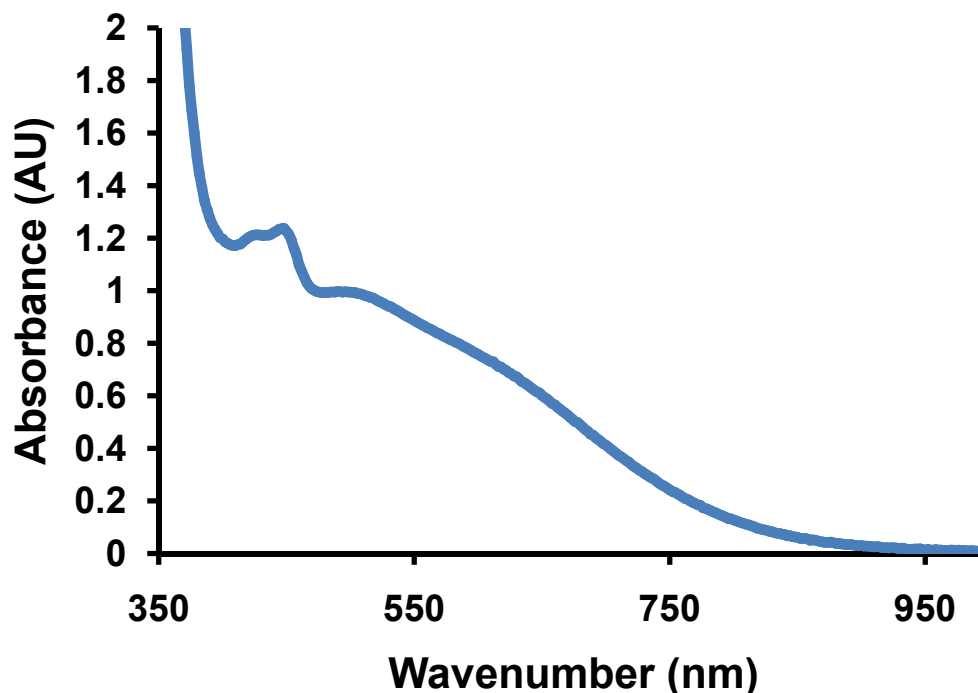


Figure 5-3. UV-vis absorption spectrum for $[\text{Fe}^{\text{III}}((\text{tBuPhO})_2\text{NHC})\text{Cl}_2][\text{Na}]$ in THF at room temperature.

Assuming that the ligand is still reduced, the complex is best thought of as Fe^{III} bound in a tridentate fashion to $[(\text{tBuPhO})_2\text{NHC}]^{2-}$, with two chlorides bound to iron to give an overall anionic complex $\text{Na}[\text{Fe}^{\text{III}}((\text{tBuPhO})_2\text{NHC})\text{Cl}_2]$ (**Figure 5-2**). The UV-Vis spectrum of the purple $\text{Na}[\text{Fe}((\text{tBuPhO})_2\text{NHC})\text{Cl}_2]$ complex shows a peaks at 428 nm and 500 nm (**Figure 5-3**). The peak at 428 nm is reminiscent of the 423 nm peak seen in the $\text{Co}^{\text{II}}((\text{tBuPhO})_2\text{NHC})$ complex (Chapter 3 of this thesis). Repeated attempts to obtain single crystals of the $\text{Na}[\text{Fe}((\text{tBuPhO})_2\text{NHC})\text{Cl}_2]$ complex did not yield X-ray quality crystals. The absence of X-ray data precludes assignment of the ligand oxidation state but based on the aforementioned data formulation as a cationic, square pyramidal Fe^{III} complex bound to a $[(\text{tBuPhO})_2\text{NHC}]^{2-}$ in a tridentate fashion with two chlorides is

reasonable. Assuming this formula is correct, an epsilon value of $4000 \text{ M}^{-1} \text{ cm}^{-1}$ (428 nm) is likely to be charge transfer bands.

The complex has an open circuit potential of -0.40 V vs Fc^+/Fc and shows a quasi-reversible oxidation wave at 0.27 V (**Figure 5-4**). An irreversible oxidation wave is seen at 0.78 V . There are two irreversible

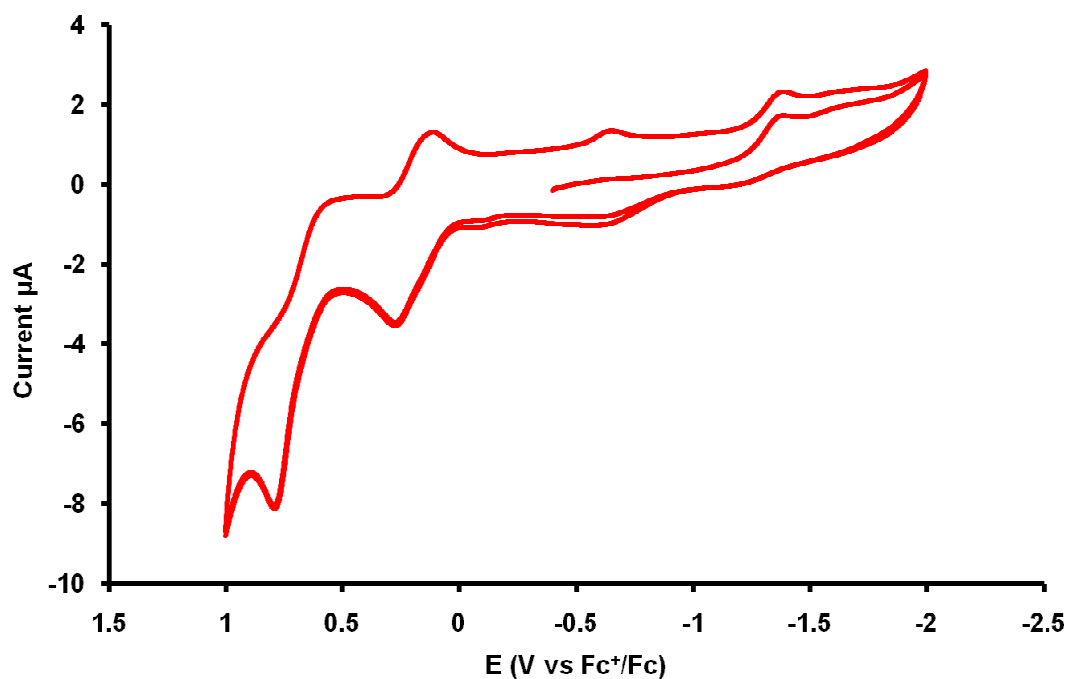


Figure 5-4. Cyclic voltammogram of $\text{Na}[\text{Fe}^{\text{III}}((\text{tBuPhO})_2\text{NHC})\text{Cl}_2]$ in THF containing 0.1 M $[\text{nBu}_4\text{N}][\text{PF}_6]$ at a 10 mm Pt electrode. Scan rate: 0.05 V s^{-1} . Temperature: $25 \text{ }^\circ\text{C}$.

reduction waves at -0.63 and -1.38 V . The complex has 2 oxidation events and 2 reduction events and the ability to span a total of 4e^- .

Exposure of $[\text{Fe}((\text{tBuPhO})_2\text{NHC})\text{Cl}_2]^-$ to air did not cleanly generate the 1 e^- oxidized product. Over the course of 24 hrs the UV-Vis intensity did decrease by 25 % however no new peaks developed and the solution remained purple. No color changes were observed upon addition of 1 equiv of AgBF_4 , as an oxidant, but, 2 equiv did lead to the loss of the 470 nm peak. Isolation of a quality single crystal was not achieved for the

silver oxidized product. Oxidation of the $[\text{Fe}((\text{tBuPhO})_2\text{NHC})\text{Cl}_2]^-$ complex using 1 equiv of WCl_6 in CH_2Cl_2 lead to a new red solution that deposited red crystals suitable for solid

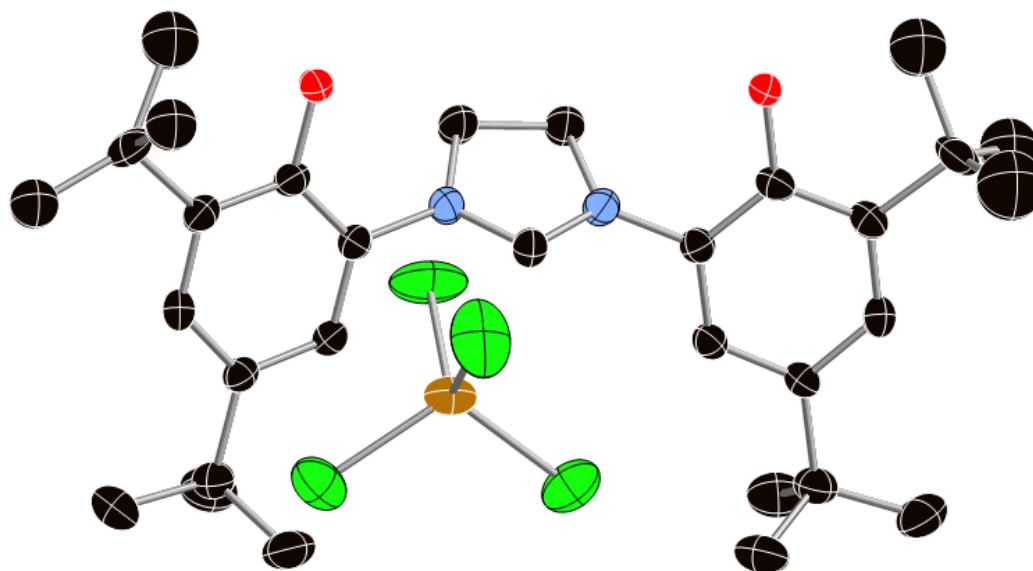


Figure 5-5. Solid-state structure of $[(\text{tBuPhO})_2\text{NHC}]\text{H}_3^+[\text{FeCl}_4]^-$ shown with 50% probability ellipsoids. Hydrogen atoms omitted for clarity.

state analysis from a solution of CH_2Cl_2 layered with pentane. The resulting crystal structure showed a fully protonated and reduced $[(\text{tBuPhO})_2\text{NHC}]^+$ with $[\text{FeCl}_4]^-$ as the counter ion (**Figure 5-5**).

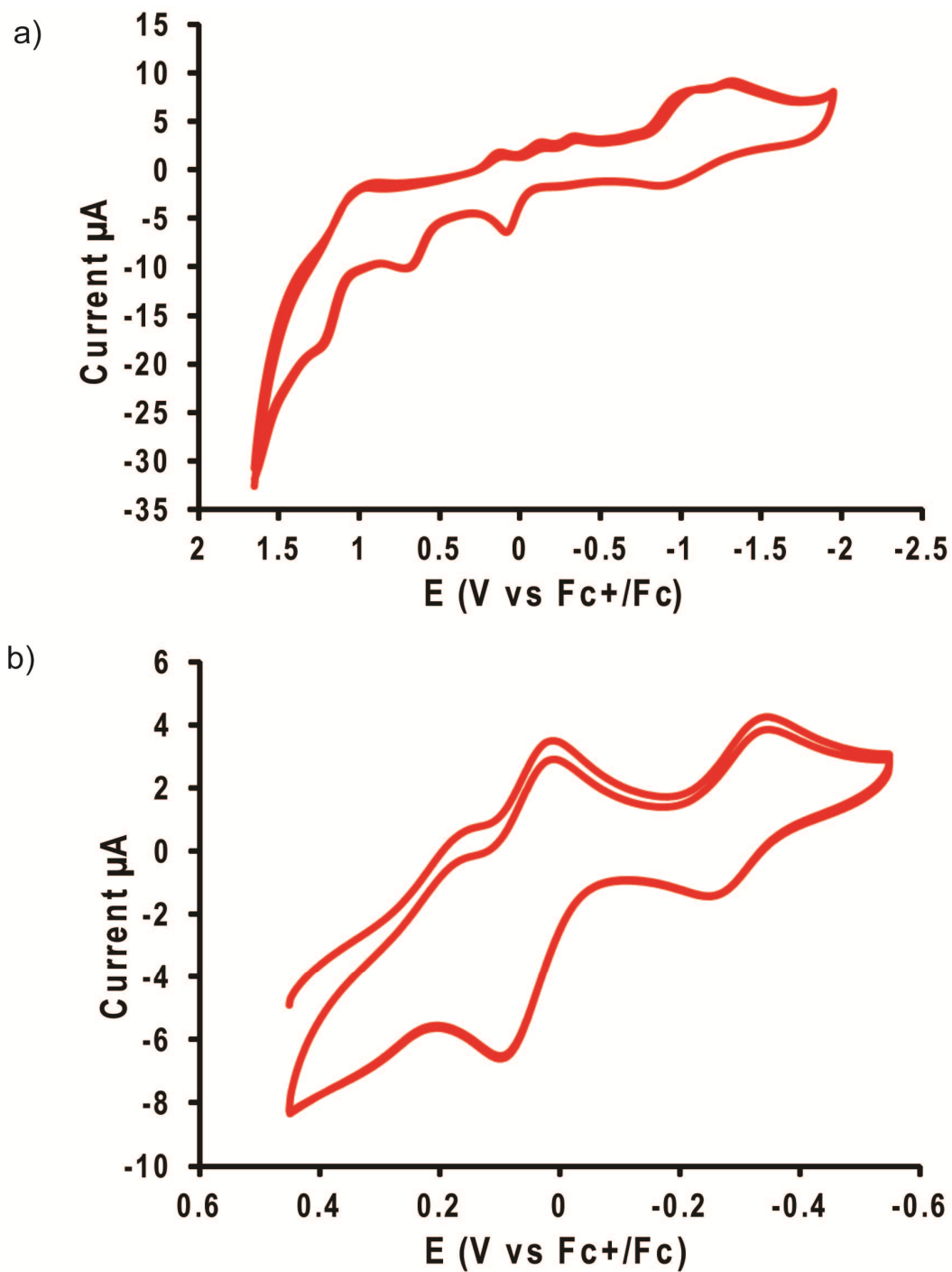


Figure 5-6. Cyclic voltammogram of $[\text{Fe}^{\text{III}}((\text{tBuPhO})_2\text{NHC})(\text{MeOH})_2]\text{ClO}_4$ in CH_3CN containing $0.1 \text{ M } [\text{nBu}_4\text{N}][\text{PF}_6]$ at a 10 mm Pt electrode. Temperature: 25°C . a) Scan rate: $0.100 \text{ V}\cdot\text{s}^{-1}$. b) Scan rate: $0.500 \text{ V}\cdot\text{s}^{-1}$.

To produce a halide free version of $\text{Na}[\text{Fe}^{\text{III}}((\text{tBuPhO})_2\text{NHC})\text{Cl}_2]$ addition of $\text{Fe}^{\text{III}}(\text{ClO}_4)_3$ to the deprotonated ligand $[(\text{tBuPhO})_2\text{NHC}]^{2-}$ in MeOH, yielded a purple solution. This new complex has a UV-Vis with a two peaks at 342 nm and 532 nm (Figure 5-7). ESI-MS shows an isotopic splitting pattern and 594.4 m/z consistent with an iron bound to one $[(\text{tBuPhO})_2\text{NHC}]^{2-}$ ligand and two associated methanols

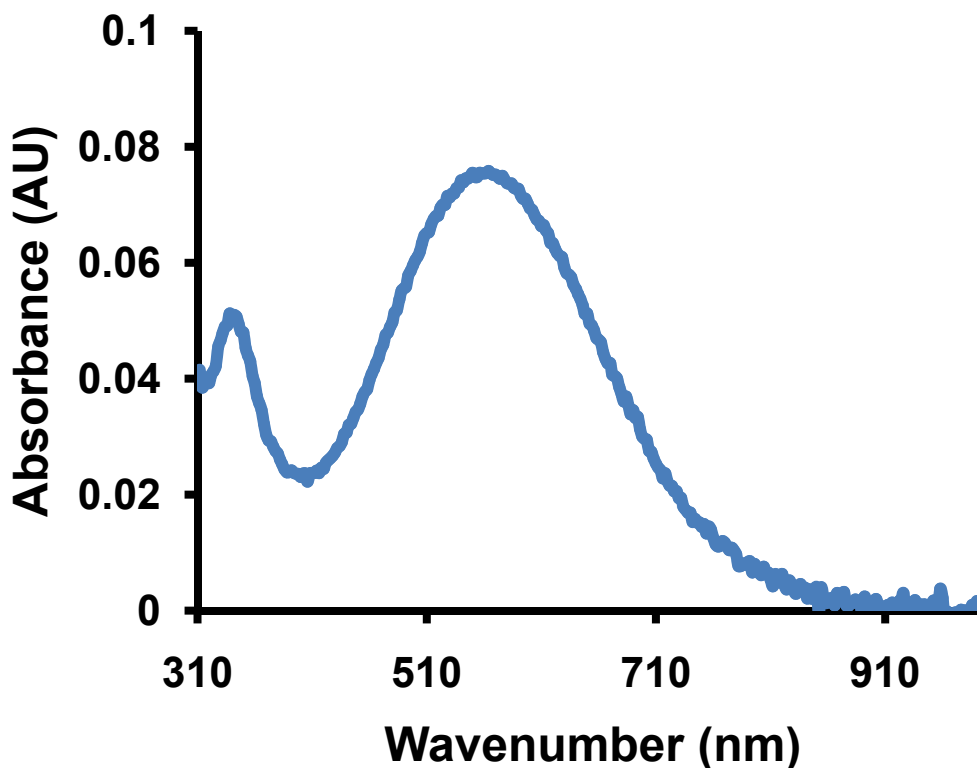


Figure 5-7. UV-vis absorption spectrum for $[\text{Fe}^{\text{III}}((\text{tBuPhO})_2\text{NHC})(\text{MeOH})_2]\text{ClO}_4$ in THF at room temperature.

$[\text{Fe}^{\text{III}}((\text{tBuPhO})_2\text{NHC})(\text{MeOH})_2]^+$ (594.4 m/z). The open circuit potential for $[\text{Fe}^{\text{III}}((\text{tBuPhO})_2\text{NHC})(\text{MeOH})_2]\text{ClO}_4$ is at -0.39 V which is the same open circuit potential as $\text{Na}[\text{Fe}((\text{tBuPhO})_2\text{NHC})\text{Cl}_2]$. The $[\text{Fe}^{\text{III}}((\text{tBuPhO})_2\text{NHC})(\text{MeOH})_2]\text{ClO}_4$ complex shows no reversible peaks when the potential window covers ~ 4.0 V at a scan rate of 100 mV s^{-1} (Figure 5-6 a). The $[\text{Fe}^{\text{III}}((\text{tBuPhO})_2\text{NHC})(\text{MeOH})_2]\text{ClO}_4$ shows two oxidation events above the open potential at 0.07 and 0.69 V. There are also two irreversible reduction

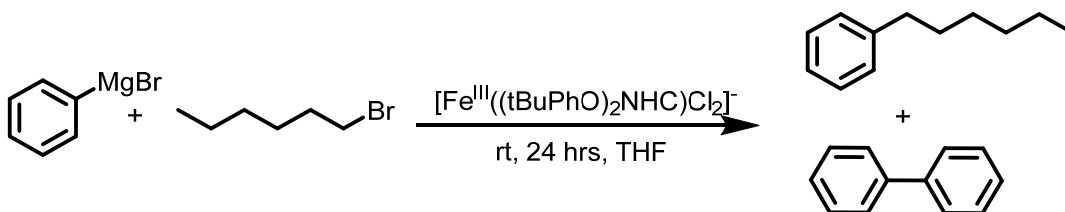
events negative of the open circuit potential at -1.02 and -1.31 V. However, when the scan rate is increased to 500 mVs⁻¹ and the potential window is narrowed, two quasi-reversible oxidation waves are seen at -0.31 and 0.09 V (**Figure 5-6 b**).

Attempts were made to chemically oxidize [Fe^{III}((tBuPhO)₂NHC)(MeOH)₂]ClO₄. Exposure of [Fe^{III}((tBuPhO)₂NHC)(MeOH)₂]ClO₄ to 1 or 2 equiv of AgBF₄ gives a distinct color change from purple to green in both cases. With 1 equiv of AgBF₄ the UV-Vis spectrum showed a blue shift of both peaks to 393 nm and 556 nm. When 2 equiv of AgBF₄ were used the peak at 393 nm remained, however, a new peak at 500 nm appeared with the disappearance of the peak at 556 nm. Numerous attempts to obtain single crystals of the oxidation products yielded only amorphous powders.

5.2.4 $[\text{Fe}((\text{tBuPhO})_2\text{NHC})(\text{MeOH})_2]^+$ catalyzed cross-coupling of alkyl halides and Grignards

Given the similarities of $[\text{Fe}((\text{tBuPhO})_2\text{NHC})\text{Cl}_2]^-$ to $\text{Co}^{\text{II}}((\text{tBuPhO})_2\text{NHC})\text{THF}$ attempts were made to utilize this new iron complex for Kumada-type cross-coupling of aryl Grignard reagents and alkyl halides. As summarized in **Table 5-2**, the $[\text{Fe}((\text{tBuPhO})_2\text{NHC})\text{Cl}_2]^-$ complex was reacted with PhMgBr in the presence of alkyl halides at room temperature under N_2 and aerobic conditions. At 16 % catalyst loading of $\text{Na}[\text{Fe}((\text{tBuPhO})_2\text{NHC})\text{Cl}_2]$ 25 % yield of the desired cross-coupled product

Table 5-2. Cross-coupling yields of PhMgBr and 1-bromohexane in the presence of $[\text{Fe}^{\text{III}}((\text{tBuPhO})_2\text{NHC})\text{Cl}_2]^-$ under N_2 or aerobic conditions.



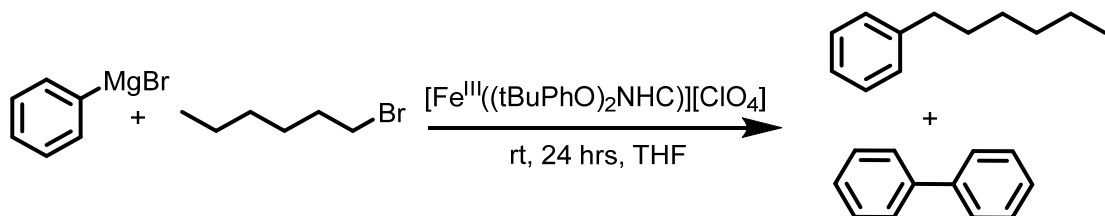
Entry	Condition	Equiv vs [Fe] used		Yield % vs organic ¹		TON vs [Fe]	
		PhMgCl	HxBr	Ph-Ph	Ph-Hx	Ph-Ph	Ph-Hx
1	N_2	0.6	0.6	79	13	0.23	0.08
2	N_2	1.2	1.2	80	20	0.48	0.25
3	N_2	3	3	67	22	1.00	0.66
4	N_2	6	6	59	25	1.77	1.50
5	Air	0.6	0.6	81	14	0.24	0.08
6	Air	1.2	1.2	81	19	0.48	0.23
7	Air	3	3	69	23	1.03	0.69
8	Air	6	6	71	22	2.13	1.32

¹Yields determined by GC-FID using decane as an internal standard.

(hexylbenzene, Ph-Hx) was achieved. This represents 1.5 TON vs $\text{Na}[\text{Fe}((\text{tBuPhO})_2\text{NHC})\text{Cl}_2]$. Also of interest, the ratio of undesired homocoupling vs

cross-coupling is nearly 1:1 vs $[\text{Fe}((\text{tBuPhO})_2\text{NHC})\text{Cl}_2]^-$ under N_2 . Under aerobic

Table 5-3. Cross-coupling yields of PhMgBr and 1-bromohexane in the presence of $[\text{Fe}^{\text{III}}((\text{tBuPhO})_2\text{NHC})(\text{MeOH})_2]\text{ClO}_4$ under N_2 or aerobic conditions.



Entry	Condition	Equiv vs [Fe] used		Yield % vs organic ¹		TON vs [Fe]	
		PhMgCl	HxBr	Ph-Ph	Ph-Hx	Ph-Ph	Ph-Hx
1	N_2	1	1	33	2	0.17	0.02
2	N_2	2	2	41	4	0.41	0.08
3	N_2	5	5	51	10	1.27	0.47
4	N_2	10	10	50	12	2.49	1.17
5	Air	1	1	31	2	0.15	0.02
6	Air	2	2	40	4	0.40	0.08
7	Air	5	5	52	9	1.29	0.47
8	Air	10	10	51	12	2.54	1.18

¹Yield determined by GC-FID using decane as an internal standard

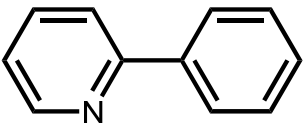
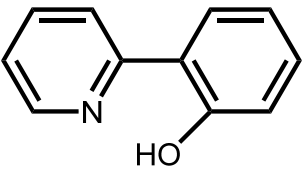
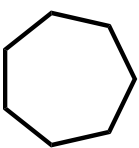
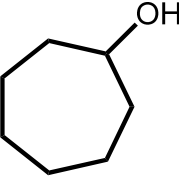
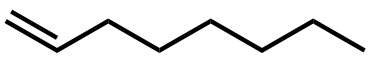
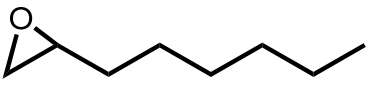

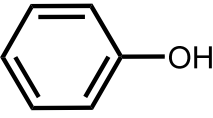
conditions the ratio of Ph-Ph to Ph-Hx is 2:1. Under an atmosphere of air the $[\text{Fe}((\text{tBuPhO})_2\text{NHC})\text{Cl}_2]^-$ appears to be acting like $\text{FeCl}(\text{isq}^{\text{Ph}})_2$ (Chapter 2) in which the Fe complex is reduced by reductive elimination of 2 equiv of Grignard and then oxidized by O_2 to reform the complex as evidenced by the homocoupling yields of nearly 50% (Table 5-3, entry 7-8).

When $[\text{Fe}^{\text{III}}((\text{tBuPhO})_2\text{NHC})(\text{MeOH})_2]\text{ClO}_4$ was used as the catalyst in the above reaction under the same conditions a lower yield of cross-coupling product, Ph-Hx, (Table 5-3) and a higher yield of the homocoupled, biphenyl, was observed. Under both N_2 and air, the ratio of homocoupled product to cross-coupled product was 2.5:1.

5.2.5 $[\text{Fe}^{\text{III}}((\text{tBuPhO})_2\text{NHC})(\text{MeOH})_2]\text{ClO}_4$ reactivity with oxygen transfer reagents

The $[\text{Fe}^{\text{III}}((\text{tBuPhO})_2\text{NHC})(\text{MeOH})_2]\text{ClO}_4$ complex was reacted with an oxygen transfer reagent (*m*-CBPA) and several organic substrates. A smaller list of substrates was chosen in comparison to $\text{Co}^{\text{II}}((\text{tBuPhO})_2\text{NHC})$ complex. In all cases no oxygenated substrate was seen except in the case of $\text{P}(\text{Ph})_3$ where the amount of $\text{O}=\text{P}(\text{Ph})_3$ did not exceed the control reaction in which no metal was present (**Table 5-4**). Color changes were observed in every reaction except in the case of $\text{P}(\text{PH})_3$. All of the other reactions changed color from purple to orange upon addition of *m*-CBPA. No identifiable metal containing product remained at the end of the reaction as judged by ESI. Furthermore, no single crystal was attained from the reaction solution.

Table 5-4. Oxygen atom transfer reactions to organic substrates in the presence of $[\text{Fe}^{\text{III}}(\text{tBuPhO})_2\text{NHC}(\text{MeOH})_2]\text{ClO}_4$.

$\text{R} + m\text{-CBPA} \xrightarrow[\text{r.t., N}_2, \text{THF, 24 hrs}]{[\text{Fe}^{\text{III}}(\text{tBuPhO})_2\text{NHC}(\text{MeOH})_2]\text{ClO}_4} [\text{R}=\text{O}] \text{ or } [\text{R}-\text{OH}]$		
R	Desired product [R=O] or [R-OH]	Yield % ¹
 $\text{P}(\text{Ph})_3$	 $\text{O}=\text{P}(\text{Ph})_3$	N.R.
		N.R. ²
		N.R.
		N.R.

¹Yields determined by GC-MS. ²Desired product was seen however did not exceed the control experiment, in which no metal was present.

5.3 Discussion

5.3.1 $\text{Co}^{\text{II}}((\text{tBuPhO})_2\text{NHC})\text{THF}$ C–H bond activation and oxygen atom transfer reactions

2-phenylpyridine was chosen as initial target for C–H bond activation for several reasons. First, the proposed mechanism of action in the palladium catalyzed case involves a nitrogen binding to the metal center, positioning one C–H bond adjacent to the metal.¹⁵ The compound 2-phenylpyridine therefore, requires open *cis* sites at the metal center. The $\text{Co}^{\text{II}}((\text{tBuPhO})_2\text{NHC})$, with its available *cis* sites, is a better candidate for C–H bond activation compared to the $\text{Fe}^{\text{III}}(\text{isq})_2\text{Cl}$, Chapter 2, and the $[\text{Co}(\text{ap})_2]^-$ complexes previously studied in the Soper Lab which have to undergo isomerization to access *cis* sites.³⁸ Second, $\text{Co}^{\text{II}}((\text{tBuPhO})_2\text{NHC})$ readily binds THF *trans* to the carbene. The nitrogen in 2-phenylpyridine would displace the solvent and bind to the metal center, which was observed by ESI–MS.

Under these conditions, no evidence of C–H bond activation by $\text{Co}^{\text{II}}((\text{tBuPhO})_2\text{NHC})$ was observed. However, a distinct orange to green color change was noticed on addition of several different oxidants including $\text{PhI}(\text{OAc})_2$, *m*-CPBA, or HCP. The resulting green solution is not just a doubly oxidized version of the $\text{Co}^{\text{II}}((\text{tBuPhO})_2\text{NHC})\text{THF}$. The doubly oxidized complex $[\text{Co}^{\text{II}}((\text{tBuPhO})_2\text{NHC})\text{THF}](\text{PF}_6)_2$ has an intense (2000 ϵ) broad peak at 850 nm (Chapter 3) which is not present in the reaction between $\text{Co}^{\text{II}}((\text{tBuPhO})_2\text{NHC})\text{THF}$ and oxygen atom transfer reagents. This could imply a new intermediate or a more complicated reaction between the oxidant and the $\text{Co}^{\text{II}}((\text{tBuPhO})_2\text{NHC})\text{THF}$. Additionally, the reaction between HCP and 2-phenylpyridine in the presence of $\text{Co}^{\text{II}}((\text{tBuPhO})_2\text{NHC})\text{THF}$ did produce a very small amount ($< 1\%$) of 2-(2-

chlorophenyl)pyridine. While this could mean that under optimized conditions $\text{Co}^{\text{II}}((\text{tBuPhO})_2\text{NHC})\text{THF}$ is able to activate the C–H bonds, the small amount of 2-(2-chlorophenyl)pyridine seen may also be the result of other routes e.g. a radical mechanism. Much more work needs to be done to determine if $\text{Co}^{\text{II}}((\text{tBuPhO})_2\text{NHC})\text{THF}$ can reproducibly activate C–H bonds in the presence of 2-phenylpyridine and HCP or an alternative oxidant.

Another parameter to explore is the effect of free rotation between the pyridine and phenyl moieties. While this rotation does not hinder C–H bond activation in the palladium system, in the cobalt system described here the steric bulk at cobalt in the complex $\text{Co}^{\text{II}}((\text{tBuPhO})_2\text{NHC})\text{THF}$ might prevent the C–H bond to have direct contact with the metal center. A more rigid system such as benzo[*h*]quinoline, which has also been used previously in palladium systems, might increase the possibility of C–H bond activation using the $\text{Co}^{\text{II}}((\text{tBuPhO})_2\text{NHC})\text{THF}$ complex by holding the C–H bond towards the metal.

The use of pyridine in the 2-phenylpyridine was designed to hold the C–H bond directly at the metal center. This system works well for palladium based catalysts. But given the propensity of the $\text{Co}^{\text{II}}((\text{tBuPhO})_2\text{NHC})\text{THF}$ complex has demonstrated affinity to bind ethers (in the form of THF) we speculated other ethers might be capable as the directing ligands for C–H bond activation in the cobalt system. To this end, several ethers were selected and tested for C–H bond activation **Scheme 5-4**. Unfortunately, none of the alkyl and aryl ethers chosen yielded products that have undergone C–H bond activation.

Cobalt complexes that are known to activate C–H bonds are generally proposed to be Co^0 species generated in situ from $\text{Co}^{\text{II}}/\text{Co}^{\text{III}}$ precursors in a very reducing

environment (e.g. 100 equiv. of methyl magnesium bromide).¹⁸ In this regard, it might be interesting to pursue the isolation of very reduced analogs of $\text{Co}^{\text{II}}((\text{tBuPhO})_2\text{NHC})\text{THF}$, such as the a $[\text{Co}^0((\text{tBuPhO})_2\text{NHC})]^{2-}$ dianion.

Several cobalt based catalyst are known to transfer oxygen atoms.³⁹⁻⁴¹ For instance, a cobalt bound to a dianionic tetradentate macrocycle was able to oxidize styrene using PhIO .⁴⁰ Additionally, work done by Nocera et. al. demonstrated a $\text{Co}^{\text{IV}}=\text{O}$ complex was present during H_2O oxidation.³² Therefore, attempts were made to transfer an oxygen atom, from oxygen atom transfer reagents, to organic substrates including phosphines, alkanes, alkenes, and aryls. The substrates chosen (**Table 5-1**) have all been shown to accept oxygen atoms from base metal complexes. Using iron complexes as a guide for oxygen atom transfer, substrates were chosen based on what previous iron complexes were able to achieve. For example, $\text{Fe}^{\text{IV}}=\text{O}$ complexes could oxygenate olefins³⁴, $\text{P}(\text{Ph})_3$ ³⁵, sulfides³⁶, and alkanes³⁷. The organic substrates also represent varying degrees of difficulty towards oxidation. For instance, thermodynamic calculations place the oxygenation of $\text{P}(\text{Ph})_3$ at a much more thermodynamically favorable value as compared to the oxygenation of alkanes.²⁶ Although no oxygen atom transfer catalysis was observed, $\text{Co}^{\text{II}}((\text{tBuPhO})_2\text{NHC})\text{THF}$ underwent color changes. These color changes were dependent on the amount of *m*-CPBA added. When 1 equiv of *m*-CPBA was used an intermediate was observed as shown in **Figure 5-1**. The intermediate disappeared over the course of an hour to generate a green solution. When 0.5 equiv *m*-CPBA was used only half of the starting complex was lost. In the case where 3 equiv *m*-CPBA was used no intermediate was observed and the solution immediately turned green. The identity of the green solution has not yet been determined. Running the reaction at low temperature might allow for the stabilization or isolation of the intermediate between $\text{Co}^{\text{II}}((\text{tBuPhO})_2\text{NHC})\text{THF}$ and 1 equiv of *m*-CPBA.

5.3.2 Na[Fe((tBuPhO)₂NHC)Cl₂] synthesis and reactivity

The reaction between FeCl₃ and deprotonated [(tBuPhO)₂NHC]²⁻ lead to a purple powder. The purple powder had an isotopic splitting pattern and molecular weight that matched the calculated m/z for [Fe((tBuPhO)₂NHC)Cl₂]⁻. Although many attempts were made to generate a single crystal of sufficient quality for solid state analysis, conditions have not been identified to produce a single crystal of sufficient quality. However, upon oxidation of [Fe((tBuPhO)₂NHC)Cl₂]⁻ with 1 equiv of WCl₆ a red crystal of sufficient quality was generated. The X-ray crystallographic data shows a fully protonated and demetallated [(tBuPhO)₂NHC]⁺ complex with [FeCl₄]⁻ as the counter ion. The oxidant WCl₆, a strong oxidant, has been known to chlorinate organic substrates.⁴² In this case the WCl₆ chlorinated the iron in [Fe((tBuPhO)₂NHC)Cl₂]⁻ to form [FeCl₄]⁻. Although other oxidants were tried, AgBF₄ and NOBF₄, no other crystals were obtained.

The Na[Fe((tBuPhO)₂NHC)Cl₂] shows an quasi-reversible oxidation wave at 0.24 V and an irreversible oxidation wave at 0.75 V. If Na[Fe((tBuPhO)₂NHC)Cl₂] is formulated as containing an Fe^{III}, then both oxidation are most likely ligand centered. The Na[Fe((tBuPhO)₂NHC)Cl₂] complex also shows two irreversible reductions at -1.2 and -1.5 V, which are assigned to metal reductions. It seems that the irreversibility of the oxidation and reduction waves are due to the bound chlorides displacing from the iron complex. Furthermore, the CV clearly shows the ability of Na[Fe((tBuPhO)₂NHC)Cl₂] to span multiple oxidations. While the oxidation state of the metal and ligand in Na[Fe((tBuPhO)₂NHC)Cl₂] cannot be unambiguously assigned, the CV suggests that both the ligand and metal are involved in the redox chemistry of the complex.

Although the solid state structure has not yet been determined, reactivity studies were performed. Cross-coupling was achieved between PhMgBr and 1-bromohexane using 15 mol % Na[Fe((tBuPhO)₂NHC)Cl₂] as the catalyst. The cross-coupled product yield was low (25 %) but was significantly higher than that seen using Co^{II}((tBuPhO)₂NHC)THF (4 % yield of cross-coupled product, Chapter 3). Additionally, the Na[Fe((tBuPhO)₂NHC)Cl₂] demonstrates selectivity towards the cross-coupled vs homocoupled product. In the case of Co^{II}((tBuPhO)₂NHC)THF the dominant organic product was homocoupled product (ratio 10:1 of homocoupled to cross-coupled). However, in the case of Na[Fe((tBuPhO)₂NHC)Cl₂] the ratio of homocoupled to cross-coupled product was nearly 1:1. When the reaction was run under aerobic conditions cross-coupling was still achieved however the reaction produced more homocoupled product than cross-coupling (~ 2:1). This mimics the reactivity seen in Chapter 2, where FeCl(isq^{Ph})₂ was able to homocouple PhMgBr using O₂ as the terminal oxidant. The increase in cross-coupling to form new C–C bonds warrants further investigation into both the coordination environment and oxidation state of the Na[Fe((tBuPhO)₂NHC)Cl₂]. Understanding both of those conditions would help to elucidate a mechanism that will aid in further rational redox-active ligand design.

5.3.3 [Fe((tBuPhO)₂NHC)(MeOH)₂]ClO₄ synthesis and reactivity

To test whether or not the irreversible peaks seen in the cyclic voltammogram were due to the halides, a halide free analog of Na[Fe((tBuPhO)₂NHC)Cl₂] was synthesized [Fe^{III}((tBuPhO)₂NHC)(MeOH)₂]ClO₄. The synthetic procedure to [Fe^{III}((tBuPhO)₂NHC)(MeOH)₂]ClO₄ was achieved using the same condition to generate Na[Fe((tBuPhO)₂NHC)Cl₂]. The UV-Vis spectrum of [Fe^{III}((tBuPhO)₂NHC)(MeOH)₂]ClO₄ is completely different from the [Fe((tBuPhO)₂NHC)Cl₂][–] complex. The CV shows a

similar open potential vs $[\text{Fe}((\text{tBuPhO})_2\text{NHC})\text{Cl}_2]^-$ (-0.39 V vs -0.40 V), however $[\text{Fe}^{\text{III}}((\text{tBuPhO})_2\text{NHC})(\text{MeOH})_2]\text{ClO}_4$ shows two quasi-reversible oxidation waves, at -0.31 V and 0.09 V. The second quasi-reversible oxidation wave at -0.31 is similar to the first quasi-reversible oxidation wave seen with $[\text{Fe}((\text{tBuPhO})_2\text{NHC})\text{Cl}_2]^-$. Both oxidation peaks for $[\text{Fe}^{\text{III}}((\text{tBuPhO})_2\text{NHC})(\text{MeOH})_2]\text{ClO}_4$ are quasi-reversible in contrast to $[\text{Fe}((\text{tBuPhO})_2\text{NHC})\text{Cl}_2]^-$ where the second oxidation is irreversible. This can be ascribed to the labile of the Cl^- ligands in $\text{Na}[\text{Fe}((\text{tBuPhO})_2\text{NHC})\text{Cl}_2]$.

Although CV data suggests the $[\text{Fe}^{\text{III}}((\text{tBuPhO})_2\text{NHC})(\text{MeOH})_2]\text{ClO}_4$ complex remains intact during oxidation and reduction, isolation of the oxidized/reduced materials has been complicated by the $[\text{Fe}^{\text{III}}((\text{tBuPhO})_2\text{NHC})(\text{MeOH})_2]\text{ClO}_4$ forming amorphous solids. However, cross-coupling reactions were attempted using $[\text{Fe}^{\text{III}}((\text{tBuPhO})_2\text{NHC})(\text{MeOH})_2]\text{ClO}_4$ as the catalyst. As seen in **Table 5-3**, cross-coupling between PhMgBr and 1-bromohexane did occur. The cross-coupling yield is less than what is seen using the $\text{Na}[\text{Fe}((\text{tBuPhO})_2\text{NHC})\text{Cl}_2]$ complex and produces more homocoupled product (Ph-Ph). The main difference between $[\text{Fe}^{\text{III}}((\text{tBuPhO})_2\text{NHC})(\text{MeOH})_2]\text{ClO}_4$ and $\text{Na}[\text{Fe}((\text{tBuPhO})_2\text{NHC})\text{Cl}_2]$ is the presents of 2 bound chlorides in the latter complex. Having the halide already bound to the metal center seems to be a requirement to increase the yield of cross-coupled product. The halides bound in the complex $\text{Na}[\text{Fe}((\text{tBuPhO})_2\text{NHC})\text{Cl}_2]$ could occupy binding sites on the metal center that aid in directing reactivity toward cross-coupling and away from undesired side reactions such as homocoupling of PhMgBr or cross-coupling of the alkyl halide and the ligand. This result is perplexing due to the large amounts of halide in solution during the reaction when using either Fe complex. The reaction is insensitive to an oxidizing environment. When the reaction is run in either N_2 or ambient atmosphere the organic products were the same. Furthermore, the ratio of homocoupled to cross-

coupled product was 2.5:1 whereas the $[\text{Fe}((\text{tBuPhO})_2\text{NHC})\text{Cl}_2]^-$ complex has a 1:1 ratio of products. This complex is not as selective for cross-coupling and does not seem to use O_2 as an oxidant to increase Ph-Ph as seen with $[\text{Fe}((\text{tBuPhO})_2\text{NHC})\text{Cl}_2]^-$ and $\text{Fe}^{\text{III}}\text{Cl}(\text{isq}^{\text{Ph}})_2$ (Chapter 2).

High valent $\text{Fe}^{\text{IV}}=\text{O}$ complexes have been very successful at oxygen atom transfer reactions to challenging organic substrates such as unactivated alkanes.⁴³ We proposed the ability of $[\text{Fe}^{\text{III}}((\text{tBuPhO})_2\text{NHC})(\text{MeOH})_2]\text{ClO}_4$ to support ligand radicals would make it a prime choice for oxygen atom transfer, catalysis, however, conditions have not been found that allow such a reaction to occur using $[\text{Fe}((\text{tBuPhO})_2\text{NHC})\text{Cl}_2]^-$ as the catalyst.

5.4 Conclusion

5.4.1 Scope of reactivity of $\text{Co}^{\text{II}}((\text{tBuPhO})_2\text{NHC})\text{THF}$

The $\text{Co}^{\text{II}}((\text{tBuPhO})_2\text{NHC})\text{THF}$ was unable to activate a C–H bond or transfer an oxygen atom to an organic substrate. In the case of C–H bond activation, cobalt has been known since the 1950's to activate C–H bonds but the use of high pressure, high temperature, and stoichiometric amount of $\text{Co}_2(\text{CO})_8$ were required.⁴⁴⁻⁴⁵ In addition, most C–H bond activation cobalt catalyst are Co^0 complexes. The mechanism for C–H bond activation by Co^0 is complicated as both a radical mechanism⁴⁶ and concerted $\text{Co}^{\text{I}}/\text{Co}^{\text{III}}$ mechanism have been reported.^{19, 47-49} While a well-defined catalyst such as $\text{Co}^{\text{II}}((\text{tBuPhO})_2\text{NHC})\text{THF}$ could shed light on the mechanism of C–H bond activation at cobalt, thus far conditions have not yet been found to allow C–H activation. It might be

that a reduced $\text{Co}^{\text{II}}((\text{tBuPhO})_2\text{NHC})\text{THF}$ complex, such as $[\text{Co}^0((\text{tBuPhO})_2\text{NHC})\text{THF}]^{2-}$, would be a better candidate for ligand assisted C–H activation.

In the case of oxygen atom transfer, $\text{Co}^{\text{II}}((\text{tBuPhO})_2\text{NHC})\text{THF}$ was unable to deliver an oxygen atom to an organic substrate. Interestingly, a distinct color change was noticed when $\text{Co}^{\text{II}}((\text{tBuPhO})_2\text{NHC})\text{THF}$ was in the presence of an oxygen atom donor. This seems to imply that an interaction between $\text{Co}^{\text{II}}((\text{tBuPhO})_2\text{NHC})\text{THF}$ and an oxygen atom is possible and that the lack of oxygen atom transfer could be due to the conditions used, i.e. temperature, oxidant, and cobalt complex oxidation state. Cooling the reaction down might decrease the rapid reaction between $\text{Co}^{\text{II}}((\text{tBuPhO})_2\text{NHC})\text{THF}$ and oxygen atom transfer reagents. The triply oxidized complex $[\text{Co}^{\text{III}}((\text{tBuPhO})_2\text{NHC})\text{THF}]^{3+}$, which has yet to be isolated, might have the best chance of oxygen atom transfer, since the ligand could support electron deficient cobalt.

5.4.2 $[\text{Fe}^{\text{III}}((\text{tBuPhO})_2\text{NHC})]^+$ synthesis and reactivity

The synthesis of $\text{Na}[\text{Fe}^{\text{III}}((\text{tBuPhO})_2\text{NHC})\text{Cl}_2]$ is very reproducible, however conditions have not yet been found to generate a single crystal of sufficient quality for X-ray crystallography. The $\text{Na}[\text{Fe}^{\text{III}}((\text{tBuPhO})_2\text{NHC})\text{Cl}_2]$ demonstrated by cyclic voltammetry implies that ligand is involved in the redox chemistry due to the four redox event observed. The irreversibility seen in the CV is believed to be due to chlorides bound to the metal center. This was remedied by synthesizing the halide free $[\text{Fe}^{\text{III}}((\text{tBuPhO})_2\text{NHC})(\text{MeOH})_2]\text{ClO}_4$ complex. The CV of $[\text{Fe}^{\text{III}}((\text{tBuPhO})_2\text{NHC})(\text{MeOH})_2]\text{ClO}_4$ shows two quasi-reversible oxidation peaks and shares the same open potential of the $\text{Na}[\text{Fe}^{\text{III}}((\text{tBuPhO})_2\text{NHC})\text{Cl}_2]$. Although a single crystal for X-ray crystallography has not yet been produced further attempts should be tried.

The cross-coupling reactivity between PhMgBr and 1-bromohexane using Na[Fe^{III}((tBuPhO)₂NHC)Cl₂] as the catalyst showed promise. The reaction in catalytic (1.5 TON vs Na[Fe^{III}((tBuPhO)₂NHC)Cl₂]) and demonstrates selectivity towards cross-coupling vs homocoupling. This is a marked improvement vs the Co^{III}((tBuPhO)₂NHC)THF reactivity from Chapter 3. Decomposition of the ligand, as seen in Chapter 3, via cross-coupling of the alkyl halide to the carbene has not been explored in either Na[Fe^{III}((tBuPhO)₂NHC)Cl₂] or [Fe^{III}((tBuPhO)₂NHC)(MeOH)₂]ClO₄. This might also hinder the cross-coupling ability of Na[Fe^{III}((tBuPhO)₂NHC)Cl₂]. Although the reactivity is, thus far, limited to C–C bond forming reactions, it warrants further investigation into the mechanism. Once a definitive structure of [Fe^{III}((tBuPhO)₂NHC)(MeOH)₂]ClO₄ has been determined and the ET series confirmed more mechanistic studies should be carried out to elucidate the steps involved in C–C bond formation. This information will serve to guide further ligand design and will provide insight into work towards oxygen atom transfer.

5.5 Methods

5.5.1 General considerations

Unless otherwise noted, all manipulations were performed under anaerobic conditions using standard vacuum line techniques, or in an inert atmosphere glove box under purified dinitrogen. All NMR spectra were acquired on a Varian Mercury 300 spectrometer (300.323 MHz for ¹H) at ambient temperature. Chemical shifts are reported in parts per million (ppm) relative to TMS, with the residual solvent peak serving as an internal reference. UV–visible absorption spectra were acquired using a Varian Cary 50 spectrophotometer. Unless otherwise specified, all electronic absorption spectra were

recorded at ambient temperatures in 1 cm quartz cells. All mass spectra were recorded in the Georgia Institute of Technology Bioanalytical Mass Spectrometry Facility. Cyclic voltammetric measurements were made using a CH Instruments CHI620C potentiostat in a three component cell consisting of a platinum disk working electrode, a platinum wire auxiliary electrode, and a non-aqueous AgNO_3/Ag reference electrode. Unless otherwise noted, all electrochemical experiments were performed in CH_3CN or THF with 0.1 M $[\text{nBu}_4\text{N}][\text{PF}_6]$ as the supporting electrolyte. Electrochemical data are referenced and reported to Fc^+/Fc as an internal standard. Elemental analyses were performed by Atlantic Microlab, Inc., Norcross, GA. All analyses were performed in duplicate, and the reported compositions are the average of the two runs. Anhydrous acetonitrile (CH_3CN), tetrahydrofuran (THF), and pentane solvents for air- and moisture- sensitive manipulations were purchased from Sigma–Aldrich, further dried by passage through columns of activated alumina, degassed by at least three freeze–pump–thaw cycles, and stored under N_2 prior to use. Methanol (anhydrous, 99.0%) was purchased from Honeywell Burdick & Jackson, and used as received. The ligand 2,4-di-tert-butyl-6-(2,6-diisopropylphenylimino) benzoquinone ($[(\text{tBuPhO})_2\text{NHC}]\text{C}$) was prepared by the method outlined in chapter 3 of this thesis. Iodosylbenzene was prepared according to literature procedures and prepared fresh monthly.⁵⁰ All other chemicals were purchased from Sigma–Aldrich and used as received.

5.5.2 $\text{Na}[\text{Fe}((\text{tBuPhO})_2\text{NHC})]$ synthesis

A scintillation vial with a magnetic stir bar was charged with $[(\text{tBuPhO})_2\text{NHC}]\text{Cl}$ (0.257 g, 0.5 mmol) and 3 equiv of 0.5 M sodium methoxide in methanol (3 mL, 1.5 mmol) in 5 mL THF. The solution immediately turned bright yellow and was stirred for

10 mins. A solution of FeCl_3 (0.0812 mg, 0.5 mmol) in 5 mL CH_3CN was added to the yellow deprotonated $[(\text{tBuPhO})_2\text{NHC}]^{2-}$ solution to generate an immediate color change to purple. The solution was allowed to stir for 15 mins. The purple solution was filtered through a Celite plug, and the filtrate was dried *in vacuo* and then taken up in THF. The purple THF solution was filtered through a Celite plug, the solvent was removed from the filtrate leaving a purple residue of the title complex $[\text{Fe}((\text{tBuPhO})_2\text{NHC})\text{Cl}_2]\text{Na}$ in 47% yield (0.1495 g). ESI-MS (m/z): $[\text{Fe}((\text{tBuPhO})_2\text{NHC})\text{Cl}_2]^-$ Calcd: 602.2, Found: 602.2. Elemental analysis: $[(\text{tBuPhO})_2\text{NHC}][\text{FeCl}_2((\text{tBuPhO})_2\text{NHC})]$ $\text{C}_{62}\text{H}_{91}\text{Cl}_2\text{FeN}_4\text{O}_4$ Anal. Calcd: C = 68.75, H = 8.47, N = 5.17 Found: C = 68.32, H = 8.41, N = 5.21.

5.5.3 X-ray crystallography

A single crystal of $[(\text{tBuPhO})_2\text{NHC}][\text{FeCl}_4]$ suitable for X-ray diffraction analysis was coated with Paratone N, suspended in a small fiber loop and placed in a nitrogen gas stream at 173 K on a Bruker D8 APEX II CCD sealed tube diffractometer. Diffraction data for $[(\text{tBuPhO})_2\text{NHC}][\text{FeCl}_4]$ was collected using graphite monochromated $\text{Cu K}\alpha$ ($\lambda = 1.54178 \text{ \AA}$) radiation. Data were measured using a series of combinations of phi and omega scans with 10 second frame exposures and 0.5° frame widths. Data collection, indexing and initial cell refinements were all carried out using APEX II software.⁵¹ Frame integration and final cell refinements were done using SAINT software.⁵² The final cell parameters were determined from least-squares refinement on 54,393 reflection for $[(\text{tBuPhO})_2\text{NHC}][\text{FeCl}_4]$. The structure was solved using direct methods and difference Fourier techniques using the shelxtl program package.⁵³ Hydrogen atoms were placed in their idealized chemical positions using the HFIX command and were included in the final cycles of least-squares with isotropic U_{ij} 's related to the atoms ridden upon. All non-

hydrogen atoms were refined anisotropically. Details of data collection and structure refinement are provided in **Table 5-5**.

Table 5-5. Crystallographic data and structure parameters for [(tBuPhO)₂NHC][FeCl₄].

Complex	[[[(tBuPhO) ₂ NHC][FeClO ₄]]
Empirical formula	C ₃₁ H ₄₅ Cl ₄ FeN ₂ O ₂
Formula weight	675.34
T (K)	173(2)
Crystal system	Orthorhombic
Space group	Pnma
Unit Cell dimensions	
<i>a</i> (Å)	11.648(4)
<i>b</i> (Å)	30.874(10)
<i>c</i> (Å)	9.621(3)
α (°)	90
β (°)	90
γ (°)	90
<i>V</i> (Å ³)	3460(2)
<i>Z</i>	4
<i>D</i> _{calc} (g/cm ³)	1.296
Absorption coefficient (mm ⁻¹)	0.773
Crystal Size (mm)	0.16 x 0.09 x 0.05
θ range for data collection (°)	2.22 to 27.48
Index ranges	-15 ≤ <i>h</i> ≤ 15
	-40 ≤ <i>k</i> ≤ 40
	-12 ≤ <i>l</i> ≤ 12
Reflections collected	54393
Reflections unique	4045
Goodness of fit on <i>F</i> ²	1.006
<i>R</i> [<i>I</i> > 2σ(<i>I</i>)]	0.06
<i>wR</i> ² (all data)	0.2044

5.5.4 General reaction for C–H bond activation

In a representative example, a scintillation vial with a magnetic stir bar and 1 mL of THF was charged with 0.500 mL of a 16.4 mM solution of $\text{Co}^{\text{II}}((\text{tBuPhO})_2\text{NHC})\text{THF}$ in THF, followed by the addition of 2.28 mL of a 72.2 mM solution of 2-phenylpyridine in THF. After 5 mins of stirring, 0.826 mL of a 0.04 M solution PhMgBr in THF was added to the solution. After 24 hours of stirring at room temperature a 0.400 mL aliquot of the solution was quenched with methanol (0.100 mL) and tested by GC-MS.

5.5.5 General reaction for oxygen atom transfer

A scintillation vial with a magnetic stir bar and 1 mL of CH_3CN was charged with 0.500 mL of a 8.23 mM solution of $\text{Co}^{\text{II}}((\text{tBuPhO})_2\text{NHC})\text{THF}$ in CH_3CN (0.050 g in 10 mL of CH_3CN), followed by the addition of 0.500 mL of a 16.46 mM solution of $\text{P}(\text{Ph})_3$ in CH_3CN . After 5 mins of stirring, 0.237 mL of a 34.8 mM solution of *m*-CPBA in CH_3CN was added to the solution. After 24 hours of stirring at room temperature a 0.400 mL aliquot of the solution was quenched with methanol (0.100 mL) and tested by GC-MS.

5.6 Works Cited

1. Baudoin, O., Transition Metal-Catalyzed Arylation of Unactivated C(sp³)-H Bonds. *Chem. Soc. Rev.* **2011**, *40*, 4902-4911.
2. Engle, K. M.; Mei, T. S.; Wasa, M.; Yu, J. Q., Weak Coordination as a Powerful Means for Developing Broadly Useful C-H Functionalization Reactions. *Acc. Chem. Res.* **2012**, *45*, 788-802.
3. Ritleng, V.; Sirlin, C.; Pfeffer, M., Ru-, Rh-, and Pd-catalyzed C-C bond formation involving C-H activation and addition on unsaturated substrates: Reactions and mechanistic aspects. *Chem. Rev. (Washington, DC, U. S.)* **2002**, *102*, 1731-1769.
4. Chen, X.; Engle, K. M.; Wang, D.-H.; Yu, J.-Q., Palladium(II)-Catalyzed C-H Activation/C-C Cross-Coupling Reactions: Versatility and Practicality. *Angew. Chem., Int. Ed.* **2009**, *48*, 5094-5115.
5. Anastas, P. T.; Kirchhoff, M. M., Origins, Current Status, and Future Challenges of Green Chemistry. *Acc. Chem. Res.* **2002**, *35*, 686-694.
6. Godula, K.; Sames, D., C-H Bond Functionalization in Complex Organic Synthesis. *Science* **2006**, *312*, 67-72.
7. Crabtree, R. H., Alkane C-H Activation and Functionalization with Homogeneous Transition Metal Catalysts: A Century of Progress-A New Millennium in Prospect. *Journal of the Chemical Society, Dalton Transactions* **2001**, 2437-2450.
8. Moritanl, I.; Fujiwara, Y., Aromatic Substitution of Styrene-Palladium Chloride Complex. *Tetrahedron Lett.* **1967**, *8*, 1119-1122.
9. Fekl, U.; Goldberg, K. I., Homogeneous Hydrocarbon C-H Bond Activation and Functionalization with Platinum. In *Adv. Inorg. Chem.*, Academic Press: **2003**; Vol. Volume 54, pp 259-320.
10. Groves, J. T., Reactivity and Mechanisms of Metalloporphyrin-Catalyzed Oxidations. *J. Porphyrins Phthalocyanines* **2000**, *04*, 350-352.
11. Sen, A., Catalytic Functionalization of Carbon-Hydrogen and Carbon-Carbon Bonds in Protic Media. *Acc. Chem. Res.* **1998**, *31*, 550-557.

12. Shilov, A. E.; Shul'pin, G. B., Activation of C–H Bonds by Metal Complexes. *Chem. Rev. (Washington, DC, U. S.)* **1997**, 97, 2879-2932.
13. Stahl, S. S.; Labinger, J. A.; Bercaw, J. E., Homogeneous Oxidation of Alkanes by Electrophilic Late Transition Metals. *Angew. Chem., Int. Ed.* **1998**, 37, 2180-2192.
14. Tisue, T.; Downs, W. J., Palladium(2)-Catalysed Nitration of Benzene. *Journal of the Chemical Society D-Chemical Communications* **1969**, 410-&.
15. Kalyani, D.; Deprez, N. R.; Desai, L. V.; Sanford, M. S., Oxidative C–H Activation/C–C Bond Forming Reactions: Synthetic Scope and Mechanistic Insights. *J. Am. Chem. Soc.* **2005**, 127, 7330-7331.
16. Dick, A. R.; Hull, K. L.; Sanford, M. S., A Highly Selective Catalytic Method for the Oxidative Functionalization of C–H Bonds. *J. Am. Chem. Soc.* **2004**, 126, 2300-2301.
17. Maleckis, A.; Kampf, J. W.; Sanford, M. S., A Detailed Study of Acetate-Assisted C–H Activation at Palladium(IV) Centers. *J. Am. Chem. Soc.* **2013**, 135, 6618-6625.
18. Gao, K.; Lee, P.-S.; Fujita, T.; Yoshikai, N., Cobalt-Catalyzed Hydroarylation of Alkynes through Chelation-Assisted C–H Bond Activation. *J. Am. Chem. Soc.* **2010**, 132, 12249-12251.
19. Li, B.; Wu, Z.-H.; Gu, Y.-F.; Sun, C.-L.; Wang, B.-Q.; Shi, Z.-J., Direct Cross-Coupling of C–H Bonds with Grignard Reagents through Cobalt Catalysis. *Angew. Chem., Int. Ed.* **2011**, 50, 1109-1113.
20. Meyer, T. J., Redox Pathways: Applications in Catalysis. *J. Electrochem. Soc.* **1984**, 131, 221C-228C.
21. Nocera, D. G., The Artificial Leaf. *Acc. Chem. Res.* **2012**, 45, 767-776.
22. Mansuy, D., Activation of alkanes : the biomimetic approach. *Coord. Chem. Rev.* **1993**, 125, 129-141.
23. Groves, J. T., High-valent iron in chemical and biological oxidations. *J. Inorg. Biochem.* **2006**, 100, 434-447.

24. Bukhtiyarov, V. I.; Knop-Gericke, A., Chapter 9 Ethylene Epoxidation over Silver Catalysts. In *Nanostructured Catalysts: Selective Oxidations*, The Royal Society of Chemistry: **2011**; pp 214-247.
25. Deubel, D. V., Ethylene Epoxidation with Tungsten Diperoxo Complexes: Is Relativity the Origin of Reactivity? *The Journal of Physical Chemistry A* **2001**, *105*, 4765-4772.
26. Holm, R. H., Metal-centered oxygen atom transfer reactions. *Chem. Rev. (Washington, DC, U. S.)* **1987**, *87*, 1401-1449.
27. Jay R. Winkler, H. B. G., *Molecular Electronic Structures of Transition Metal Complexes I*. Springer Berlin Heidelberg: **2012**.
28. Hay-Motherwell, R. S.; Wilkinson, G.; Hussain-Bates, B.; Hursthouse, M. B., Synthesis and X-ray crystal structure of oxotrimesityliridium(V). *Polyhedron* **1993**, *12*, 2009-2012.
29. Poverenov, E.; Efremenko, I.; Frenkel, A. I.; Ben-David, Y.; Shimon, L. J. W.; Leitun, G.; Konstantinovski, L.; Martin, J. M. L.; Milstein, D., Evidence for a terminal Pt(IV)-oxo complex exhibiting diverse reactivity. *Nature* **2008**, *455*, 1093-1096.
30. Lutterman, D. A.; Surendranath, Y.; Nocera, D. G., A Self-Healing Oxygen-Evolving Catalyst. *J. Am. Chem. Soc.* **2009**, *131*, 3838-+.
31. Surendranath, Y.; Dinca, M.; Nocera, D. G., Electrolyte-Dependent Electrosynthesis and Activity of Cobalt-Based Water Oxidation Catalysts. *J. Am. Chem. Soc.* **2009**, *131*, 2615-2620.
32. Kanan, M. W.; Yano, J.; Surendranath, Y.; Dinca, M.; Yachandra, V. K.; Nocera, D. G., Structure and Valency of a Cobalt-Phosphate Water Oxidation Catalyst Determined by in Situ X-ray Spectroscopy. *J. Am. Chem. Soc.* **2010**, *132*, 13692-13701.
33. Stieber, S. C. E.; Milsman, C.; Hoyt, J. M.; Turner, Z. R.; Finkelstein, K. D.; Wieghardt, K.; DeBeer, S.; Chirik, P. J., Bis(imino)pyridine Iron Dinitrogen Compounds Revisited: Differences in Electronic Structure Between Four- and Five-Coordinate Derivatives. *Inorg. Chem.* **2012**, *51*, 3770-3785.
34. Groves, J. T.; Nemo, T. E.; Myers, R. S., Hydroxylation and epoxidation catalyzed by iron-porphine complexes. Oxygen transfer from iodosylbenzene. *J. Am. Chem. Soc.* **1979**, *101*, 1032.

35. Rohde, J. U.; In, J. H.; Lim, M. H.; Brennessel, W. W.; Bukowski, M. R.; Stubna, A.; Münck, E.; Nam, W.; Que, L., Crystallographic and spectroscopic characterization of a nonheme Fe(IV)=O complex. *Science* **2003**, 299, 1037.
36. Sastri, C. V.; Oh, K.; Lee, Y. J.; Seo, M. S.; Shin, W.; Nam, W., Oxygen-atom transfer between mononuclear nonheme iron(IV)-oxo and iron(II) complexes. *Angew. Chem., Int. Ed.* **2006**, 45, 3992.
37. Kaizer, J.; Klinker, E. J.; Oh, N. Y.; Rohde, J. U.; Song, W. J.; Stubna, A.; Kim, J.; Münck, E.; Nam, W.; Que, L., Nonheme FeIVO complexes that can oxidize the C–H bonds of cyclohexane at room temperature. *J. Am. Chem. Soc.* **2004**, 126, 472.
38. Smith, A. L.; Clapp, L. A.; Hardcastle, K. I.; Soper, J. D., Redox-active ligand-mediated Co-Cl bond-forming reactions at reducing square planar cobalt(III) centers. *Polyhedron* **2010**, 29, 164-169.
39. Levason, W.; McAuliffe, C. A., Higher oxidation state chemistry of iron, cobalt, and nickel. *Coord. Chem. Rev.* **1974**, 12, 151-184.
40. Collins, T. J.; Ozaki, S.; Richmond, T. G., Catalytic oxidation of styrene in the presence of square planar cobalt(III) complexes of polyanionic chelating ligands. *J. Chem. Soc., Chem. Commun.* **1987**, 803-804.
41. Koola, J. D.; Kochi, J. K., Cobalt-catalyzed epoxidation of olefins. Dual pathways for oxygen-atom transfer. *The Journal of Organic Chemistry* **1987**, 52, 4545-4553.
42. Connelly, N. G.; Geiger, W. E., Chemical Redox Agents for Organometallic Chemistry. *Chem. Rev. (Washington, DC, U. S.)* **1996**, 96, 877-910.
43. Nam, W., High-Valent Iron(IV)–Oxo Complexes of Heme and Non-Heme Ligands in Oxygenation Reactions. *Acc. Chem. Res.* **2007**, 40, 522-531.
44. Murahashi, S., Synthesis of Phtahlimidines from Schiff Bases and Carbon Monoxide. *J. Am. Chem. Soc.* **1955**, 77, 6403-6404.
45. Murahashi, S.; Horie, S., The Reaction of Azobenzene and Carbon Monoxide. *J. Am. Chem. Soc.* **1956**, 78, 4816-4817.

46. Wakabayashi, K.; Yorimitsu, H.; Oshima, K., Cobalt-Catalyzed Tandem Radical Cyclization and Cross-Coupling Reaction: Its Application to Benzyl-Substituted Heterocycles. *J. Am. Chem. Soc.* **2001**, *123*, 5374-5375.
47. Obligacion, J. V.; Semproni, S. P.; Chirik, P. J., Cobalt-Catalyzed C–H Borylation. *J. Am. Chem. Soc.* **2014**, *136*, 4133-4136.
48. Gao, K.; Yoshikai, N., Low-Valent Cobalt Catalysis: New Opportunities for C–H Functionalization. *Acc. Chem. Res.* **2014**, *47*, 1208-1219.
49. Ding, Z.; Yoshikai, N., Cobalt-Catalyzed Addition of Azoles to Alkynes. *Org. Lett.* **2010**, *12*, 4180-4183.
50. Dauban, P.; Sanière, L.; Tarrade, A.; Dodd, R. H., Copper-Catalyzed Nitrogen Transfer Mediated by Iodosylbenzene PhIO. *J. Am. Chem. Soc.* **2001**, *123*, 7707-7708.
51. Systems, A. X.-r. *APEX II*, Bruker AXS, Inc.: Madison, WI, **2005**.
52. Systems, A. X.-r. *saint Version 6.45A*, Bruker AXS, Inc.: Madison, WI, **2003**.
53. Systems, A. X.-r. *shelxtl Version 6.12*, Bruker AXS, Inc.: Madison, WI, **2002**.

Chapter 6

Conclusions and Future Directions

Redox-active ligands can act as an electron reservoir to impart multiple electron redox events at metal centers prone to one electron transformation. This allows for the development of well-defined 3d metal complexes to carry out C–C bond forming reactions. My graduate work was aimed at catalyzing C–C bond formation at well-defined 3d metal catalyst using redox-active ligands. To achieve this goal previously reported complexes and new complexes containing 3d metals bound to redox-active ligands were synthesized and tested for C–C bond forming reactivity.

Several redox-active ligand containing complexes were synthesized including $(\text{Fe}^{\text{III}}\text{Cl}(\text{isq}^{\text{Ph}})_2, \text{Co}^{\text{II}}((\text{tBuPhO})_2\text{NHC})\text{THF}$, and $[\text{Fe}^{\text{III}}((\text{tBuPhO})_2\text{NHC})\text{Cl}_2]^-$) and tested for C–C bond forming reactivity. All of the complexes showed varying degrees of C–C coupling. $\text{Fe}^{\text{III}}\text{Cl}(\text{isq}^{\text{Ph}})_2$ could homocouple PhMgBr to biphenyl with moderate yields (45 %) using O_2 as the terminal oxidant, however this complex was not competent at cross-coupling. $\text{Co}^{\text{II}}((\text{tBuPhO})_2\text{NHC})\text{THF}$ could activate C–O bonds for subsequent cross-coupling to aryl Grignards forming new C–C bonds. As an example, 3-butoxypropanenitrile reacted with PhMgBr using $\text{Co}^{\text{II}}((\text{tBuPhO})_2\text{NHC})\text{THF}$ as the catalyst to produce 3-phenylpropanenitrile in 70 % yield. Kumada coupling was less successful, cross-coupling between PhMgBr and 1-bromohexane using 10 mol % of $\text{Co}^{\text{II}}((\text{tBuPhO})_2\text{NHC})\text{THF}$ produced Ph-Hx (1.4 % yield) and biphenyl (26 % yield).

$\text{Fe}^{\text{III}}((\text{tBuPhO})_2\text{NHC})\text{Cl}_2]^-$ was more successful at Kumada coupling, producing a 25 % yield of cross-coupled product (Ph–Hx) and an 80 % yield of homocoupled product (Ph–Ph) from the reaction of PhMgBr and 1-bromohexane at 15 mol % catalyst loading.

To explain the resulting yields shown above attempts at generating ET series of the three catalysts were pursued to elucidate intermediates in their respective catalytic cycles. While the $\text{Co}^{\text{II}}((\text{tBuPhO})_2\text{NHC})\text{THF}$ ET series was isolated and characterized neither iron ET series has been generated, isolated and completely characterized. This should be the focus of future work, especially in the case of $[\text{Fe}^{\text{III}}((\text{tBuPhO})_2\text{NHC})\text{Cl}_2]^-$, where cross-coupling yields are 25 %. The benefit to generating the ET series is demonstrated by the $\text{Co}^{\text{II}}((\text{tBuPhO})_2\text{NHC})\text{THF}$ complex. The ET series allowed mechanistic investigation into the ligand degradation pathway that prevents Kumada coupling. Furthermore, by noticing that all three complexes in the cobalt ET series had a proclivity for oxygen (in the form of THF), other ethers were tested for reactivity, in the hopes that an ether could direct reactivity at a particular bond. This led to the discovery of C–O activation using ether nitriles as directing groups, this kind of reactivity would have not been explored if the ET series was not isolated and characterized. Exploration of nitrile directed C–O bond activation should also be continued. Thus far $\text{Co}^{\text{II}}((\text{tBuPhO})_2\text{NHC})\text{THF}$ can only activate ether nitriles, however other nitrile containing substrates are unexplored. This could lead to a new strategy for C–H bond activation and should be the focus of future studies.

Additionally, $\text{Fe}^{\text{III}}\text{Cl}(\text{isq}^{\text{Ph}})_2$, $\text{Co}^{\text{II}}((\text{tBuPhO})_2\text{NHC})\text{THF}$, and $[\text{Fe}^{\text{III}}((\text{tBuPhO})_2\text{NHC})\text{Cl}_2]^-$ are unable to carry out stoichiometric oxidative addition of alkyl halides. One attractive strategy that could alleviate this problem is extending the π system of the N-heterocyclic carbene. This would decrease the π back donation of the metal d orbitals to the NHC making the metal center more electron rich.¹⁻² Therefore I

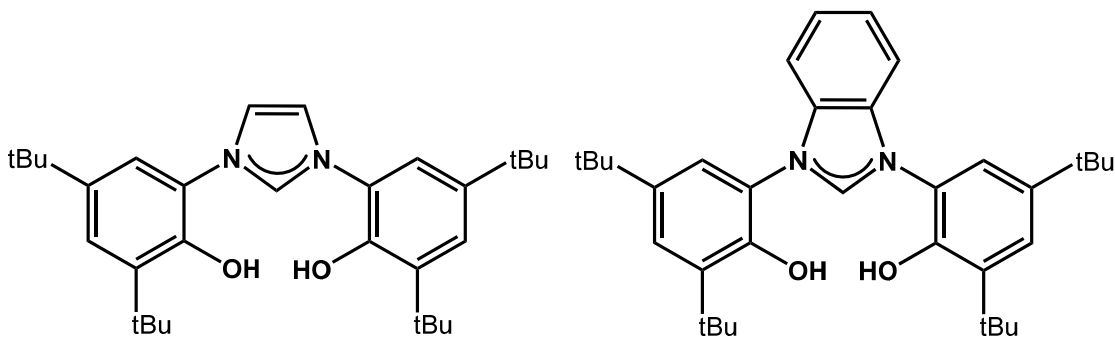


Figure 6-1 Proposed ligands to increase electron density at the metal center.

propose that future work pursue this strategy by making analogous cobalt ET series of the ligands shown in **Figure 6-1**. Both ligands have been previously published but cobalt complexes based on the ligands in **Figure 6-1** are unknown.³⁻⁴

In sum, redox-active ligands on 3d metals can function as well-defined catalysts for C–C bond forming reactions. Studies that elucidate the mechanism that allow for C–C bond forming reaction should be pursued. Furthermore, ligands that increase the electron density at the metal center should be explored.

6.1 Work cited

1. Khramov, D. M.; Lynch, V. M.; Bielawski, C. W., N-Heterocyclic Carbene–Transition Metal Complexes: Spectroscopic and Crystallographic Analyses of π -Back-bonding Interactions. *Organometallics* **2007**, 26, 6042-6049.
2. Cavallo, L.; Correa, A.; Costabile, C.; Jacobsen, H., Steric and electronic effects in the bonding of N-heterocyclic ligands to transition metals. *J. Organomet. Chem.* **2005**, 690, 5407-5413.

3. Despagnet-Ayoub, E.; Henling, L. M.; Labinger, J. A.; Bercaw, J. E., Addition of a phosphine ligand switches an N-heterocyclic carbene-zirconium catalyst from oligomerization to polymerization of 1-hexene. *Dalton Trans.* **2013**, 42, 15544-15547.
4. Yagyu, T.; Oya, S.; Maeda, M.; Jitsukawa, K., Syntheses and Characterization of Palladium(II) Complexes with Tridentate N-Heterocyclic Carbene Ligands Containing Aryloxy Groups and Their Application to Heck Reaction. *Chem. Lett.* **2006**, 35, 154-155.

Appendix A.

Work Towards a Pacman Type Redox-Active Ligand

A.1 Introduction

A.1.1 Pacman Type Ligands

Whereas this thesis has focused on the application of redox-active ligands for multielectron chemistry at a single base metal, nature has developed alternative strategies to catalyze multielectron redox reactions required for nitrogen fixation and water oxidation. To carry out these multielectron redox reactions nature employs enzymatic systems such as nitrogenase,¹ hydrogenase²⁻³, photosystem II,⁴⁻⁵ and cytochrome *c* oxidase, that use multiple metal centers working in concert.⁶ By working cooperatively, the bimetallic centers can alter the reactivity of substrates and direct the timing and redox potential of the redox equivalents.⁷ Dinuclear metal center complexes have been pursued to mimic the reactivity of enzymatic systems or to model their intrinsic behavior.⁸⁻¹³ Furthermore, dinuclear metal center complexes can be used to catalytically convert small molecules. For instance, the thermodynamic reduction potential for the catalytic four e^- oxidation of O_2 to H_2O is 1.23 V vs. NHE if all four e^- and protons are delivered in a concerted manner. If the reaction proceeds via two 2 e^- steps, producing either H_2O_2 or HO_2 , then the overall thermodynamic potential is increased to 1.65 V and 1.763 V respectively. Cofacial bis(cobalt) diporphyrin could deliver, electrocatalytically, the 4 e^- in a concerted manner to O_2 and avoid the two 2 e^- reduced intermediates. The cofacial arrangement enforced by the pacman ligand allows

the concerted interaction of O_2 and both metal centers.^{7, 14} Other pacman complexes containing two metals exhibit increased reactivity compared to their monometal counterparts or generated new reactivity. For instance, a dinuclear Cu^I complex synthesized by Bouwman and co-workers can reductively couple CO_2 to oxalate.¹⁵

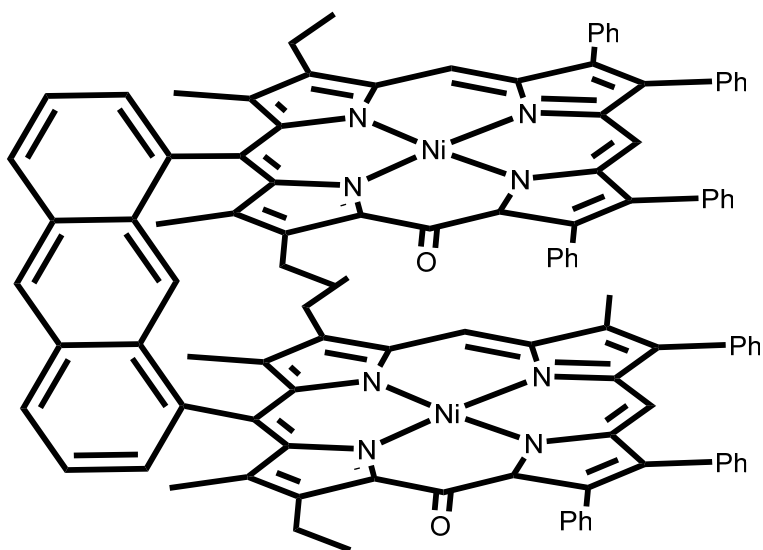
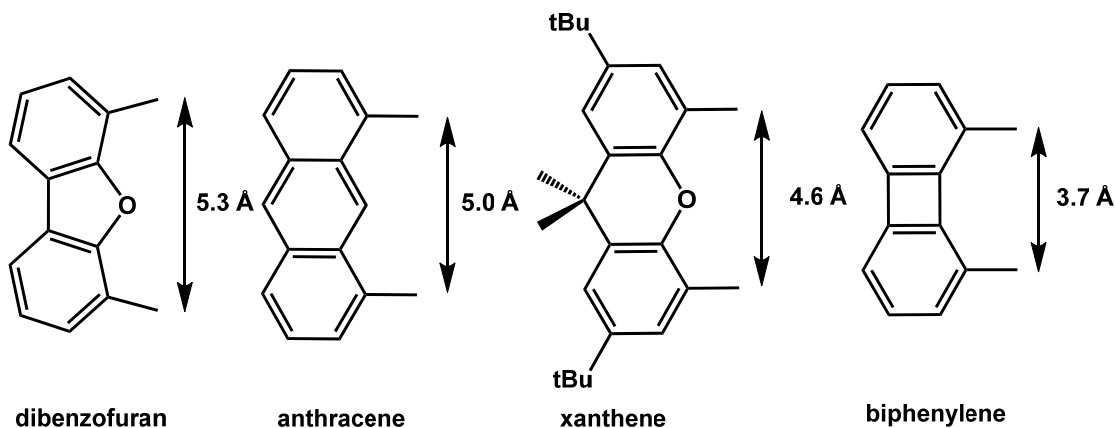


Figure A-1. A pacman ligand with bis(Ni(II)oxocorrole) and an anthracene backbone.

Pacman ligands, a subset of dinuclear metal center complexes, have two metals connected by a linker, or backbone, in such a way to allow either metal-metal bonding or a space between metals that allows single element bridging, referred to as bite angle.^{7, 16} A representative example of the basic ligand configuration is shown in **Figure A-1**. In this complex two modified nickel porphyrin moieties are linked by a rigid anthracene spacer.¹⁷ Pacman ligands typically involve anthracene, dibenzofuran, biphenylene or xanthene as the backbone moieties. The backbone serves two roles: first, it provides a chemically inert linker that holds the two metal containing moiety in a cofacial arrangement; second, it is the source of the bite angle *i.e.* the distance between attachment sites on the linker as shown in **Scheme A-1**.

Scheme A-1. Distance between the typical binding sites for macrocyclic ligands of several pacman ligand linkers.



The space between metal centers is crucial for small molecule activation. If the metals are too close together, they preclude small molecule binding. Additionally, if they are spaced too far apart they will act in concert on the small molecule. The spacer, in the case of biphenylene, can also provide a certain amount of translational freedom to the cofacial metals which is believed to aid in small molecule activation.⁷ The metal containing macrocycles can range from porphyrins and modified porphyrins to Schiff-base calixpyrrole.^{7, 18}

The overall geometric design of pacman ligands allows small molecules to interact with both metals. This feature allows the concerted delivery of multiple electrons. Delivering multiple electrons avoids high energy intermediates that prevent the economical transformation of inert small molecules, N₂, O₂, and H₂O, to chemically useful feed stocks.

A.1.2 Redox-Active Pacman Type Ligands

Incorporating redox-active ligands into the pacman scaffold can carry out difficult reactions such as H₂O oxidation. A dinuclear Ru redox-active pacman ligand (**Figure**

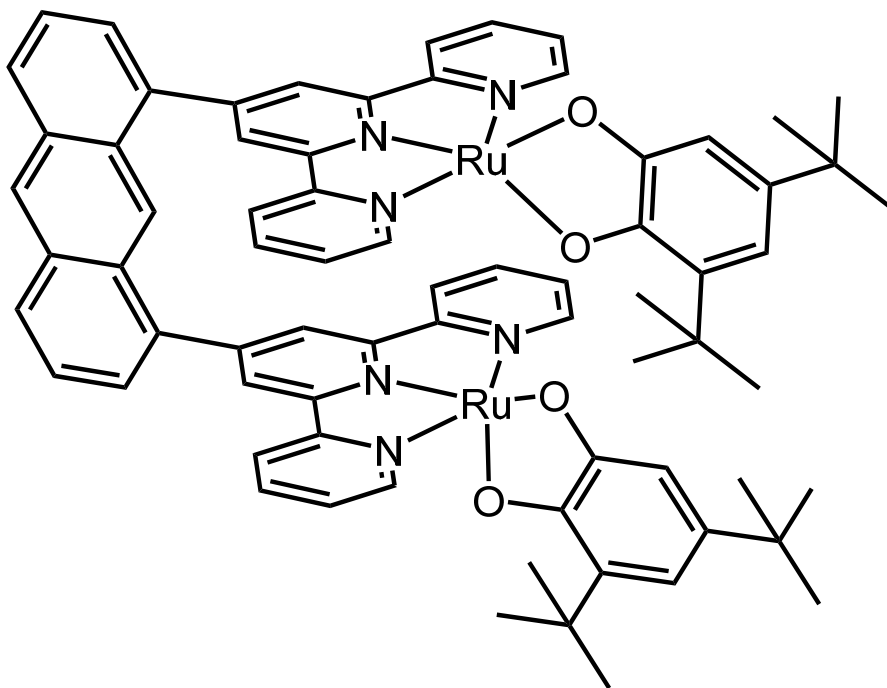


Figure A-2. A redox-active pacman ligand consisting of an anthracene backbone and bis(Ru(terpyridine)(3,5-ditertbutylcatechol))

A-2) was able to electrocatalytically (1.92 V) oxidize water with TONs of 33500.¹⁹⁻²⁰ The two redox-active ligands in close proximity to one another allow for delivery of 4 redox equivalents and the specific geometrical constraints aid in the oxidation of H₂O. Cofacial bis(porphyrins) are the prototypical pacman ligand. Cofacial bis(porphyrins) pacman-type ligands can support a variety of metals including Cu,²¹ Ni,¹⁷ Zn,²¹ Fe,²² Ru²³ and Co.^{7, 22} The porphyrin based redox-active ligands have been shown catalyzed O₂ reduction.⁷ Furthermore, work by Nocera *et.al.* demonstrated oxygen atom transfer to organic substrates via a cofacial diiron porphyrin complex using visible light and O₂ at the terminal oxidant.²⁴

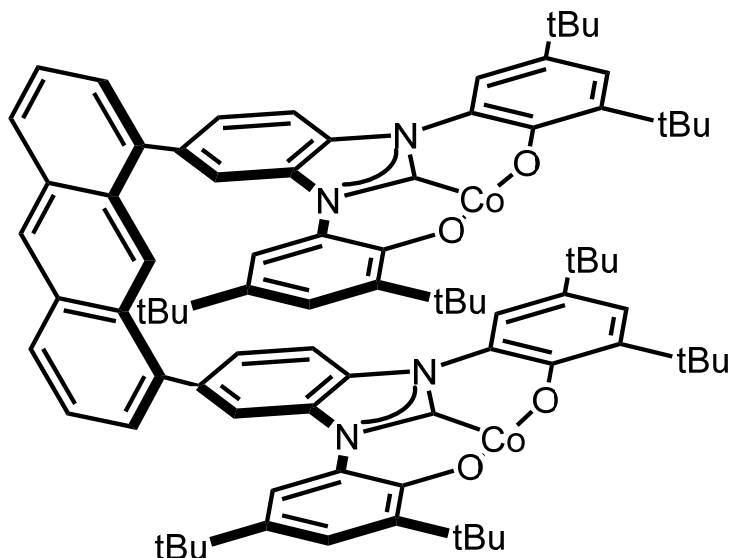
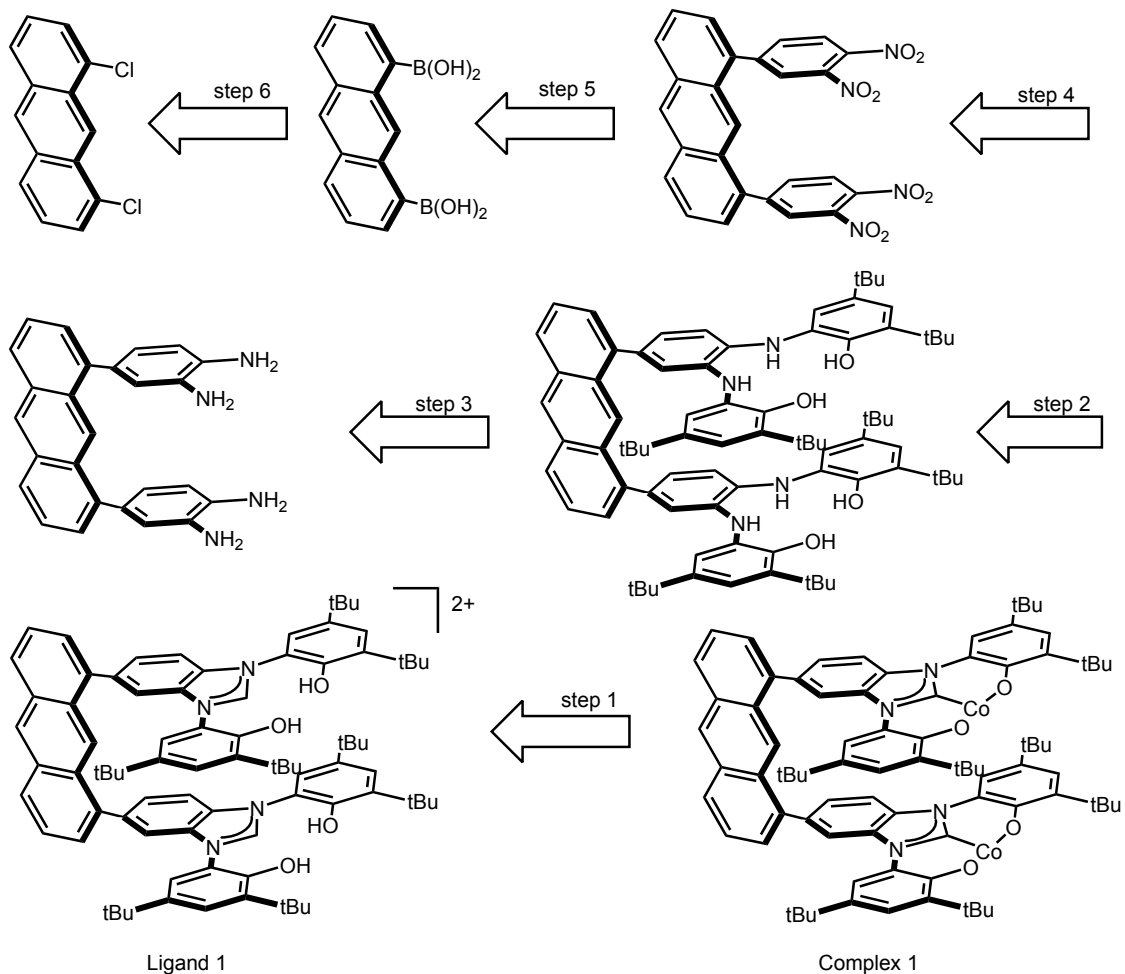


Figure A-3. Proposed redox-active pacman complex

Ammonia production is estimated to be 150 million tonnes annually and consumes 1 % of the world total annual energy supply.²⁵⁻²⁶ Ammonia is produced by the Haber-Bosch process which converts N_2 to NH_3 , referred to as nitrogen fixation.²⁷ Nitrogen fixation is difficult because N_2 requires $6 e^-$ and $6 H^+$ to produce 2 equiv of NH_3 . Industrially, a heterogeneous iron catalyst is used but requires high temperatures and pressures to catalytically produce NH_3 .²⁷ The $Co^{II}((tBuPhO)_2NHC)THF$ complex, Chapter 3, can be oxidized by $3 e^-$. For this complex to deliver the $6 e^-$ required to convert N_2 to NH_3 , two $Co^{II}((tBuPhO)_2NHC)THF$ complexes must be combined in a pacman-type ligand (**Figure A-3**). The two $[(tBuPhO)_2NHC]^{2-}$ macrocycles can each be oxidized by $2 e^-$, delivering a total of $4 e^-$. This combined with a 3d metal could provide up to six redox equivalences in a concerted manner to carry out the difficult reaction of nitrogen fixation that could avoid the high temperatures and pressures currently used in industry. This chapter shows the progress made toward realizing a new redox-active pacman type ligand.

Scheme A-2. Retrosynthetic analysis of redox-active pacman ligand with bis($\text{Co}((\text{tBuPhO})_2\text{NHC}^{\text{Bz}})$) and an anthracene backbone.



A.1.3 Retrosynthetic analysis of Redox-Active Pacman Type Ligands

To generate a redox-active pacman type ligand a retrosynthetic analysis was employed (**Scheme A-2**). The final complex features two redox-active ligand macrocycles ($[\text{tBuPhO})_2\text{NHC}^{\text{Bz}}]^{2-}$ bound to a Co where each arm is connected by an anthracene backbone (complex **1**). Complex **1** is achieved by metallation of ligand **1**; Step 1 in the retrosynthetic analysis. This step was proposed to follow metallation of the

parent macrocycle; a deprotonated pincer ligand $[\text{tBuPhO})_2\text{NHC}]^{2-}$ can be directly metallated with CoCl_2 as described in Chapter 3. The bis(NHC) anthracene complex (Step 2) can be prepared by a procedure from Chapter 3 from the reaction of 6,6'-(1,2-phenylenebis(azanediyl))bis(2,4-di-tert-butylphenol)-1,8-anthracene and triethyl orthoformate to generate the bis(NHC) compound. The conversion of bis(phenyl diamine)-1,8 anthracene to bis6,6'-(1,2-phenylenebis(azanediyl))bis(2,4-di-tert-butylphenol)-1,8-anthracene in Step 3 is accomplished via a condensation reaction with 3,5-ditertbutyl catechol.²⁸ Reduction of nitro groups to amines (Step 4) has good literature precedence.²⁹⁻³² Step 5 represents the largest challenge. There are several examples of cross-coupling to an activated anthracene,³³⁻⁴⁰ but fewer examples of multiple cross-coupling reactions to activated anthracene involving a functionalized beznene.⁴¹⁻⁴² It was anticipated that determining the right catalyst and conditions needed to facilitate multiple cross-coupling at a single reagent would require extensive screening. Conversion of 1,8-dichloroanthracene to the diboronic ester in Step 6 follows a previously published procedure via Pd cross-coupling with 5,5,5',5'-tetramethyl-2,2'-bi(1,3,2-dioxaborinane) to form 1,8-bis(5,5-dimethyl-1,3,2-dioxaborinan-2-yl)anthracene followed by acidic work up to generate anthracene-1,8-diylidiboronic acid.¹⁹

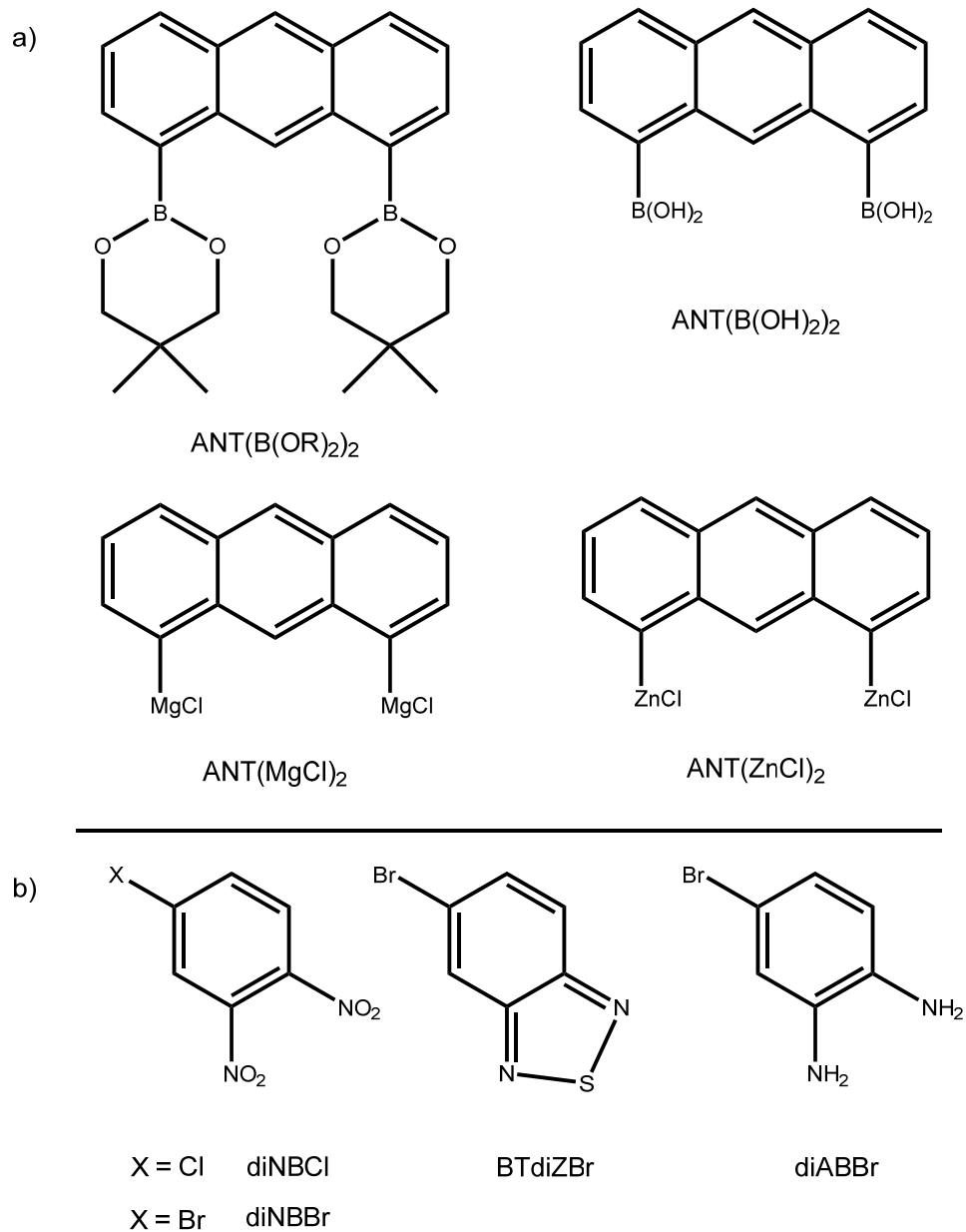
The precursors to Step 5 in the retrosynthetic analysis are either literature compounds or easily synthesized. However, little literature precedence exist for the dicoupling of functionalized aryls to activated anthracenes. Therefore, this chapter is focused on the synthetic protocol to achieve Step 5.

A.2 Results

A.2.1 Attempts at Anthracene Backbone Pacman Type Ligand

A.2.1.1 Cross-coupling Attempts Using Anthracene Nucleophiles and Substituted Aryl Halides

Scheme A-3. Aryl nucleophiles and protected and non-protected amines used for cross-coupling.



A total of four anthracene dinucleophiles were chosen (**Scheme A-3 a**). Two anthracene dinucleophiles were synthesized from literature procedures, anthracenyl-1,8-diboronic acid (ANT(B(OH)₂)₂)¹⁹ and 1,8-bis(neopentylglycolato)boryl)anthracene

(ANT(B(OR)₂)₂).¹⁹ Two new anthracene dinucleophiles were synthesized: 1,8-bis(chloromagnesio)anthracene (ANT(MgCl)₂) and anthracene-1,8-dizincchloride (ANT(ZnCl)₂). ANT(B(OR)₂)₂ was obtained from a reaction between 1,8-dichloroanthracene and bis(neopentylglycolate)diborane in the presence of a Pd⁰ catalyst (Pd₂(dba)₃), base (NaOAc), and ligand (2-dicyclohexylphosphino-2',4',6'-trisisopropylbiphenyl = xPhos) at 90 °C under N₂ for 48 hours. Subsequent recrystallization lead to a 68 % yield of the desired ANT(B(OR)₂)₂ as yellow needles. To produce anthracenyl-1,8-diboronic acid, the borate esters of ANT(B(OR)₂)₂ were converted to boronic acids in the presence of diethanolamine in isopropanol for 3 hours followed by an excess of 1 M HCl (70 % yield). ANT(MgCl)₂ was made from activating 2.5 equiv Mg (s) with 1 drop of 1,2-dibromoethane in THF and adding the 1,8-dichloroanthracene followed by heating for at 100 °C for 6 hours. During the course of the reaction, the Mg (s) shavings turn black and reduced in volume which is followed by the solution turning from yellow to colorless. Once cooled to room temperature, the solution is filtered to remove excess Mg (s). Iodometric titrations indicate the desired ANT(MgCl)₂ was obtained in a yield of 70 %. When the solution is quenched with MeOH the only remaining product is anthracene, as judged by NMR and GC-MS. However, anthracene is known as a Mg⁰ transfer reagent.⁴³ When magnesium anthracene (MgC₁₄H₁₀•3THF) is formed an insoluble blue material precipitates out. This was not seen in the 1,8-dichloroanthracene reaction. However, it could not be ruled out as a possible product. Nevertheless, given the ease of synthesis, the ANT(MgCl)₂ would be screened as an anthracene dinucleophile. To make the ANT(ZnCl)₂ complex 1,8-dichloroanthracene was reacted with 2 equiv of Zn dust and a catalytic amount of I₂ in THF. Upon quenching an aliquot with MeOH, the major product was anthracene with lesser amounts of 1,8-dichloroanthracene and chloroanthracene.

Three aryl halide complexes with protected nitrogens and one aryl halide with primary amines were chosen to cross-couple with the above mentioned anthracenedinucleophiles. 5-bromo-1,2-dinitrobenzene (diNBBr), 5-chloro-1,2-dinitrobenzene (diNBCl), and 5-bromo-1,2-diaminebenzene (diABBr) were commercially available (**Scheme A-3 b**). The complex 5-bromo-2,1,3 benzothiadiazole (BTdiZBr) was made by a literature procedure.⁴⁴

With both coupling partners in hand, attempts were made to generate the diaryl substituted anthracene compound. In a typical reaction, an anthracene dinucleophile and 2 equiv of an aryl halide were heated for up to 48 h. The reaction was cooled and in the case of Grignard or organozinc anthracene the crude product was tested using GC-MS and ESI for the desired product without further purification. In the case of the $\text{ANT}(\text{B}(\text{OR})_2)_2$ and $\text{ANT}(\text{B}(\text{OH})_2)_2$, after heating and cooling, the solution was washed with 3x H_2O and the organic phases combined and tested using GC-MS and ESI. The results of the cross-coupling reactions are listed in **Table A-1**. In all cases the desired disubstituted anthracene was not observed. Anthracene was seen as a product in all reactions. Interestingly, entry 1 and 4 from **Table A-1** and entry 2 from Table A-2 showed a mass of 538 m/z as the major product. The desired product 1,8-di(1,2-dinitrobenzene)anthracene has a mass of 510 m/z. Since all three reactions use different catalyst and different anthracene dinucleophiles, the resulting 538 m/z peak might be of interest even though it is not the desired product. The identity of the 538 m/z has not been determined. The monosubstituted anthracene was also not seen in any reaction.

Table A-1. Reactions between anthracenedigrignard or diorganozinc and aryl halides catalyzed by Pd or Ni.

Entry	Aryl dinucleophile	Aryl halide	Catalyst (mol %)	Solvent	Base	Temperature °C	Time hrs	Result ¹
1	ANT(ZnCl) ₂	diNBCl	PdCl ₂ (P(Ph) ₃) ₂ (5)	THF	N.A.	80	16	N.P.
2	ANT(MgCl) ₂	diNBCl	PdCl ₂ (P(Ph) ₃) ₂ (5)	THF	N.A.	100	24	N.P.
3	ANT(MgCl) ₂	BTdiZBr	Ni(acac) ₂ /PPh ₃ (10) ²	THF	N.A.	100	24	N.P.
4	ANT(MgCl) ₂	diNBBr	Ni(acac) ₂ /PPh ₃ (10) ²	THF	N.A.	100	24	N.P.
5	ANT(MgCl) ₂	BTdiZBr	NiCl ₂ /I ₂ (10) ²	xylene	N.A.	140	36	N.P.

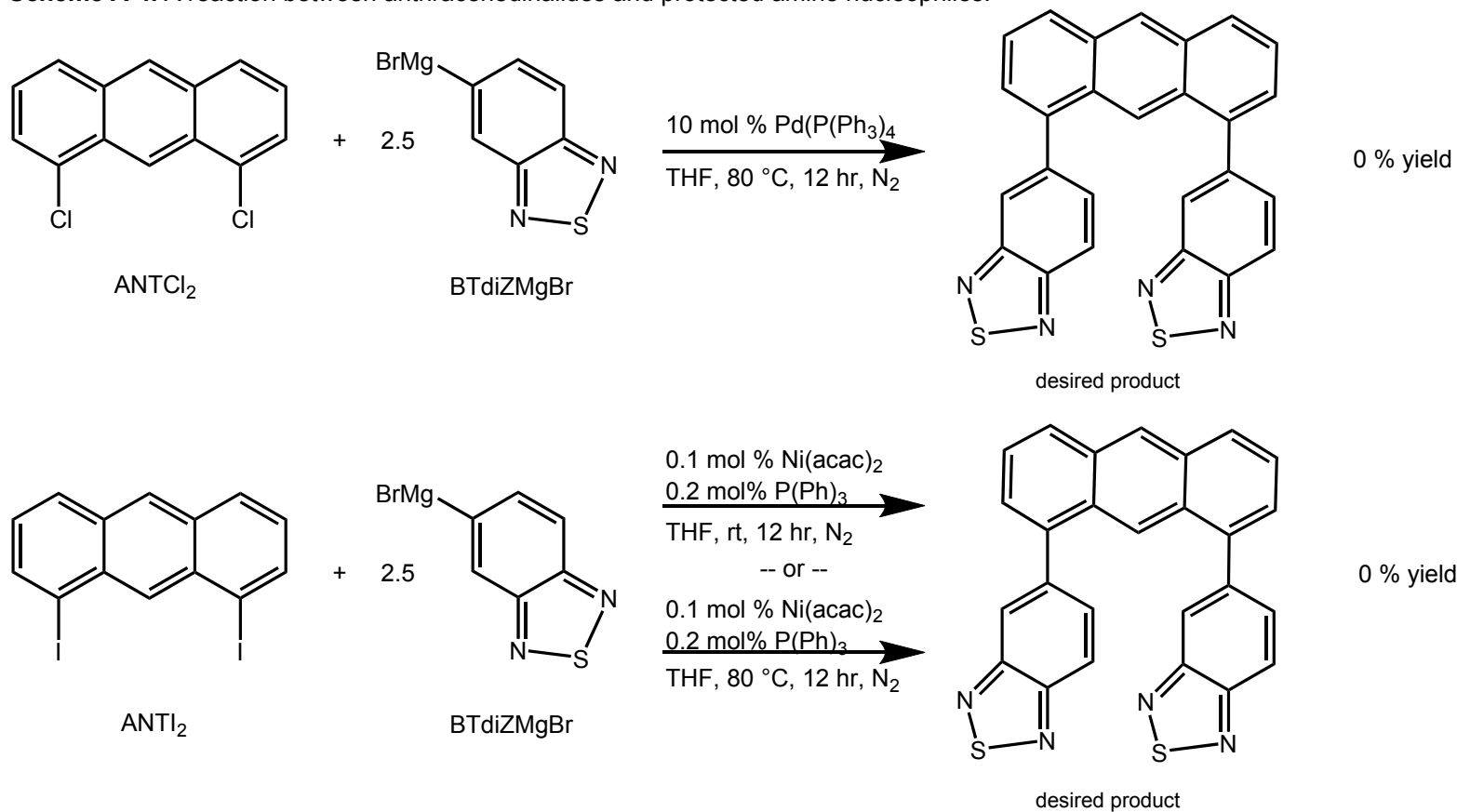
The reactions are carried out on a 4.0 mmol scale with 2 equiv of aryl halide under N₂. At the end of the reaction the solution was cooled and tested without further purification. ¹Products determined by ESI, MALDI and NMR. ² 20 mol % of PPh₃ and 1 equiv I₂ was added to the reaction.

Table A-2. Reactions between aryl borate esters or boronic acid and aryl halides catalyzed by Pd.

Entry	Aryl dinucleophile	Aryl halide	Catalyst (mol %)	Solvent (ratio)	Base	Temperature °C	Time hrs	Result ¹
1	ANT(B(OR) ₂) ₂	diABBr	Pd(dppf)Cl ₂ (1)	dioxane	K ₂ CO ₃	90	24	N.P.
2	ANT(B(OR) ₂) ₂	diNBrCl	Pd(OAc) ₂ (5)	EtOH/DMA (1:1)	K ₂ CO ₃	80	48 or 24	N.P.
3	ANT(B(OH) ₂) ₂	diNBrCl	Pd ₂ (dba) ₃ (10)	toluene	K ₃ PO ₄	80	48	N.P.
4	ANT(B(OH) ₂) ₂	diNBrCl	PdCl ₂ (P(Ph) ₃) ₂ (5)	DMSO	K ₂ CO ₃	100	24	N.P.
5	ANT(B(OH) ₂) ₂	diABBr	Pd(PPh ₃) ₄ (10)	dioxane/H ₂ O (10:1)	K ₂ CO ₃	110	24	N.P.
6	ANT(B(OH) ₂) ₂	BTdiZBr	Pd(OAc) ₂ (1)	THF/H ₂ O (10:1)	K ₂ CO ₃	100	24	N.P.
7	ANT(B(OH) ₂) ₂	BTdiZBr	Pd(OAc) ₂ (1)	EtOH/DMA (1:1)	K ₂ CO ₃	120	1	N.P.

The reactions are carried out on a 4.0 mmol scale with 2 equiv of aryl halide under N₂. At the end of the reaction the solution was cooled quenched with H₂O and the organic layer removed. ¹Products determined by ESI, MALDI and NMR.

Scheme A-4. A reaction between anthracenedihalides and protected amine nucleophiles.



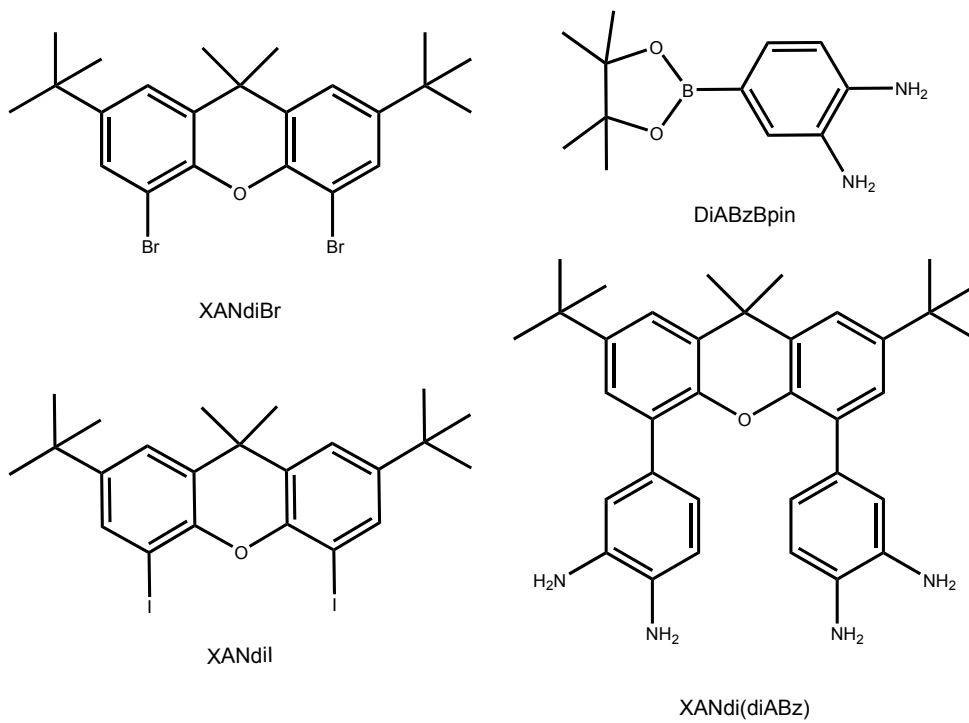


Figure A-4. Chosen dihalidexanthenes and diamine nucleophiles for cross-coupling.

Table A-3. Reaction conditions and results between dihalide xanthene and borate ester diamines catalyzed by Pd.

Entry	Aryl dinucleophile	Aryl halide (equiv)	Catalyst (mol %)	Solvent (ratio)	Base (equiv)	Temperature °C	Time hrs	Result ¹
1	XANdiBr	DiABzBpin (2)	Pd(dppf)Cl ₂ (5)	dioxane/H ₂ O (10:1)	K ₂ CO ₃ (5)	100	72	N.P.
2	XANdiBr	DiABzBpin (2)	Pd(dppf)Cl ₂ (5)	dioxane	K ₂ CO ₃ (5)	100	24	N.P.
3	XANdiBr	DiABzBpin (2)	Pd(dppf)Cl ₂ (5)	dioxane	K ₂ CO ₃ (5)	100	72	N.P.
4	XANdiBr	DiABzBpin (2)	Pd(dppf)Cl ₂ (5)	toulene	Ba(OH) ₂ (5)	90	24	N.P.
5	XANdil	DiABzBpin (2)	Pd(dppf)Cl ₂ (5)	dioxane/H ₂ O (10:1)	K ₂ CO ₃ (5)	100	24	N.P.
6	XANdil	DiABzBpin (3)	Pd(dppf)Cl ₂ (20)	dioxane/H ₂ O (10:1)	K ₂ CO ₃ (5)	130	48	XANdi(diABz)

¹ Products determined by ESI, MALDI and NMR.² 5 equiv of K₂CO₃ were used.

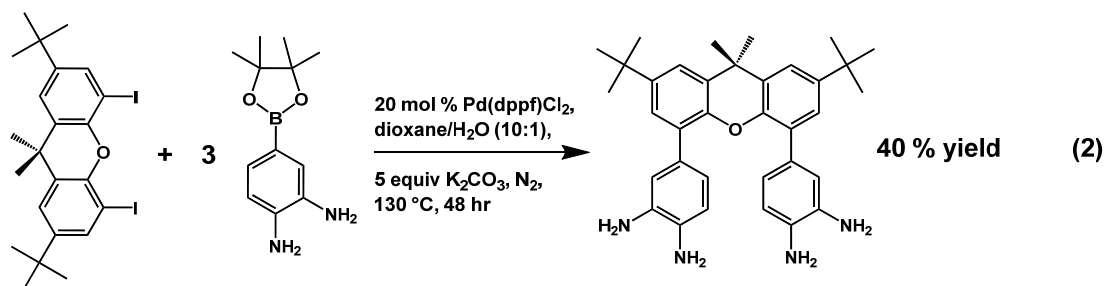
A.2.1.2 Cross-coupling Attempts Using Anthracene Halides and Nucleophilic aryl Protected Amines

The two complexes 1,8-dichloroanthracene or 1,8-diiodoanthracene were used as the anthracene halide due to easy of synthesis (1,8-dichloroanthracene) or commercial availability (1,8-diiodoanthracene). Converting BTdiZNr to a Grignard reagent was accomplished by exposure of BTdiZNr to activated Mg (s) at 80 °C giving a 79 % yield as determined by MeOH quench and NMR analysis. A reaction between either dichloro- or diiodo- anthracene and 2.5 equiv of benzo[c][1,2,5]thiadiazol-5-yl magnesium bromide (BTdiZMgBr) in THF at r.t. or 100 °C did not lead to cross-coupled product, nor did any of the reactions in **Scheme A-4** show the monosubstituted product.

A.2.2 Synthesis of Xanthene Backbone Pacman Type Ligand

Switching the backbone from anthracene to xanthene immediately gave improvement. A reaction between 4,5-dibromo-2,7-di-tert-butyl-9,9-dimethyl-9H-xanthene (XANdiBr) and 2 equiv of 4-(4,4,5,5-tetramethyl-1,3,2-dioxaborolan-2-yl)benzene-1,2-diamine (diABzBpin) lead to the monosubstituted xanthene and a small amount of the disubstituted product as judged by ESI (entry 1 in **Table A-3**). The amount of disubstituted product was not sufficient for isolation. Encouraged by the result, the parameters were varied until the desired product was achieved (40 % yield, entry 6 **Table A-3**). The reaction that ultimately led to disubstituted xanthane (4,4'-(2,7-di-tert-butyl-9,9-dimethyl-9H-xanthene-4,5-diyl)bis(benzene-1,2-diamine) = XANdi(diABz)) complex involved replacing the bromides with iodines, increasing the catalyst loading, increasing the equivalents of diABzBpin from 2 to 3, increasing the temperature to 130 °C, and running the reaction for 48 hr. After washing the solution 3x with water, the crude organic layer showed a high resolution mass spectrum of 534.3359

m/z vs the calculated mass for XANdi(diABz) = 534.33587 m/z . Attempts to isolate XANdi(diABz) as a HCl salt have been unsuccessful. Excess phenylenediamine and benzo[c][1,2,5]thiadiazole could be sublimed off, however this alone was insufficient at producing pure XANdi(diABz). Isolation of XANdi(diABz) was challenging because of its propensity to irreversibly bind the silica or alumina column materials. Nevertheless, a separation protocol was developed. Separation involved column chromatography on silica gel using a series of increasingly polar solvents ending with MeOH as the final eluent. This produced the desired compound (XANdi(diABz)) as the last analyte-containing fraction. The overall synthetic procedure is shown in **equation 2**.



A.3 Discussion

Step 5 is challenging due to the requirement of two cross-coupling event involving functionalized aryl reagents to one substrate. While several systems can cross-couple two substrates on to an activated anthracene,^{19, 33-34, 37-39, 45-46} to the best of my knowledge there are no examples of cross-coupling 2 1,2-dinitrobenzene or 1,2-diaminebenzene to an activated anthracene. A significant challenge to Step 5 is the multitude of synthetic protocols available for Pd and Ni coupling. Therefore, several different activated anthracenes and xanthenes; palladium and nickel catalysts; and

activated, functionalized aryls were screened to address this problem. Discussed here are the challenges and synthetic protocols pursued that eventually led to conditions that completed Step 5.

A.3.1 Cross-coupling attempts anthracene

Anthracene is an attractive backbone for a pacman type ligand for three reasons. First, it is chemically inert.⁷ Second, it is cheap to synthesize on a large scale. 1,8-dichloroanthracene is easily made from inexpensive and commercially available 1,8-dichloro-9,10-anthraquinone.³⁵ This process is also amenable to scale up where up to 78 g of 1,8-dichloroanthracene can be produced in good yield (88 %). Third, modifying the 1,8-dichloroanthracene is relatively straight forward providing a range of cross-coupling platforms and subsequent cross-coupling reactions. For instance, both halides on ANTCl_2 can be substituted for o-xylenes and porphyrins.^{32-33, 36-38, 40, 42-44} It was believed that one of these platforms would allow a double cross-coupling event with activated and functionalized aryl compounds to occur.

A.3.1.1 Cross-coupling attempts at nucleophilic anthracene ($\text{ANT}(\text{MgCl})_2$, $\text{ANT}(\text{ZnCl})_2$, $\text{ANT}(\text{B}(\text{OH})_2)_2$, $\text{ANTB}(\text{OR})_2$)

Although $\text{ANT}(\text{ZnCl})_2$ was been previously prepared,⁴¹ it has not been isolated or characterized, and was used *in situ*. Therefore a new synthetic procedure was developed and employed. Although the conversion of ANTCl_2 to $\text{ANT}(\text{ZnCl})_2$ was not complete, cross-coupling was attempted. However a reaction between $\text{ANT}(\text{ZnCl})_2$ and diNBCl did not produce the desired product. The $\text{ANT}(\text{MgCl})_2$ synthetic procedure lead to a 95 % conversion of ANTCl_2 to $\text{ANT}(\text{MgCl})_2$ and allowed for screening of several different activated aryls and catalysts (**Table A-1**). Generally, Grignard and organozinc reagents react with primary amines, however nitro groups are tolerant of Grignards,

organozincs, and Suzuki cross-coupling reactions and act as protected amines.⁴⁷⁻⁴⁹ Another way to protect 1,2-diaminebenzene involves conversion of the diamines to thiadiazole (BTdiZBr **Scheme A-3 b**).⁵⁰ This protected amine has been shown to tolerate cross-coupling reactions including Grignard reagents.⁵¹⁻⁵⁴ Furthermore, conversion of the thiadiazole complex to diaminebenzene is a known literature procedure.⁵⁵ Therefore, dinitro or benzo[c][1,2,5]thiadiazole halides were employed. However, neither the $\text{ANT}(\text{MgCl})_2$ or $\text{ANT}(\text{ZnCl})_2$ cross-coupled with the protected amines in the presence of either a palladium ($\text{Pd}^{\text{II}}\text{Cl}_2(\text{P}(\text{Ph}_3)_2)$ or nickel ($\text{Ni}(\text{acac})_2$ or NiCl_2) catalyst (**Table A-1**).

Both $\text{ANT}(\text{B}(\text{OH})_2)_2$ and $\text{ANT}(\text{B}(\text{OR})_2)_2$ were prepared from literature procedures. The boronic acids have enhanced reactivity (aryl cross-coupling) compared to borate esters however pinacol boronic esters are still very commonly used especially in Miyaura borylation reactions due to pinacol boronic esters being tolerant of ambient atmosphere and chromatographic purification.⁵⁶ Both $\text{ANT}(\text{B}(\text{OH})_2)_2$ and $\text{ANT}(\text{B}(\text{OR})_2)_2$ are tolerant of many solvents, unlike $\text{ANT}(\text{MgCl})_2$ or $\text{ANT}(\text{ZnCl})_2$ where only THF, o-xylene or ethers could be employed. Most palladium based cross-coupling protocols cannot tolerate primary amines as functional groups. In fact, the Buckwald-Hartwig amination exploits primary amines ability to cross-couple with carbon nucleophiles to form new N-C bonds in the presence of a palladium catalyst.⁵⁷⁻⁵⁹ Therefore, to avoid reactions between amines and carbon nucleophilicities, primary amines generally must be protected. To this end, diNBCl, diNBBr, and BTdiZBr were used as coupling partners. However, a few examples exist of Suzuki cross-coupling with a primary amine functional groups that avoid forming new N-C bonds.⁶⁰⁻⁶² For instance, in the synthesis of a hangman porphyrin xanthene (HPX) complex a borate ester diamine benzene was directly cross-coupled to a bromoxanthene.⁶³

A.3.1.2 Cross-coupling attempts at dihalide anthracene

Starting with the dihalide anthracene requires that the coupling partner be nucleophilic. Converting 5-bromo-2,1,3-benzothiadiazole to a Grignard reagent was the most straightforward way to turn the protected diamine into an aryl nucleophile. However, neither ANTl_2 or ANTCl_2 cross-coupled with benzo[c][1,2,5]thiadiazol-5-yl magnesium bromide using either a palladium or nickel catalyst (**Scheme A-4**).

A.3.2 Cross-coupling of a borate ester aryl diamine and dihalidexanthane

Using diiodoxanthane and 3 equiv diABzBpin lead to the desired product ($\text{XAN}(\text{diABz})_2$). The system required to carry out this cross-coupling is harsh, 3 equiv diABzBpin, 5 equiv of base, 20 mol % catalyst loading at 130 °C for 48 hours. The halide is also important for cross-coupling to occur. The XANdiBr lead to monosubstituted product. Interestingly, using a better base ($\text{Ba}(\text{OH})_2$, entry 4, Table A-3) did not lead to the desired product and K_2CO_3 was the preferred base when used in a large excess (5 equiv). Solvent choice was also important. The dioxane/ H_2O (10:1) solution proved to be the best solvent however different ratios of dioxane to H_2O have not been explored. Temperature was also crucial in the synthesis of $\text{XAN}(\text{diABz})_2$. At 100 °C in a sealed bomb only the monosubstituted product was isolated, however when the reaction temperature was increased to 130 °C the major product was $\text{XAN}(\text{diABz})_2$. Although isolation by column chromatography is difficult, due to the four primary amines, isolation was achieved by silica gel column chromatography using several different solvents (*vide infra*).

A.4 Conclusion

Given the cost of anthracene and the wide variety of dihalides and dinucleophiles available, work should continue to elucidate conditions that would make anthracene the backbone in the proposed pacman ligand. While the cost of catalyst and XANdI_2 make this system less desirable than anthracene, XANdI_2 is the only complex where cross-coupling has been achieved. Production of $\text{XAN}(\text{diABz})_2$ completes Steps 6 to 4 in an overall 28 % yield. Only two more synthetic steps are required to synthesis the desired ligand **1**. However achievement of Step 3 will require scale up of $\text{XAN}(\text{diABz})_2$ due to the low yielding nature of the condensation reaction between 3,5-di-tert-butylcatechol and the $\text{XAN}(\text{diABz})_2$. Regardless, a significant challenge has been overcome in the progress toward a redox-active pacman-type ligand based on the $[(\text{tBuPhO})_2\text{NHC}]^{2-}$ moiety.

A.5 Materials and Methods

General consideration

Unless otherwise noted, all manipulations were performed under anaerobic conditions using standard vacuum line techniques, or in an inert atmosphere glove box under purified nitrogen. All NMR spectra were acquired on a Varian Mercury 300 spectrometer (300.323 MHz for ^1H) at ambient temperature. Chemical shifts are reported in parts per million (ppm) relative to TMS, with the residual solvent peak serving as an internal reference. All mass spectra were recorded in the Georgia Institute of Technology Bioanalytical Mass Spectrometry Facility. Anhydrous toluene, tetrahydrofuran (THF), and pentane solvents for air- and moisture-sensitive manipulations were purchased from Sigma–Aldrich, further dried by passage through columns of activated alumina, degassed by at least three freeze–pump–thaw cycles, and

stored under N₂ prior to use. Dimethylsulfoxide, dimethylformamide, diethyl ether, 1,4-dioxane, methanol (MeOH), ethanol (EtOH), and xylene were purchased from Sigma–Aldrich, degassed by nitrogen sparge for 20 mins and stored under N₂ until used. Distilled H₂O was degassed by nitrogen sparge for 20 mins and stored under N₂ until used. The compounds 1,8-dichloroanthracene,⁶⁴ anthracene-1,8-diyl diboronic acid,¹⁹ 1,8-bis(5,5-dimethyl-1,3,2-dioxaborinan-2-yl)anthracene,¹⁹ 4-(4,4,5,5-tetramethyl-1,3,2-dioxaborolan-2-yl)benzene-1,2-diamine,⁶³ 5-bromobenzo[c][1,2,5]thiadiazole,⁶⁵ and 2,7-di-tert-butyl-4,5-diiodo-9,9-dimethyl-9H-xanthene⁶⁶ were prepared according to literature methods. All characterization data matched those referenced. All other chemicals were purchased from Sigma–Aldrich and used as received.

Synthesis of 1,8-bis(chloromagnesio)anthracene

A dried round bottom flask was charged with a magnetic stir bar, 20 mL of THF and magnesium shavings (0.123 g, 5.0 mmol). 1,2-dibromoethane (150 µL, 1.7 mmol) was added with stirring. After effervescence ceased, 1,8-dichloroanthracene (0.224 g, 0.9 mmol) was added and the solution was stirred for 24 hours to produce 1,8-bis(chloromagnesio)anthracene yield 95 %. Yield was determined by MeOH quench of the resulting di-Grignard to generate anthracene. The ratio of anthracene to 1,8-dichloroanthracene, as judged by ¹H NMR, was used to determine yield of the reaction.

Synthesis of 1,8-dizinchlorideanthracene

A dried thick-walled glass bomb with a Knotes valve was charged with a magnetic stir bar, 1,8-dichloroanthracene (0.800 g, 3.2 mmol), Zn (dust) (0.422 g, 6.4 mmol), 1 crystal of I₂, LiBr (0.282 g, 3.2 mmol) and 40 mL of THF under N₂. The bomb was sealed and heated to 80 °C for 12 hr with stirring to produce a 50 % yield of the title

complex. Yield of the di-organozinc reagent was determined by quenching an aliquot of the solution with MeOH and measured the amount of anthracene generated by GC-MS.

Synthesis of benzo[c][1,2,5]thiadiazol-5-yl magnesium bromide

A dried round bottom flask was charged with a magnetic stir bar, Mg shavings (0.074 g, 3.0mmol) and 10 mL THF under N₂. Then, 1,2-dibromoethane (50 μ L, 0.5 mmol) and 1 crystal of I₂ was added. After effervescence ceased, 5-bromobenzo[c][1,2,5]thiadiazole (0.538 g, 2.5 mmol) was added. The reaction was then stirred for 48 hrs to yield 79 % of the title complex. Yield was determined by MeOH quench of the resulting Grignard to generate benzo[c][1,2,5]thiadiazole. The ratio of benzo[c][1,2,5]thiadiazole to 5-bromobenzo[c][1,2,5]thiadiazole, as judged by ¹H NMR, was used to determine yield of the reaction.

Typical cross-coupling procedure

In a representative procedure, a dried thick-walled glass bomb with a Knotes valve was charged with a magnetic stir bar, 1,8-bis(5,5-dimethyl-1,3,2-dioxaborinan-2-yl)anthracene (1.02g, 2.4 mmol), 4-bromobenzene-1,2-diamine (1.34 g, 7.2 mmol), Pd(dppf)Cl₂ (0.196 g, 0.24 mmol), and K₂CO₃ (0.828 g, 6.0 mmol). The bomb was evacuated and refilled with N₂ 3x. Nitrogen sparged dioxane (20 mL) was transferred by cannula and the bomb was sealed. The reaction was heated with stirring to 90 °C for 24 hr. After 24 hr the reaction was cooled, and diethyl ether (~60 mL) was added. The organic layer was 3x washed with H₂O. The organic layer was then run in GC-MS to determine product composition.

Synthesis of 4,4'-(2,7-di-tert-butyl-9,9-dimethyl-9H-xanthene-4,5-diyl)bis(benzene-1,2-diamine)

A dried thick-walled glass bomb with a Knotes valve was charged with a magnetic stir bar, 2,7-di-tert-butyl-4,5-diiodo-9,9-dimethyl-9H-xanthene (1.01 g, 1.75 mmol), 4-(4,4,5,5-tetramethyl-1,3,2-dioxaborolan-2-yl)benzene-1,2-diamine (1.23 g, 5.27 mmol), Pd(dppf)Cl₂ (0.287 g, 0.35 mmol), and K₂CO₃ (1.21 g, 8.75 mmol). The bomb was evacuated and refilled with N₂ 3 times. Nitrogen sparged 1,4-dioxane/H₂O (40 mL, ratio (10:1)) was transferred by cannula and the bomb was sealed. The reaction was heated with stirring to 130 °C for 48 hr. After 48 hr the reaction was cooled, and diethyl ether (~60 mL) was added. The organic layer was 3x washed with H₂O. The organic layer was dried and taken up in a minimum amount of CH₂Cl₂. Isolation was achieved by column chromatography. To a 30 cm x 3 cm glass column with a porous frit was added 50 g of silica gel in CH₂Cl₂ and topped off with 1 cm of sand. The CH₂Cl₂ solution containing the desired product was loaded, by aliquots, to the column. Methylene chloride was run through the column until the eluent no longer contained analytes, as judged by TLC. The eluent was then changed to CH₂Cl₂/NEt₃ (ratio 5/2) and run through the column until the eluent no longer contained analytes, as judged by TLC. The column was then washed with CH₂Cl₂ (300 mL) to remove any excess NEt₃. Finally, the eluent was changed to MeOH and fractions were collected. The last analyte-containing fractions removed from the column were the desired product. The like fractions were combined and dried *in vacuo* to produce a brown solid of the title complex (0.356 g, 40 % yield). ¹H NMR (300 MHz, CDCl₃) δ 7.36 (d, *J* = 2.4 Hz, 2H), 7.20 (d, *J* = 2.4 Hz, 2H), 6.80 – 6.69 (m, 4H), 6.61 (d, *J* = 7.9 Hz, 2H), 3.30 (s, 8H), 1.71 (s, 6H), 1.34 (s, 18H). ¹³C NMR (75 MHz, CDCl₃) δ 145.81, 145.14, 134.08, 134.05, 130.67, 130.07, 129.20,

125.83, 121.76, 121.05, 119.73, 115.88, 35.15, 34.62, 32.24, 31.71. HRMS (ESI) Calcd
for $C_{35}H_{42}N_4O$: $[M] = 534.33587$ m/z. Found = 534.3359 m/z.

A.6 Work Cited

1. Burgess, B. K.; Lowe, D. J., Mechanism of Molybdenum Nitrogenase. *Chem. Rev.* **1996**, *96*, 2983-3012.
2. Holm, R. H.; Kennepohl, P.; Solomon, E. I., Structural and Functional Aspects of Metal Sites in Biology. *Chem. Rev.* **1996**, *96*, 2239-2314.
3. Fontecilla-Camps, J. C.; Volbeda, A.; Cavazza, C.; Nicolet, Y., Structure/Function Relationships of [NiFe]- and [FeFe]-Hydrogenases. *Chem. Rev.* **2007**, *107*, 4273-4303.
4. Yachandra, V. K.; Sauer, K.; Klein, M. P., Manganese Cluster in Photosynthesis: Where Plants Oxidize Water to Dioxygen. *Chem. Rev.* **1996**, *96*, 2927-2950.
5. McEvoy, J. P.; Brudvig, G. W., Water-Splitting Chemistry of Photosystem II. *Chem. Rev.* **2006**, *106*, 4455-4483.
6. Liu, F.; Concepcion, J. J.; Jurss, J. W.; Cardolaccia, T.; Templeton, J. L.; Meyer, T. J., Mechanisms of Water Oxidation from the Blue Dimer to Photosystem II. *Inorg. Chem.* **2008**, *47*, 1727-1752.
7. Collman, J. P.; Wagenknecht, P. S.; Hutchison, J. E., Molecular Catalysts for Multielectron Redox Reactions of Small Molecules: The "Cofacial Metallodiporphyrin" Approach. *Angew. Chem., Int. Ed. Engl.* **1994**, *33*, 1537-1554.
8. van der Vlugt, J. I., Cooperative Catalysis with First-Row Late Transition Metals. *Eur. J. Inorg. Chem.* **2012**, 363-375.
9. Esteruelas, M. A.; Garcia, M. P.; Lopez, A. M.; Oro, L. A., Indirect cooperative effects leading to synergism in bimetallic homogenous catalysts containing azolates as bridging ligands. *Organometallics* **1991**, *10*, 127-133.
10. van den Beuken, E. K.; Feringa, B. L., Bimetallic catalysis by late transition metal complexes. *Tetrahedron* **1998**, *54*, 12985-13011.
11. Li, L. T.; Metz, M. V.; Li, H. B.; Chen, M. C.; Marks, T. J.; Liable-Sands, L.; Rheingold, A. L., Catalyst/cocatalyst nuclearity effects in single-site polymerization. Enhanced polyethylene branching and alpha-olefin comonomer enchainment in polymerizations mediated by binuclear catalysts and cocatalysts via a new enchainment pathway. *J. Am. Chem. Soc.* **2002**, *124*, 12725-12741.

12. Salata, M. R.; Marks, T. J., Catalyst Nuclearity Effects in Olefin Polymerization. Enhanced Activity and Comonomer Enchainment in Ethylene plus Olefin Copolymerizations Mediated by Bimetallic Group 4 Phenoxyminato Catalysts. *Macromolecules* **2009**, *42*, 1920-1933.
13. Klaus, S.; Lehenmeier, M. W.; Anderson, C. E.; Rieger, B., Recent advances in CO₂/epoxide copolymerization-New strategies and cooperative mechanisms. *Coord. Chem. Rev.* **2011**, *255*, 1460-1479.
14. Collman, J. P.; Anson, F. C.; Barnes, C. E.; Bencosme, C. S.; Geiger, T.; Evitt, E. R.; Kreh, R. P.; Meier, K.; Pettman, R. B., Further studies of the dimeric .beta.-linked "face-to-face four" porphyrin: FTF4. *J. Am. Chem. Soc.* **1983**, *105*, 2694-2699.
15. Angewandte Chemie, I. E. i. E., Raja; Byers, P.; Lutz, M.; Spek, A. L.; Bouwman, E., Electrocatalytic CO₂ Conversion to Oxalate by a Copper Complex. *Science* **2010**, *327*, 313-315.
16. Chang, C. K.; Liu, H. Y.; Abdalmuhdi, I., Electroreduction of oxygen by pillared cobalt(II) cofacial diporphyrin catalysts. *J. Am. Chem. Soc.* **1984**, *106*, 2725-2726.
17. Jerome, F.; Barbe, J.-M.; Gros, C. P.; Guillard, R.; Fischer, J.; Weiss, R., Peculiar reactivity of face to face biscorrole and porphyrin-corrole with a nickel(II) salt. X-Ray structural characterization of a new nickel(II) bisoxocorrole. *New J. Chem.* **2001**, *25*, 93-101.
18. Rosenthal, J.; Nocera, D. G., Role of Proton-Coupled Electron Transfer in O–O Bond Activation. *Acc. Chem. Res.* **2007**, *40*, 543-553.
19. Wada, T.; Muckerman, J. T.; Fujita, E.; Tanaka, K., Substituents dependent capability of bis(ruthenium-dioxolene-terpyridine) complexes toward water oxidation. *Dalton Trans.* **2011**, *40*, 2225-2233.
20. Wada, T.; Tsuge, K.; Tanaka, K., Syntheses and redox properties of bis(hydroxoruthenium) complexes with quinone and bipyridine ligands. Water-oxidation catalysis. *Inorg. Chem.* **2001**, *40*, 329-337.
21. Barbe, J. M.; Habermeyer, B.; Khoury, T.; Gros, C. P.; Richard, P.; Chen, P.; Kadish, K. M., Three-Metal Coordination by Novel Bisporphyrin Architectures. *Inorg. Chem.* **2010**, *49*, 8929-8940.

22. Kadish, K. M.; Fremond, L.; Burdet, F.; Barbe, J. M.; Gros, C. P.; Guillard, R., Cobalt(IV) corroles as catalysts for the electro reduction of O₂: Reactions of heterobimetallic dyads containing a face-to-face linked Fe(III) or Mn(III) porphyrin. *J. Inorg. Biochem.* **2006**, *100*, 858-868.
23. Collman, J. P.; Fish, H. T., A bis-capped cofacial metallodiporphyrin: Synthesis and electrochemistry of a molecule containing two coaxial metal-metal multiple bonds in close proximity. *Inorg. Chem.* **1996**, *35*, 7922-7923.
24. Rosenthal, J.; Pistorio, B. J.; Chng, L. L.; Nocera, D. G., Aerobic Catalytic Photooxidation of Olefins by an Electron-Deficient Pacman Bisiron(III) μ -Oxo Porphyrin. *J. Org. Chem.* **2005**, *70*, 1885-1888.
25. Appl, M., Ammonia. In *Ullmann's Encyclopedia of Industrial Chemistry*, Wiley-VCH Verlag GmbH & Co. KGaA: **2000**.
26. Smith, B. E., Nitrogenase Reveals Its Inner Secrets. *Science* **2002**, *297*, 1654-1655.
27. Michalsky, R.; Pfromm, P. H., Thermodynamics of metal reactants for ammonia synthesis from steam, nitrogen and biomass at atmospheric pressure. *AIChE J.* **2012**, *58*, 3203-3213.
28. Blackmore, K. J.; Lal, N.; Ziller, J. W.; Heyduk, A. F., Group IV Coordination Chemistry of a Tetradentate Redox-Active Ligand in Two Oxidation States. *Eur. J. Inorg. Chem.* **2009**, *2009*, 735-743.
29. Alexander, E. R.; Burge, R. E., The hypophosphorous acid deamination of diazonium salts in deuterium oxide. *J. Am. Chem. Soc.* **1950**, *72*, 3100-3103.
30. Chung, J.-K.; Dong, S. L.; Hyung, W. K.; Jae, M. J.; Lee, Y.-S.; Myung, C. L.; Rai, G.; Jae, M. J.; Lee, Y.-S.; Myung, C. L.; Rai, G.; Chung, J.-K.; Jae, M. J., Ionic liquid mediated efficient reduction of nitroarenes using stannous chloride under sonication. *Tetrahedron Lett.* **2005**, *46*, 3987 - 3990.
31. Dash, J.; Gupta, R. K.; Khan, F. A.; Sudheer, Chemoselective reduction of aromatic nitro and azo compounds in ionic liquids using zinc and ammonium salts. *Tetrahedron Lett.* **2003**, *44*, 7783 - 7787.
32. Ragul; Raju; Sivasankar, A new reagent for selective reduction of nitro group. *Indian Journal of Chemistry - Section B Organic and Medicinal Chemistry* **2009**, *48*, 1315 - 1318.

33. Averin, A. D.; Beletskaya, I. P.; Bessmertnykh, A. G.; Averin, A. D.; Bessmertnykh, A. G.; Denat, F.; Guillard, R., Palladium-catalysed amination of 1,8- and 1,5-dichloroanthracenes and 1,8- and 1,5-dichloroanthraquinones. *Eur. J. Org. Chem.* **2005**, 281 - 305.
34. Beletskaya, I. P.; Averin, A. D.; Bessmertnykh, A. G.; Denat, F.; Guillard, R., Synthesis of 1,8-bis(cyclam) and 1,8-bis(azacrown) substituted anthracenes by palladium-catalyzed arylation of cyclam. *Tetrahedron Lett.* **2002**, 43, 1193 - 1196.
35. Brandes, S.; Guillard, R.; Lopez, M. A.; Richard, P.; Tabard, A.; Lecomte, C.; Collman, J. P.; Hutchison, J. E., Synthesis and characterization of novel cobalt aluminum cofacial porphyrins. First crystal and molecular structure of a heterobimetallic biphenylene pillared cofacial diporphyrin. *J. Am. Chem. Soc.* **1992**, 114, 9877 - 9889.
36. Gelman, D.; Grossman, O.; Rueck-Braun, K., Trans-spanned palladium catalyst for mild and efficient amination of aryl halides with benzophenone imine. *Synthesis* **2008**, 537 - 542.
37. Holt; House; VanDerveer, Unsymmetrically substituted 2,7-dimethyl-1,8-diarylanthracenes. *J. Org. Chem.* **1993**, 58, 7516 - 7523.
38. House, H. O.; Ghali, N. I.; Haack, J. L.; VanDerveer, D., Reactions of the 1,8-Diphenylantracene System. *J. Org. Chem.* **1980**, 45, 1807 - 1817.
39. House, H. O.; Hrabie, J. A.; VanDerveer, D., Unsymmetrically Substituted 1,8-Diarylanthracenes. *J. Org. Chem.* **1986**, 51, 921 - 929.
40. Katz, H. E., 1,8-Anthracenediethynylbis(catechol boronate): A Bidentate Lewis Acid on a Novel Framework. *J. Org. Chem.* **1989**, 54, 2179 - 2183.
41. Lam, H.; Marcuccio, S. M.; Svirskaya, P. I.; Greenberg, S.; Lever, A. B. P.; et al., Binuclear phthalocyanines with aromatic bridges. *Can. J. Chem.* **1989**, 67, 1087 - 1097.
42. Wada, T.; Fujita, E.; Muckerman, J. T.; Tanaka, K., Substituents dependent capability of bis(ruthenium-dioxolene-terpyridine) complexes toward water oxidation. *Dalton Trans.* **2011**, 40, 2225 - 2233.
43. Bogdanovic, B., Magnesium Anthracene Systems and their Application in Synthesis and Catalysis. *Acc. Chem. Res.* **1988**, 21, 261-267.

44. Yasuda, H. D., Orlov Varelly Method of Manufacturing 3,3',4,4'-tetraaminobiphenyl. 20090149676, **2008**.
45. Effenberger; Heid; Merkle; Zimmermann, Synthesis of conjugated polyenes with alkylanthryl and N-alkylpyridinium terminal groups. *Synthesis* **1995**, 1115 - 1120.
46. Oliver, H.; Chauvin, Y.; Saussine, L., Reduction of aromatic ketones by some rare earth metals in ether. Reversibility of the reduction steps. *Tetrahedron* **1989**, 45, 165 - 170.
47. Knochel, P.; Calaza, M. I.; Hupe, E., Carbon-Carbon Bond-Forming Reactions Mediated by Organozinc Reagents. In *Metal-Catalyzed Cross-Coupling Reactions*, Wiley-VCH Verlag GmbH: **2008**; pp 619-670.
48. Knochel, P.; Sapountzis, I.; Gommermann, N., Carbon-Carbon Bond-Forming Reactions Mediated by Organomagnesium Reagents. In *Metal-Catalyzed Cross-Coupling Reactions*, Wiley-VCH Verlag GmbH: **2008**; pp 671-698.
49. Miyaura, N., Metal-Catalyzed Cross-Coupling Reactions of Organoboron Compounds with Organic Halides. In *Metal-Catalyzed Cross-Coupling Reactions*, Wiley-VCH Verlag GmbH: **2008**; pp 41-123.
50. Method of Manufacturing 3, 3' , 4, 4'-tetraaminobiphenyl. US2009/149676, **2009**.
51. Avola, S.; Dubovyk, I.; Hadei, N.; Kantchev, E. A. B.; O'Brien, C. J.; Organ, M. G.; Valente, G., A user-friendly, all-purpose Pd-NHC (NHC = N-heterocyclic carbene) precatalyst for the Negishi reaction: A step towards a universal cross-coupling catalyst. *Chem. Eur. J.* **2006**, 12, 4749 - 4755.
52. Chass, G. A.; Hadei, N.; Hopkinson, A. C.; Kantchev, E. A. B.; O'Brien, C. J.; Organ, M. G.; Valente, C.; Lough, A., Easily prepared air- and moisture-stable Pd-NHC (NHC = N-heterocyclic carbene) complexes: A reliable, user-friendly, highly active palladium precatalyst for the Suzuki-Miyaura reaction. *Chem. Eur. J.* **2006**, 12, 4743 - 4748.
53. Transition metal complexes of N-heterocyclic carbenes, method of preparation and use in transition metal catalyzed organic transformations. US2007/73055, **2007**.
54. Abdel-Hadi, M.; Avola, S.; Hadei, N.; Nasielski, J.; O'Brien, C. J.; Organ, M. G.; Valente, C., Biaryls made easy: PEPPSI and the Kumada-Tamao-Corriu reaction. *Chem. Eur. J.* **2007**, 13, 150 - 157.

55. Costa, V. E. U.; DaSilveira Neto, B. A.; Dupont, J.; Ebeling, G.; Lopes, A. S.; Wuest, M., Reductive sulfur extrusion reaction of 2,1,3-benzothiadiazole compounds: A new methodology using NaBH₄/CoCl₂·6H₂O(cat) as the reducing system. *Tetrahedron Lett.* **2005**, *46*, 6843 - 6846.
56. Lennox, A. J. J.; Lloyd-Jones, G. C., Selection of boron reagents for Suzuki-Miyaura coupling. *Chem. Soc. Rev.* **2014**, *43*, 412-443.
57. Wagaw, S.; Buchwald, S. L., The Synthesis of Aminopyridines: A Method Employing Palladium-Catalyzed Carbon–Nitrogen Bond Formation. *J. Org. Chem.* **1996**, *61*, 7240-7241.
58. Jiang, L.; Buchwald, S. L., Palladium-Catalyzed Aromatic Carbon-Nitrogen Bond Formation. In *Metal-Catalyzed Cross-Coupling Reactions*, Wiley-VCH Verlag GmbH: **2008**; pp 699-760.
59. Louie, J.; Hartwig, J. F., Palladium-catalyzed synthesis of arylamines from aryl halides. Mechanistic studies lead to coupling in the absence of tin reagents. *Tetrahedron Lett.* **1995**, *36*, 3609-3612.
60. Parrish, C. A.; Adams, N. D.; Auger, K. R.; Burgess, J. L.; Carson, J. D.; Chaudhari, A. M.; Copeland, R. A.; Diamond, M. A.; Donatelli, C. A.; Duffy, K. J.; Faucette, L. F.; Finer, J. T.; Huffman, W. F.; Hugger, E. D.; Jackson, J. R.; Knight, S. D.; Luo, L.; Moore, M. L.; Newlander, K. A.; Ridgers, L. H.; Sakowicz, R.; Shaw, A. N.; Sung, C.-M. M.; Sutton, D.; Wood, K. W.; Zhang, S.-Y.; Zimmerman, M. N.; Dhanak, D., Novel ATP-Competitive Kinesin Spindle Protein Inhibitors. *J. Med. Chem.* **2007**, *50*, 4939-4952.
61. Parks, D. J.; Parsons, W. H.; Colburn, R. W.; Meegalla, S. K.; Ballentine, S. K.; Illig, C. R.; Qin, N.; Liu, Y.; Hutchinson, T. L.; Lubin, M. L.; Stone, D. J.; Baker, J. F.; Schneider, C. R.; Ma, J.; Damiano, B. P.; Flores, C. M.; Player, M. R., Design and Optimization of Benzimidazole-Containing Transient Receptor Potential Melastatin 8 (TRPM8) Antagonists. *J. Med. Chem.* **2010**, *54*, 233-247.
62. Ren, D.; McClelland, R. A., Carbocation-like reactivity patterns in X'-substituted-4-biphenylnitrenium ions. *Can. J. Chem.* **1998**, *76*, 78-84.
63. Liu, S.-Y.; Nocera, D. G., Hangman salophens. *J. Am. Chem. Soc.* **2005**, *127*, 5278 - 5279.
64. Guillard, R.; Lopez, M. A.; Tabard, A.; Richard, P.; Lecomte, C.; Brandes, S.; Hutchison, J. E.; Collman, J. P., Synthesis and characterization of novel cobalt aluminum cofacial porphyrins. First crystal and molecular structure of a

heterobimetallic biphenylene pillared cofacial diporphyrin. *J. Am. Chem. Soc.* **1992**, *114*, 9877-9889.

65. Wąsik, R.; Wińska, P.; Poznański, J.; Shugar, D., Synthesis and Physico-Chemical Properties in Aqueous Medium of All Possible Isomeric Bromo Analogues of Benzo-1H-Triazole, Potential Inhibitors of Protein Kinases. *J. Phys. Chem. B* **2012**, *116*, 7259-7268.
66. van der Veen, L. A.; Keeven, P. K.; Kamer, P. C. J.; van Leeuwen, P. W. N. M., Wide bite angle amine, arsine and phosphine ligands in rhodium- and platinum/tin-catalysed hydroformylation. *J. Chem. Soc., Dalton Trans.* **2000**, 2105-2112.